To my grandparents, Felicidade e José, and my mother.

UNIVERSITY OF SOUTHAMPTON

FACULTY OF ENGINEERING, SCIENCE & MATHEMATICS

SCHOOL OF CHEMISTRY

ELECTRODEPOSITION OF Cu AND Cu-Pd ALLOYS FROM AQUEOUS AND LIQUID CRYSTAL MEDIA AND THEIR ACTIVITY FOR NITRATE REDUCTION

by

Clélia Alexandre Claudino Milhano

Thesis for the degree of Doctor of Philosophy

April 2007

UNIVERSITY OF SOUTHAMPTON

ABSTRACT

FACULTY OF ENGINEERING, SCIENCE & MATHEMATICS

SCHOOL OF CHEMISTRY

Doctor of Philosophy

ELECTRODEPOSITION OF Cu AND Cu-Pd ALLOYS FROM AQUEOUS AND LIQUID CRYSTAL MEDIA AND THEIR ACTIVITY FOR NITRATE REDUCTION

by Clélia Alexandre Claudino Milhano

This thesis describes the preparation and characterisation of palladium, copper and copper-palladium alloy films for nitrate and nitrite electroreduction. Palladium, copper and copper-palladium films were prepared by electroreduction of the respective salt precursors within the aqueous domain of the hexagonal (H_1) lyotropic liquid crystalline phase of $C_{16}EO_8$. These materials were characterised structurally and electrochemically. Mesoporous palladium films were electrodeposited onto platinum microdisc electrodes and the voltammetry of these high area films was study predominantly in basic media (2 M NaOH). Interesting features that usually are not possible to observe and to study with smooth palladium films were revealed and the palladium films also showed particular good activity for nitrite electroreduction.

Different templating baths and experimental conditions were studied for the electrodeposition of mesoporous copper films and all the attempts are discussed in detail. Electrochemical methods for the quantification of high area copper films are also discussed. The response for nitrate reduction at copper films electrodeposited in the presence of surfactant is compared with the response obtained at polished Cu discs and Cu films deposited *in situ* from $CuSO_4$ and a significantly positive shift in the potential can be observed for the former Cu films.

Several aqueous Cu(II)-Pd(II) solutions containing different ratios of the two metal precursors were electrochemical studied and a series of interesting results showing the formation of Cu-Pd alloys is presented. It is also shown in this work that Pd(II) catalyses the electrodeposition of Cu(II) when both cations are present in solution. A number of Cu-Pd films were electrodeposited from aqueous Cu(II)-Pd(II) solutions and

it was found by EDX analysis that the films composition strongly depends on the Cu(II):Pd(II) ratio and the deposition potential. The electrodeposition of Cu-Pd films in the presence of $C_{16}EO_8$ introduces even more variables in the system, but smooth and well adherent film with a uniform composition can be obtained.

Nitrate reduction studies were performed at Cu-Pd films electrodeposited from aqueous solution and in the presence of surfactant and in both cases the response seems to be dependent on the film composition.

List of Contents

Author's Declaration

Except where specific reference is made to other sources, the work presented within this thesis is the original work of the author. It has not been submitted, in whole or part, for any other degree.

Acknowledgements

First, I would like to thank Professor Derek Pletcher for his supervision and continuous encouragement during my project. Derek has a special gift for explaining things, which together with his knowledge, experience, infinite patience and simplicity make him a unique supervisor and a very special person. I might be loosing a supervisor now, but I have certainly gained a friend. Thank you for everything, Derek!

Dr. Guy Denuault (my advisor), Professor George Attard and Professor Phil Bartlett I would like to thank for the useful discussions and suggestions at different stages of my research.

My work was also made easier thanks to the skilled technicians that we have at Southampton who are always working in the background and provide strong support for our research to continue, namely our glassblowers, the people at the workshop and Alistair Clark.

The faces in Derek's group kept changing during my PhD, but to all of them I would like to say thank you. To Richard, Dmitry and Yusairie for their help when I arrived and to Jyo, Miss Hartini and Miss Maria for their kindness and patience. I also would like to thank the more recent students in the group, Alicja, Jacek and Hantao who, despite not seeing me that often, always have a smile to offer. To all of you I wish the best!
I also would like to thank Xiaohong Li for all her help and for all the discussions we shared, to Doug Offin for making my potentiostat work, Marcus Dymond for his help with liquid crystal phase identification and Jenny Armstrong for the interpretation of X-ray data.
Thank you to all groups in the 7^{th} and 6^{th} floor of building 29 for the enjoyable and friendly atmosphere and in particular to Nefeli.

If there is someone "to blame" for choosing Southampton to do my PhD, it is Professor Irene Montenegro, who introduced me to electrochemistry during my degree in Portugal and who became my supervisor later in my first electrochemistry related research

project. Irene was the one who introduced me to Derek and who always supported me in coming to Southampton. Obrigada, Grande Chefe!

Thank you to Fundação para a Ciência e a Tecnologia (FCT, Portugal) for sponsoring my PhD.

To my family, in particular my grandparents, my mother and my sister Inês, who were always there for me and supporting my decisions. To Phil, for all his patience, motivation and encouragement (specially in the last couple of months!) but most of all, for his love. To all of you I give thanks.

My time in Southampton has been a very rewarding one, not only for all the scientific knowledge acquired, but also for all the people I had the chance to meet, the friends that I have made and for the many experiences that I have been through. And if our life is like a book, where we can write our own story, I am certain that I have written in the last three and a half years some beautiful pages. The names above are only some of those who helped these pages to be happy ones. To those who I did not mention, including so many friends in Portugal, my big thank you!

Chapter 1- Introduction

1.1- The Need for Electrocatalysis

The need to increase the rate of many electrochemical reactions, especially those with a practical application, has always been a challenge and has motivated intensive research in different areas of electrochemistry.

In electrocatalysis, an increase in the reaction rate is manifested by (i) an increase in current density at a fixed potential or (ii) a decrease in the overpotential during electrolysis at fixed current density[1]. For those reactions which are not mass transport controlled, a high reaction rate can be achieved by increasing the overpotential at the electrode (η), as dictated by the Tafel equation (written here for an oxidation):

$$\log i = \log i_0 + \frac{\alpha_A nF}{2.3RT}\eta \qquad (1.1)$$

where i is the current density, i_0 the exchange current density, α_A is the transfer coefficient, n the number of electrons involved in the electrode reaction and the other symbols have their usual meaning.

However, increasing the overpotential increases the energy consumption of an electrolysis cell or decreases the energy efficiency of a battery or fuel cell. It can also lead to loss in current efficiency because competing reactions (e.g. H_2 evolution) become more important with the increased overpotential. The objective of electrocatalysis is therefore to provide alternative ways for the reaction of interest to occur at high current densities close to the equilibrium potential. In practice, this can be achieved by selecting an electrode composition of higher catalytic activity and/or increasing the active area of the electrode by preparation of rough, porous or other high area surfaces.

Hydrogen evolution was one of the first reactions where the effect of the electrode material on the reaction rate was studied in detail and it is a classical example where electrocatalysis plays a major role[2]. The performance of different cathode materials for this process changes dramatically and if one wants to achieve a high rate for the hydrogen evolution reaction it is necessary to use precious metals like platinum, palladium or its alloys.

With the increasing interest in fuel cell technology over the last years, methanol oxidation[3, 4] and oxygen reduction[5] have also been the subject of extensive research to find the best materials in order to achieve maximum efficiency. For methanol oxidation, a major problem arises from poisoning of the surface. Species such as CHO and CO are intermediates or can result from side reactions and adsorb to the surface, reducing considerably the number of active sites for the reaction of interest. In the case of oxygen reduction, and particularly in acid solutions, few materials are stable to anodic dissolution close to the equilibrium potential for oxygen reduction and even the more noble metals, which do not dissolve, suffer from the oxidation and/ or reduction of their surfaces within the potential range of interest. Considering these two last examples, it is easy to understand that the selection of the best electrocatalyst for a particular electrochemical process cannot be simply based on the increase of the reaction rate. It is also necessary to take into account the selectivity of the electrode material for the reaction of interest and its stability.

Very often in electrocatalytic processes there is bond formation, or at least a strong interaction of the reactants, intermediates or the products with the electrode surface[6, 7] and it is common that the rate determining step is a surface reaction. In such cases, the measured current density depends not only on the electrode material, but also on its real surface area and for most catalytic processes a high surface area is desirable. Since for many reactions the best electrocatalysts are found among precious metals, which are expensive, it is often necessary to use them in a form requiring only a low loading. Coating a cheaper substrate or using a highly dispersed form of the precious metal are some of the possible approaches. Carbon substrates, particularly powders but also highly pyrolitic graphite (HOPG)[8], carbon nanotubes (CNTs)[9] and mesoporous carbon[10] are common materials for the immobilization of dispersed noble metals. Different electron conducting polymers (e.g. polyaniline and polypyrrole) are also considered as convenient substrates[11].

A high chemical and electrochemical stability, a low background current and a wide electrochemical window of polarizability make highly boron-doped diamond electrodes (BDD) also attractive as support materials[12, 13] and they have been used, for example, for the deposition of IrO_2, Au and Pt nanoparticles, which are catalytically active components for oxygen evolution, CO and methanol oxidation[14].

Many physical and chemical properties of materials are determined not only by the materials themselves, but also by their geometric dimensions. It is well known that the size of nanoparticles influences their catalytic activity, not only due to the enhanced surface area, but also due to particular electronic and chemical properties, different from those of bulk materials[15]. Several different approaches for the fabrication of nanoparticles have been described in the literature[14-17] and this is an area of intensive research in electrocatalysis, where techniques such as high resolution transmission electron microscopy (HRTEM), *in situ* scanning tunnelling microscopy (STM) and Fourier transformed infrared (FTIR) play a major role in the characterisation and optimization of the electrode surface.

The list of electrode materials and ways to modified and modulate their surface is immense. Single-crystal surfaces[18], supported nanostructured metal colloids[16, 19], metallic alloys[3, 20-22], oxides[7, 23, 24] and non-precious metals[25] have been extensively studied both in fundamental aspects and applications of electrocatalysis.

Therefore, the development of improved performance electrocatalysts depends on understanding and exploiting the roles of catalyst composition, catalyst structure and catalyst substrate. All high surface area forms of metals are of interest and this thesis focuses on a particular high surface area structure.

1.2- Metal Electroplating

The electrodeposition of metals involves the reduction of metal ions, M^{n+}, usually from aqueous or organic electrolytes at the electrode surface. In a general way, the reaction in aqueous medium at the cathode follows Equation 1.2

$$M^{n+} + ne^- \longrightarrow M \qquad (1.2)$$

In recent years, metal electroplating has evolved from the deposition of smooth and uniform metal layers with desired characteristics (e.g. abrasion or wear resistance and corrosion protection or to improve the appearance or mechanical properties) to the electrodeposition of nanoscale structures showing new optical, electrical, magnetic, chemical and mechanical properties[26, 27].

Several approaches have been reported for the electrodeposition of metallic nanostuctures such as nanometer sized particles, wires, tubules and nanoporous layers[28, 29]. Some of the methods used include preferential metal electrodeposition at step edges of highly orientated pyrolytic graphite[30, 31], the electrodeposition of metals within the pores of nanoporous template membranes[32, 33], into self assembled layers of microspheres[34] and also the deposition into liquid crystal solutions[29]. This last method was the one used throughout the present work and will be covered in more detail in Section 1.4, but first some of the basic concepts related with metal electroplating will be discussed.

1.2.1- Nucleation and growth

Real surfaces for electrodeposition (substrates) are likely to contain a large number of defects and sites more advantageous than others for nucleation[35], but in the following discussion an ideal cathode surface, atomically smooth and defect free, will be assumed. Since metal ions in an aqueous solution are hydrated, it is necessary to consider a series of stages in the formation and growth of a single nucleus of the metal on an inert cathode. These include the transport of hydrated metal ions through the solution to the electrode surface, the electron transfer between the cathode and the hydrated metal ion, the formation and clustering of adatoms leading to each stable nucleus and finally, the growth of the nucleus by incorporation of adatoms at favourable sites in the lattice structure of the metal. For thermodynamic reasons, the nucleus must reach a critical size to become stable and this can be achieved only if the adatoms collect together very rapidly. In electrodeposition, a very high concentration of adatoms is favoured by using a solution with high concentration of metal ions and driving the electron transfer process hard by applying a sufficient overpotential.

In terms of nucleation, two limiting forms can occur, one where all the nuclei are formed immediately (instantaneous nucleation) and another one where the nuclei are formed gradually (progressive nucleation). A difference resulting from these two

limiting forms of nucleation is the size distribution of the nuclei after a period of growth. Following instantaneous nucleation, the centres would be expected to be the same size, while progressive nucleation would be expected to lead to a broad range of sizes.

Once stable nuclei have been created, they will grow readily, unless the deposition conditions (e.g. potential) are changed. The growth may be either (a) two dimensional, when only a monolayer can be deposited without further nucleation or (b) three dimensional (3D), when thick layers can be formed simply by a continuous growth process[35]. A thick layer can arise either by repetitive nucleation and monolayer by monolayer thickening or growth and overlap of 3D centres.

In the growth and overlap mechanism the structural components are 3D crystallites and the growth sequence consists of five stages:

(i) formation of isolated nuclei;

(ii) growth of each nucleus to a 3D crystallite;

(iii) overlap of the 3D crystallites;

(iv) formation of a continuous layer over the whole cathode surface;

(v) thickening of this complete layer.

The formation of nuclei leading to the deposition of a thick metal layer is then a multistep process where each of the above processes may be the rate determining step. Hence, a wide range of responses to potential step and sweep experiments might be expected.

The rate of growth of the nuclei is generally determined by the rate of conversion of metal ions to adatoms at the expanding surface of the centres (either at the perimeter of the monolayer or at the surface of the hemisphere). As the nuclei grow, their surface area increases and hence the rate of metal deposition will initially increase, i.e., the deposition of metal leads to an extension of the area available for further reduction and a rising current-time transient will be observed. The rate of reduction of metal ions and, therefore, the rate of metal deposition can, however, depend either on the kinetics of the electron transfer process at the surface or on the rate of mass transport of ions in solution. Diffusion will, however, occur in a spherical field to each growing centre and hence its rate will be higher than predicted by linear diffusion to a plane electrode of area equivalent to the surface of the centre.

When the cathode surface reaches the stage where the growing centres start to overlap, these will no longer grow at the expected rate and the current will increase less rapidly than previously.
Once overlap of growing centres has occurred over the whole surface, the layer will thicken as deposition continues over the total area of the cathode. The rate determining step can again be either electron transfer or mass transport.

The early stages of metal deposition can be studied by stepping the potential of a polished electrode, free from metal, M, from a value where no reduction occurs to one where nucleation of the metal phase can occur. Such experiments lead to rising current-time transients. At the instant the potential is changed, there are no nuclei on the surface and, hence, the initial current for the deposition must be zero. Thereafter, the current increases because (a) the number of nuclei may increase (if the nucleation is progressive) and (b) the surface area of each nucleus increases with time. The detailed shape of the rising transient depends on the kinetics of nucleation, whether growth is two or three dimensional, and the rate determining step during growth. When overlap of the centres begins, the slope of the transient will decrease and when a complete layer is formed, the current will plateau (if thickening is electron transferred controlled) or pass through a peak and decrease (if thickening is diffusion controlled). The analysis of the transients in such a linear way, however, is not always possible and several practical problems such as charging currents and cleaning of the electrode can interfere with the response.

The deposition of metals into the aqueous phase around the surfactant rods of a liquid crystal structure presents new challenges to the theory of nucleation and growth. With the restricted aqueous phase having characteristic scales ~ 5 nm, growth cannot be either two dimensional or 3D in the accepted sense. I am not aware of any literature considering this problem.

1.2.2- Electrodeposition of alloys

It is generally recognized that alloy deposits show not only better properties than those of the single component metals but also different properties in certain composition ranges and these two factors have been motivating the research and development of numerous alloy systems in diverse areas and for different technological applications[26, 36].

A comprehensive compilation of principles and electrochemical conditions for the electrodeposition of alloys has been published by Brenner[37] in 1963. Despite the technological advances over the last years, this work covers the most important theoretical and practical aspects of alloy electrodeposition. More recent overviews on electrodeposition of different alloys can be found in the literature[26, 36].

The electrodeposition of alloys follows the basic principles of single metal electroplating, namely the transport of the hydrated ions, the electron transfer at the cathode surface and the incorporation of the adsorbed atoms in the growing lattice. However, the co-deposition of at least two different metals in order to form an alloy introduces two particular aspects to the process that are worthy to be mentioned in more detail:

(i) the deposition potential of the two individual metals should be nearly the same. This implies that the formal electrode potentials of the two metals are similar or, that some concentration adjustment of one of the metal ions needs to be done (e.g. by addition of complexing agent) in order to bring to the deposition potentials close together;

(ii) the plating bath may be depleted of one metal ion faster than the other. Thus, in order to keep deposition conditions under control, metal ions must be replenished in direct proportion to their rates of deposition.

1.2.3- Faraday's law and current efficiency

The total amount of electrochemical reaction that occurs at the electrode surface is proportional to the quantity of electric charge, Q, passed through an electrochemical cell, as stated by Faraday's law

$$Q = mnF \qquad (1.3)$$

where m is the number of moles of product formed, n is the number of electrons required to convert reactant into product and F is the Faraday constant.

The film thickness can then be estimated considering the charge passed during deposition, the area of the deposit, a, the atomic weight of the metal deposited, w, and its density, ρ, according to Equation 1.4

$$\text{film thickness} = \frac{Qw}{nFa\rho} \qquad (1.4)$$

Assuming that only the reaction of interest occurs at the electrode surface, a current efficiency, CE, of 100% can be expected, but if two or more reactions occur simultaneously (competing reactions), the current efficiency is defined by

$$\text{CE} = \frac{\text{charge consumed in the reaction of interest}}{\text{total charge passed}} \qquad (1.5)$$

The evolution of hydrogen during metal electrodeposition is a typical example of a competing reaction that affects the current efficiency of plating processes. Besides the energetic losses, the electrochemical production of hydrogen can also interfere with the properties of various metal deposits[38], leading to the formation of cracks due to lattice expansions when H_2 gas is evolved from the deposit (hydrogen embrittlement), or the appearance of pores if the deposit forms around gas bubbles before they are released.

1.2.4- Electrodeposition of palladium and copper

Commonly plated metals include nickel, gold, silver, tin, chromium, lead, zinc, iron, cobalt, copper and palladium. In this section special attention will be given to the last two metals.

The composition of a commercial plating bath can be complex and vary according to the metal deposited, but in general, in addition to the metal source, electrolyte, complexing agent and buffer, additives for brightening, hardening, grain refining and surface smoothing (levelling agents) are included in the solution to improve the morphology and performance of the deposits. These additives affect in different ways the deposition and crystal growth processes, but their specific role is out of the scope of this thesis.

Below, only a general idea of the main constituents of commercial palladium and copper baths will be given. Further details can be found in the numerous existing patents and in the literature [39, 40].

1.2.4.1- Palladium

Electroplated palladium became technologically significant in the mid-1970s and since then it has found application in interconnect products especially for telecommunication, computer and automotive connectors, semiconductor packaging, printed circuit industry and in the decorative industry [40].

Palladium has been electroplated from alkaline (pH 8-13), neutral (pH 5-8) and acidic (pH <1 to 5) electrolytes. In alkaline electrolytes, the systems with more practical application involve the formation of stable complexes between Pd ions and diamines (e.g. 1,3-diaminopropane), with the palladium precursor being in general $PdCl_2$. Hydrochloric acid and sulphuric acid are used in the preparation of acidic media and in neutral media the attention goes to systems with oxalates, sulfamates and in particular ammonia ligands.

Palladium is known to form alloys with other metals of group VIII and IB that show improved characteristics over the pure metals. Alloys such as Pd-Ni, Pd-Co, Pd-Fe, Pd-Au, Pd-In and Pd-Ag are only examples of the numerous binary systems that have been reported[40].

The electrodeposition of palladium and its alloys from aqueous solutions can suffer interferences from the co-deposition of hydrogen and the formation of palladium hydrides, PdH_x. Thus, in order to achieve good quality palladium films and high current efficiencies, it is necessary to control deposition parameters such as temperature and pH to avoid co-deposition of hydrogen.

1.2.4.2- Copper

Copper has been extensively electroplated for more than 100 years with major applications on plastics, printed circuit boards, die castings, automotive bumpers, rotogravure rolls, electrorefining and electroforming[39].

The main commercial solutions that have been used for the electrodeposition of copper are: the alkaline cyanide and pyrophosphate complex ion systems and the acid sulphate and fluoroborate simple ion systems[39]. Cyanide solutions are progressively being replaced by non-cyanide solutions because of their toxicity and waste treatment

problems and from all the baths, the acid copper sulphate is clearly the most common for copper plating.

The structure of the copper deposit depends on the deposition rate, the substrate surface nature and the deposition technique and the characteristics of the deposits are influenced by the concentration of copper salts, additives, free acid, temperature, cathode current density and the nature and degree of agitation.

Examples of copper alloys that have been reported include Cu-Pb, Cu-Ni, Cu-Sn and Cu-Zn. Surprisingly, there are only few works reporting the electrodeposition of Cu-Pd alloys[41-43].

Considering that electrodeposited alloys are similar to thermally prepared alloys in structure, in that they usually contain the same phases[37] and according to the solidification diagram shown in Figure 1.1, one can expect the electrodeposition of Cu-Pd alloys to form Cu_3Pd and CuPd phases.

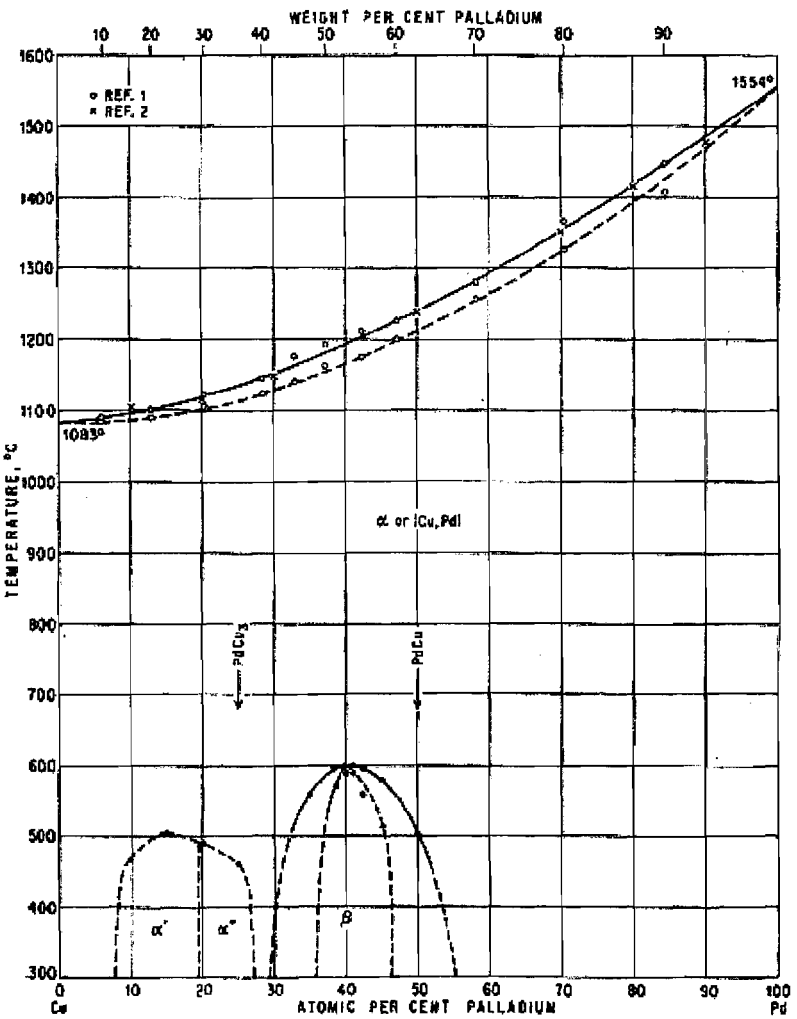

Figure 1.1 *Solidification diagram for Cu-Pd obtained from reference*[44].

1.3- Microelectrodes

1.3.1- Advantages

The geometric dimensions of a microelectrode (dimensions of tens of micrometers or less) introduce significant changes in the mass transport from the bulk of a solution towards the electrode surface, offering several advantages over normal size electrodes[45], namely:

(i) decreased ohmic drop of potential, IR;

(ii) fast establishment of a steady-state signal;

(iii) current increase due to enhanced mass transport at the electrode boundary;

(iv) increased signal-to-noise ratio.

Besides these characteristics, the convenience of microelectrodes for analysis, and the use of viscous and expensive templating mixtures were the main reasons why microelectrodes were chosen to perform the metal deposition and the nitrate and nitrite studies reported in the present work.

1.3.2- Steady state voltammetry

In the steady state, a microdisc electrode is surrounded by a hemispherical diffusion field, with the rate of diffusion being higher to the edge of the disc than to the centre. When the steady state is achieved, the diffusion controlled current is given by

$$I_L = 4nFDcr \qquad (1.6)$$

where n is the number of electrons involved in the reaction, F is the Faraday constant, D is the diffusion coefficient, c is the concentration of reactant and r is the radius of the disc. Figure 1.2 illustrates a typical steady state voltammogram for a reversible electron transfer process at a microdisc electrode. As it is possible to observe, the response is a well defined wave reaching a limiting current (I_L) for a diffusion controlled process.

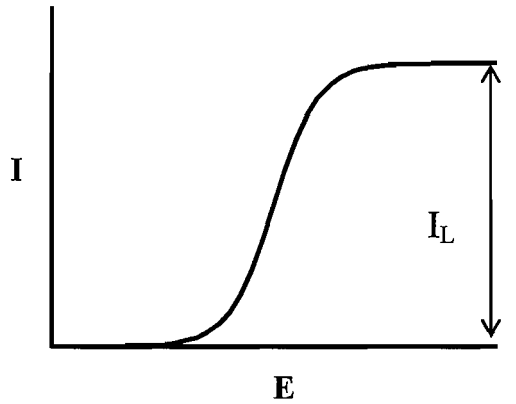

Figure 1.2 *Steady state voltammogram for a microdisc electrode.*

1.3.3- Metal deposition

The metal deposition at a microdisc electrode follows, in general, the same principles discussed before for metal deposition at a macroelectrode. An unfortunate characteristic is related with the thickening of the metal layer. Once it occurs in a spherical diffusion field, the growth of the deposit tends to occur predominantly at the edge of the microdisc (edge effect) and if the deposit becomes sufficiently thick, then growth will start to occur at the perimeter of the growing layer and the deposit starts to spread over the insulating substrate around the disc[46].

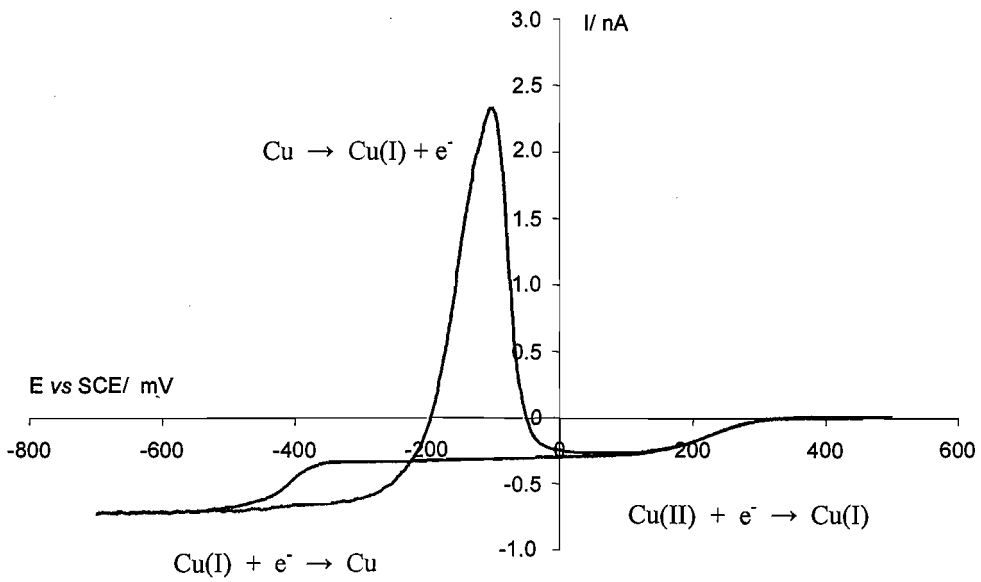

Figure 1.3 *Cyclic voltammogram for the deposition of copper at a Au microdisc electrode from a chloride electrolyte.*

Figure 1.3 shows a cyclic voltammogram for a polished microdisc in a Cu(II) aqueous chloride solution. The following features should be noted:

(i) on the forward scan, the current is very low until an overpotential (at 300 mV *vs* SCE) where Cu(II) starts to reduce to Cu(I), giving rise to a very well defined wave. The current reaches then a steady state until the overpotential where nucleation of copper can take place (~ -375 mV *vs* SCE). A very well formed wave is observed again for this process and the current reaches for the second time a steady state value corresponding to mass transport control, I_L. The copper deposition continues until the scan is reversed at -700 mV;

(ii) on reversing the direction of the scan, a nucleation loop is observed between -400 and -225 mV *vs* SCE. On the forward scan nucleation of the Cu has not occurred at such positive potentials, but on the reverse scan the Cu layer exists and thickening can continue to happen;

(iii) continuing the scan in the positive direction, the copper is oxidised and a sharp stripping peak is observed at -100 mV *vs* SCE. The symmetrical anodic peak shape results from the fixed amount of Cu available for oxidation. Comparison of the charge under the stripping peak and the cathodic charge corresponding to reaction $Cu(I) + e^- \rightarrow Cu$ shows that they are very similar and hence the stripping peak corresponds to the process $Cu \rightarrow Cu(I) + e^-$.

1.3.4- Adsorption

As for macroelectrodes, also at microelectrodes an electrode reaction involving adsorption processes or the formation/ removal of a monolayer or a fixed amount of reactant/ product (e.g. the underpotential deposition (UPD) of metals) will give a response significantly different from the one obtained for a simple electron transfer process, see Figure 1.4. The characteristics of the voltammogram largely arise because the amount of reaction is determined by the number of sites on the electrode surface where adsorption can occur[47]. As it is possible to observe in Figure 1.4,

(i) the reduction peak is symmetrical with the current dropping to zero beyond the peak when the reactant is fully consumed or the surface fully covered and the same behaviour is observed for the anodic peak;

(ii) the separation between the cathodic and anodic peaks is 0 mV for a rapid electron transfer since diffusion does not play any role in the process;

(iii) the charge is the same under both peaks and it must be below or equal to the charge associated to the formation of a monolayer.

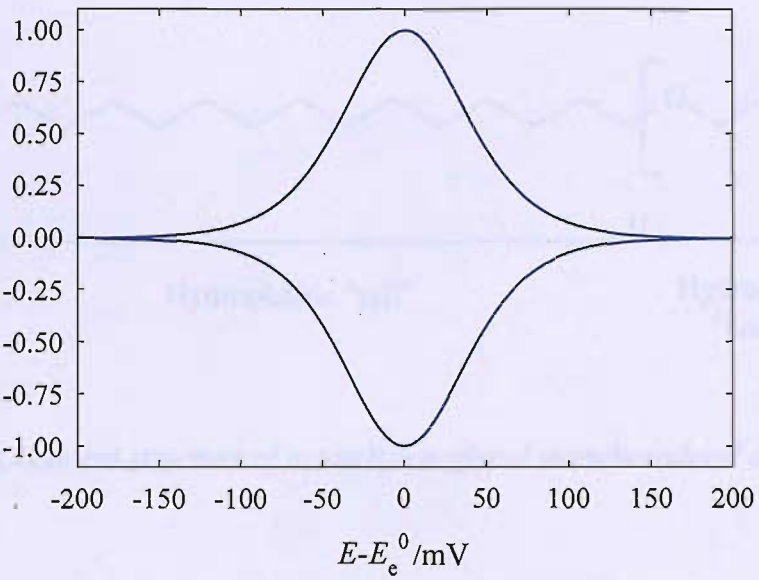

Figure 1.4 *Typical cyclic voltammogram for a reversible process involving the formation/ removal of a surface layer.*

Also for a surface process one can expect the peak current to be proportional to potential scan rate, i.e., the charge required to reduce the adsorbed layer is independent of potential scan rate and a similar behaviour can be expected for the peak potential.

1.4- Lyotropic Liquid Crystalline Phases

Surfactants, or surface active agents, have been used for centuries and play an important role in everyday life products such as detergents, cosmetics, paints, coatings and even food. They are amphipilic molecules consisting of two distinctive parts: a polar (hydrophilic) moiety, which is usually designated as the "head" of the molecule and a non-polar (hydrophobic) linear or ramified hydrocarbon chain also know as the "tail". Due to this dual character, the molecules have a unique ability to self-organize at interfaces and in solution, giving rise to supramolecular assemblies such as micelles and liquid crystals, with different structures, at higher concentrations. Figure 1.5 illustrates

the structure of the octaethyleneglycol monohexadecyl ether, a pure non-ionic surfactant commonly known as $C_{16}EO_8$. Together with Brij® 56, these were the two surfactants studied throughout this work. Brij® 56 has a similar structure to $C_{16}EO_8$, but it is not a single compound, so the number of ethylene groups changes from molecule to molecule, with an average number of ten.

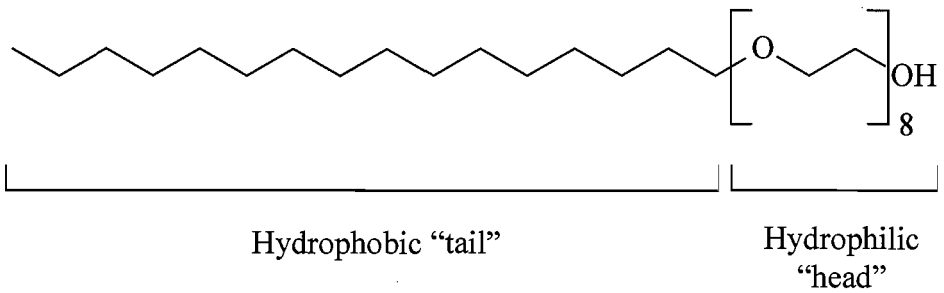

Figure 1.5 *Chemical structure of octaethyleneglycol monohexadecyl ether ($C_{16}EO_8$).*

At very low concentrations of surfactant in water, the amphiphilic molecules are present as monomers[48]. As the concentration of surfactant increases and reaches the 'critical micelle concentration' (CMC), the molecules start to aggregate in bulk solution to form nanosized spherical micelles. This configuration minimises the contact between the hydrophobic part of the molecule and surrounding water by keeping the hydrocarbon tail (non-polar) in the interior of the structure and shielding it with the hydrophilic (polar) head of the molecule[49]. This configuration is known as the micellar solution (denoted L_1) and is illustrated in Figure 1.6. A further increase in surfactant concentration leads to an increase in the density of the micelles and consequently a less random configuration is adopted. In this cubic micellar phase (I_1), the micelles still retain their spherical structure, but they are usually packed on a body-centred cubic (bcc) lattice. The I_1 phase is the first of the lyotropic liquid crystalline phases, also known as mesophases, to be observed in a surfactant/ water system. At higher surfactant concentrations rod-like micelles start to form, with the amphiphilic molecules in a radial arrangement. The rods are surrounded by the aqueous media, so the molecules keep their hydrophobic part within the centre of the rod. These indefinitely long cylindrical rods self-assemble in an hexagonal array and form the hexagonal phase (H_1). A second cubic morphology arises with further increased surfactant/water ratio. This is the

bicontinuous cubic phase (V_1), which is characterised by short surfactant rod-like micelles interconnect in a three-dimensional and continuous network. The lamellar phase (L_α), the last of the lyotropic liquid crystalline phases considered here, consists of equidistant parallel surfactant bilayers separated by layers of water[50].

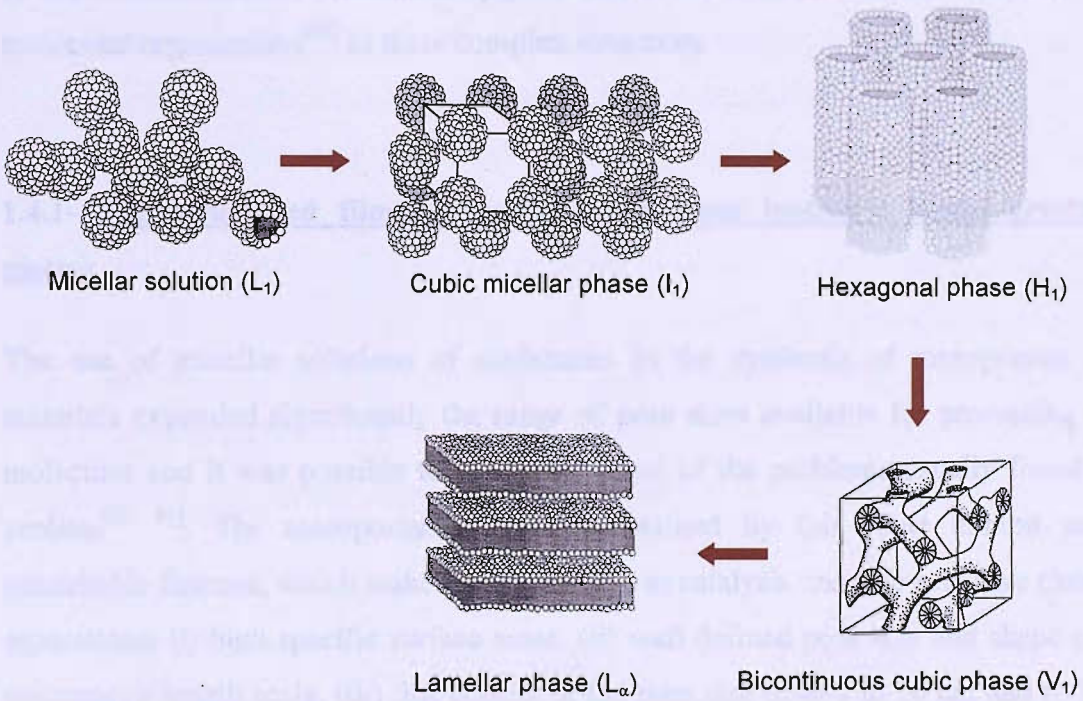

Figure 1.6 *Structure of micellar solution and liquid crystalline phases formed with increasing surfactant concentration. Figure reproduced with permission from Prof. George Attard.*

Besides the normal mesophases described above, which were designated by the index 1, some surfactants also show reversed mesophases, where the polar "heads" assemble together into the interior of the micelles and the "tails" are in contact with the solvent. These reversed phases might be due to different alkyl-chain conformations and also different alkyl-chain/water or head-group repulsions occurring in the system[50], or when the amphiphilic molecules are mixed with a non-polar solvent, like hexane[51]. In these cases, the phases are denoted with the index 2 (e.g. reversed hexagonal phase, H_2).

The hexagonal and lamellar phases are both birefringent and show different textures under polarized light. The micellar (L_1) and cubic phases (I_1 and V_1) are optically

isotropic, so they do not show any distinctive pattern but, on the other hand, they can be easily distinguished by the difference in their viscosities.

Polarized light microscopy is the most widely used technique for liquid crystalline phase identification, however, it is often difficult and requires some experience[51]. Techniques like X-ray or neutron diffraction and NMR spectroscopy are also employed in the characterization of different phases and allow a more detailed study about he molecular organization[49] in these complex structures.

1.4.1- Nanostructured films electrodeposited from lyotropic liquid crystalline phases

The use of micellar solutions of surfactants in the synthesis of mesoporous silica materials expanded significantly the range of pore sizes available for processing large molecules and it was possible to overcome some of the problems usually found with zeolites[52, 53]. The mesoporous structures obtained by this route exhibit several remarkable features, which make them attractive in catalysis and size-selective chemical separations: (i) high specific surface areas, (ii) well defined pore size and shape over a micrometer length scale, (iii) fine control of the pore size from 2 to 10 nm and (iv) high thermal and hydrolytic stability.

It is clear that the surfactant plays a vital role in the synthesis of these materials, but its concentration is too low to permit formation of bulk liquid crystalline phases throughout the entire mixture and different formation mechanisms have been proposed[53-55].

The templating of silica mesostructures from ordered liquid crystalline mesophases was achieved by Attard *et al.*[56], using higher surfactant concentrations (>30 weight %). In this route, which was termed 'direct liquid crystal templating' (DLCT), the reaction mixture is in fact a single phase and the nanostuctures produced are casts of the structures of the liquid crystalline phases in which they are formed. One of the advantages of this method is that it allows a great degree of predictability in the deposition process through the use of different crystalline phases (H_1, V_1 or L_α), together with the control that can be achieved over the characteristic dimensions of the channels just by working with different surfactants.

In 1997, the templating from liquid crystalline phases was extended to the electrodeposition of mesoporous metallic films[29]. As with the silicas, it allows a significant control over the pore size and morphology of the structures, e.g. the

deposition from an H_1 phase gives a porous nanostructure, while templating from the H_2 phase allows the formation of nanowire arrays[57]. To date, most studies have been concentrated on the use of the H_1 phase[58] and this is the approach also followed in this work. The principle for metal electrodeposition by this method is illustrated in Figure 1.7 and can be described in the following way:

(a) The composition of the plating mixture, which includes the metal precursor, is chosen in a way that the bath consists of the hexagonal phase of the non-ionic surfactant, with the rods aggregating in an hexagonal lattice;

(b) Upon application of the desired potential, the electrochemical deposition of the metal takes place within the aqueous domain surrounding the surfactant rods;

(c) After deposition, the liquid crystalline template is removed by soaking the deposits in water or some other suitable solvent (e.g. isopropanol), to leave a metallic film with nanostructured pores. These metallic films are usually denoted by H_1-eMetal to indicate that they were electrochemically deposited from the hexagonal phase.

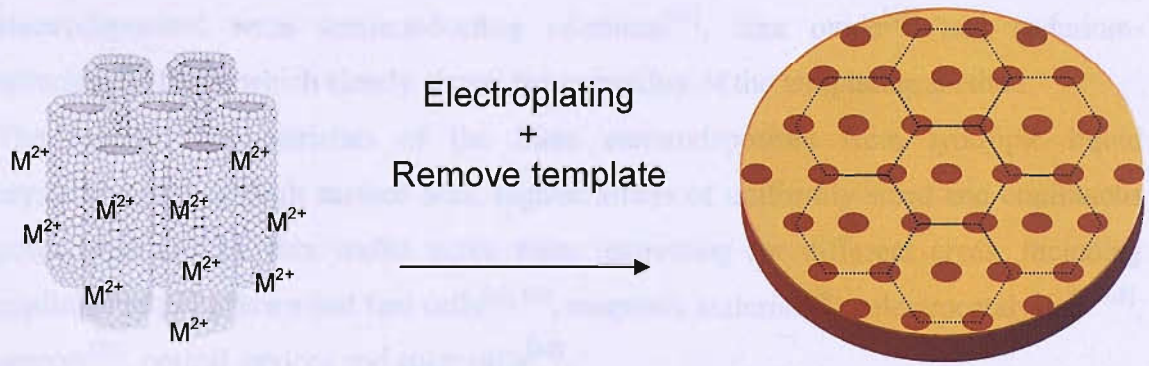

Figure 1.7 *Electrodeposition of metal films within the aqueous domain of an H_1 liquid crystalline phase. Mesoporosity is created on removal of the surfactant template.*

This method was first applied to the electrodeposition of nanostructured platinum films from a plating mixture containing $C_{16}EO_8$ (octaethyleneglycol monohexadecyl ether), hexachloroplatinic acid (H_2PtCl_6) and water[29]. Transmission electron microscopy (TEM) studies of the electrodeposited platinum film (H_1-ePt) revealed a highly porous structure consisting of cylindrical pores ~2.5 nm in diameter arranged on a hexagonal lattice. The platinum wall thickness was found to be ~ 2.5 nm and the specific surface area of the film was estimated to be ~ 22 $m^2\ g^{-1}$. It was observed that altering the alkyl

chain length of the surfactant or using a hydrophobic additive such as *n*-heptane it was possible to control the pore size over a range of 1.7 to 10 nm. The effects of electrodeposition conditions (deposition potential, charge density and electrodeposition temperature) on H_1-ePt films were studied in more detail later[59] and it was concluded that the films with the most ordered nanostructure were the ones deposited at potentials positive to -0.1 V *vs* SCE and at 25 °C. Following the same approach, the electrodeposition of H_1-ePt was also carried out onto Pt microelectrodes[60] and it was shown that, despite the high surface area, the electrodes still retain efficient mass transport characteristics. Roughness factors ~ 220 were obtained in this case for a 25 μm diameter disc, but the estimated specific surface area (~6.45 $m^2\ g^{-1}$) was considerably smaller than the value reported before (~22 $m^2\ g^{-1}$) for 1 mm diameter gold disc. This was attributed to a decrease in the deposition efficiency on the microdisc. Besides platinum, the method has been successfully applied to other metals such as cobalt[61], nickel[62], palladium[63], rhodium[64] and tin[65] although in this last example the TEM studies revealed a less organized structure. The production and characterisation of co-deposited palladium + platinum films has also been reported by Guerin *et al.*[66]. Also electrodeposited were semiconducting selenium[67], zinc oxide[68] and cadmium-tellurium[69] films, which clearly shows the versatility of the templating method.

The specific characteristics of the films electrodeposited from lyotropic liquid crystalline phases (high surface area, regular arrays of uniformly sized and continuous pores separated by thin walls) make them interesting for different areas, including applications in batteries and fuel cells[62, 65], magnetic materials[61], electrocatalysis[64, 66], sensors[70], optical devices and solar cells[67].

1.4.2- A closer look at H_1-ePd films

The electrodeposition of palladium films from the hexagonal phase of non-ionic surfactants such as $C_{16}EO_8$ and Brij® 56 was carried out by Bartlett *et al.*[63] on 1 mm diameter Au electrodes. In this work, the phase behaviour of the mixtures of each surfactant with $(NH_4)_2PdCl_4$ solution was investigated in detail and in both cases the H_1 phase was stable over a wide range of composition and temperature. The characterisation of the mesoporous Pd films showed a regular hexagonal array of cylindrical pores with diameter between 2.0 to 2.5 nm, wall thickness around the same values and very high surface areas (typical roughness factor of 250). In 1 M H_2SO_4

these films show very well resolved and sharp peaks in the hydrogen region, allowing the differentiation between adsorption and absorption processes and also between the formation of α and β-hydride phases. Taking advantage of the behaviour of the mesoporous Pd in acidic conditions (fast hydrogen absorption/ desorption reactions, fast hydrogen loading and stability of the structure towards repeated cycling to form the β-hydride phase), Imokawa *et al.*[71] have also carried out a significant amount of work with H_1-ePd films, but this time deposited onto Pt microelectrodes with the aim of developing a new pH microsensor.

1.5- Nitrate and Nitrite Electrocatalysis

The reduction of nitrate and nitrite in aqueous solutions plays an important role in different systems and in the last decades a big effort has been made to understand the chemistry involved in such reactions and also to reduce these ions to less harmful species in some situations. A review article about several treatment processes to remove nitrate from drinking water has been published by Kappor and co-workers[72] and more recently a review by Fanning[73] has covered some of the most important chemical reducing agents used for nitrate reduction, as well as a brief reference to electrochemical, photochemical and thermal methods. In this thesis, however, only the electrochemical reduction of nitrate and nitrite will be discussed.

The electrochemical reduction of nitrate and nitrite in aqueous solution has been the focus of many studies[74], but in the last years the research has been driven for three main reasons. Namely, (i) the need to develop sensitive and selective methods for the analysis of nitrate and nitrite[75-78], (ii) the treatment of low-level nuclear wastes and reduction of environmental problems caused by the extensive use of nitrogen-based fertilizers[79-82] and (iii) the purification of drinking water[83-85]. The most important aspects of the electrochemistry and electrochemical technology of nitrate have been recently reviewed[86].

It is well known that the mechanism for NO_3^- and NO_2^- electroreduction is very complex and strongly dependent on experimental conditions such as electrode material, pH and medium composition[87-90], with the possible formation of a large number of nitrogen compounds (Equation 1.7 to 1.18 , with $E°$ *vs* SHE /V values obtained from[91]):

$NO_3^- + 2H^+ + e^- \rightarrow NO_2(g) + H_2O$ $E^o = 0.775$ (1.7)

$NO_3^- + 3H^+ + 2e^- \rightarrow HNO_2 + H_2O$ $E^o = 0.94$ (1.8)

$NO_3^- + 2H^+ + 2e^- \rightarrow NO_2^- + H_2O$ $E^o = 0.835$ (1.9)

$NO_3^- + 4H^+ + 3e^- \rightarrow NO(g) + 2H_2O$ $E^o = 0.957$ (1.10)

$2NO_3^- + 10H^+ + 8e^- \rightarrow N_2O(g) + 5H_2O$ $E^o = 1.116$ (1.11)

$2NO_3^- + 12H^+ + 10e^- \rightarrow N_2(g) + 6H_2O$ $E^o = 1.246$ (1.12)

$NO_3^- + 10H^+ + 8e^- \rightarrow NH_4^+ + 3H_2O$ $E^o = 0.875$ (1.13)

$NO_2^- + 2H^+ + e^- \rightarrow NO(g) + H_2O$ $E^o = 1.202$ (1.14)

$2NO_2^- + 6H^+ + 4e^- \rightarrow N_2O(g) + 3H_2O$ $E^o = 1.396$ (1.15)

$2NO_2^- + 8H^+ + 6e^- \rightarrow N_2(g) + 4H_2O$ $E^o = 1.520$ (1.16)

$NO_2^- + 8H^+ + 6e^- \rightarrow NH_4^+ + 2H_2O$ $E^o = 0.897$ (1.17)

$NO_2^- + 7H^+ + 6e^- \rightarrow NH_3(g) + 2H_2O$ $E^o = 0.789$ (1.18)

From an environmental point of view, the desired cathodic process is the reduction of NO_3^- and NO_2^- to nitrogen gas (Eq. 1.12 and 1.16), but most of the electrode materials reported so far show no selectivity to N_2 and products such as NO_2^-, NO, NH_3 or NH_4^+ are among the most commonly found[80-84, 87, 92].

Despite the extensive literature published about nitrate and nitrite reduction, there are only a few examples where the reaction mechanism has been discussed[87, 93-96] and most part of them have been devoted to the electrocatalytic reduction of nitrate at precious metals in acidic media. In this case, a distinction is made between two possible mechanisms[96]: (i) a "direct" reduction mechanism which develops at all nitrate and acid concentrations and (ii) an "indirect" reduction mechanism that develops only at high concentrations of nitric acid (>1 M) in the presence of nitrite. A summary of the conditions for the two mechanisms is given below:

(i) <u>"Direct" nitrate reduction</u>

The reduction of nitrate at low concentrations (below 0.1 M) starts at potentials below 0.4 V *vs* SHE and its inhibition occurs at potentials below 0.1 V, which has been ascribed to the increasing surface coverage of adsorbed hydrogen (H_{ads}) and hence the impossibility for NO_3^- to adsorb on the surface. The following mechanism has been proposed by Dima *et al.*[87]:

$$NO_3^- \rightleftarrows NO_{3(ads)}^- \quad (1.19)$$

$$NO_{3(ads)}^- + 2H^+ + 2e^- \rightarrow NO_{2(ads)}^- + H_2O \text{ (rate-determining)} \quad (1.20)$$

$$NO_{2(ads)}^- + 2H^+ + e^- \rightarrow NO_{(ads)} + H_2O \text{ (fast)} \quad (1.21)$$

Since no N_2O or N_2 were formed during the reduction of 0.1 M nitrate, the authors concluded that the further reduction of $NO_{(ads)}$ leads to either NH_3 or NH_2OH.

(ii) "Indirect" nitrate reduction

- In the presence of nitrite

Nitrate can be reduced to nitrite at potentials as positive as 0.9 V *vs* SHE[96]. However, this is possible only in highly acidic environments (> 1 M) and if nitrite is present in solution, since nitrite is needed to initiate an autocatalytic cycle:

$$HNO_2 + H^+ \rightarrow NO^+ + H_2O \quad (1.22)$$

$$NO^+ + e^- \rightarrow NO \quad (1.23)$$

$$2NO + HNO_3 + H_2O \rightarrow 3HNO_2 \quad (1.24)$$

The reaction rate of the indirect reduction mechanism starts to decline around 0.65 V *vs* SHE, since NO itself starts to reduce instead of reacting with HNO_3. HNO_2 is no longer regenerated and hence its concentration starts to drop, resulting in a lower overall reaction rate.

- Without the presence of nitrite

If no nitrite and acid are added to a solution of low nitrate concentration, the indirect reduction does not develop. However, nitric acid is thermodynamically unstable at high concentrations (> 4 M) and therefore, small amounts of HNO_2, NO and NO_2 (10^{-6} to 10^{-5} mol L^{-1}) are formed without the addition of nitrite. These small amounts can initiate the indirect reduction, as has been shown by Groot *et al.*[96].

Nitrate and nitrite reduction has been extensively studied in acidic[87-89, 92, 94, 96-98], neutral[81, 84, 99-101] and alkaline[80, 83, 90, 102-104] media on a large number of electrodes, e.g. polycrystalline[87, 96] and single-crystal metals[105, 106], bimetallic systems[92, 102, 103, 107-110], graphite[84, 111] and B-doped diamond electrodes[112]. Several modified electrodes

have also been reported and different approaches have been carried out, including the metallic coating of carbon cloths[81], carbon fibers[85, 99, 100] and pyrolytic graphite[101], the underpotential deposition of different metals[113, 114] and surface modification with metal complexes[115-117]. The number and variety of electrode materials that have been used in the study of both anions is immense and difficult to report here. In the following sections, special attention will be given to selected papers and in particular to those where copper and palladium have been used.

As already mentioned, the electroreduction of both NO_3^- and NO_2^- can be affected by the presence of different species in solution. Some species can enhance the reduction current, while others have the opposite effect. Thus, the anion effect observed in some studies will be mentioned a bit more in detail in Section 1.5.3.

1.5.1- Polycrystalline metal electrodes

1.5.1.1- Bulk and plated metal electrodes

A comparative study to determine the activity of eight different polycrystalline electrodes (platinum, palladium, rhodium, ruthenium, iridium, copper, silver and gold) for nitrate reduction in acidic solution was carried out by Dima and co-workers[87]. Using different electrochemical techniques, it was shown that the activities decreased in the order Rh> Ru> Ir> Pd> Pt for the precious metal electrodes and in the order Cu> Ag> Au for the coinage metals. It was concluded that the rate determining step on Ru, Rh, Ir, Pt, Cu and Ag is the reduction of nitrate to nitrite, with a previous adsorption of nitrate ions onto the surface, according to Equation 1.20.

DEMS (differential electrochemical mass spectroscopy) measurements were performed on Pt, Rh and Cu electrodes to identify some of the reaction products as a function of potential. For Pt and Rh no gaseous products were detected and the authors have suggested that ammonia and hydroxylamine are the main products on precious metal electrodes. On the other hand, the results on Cu showed an increasing production of NO along with the reduction current.

Petrii *et al.*[88] carried out a comparative study for nitrate and nitrite reduction at electroplated Pt, Pd and Rh on Pt electrodes and an increase in the electroreduction rate of NO_3^- during the transition from Pt and Pd to Rh was also observed.

Pletcher *et al.*[118] studied the reduction of NO_3^- at a Cu cathode, for pH values between 0 and 4, using cyclic voltammetry and rotating disc techniques. With a Cu RDE, in 1 M

$HClO_4$, well formed reduction waves were observed with $E_{1/2}$ = -0.30 V (*vs* SCE) and the current being determined by the rate of mass transport of nitrate to the electrode. Reducing the proton concentration, the half wave potential shifted to more negative values and without an excess of protons, the reaction is no longer diffusion controlled. Based on the results obtained from controlled potential electrolysis and providing that there are sufficient protons in the catholyte, the authors suggest that the reduction of nitrate ions occurs by the overall reaction

$$NO_3^- + 8e^- + 9H^+ \rightarrow 3H_2O + NH_3 \qquad (1.25)$$

In alkaline conditions, a double peak around -1.3 V (*vs* SCE) was observed for both NO_3^- and NO_2^- reduction at a Cu disc[119]. In this work, Cattarin has shown that the voltammetric features depend on the positive potential limit used during cyclic voltammetry and suggests that the variations may be attributed to surface modifications affecting interfacial properties relevant to the catalytic behaviour, but no further explanation is given.

Freshly deposited metal surfaces generally give very reproducible results and can even be more active than the bulk material. For these reasons, several electrochemical studies of nitrate reduction have been concentrated on the use of metal electrodes formed by *in situ* deposition of the metal from solution onto a suitable substrate.

Carpenter *et al.*[75] carried out the reduction of nitrate at a copper cathode formed *in situ*, by plating Cu from $CuSO_4$ in solution onto a vitreous carbon disc electrode and reported that the freshly deposited Cu layers were more active than a freshly polished bulk Cu electrode and also increased significantly the reproducibility of the results. Using a potential pulse sequence technique, it was shown that this approach could be successfully applied to the determination of nitrate in drinking water.

An *in situ* copper plated boron-doped diamond microelectrode array for the sensitive electrochemical detection of nitrate was reported by Ward-Jones and co-workers[77]. This array consisted of 130 individual copper plated BDD-microdiscs with 40 μm diameter each and allowed a detection limit of 0.76(±0.5) μM.

Paidar and co-workers[83] found that the addition of Cu ions to the solution (~ 6 mg L^{-1}) effectively prevents a decrease in the activity of a Cu cathode used for electrochemical reduction of NO_3^- in the regeneration of ion exchange columns. It is suggested in this

study that the Cu^{2+} deposits slowly and continuously on the cathode surface, forming new active sites during the electrolysis time.

Vooys *et al.*[102] obtained submonolayers of Cu on Pd electrodes by *in situ* under-potential deposition to investigate the electrocatalytic reduction of nitrate and some of the possible reaction intermediates (NO_2^-, NO, and N_2O) in acidic and alkaline media. They found that, in acidic electrolytes, the activity increases linearly with Cu coverage, but in alkaline conditions a different dependence is observed. According to this study, the Cu activates the first electron transfer (from NO_3^- to NO_2^-) and the role of Pd is to steer the selectivity towards N_2. In both acidic and basic electrolytes the selectivity towards N_2 decreases with increasing Cu coverage, while the selectivity towards N_2O increases linearly.

1.5.1.2- Bimetallic electrodes

Various bimetallic electrode surfaces have shown improved activity for NO_3^- and NO_2^- reduction when compared to the pure component metals.

Casella *et al.*[103] studied the electrochemical behaviour of copper-thallium films on glassy carbon in 10 mM NaOH solutions, for a potential range between 0.0 and -1.4 V *vs* SCE. The binary film $Cu_{45}Tl_{55}$ exhibited a higher electrocatalytic activity for the reduction of NO_3^- and NO_2^- than copper and thallium alone. The presence of Tl causes a marked increase of the roughness factor accompanied by a favourable adsorption process of reactant molecules, with subsequent increase of the catalytic response.

A better voltammetric response for Cu-Ni alloys when compared to the responses at pure Cu and Ni electrodes was reported by Simpson *et al.*[107]. This effect was attributed to the synergism of the two different metal sites at the alloy surface. It was suggested that adsorbed H-atoms are generated by cathodic discharge of H^+ at Ni-sites, whereas adsorption of NO_3^- occurs at Cu-sites. The number of electrons involved in the reduction seems to depend on the composition of the alloy, with NH_3 or NH_2OH being the two major products.

A positive synergetic effect was also observed with Pd-Sn electrodes for NO_3^- reduction in slightly acidic solutions[109]. Different compositions were studied and the best electrocatalytic performance was obtained for $Pd_{33}Sn_{67}$ (Pd:Sn chemical composition determined by XPS analysis). Based on their experimental results, the authors suggest that the tin metal induces a significant increase of the catalytic performance by avoiding the massive hydrogen adsorption characteristic of palladium and also by a beneficial

interaction with the oxygen atoms of the nitrate species, which facilitates the dissociation reaction.

1.5.2- Modified electrodes

The modification of a copper electrode for the electrochemical detection of nitrate and nitrite was carried out by Davis *et al.*[76]. In this work a high surface area copper structure was deposited on a copper electrode by fixed potential electrolysis in a solution consisting of 0.05 M $CuSO_4$ and 0.1 M Na_2SO_4, which was adjusted to pH 3 with 0.1 M HCl. This approach is very similar to the one reported before by Carpenter and Pletcher[75]. The main difference is that the deposition was not carried out *in situ* and the electrode was transferred between solutions after deposition. The authors reported a significant improvement in the response comparing with a bare Cu electrode and also the presence of two distinct peaks for NO_3^- and NO_2^- reduction, in contrast with previous studies on copper where the reduction of NO_2^- was found to occur at similar or more negative potential values[75, 77, 118].

Carbon cloths with and without a 30% Rh coated on the surface (1 $\mu g\ cm^{-1}$) were used in cyclic voltammetric studies, in aqueous solutions containing 1mM $NaNO_3$[81]. It was observed that for Rh loaded electrodes there is a 20 to 50% current enhancement (depending on potential) comparing with the unloaded carbon electrodes.

De and co-workers[99, 100] have shown that the surface modification of carbon fibers by electrodeposition of iridium can improve significantly the electrochemical reduction of nitrates and nitrites in a neutral pH solution. In the presence of the metal, the current densities increase and the reduction of both anions occurs at a potential ~ 0.5 V more positive than at plain carbon fiber electrodes. It was determined that the adsorption of nitrogen dioxide on the electrode surface is the rate limiting step and the authors suggest that hydrogen adsorbed on the electrode surface and a product of the adsorption of NO_3^- and NO_2^- ions simultaneously take part in the limiting stage of the electrochemical reaction process.

An improvement in the catalytical activity of Pt, Pd and Pt + Pd electrodes for nitrate reduction after deposition of a submonolayer of germanium on the metal surfaces was found by Gootzen *et al.*[113]. The linear relationship between the activity and the Ge coverage showed that Ge is involved in the rate determining step (reduction of nitrate to nitrite). The specific action of germanium in the system is explained on the basis of a

stronger interaction of oxygen with this metal than with Pt or Pd. According to the authors, a stronger interaction of the catalyst surface with the oxygen atom of the nitrate molecule will lead to a weakening of the N-O bond and therefore facilitate dissociation. The enhancing effect of Ge was also observed for NO_2^-, although to a lesser extent.

1.5.3- Effect of inorganic ions

The specific adsorption of different chemical species at the electrode surface during nitrate reduction has been reported several times in acid media[87-89, 96-98, 106, 108, 118, 120], but some attempts to observe similar results in alkaline media have failed[90, 102].

Dima and co-workers[87] reported a higher activity for Pt, Cu and Ag electrodes in $HClO_4$ than in H_2SO_4. For Ir, Ru, Rh, Au and Pd, however, the influence of the anion was not so large. This electrolyte effect is usually explained by the difference in adsorption strength between ClO_4^- and SO_4^{2-} ions, with the adsorption of NO_3^- being hindered by the adsorption of SO_4^{2-}. Similar results were observed by Groot *et al.*[96] for the same concentration of nitrate (0.1 M), on Pt electrodes. For higher nitrate concentrations (> 1 M), however, the reaction rate in sulphuric and perchloric acid were similar and it seems that the nitrate ions are more able to compete for the available surface sites.

Horányi *et al.*[97] compared the electrocatalytic reduction of nitric acid at platinized platinum electrodes in $HClO_4$, H_2SO_4 and HCl and showed that the supporting electrolyte exerts a significant influence on the reduction rate and on the shape of the polarization curves. Once again, the currents in H_2SO_4 are very low in comparison to those obtained in $HClO_4$ and the same explanation is given. The addition of HCl to nitric acid dissolved either in H_2SO_4 or $HClO_4$ also results in a current decrease, and significant changes can be observed even for low chloride concentrations (7×10^{-5} M) in the presence of $HClO_4$. The same effect was found later, for the reduction of HNO_3 at a rhodized gold electrode[98] and in both cases the decrease in current is attributed to the high adsorbability of Cl^- to the electrode surfaces.

The influence of iodide, bromide and chloride ions and the effect of different concentrations on the reduction of NO_3^- at a copper electrode was studied by cyclic voltammetry[120]. In the presence of I^- and Br^- the nitrate reduction peak current decreased for very small addition of these ions (1×10^{-6} M) and almost disappeared for higher concentrations (1×10^{-5} M I^- and 2.5×10^{-5} M Br^-). The influence of chloride ions

seemed more complex. At 1×10^{-5} and 1×10^{-4} M of Cl^-, the peak current decreased, but at higher concentrations (1×10^{-3} M) an opposite effect was observed, i.e. the current increased and it was even slightly higher than in the absence of halide ions. Based on these results, Radovici *et al.* suggested that chloride ions may act both as inhibitors and accelerators of the electrochemical reduction of nitrate, depending on the experimental conditions. In their work with Cu electrodes, Pletcher *et al.*[118] carried out a very similar study (the main difference being only the supporting electrolyte: perchlorate medium pH 1 instead of 0.1 M H_2SO_4) but in this case, despite working with the same concentrations of nitrate and Cl^-, only a decrease in current and a negative shift in the potential was observed with increasing halide concentration.

The effect of Cs^+, La^{3+}, Cd^{2+}, Ni^{2+}, Co^{2+}, Zn^{2+} and Ge^{4+} has been reported by Petrii and Safonova[88, 89]. La^{3+}, Cd^{2+} and Zn^{2+} were found to decrease the rate of the process, while Ni^{2+} and Ge^{4+} show a positive effect. Apparently, the accelerating mechanism effect depends on the cation, but no attempt has been made to explain it.

1.6- Objectives of This Project

The overall objective of this project was to develop electrocatalysts that allowed the selective reduction of nitrate at a high current density close to the equilibrium potential. The idea was to combine the selection of cathode material with the application of a reproducible and controllable high surface area architecture, i.e., mesoporous coatings of the electrocatalyst.

It has been reported that, in the gas phase, Cu-Pd alloys show a high activity for the reduction of nitrate by hydrogen[121-124] and surfaces with exposed Cu and Pd have also been shown to be effective cathodes[125]. Hence, Cu-Pd alloys were chosen as the target electrocatalysts.

In order to achieve the goal of studying nitrate reduction at mesoporous layers of Cu-Pd alloys, it is first clearly necessary to prepare and characterise such electrodeposits from liquid crystal media. This is a challenging goal since few bimetallic systems have been electrodeposited as mesoporous layers[66, 69] and, indeed, earlier attempts to electroplate mesoporous copper layers were unsuccessful. Therefore, it was decided to approach the goal in stages, i.e.,

(i) to confirm the electrodeposition of mesoporous palladium[63];

(ii) to investigate the electrodeposition of mesoporous copper;

(iii) to define conditions where uniform layers of Cu-Pd alloys of known composition could be electroplated;

(iv) to electrodeposit mesoporous Cu-Pd layers.

Each stage required the definition of suitable electroplating media, the study of the voltammetry of the baths and the characterisation of the materials produced. In addition, a better understanding of the surface electrochemistry of the materials was also required before the mechanism of nitrate reduction could be considered. Not surprisingly, some difficulties were encountered and, indeed, the final stage could not be achieved within the allowed timescale. This thesis, however, reports interesting data from the steps along the way.

We were also aware that the number of electrons involved in the reduction of nitrate depends on the concentration of nitrate and the availability of proton donors, as well as the cathode material. Indeed, the nitrate reduction reaction itself can lead to strong pH changes at the cathode surface and effective buffering is essential if conditions (and therefore mechanism and/ or products) are not to change during the timescale of the experiment. Hence, the experiments are generally restricted to one concentration of nitrate, 30 mM, and to either strongly acid or strongly alkaline solutions.

1.7- References

[1] A. M. Couper, D. Pletcher, F. C. Walsh, *Chem. Rev.* **1990**, *90*, 837.

[2] L. A. Kibler, *ChemPhysChem* **2006**, *7*, 985.

[3] P. N. Ross, in *Electrocatalysis* (Eds.: J. Lipkowski, P. N. Ross), Wiley-VCH, New York, **1998**, p. 43.

[4] T. D. Jarvi, E. M. Stuve, in *Electrocatalysis* (Eds.: J. Lipkowski, P. N. Ross), Wiley-VCH, New York, **1998**, p. 75.

[5] R. Adzic, in *Electrocatalysis* (Eds.: J. Lipkowski, P. N. Ross), Wiley-VCH, New York, **1998**, p. 197.

[6] R. Parsons, *Surf. Sci* **1964**, *2*, 418.

[7] S. Trasatti, *Electrochim. Acta* **1984**, *29*, 1503.

[8] A. J. Arvia, R. C. Salvarezza, W. E. Triaca, *J. New Mat. Electrochem. Systems* **2004**, *7*, 133.

[9] W. Z. Li, C. H. Liang, J. S. Qiu, W. J. Zhou, H. M. Han, Z. B. Wei, G. Q. Sun, Q. Xin, *Carbon* **2002**, *40*, 791.

[10] P. V. Samant, C. M. Rangel, M. H. Romero, J. B. Fernandes, J. L. Figueiredo, *J. Power Sources* **2005**, *151*, 79.

[11] A. Malinauskas, *Synth. Met.* **1999**, *107*, 75.

[12] Q. Y. Chen, M. C. Granger, T. E. Lister, G. M. Swain, *J. Electrochem. Soc.* **1997**, *144*, 3806.

[13] S. Ferro, A. De Battisti, I. Duo, C. Comninellis, W. Haenni, A. Perret, *J. Electrochem. Soc.* **2000**, *147*, 2614.

[14] G. Sine, I. Duo, B. El Roustom, G. Foti, C. Comninellis, *J. Appl. Electrochem.* **2006**, *36*, 847.

[15] R. Schuster, G. Ertl, in *Catalysis and Electrocatalysis at Nanoparticle Surfaces* (Eds.: A. Wieckowski, E. R. Savinova, C. G. Vayenas), Marcel Dekker, Inc., New York, **2003**, p. 211.

[16] H. Bonnemann, R. Richards, in *Catalysis and Electrocatalysis at Nanoparticle Surfaces* (Eds.: A. Wieckowski, E. R. Savinova, C. G. Vayenas), Marcel Dekker, Inc., New York, **2003**, p. 343.

[17] S. Guerin, B. E. Hayden, D. Pletcher, M. E. Rendall, J. P. Suchsland, L. J. Williams, *J. Comb. Chem.* **2006**, *8*, 791.

[18] B. E. Hayden, in *Catalysis and Electrocatalysis at Nanoparticle Surfaces* (Eds.: A. Wieckowski, E. R. Savinova, C. G. Vayenas), Marcel Dekker, Inc., New York, **2003**, p. 171.

[19] D. R. Rolison, *Science* **2003**, *299*, 1698.

[20] T. Toda, H. Igarashi, H. Uchida, M. Watanabe, *J. Electrochem Soc.* **1999**, *146*, 3750.

[21] V. Stamenkovic, T. J. Schmidt, P. N. Ross, N. M. Markovic, *J. Electroanal. Chem.* **2003**, *554-555*, 191.

[22] V. R. Stamenkovic, B. S. Mun, K. J. J. Mayrhofer, P. N. Ross, N. M. Markovic, *J. Am. Chem. Soc.* **2006**, *128*, 8813.

[23] J. S. Rebello, P. V. Samant, J. L. Figueiredo, J. B. Fernandes, *J. Power Sources* **2006**, *153*, 36.

[24] C. Iwakura, N. Furukawa, M. Tanaka, *Electrochim. Acta* **1992**, *37*, 757.

[25] S. H. Jordanov, P. Paunovic, O. Popovski, A. Dimitrov, D. Slavkov, *Bull. Chem. Technol. Macedonia* **2004**, *23*, 101.

[26] D. Landolt, *J. Electrochem Soc.* **2002**, *149*, S9.

[27] J. A. Switzer, *Interface* **1998**, 1.

[28] D. Bera, S. C. Kuiry, S. Seal, *JOM* **2004**, *56*, 49.

[29] G. S. Attard, P. N. Bartlett, N. R. B. Coleman, J. M. Elliott, J. R. Owen, J. H. Wang, *Science* **1997**, *278*, 838.

[30] E. C. Walter, B. J. Murray, F. Favier, G. Kaltenpoth, M. Grunze, R. M. Penner, *J. Phys. Chem. B* **2002**, *106*, 11407.

[31] E. C. Walter, M. P. Zach, F. Favier, B. J. Murray, K. Inazu, J. C. Hemminger, R. M. Penner, *Chemphyschem* **2003**, *4*, 131.

[32] R. M. Penner, C. R. Martin, *Anal. Chem.* **1987**, *59*, 2625.

[33] G. Yi, W. Schwarzacher, *Appl. Phys. Lett.* **1999**, *74*, 1746.

[34] P. N. Bartlett, P. R. Birkin, M. A. Ghanem, *Chem. Commun.* **2000**, 1671.

[35] M. Paunovic, M. Schlesinger, *Fundamentals of Electrochemical Deposition*, 2nd ed., John Wiley & Sons, New York, **2006**.

[36] M. Schlesinger, M. Paunovic, *Modern Electroplating*, 4th ed., John Wiley & Sons, New York, **2000**.

[37] A. Brenner, *Electrodeposition of Alloys, Vol. I and II*, Academic Press, New York, **1963**.

[38] D. R. Gabe, *J. Appl. Electrochem.* **1997**, *27*, 908.

[39] J. W. Dini, in *Modern Electroplating*, 4th ed. (Eds.: M. Schlesinger, M. Paunovic), John Wiley & Sons, New York, **2000**, p. 61.

[40] J. A. Abys, C. A. Dullaghan, in *Modern Electroplating* (Eds.: M. Schlesinger, M. Paunovic), John Wiley & Sons, New York, **2000**, p. 483.

[41] S. N. Vinogradov, G. N. Mal'tseva, N. A. Gulyaeva, *Russ. J. Electrochem.* **2001**, *37*, 715.

[42] D. L. Lu, M. Ichihara, K. Tanaka, *Electrochim. Acta* **1998**, *43*, 2325.

[43] C. C. Yang, A. S. Kumar, M. C. Kuo, S. H. Chien, J. M. Zen, *Analytica Chimica Acta* **2005**, *554*, 66.

[44] M. Hansen, K. Anderko, *Constitution of Binary Alloys*, McGraw Hill, **1958**.

[45] K. Stulik, C. Amatore, K. Holub, V. Marecek, W. Kutner, *Pure Appl. Chem.* **2000**, *72*, 1483.

[46] D. Pletcher, in *Microelectrodes: Theory and Applications, Vol. 197* (Eds.: M. I. Montenegro, M. A. Queiros, J. L. Daschbach), Kluwer Academic Publishers, Dordrecht, **1991**, p. 463.

[47] R. Greef, R. Peat, L. M. Peter, D. Pletcher, J. Robinson, *Instrumental Methods in Electrochemistry*, Ellis Horwood, Chichester, **1993**.

[48] C. E. Fairhurst, S. Fuller, J. Gray, M. C. Holmes, G. J. T. Tiddy, in *Handbook of Liquid Crystals - High Molecular Weight Liquid Crystals, Vol. 3* (Eds.: D. Demus, J. W. Goodby, G. W. Gray, H. W. Spiess, V. Vill), Wiley-VCH, New York, **1998**, pp. 341.

[49] G. Burducea, *Rom. Repts. Phys.* **2004**, *56*, 66.

[50] D. J. Mitchell, G. J. T. Tiddy, L. Waring, T. Bostock, M. P. McDonald, *J. Chem. Soc., Faraday Trans. 1* **1983**, *79*, 975.

[51] P. J. Collings, M. Hird, *Introduction to Liquid Crystals*, Taylor & Francis Ltd, London, **1998**.

[52] C. T. Kresge, M. E. Leonowicz, W. J. Roth, J. C. Vartuli, J. S. Beck, *Nature* **1992**, *359*, 710.

[53] J. S. Beck, J. C. Vartuli, W. J. Roth, M. E. Leonowicz, C. T. Kresge, K. D. Schmitt, C. T. W. Chu, D. H. Olson, E. W. Sheppard, S. B. McCullen, J. B. Higgins, J. L. Schlenker, *J. Am. Chem. Soc.* **1992**, *114*, 10834.

[54] A. Monnier, F. Schuth, Q. Huo, D. Kumar, D. Margolese, R. S. Maxwell, G. D. Stucky, M. Krishnamurty, P. Petroff, A. Firouzi, M. Janicke, B. F. Chmelka, *Science* **1993**, *261*, 1299.

[55] C. F. Cheng, Z. H. Luan, J. Klinowski, *Langmuir* **1995**, *11*, 2815.

[56] G. S. Attard, J. C. Glyde, C. G. Goltner, *Nature* **1995**, *378*, 366.

[57] L. M. Huang, H. T. Wang, Z. B. Wang, A. Mitra, K. N. Bozhilov, Y. S. Yan, *Adv. Mater.* **2002**, *14*, 61.

[58] P. N. Bartllet, *Interface* **2004**, *13*, 28.

[59] J. M. Elliott, G. S. Attard, P. N. Bartlett, N. R. B. Coleman, D. A. S. Merckel, J. R. Owen, *Chem. Mater.* **1999**, *11*, 3602.

[60] J. M. Elliott, P. R. Birkin, P. N. Bartlett, G. S. Attard, *Langmuir* **1999**, *15*, 7411.

[61] P. N. Bartlett, P. N. Birkin, M. A. Ghanem, P. de Groot, M. Sawicki, *J. Electrochem. Soc.* **2001**, *148*, C119.

[62] P. A. Nelson, J. M. Elliott, G. S. Attard, J. R. Owen, *Chem. Mater.* **2002**, *14*, 524.

[63] P. N. Bartlett, B. Gollas, S. Guerin, J. Marwan, *Phys. Chem. Chem. Phys.* **2002**, *4*, 3835.

[64] P. N. Bartlett, J. Marwan, *Microporous and Mesoporous Materials* **2003**, *62*, 73.

[65] A. H. Whitehead, J. M. Elliott, J. R. Owen, G. S. Attard, *Chem. Commun.* **1999**, 331.

[66] S. Guerin, G. S. Attard, *Electrochem. Commun.* **2001**, *3*, 544.

[67] I. Nandhakumar, J. M. Elliott, G. S. Attard, *Chem. Mater.* **2001**, *13*, 3840.

[68] H. M. Luo, J. F. Zhang, Y. S. Yan, *Chem. Mater.* **2003**, *15*, 3769.

[69] X. Li, I. Nandhakumar, T. Gabriel, G. Attard, M. Markham, D. Smith, J. Baumberg, K. Govender, P. O'Brien, D. Smyth-Boyle, *J. Mater. Chem.* **2006**, *16*, 3207.

[70] P. N. Bartlett, S. Guerin, *Anal. Chem.* **2003**, *75*, 126.

[71] T. Imokawa, K. J. Williams, G. Denuault, *Anal. Chem.* **2006**, *78*, 265.

[72] A. Kapoor, T. Viraraghavan, *J. Envir. Technol.* **1997**, 371.

[73] J. C. Fanning, *Coord. Chem. Rev.* **2000**, *199*, 159.

[74] W. J. Plieth, in *Encyclopedia of Electrochemistry of the Elements, Vol. VIII* (Ed.: A. J. Bard), Marcel Dekker, Inc., New York, **1973**, p. 321.

[75] N. G. Carpenter, D. Pletcher, *Anal. Chim. Acta* **1995**, *317*, 287.

[76] J. Davis, M. J. Moorcroft, S. J. Wilkins, R. G. Compton, M. F. Cardosi, *Analyst* **2000**, *125*, 737.

[77] S. Ward-Jones, C. E. Banks, A. O. Simm, L. Jiang, R. G. Compton, *Electroanalysis* **2005**, *17*, 1806.

[78] M. J. Moorcroft, J. Davis, R. G. Compton, *Talanta* **2001**, *54*, 785.

[79] J. O. Bockris, J. Kim, *J. Electrochem. Soc.* **1996**, *143*, 3801.

[80] J. O. Bockris, J. Kim, *J. Appl. Electrochem.* **1997**, *27*, 623.

[81] J. W. Peel, K. J. Reddy, B. P. Sullivan, J. M. Bowen, *Water Res.* **2003**, *37*, 2512.

[82] L. Szpyrkowicz, S. Daniele, M. Radaelli, S. Specchia, *Appl. Catal. B: Environ.* **2006**, *66*, 40.

[83] M. Paidar, I. Rousar, K. Bouzek, *J. Appl. Electrochem.* **1999**, *29*, 611.

[84] B. P. Dash, S. Chaudhari, *Water Res.* **2005**, *39*, 4065.

[85] Y. Wang, J. H. Qu, R. C. Wu, P. J. Lei, *Water Res.* **2006**, *40*, 1224.

[86] C. Milhano, D. Pletcher, in *Modern Aspects of Electrochemistry, in press.*

[87] G. E. Dima, A. C. A. de Vooys, M. T. M. Koper, *J. Electroanal. Chem.* **2003**, *554*, 15.

[88] O. A. Petrii, T. Y. Safonova, *J. Electroanal. Chem.* **1992**, *331*, 897.

[89] T. Y. Safonova, O. A. Petrii, *J. Electroanal. Chem.* **1998**, *448*, 211.

[90] G. Horanyi, E. M. Rizmayer, *J. Electroanal. Chem.* **1985**, *188*, 265.

[91] J. T. Maloy, in *Standard Potentials in Aqueous Solution* (Eds.: A. J. Bard, R. Parsons, J. Jordan), Marcel Dekker, Inc., New York, **1985**, p. 127.

[92] M. Cunha, J. D. Souza, F. Nart, *Langmuir* **2000**, *16*, 771.

[93] K. Nishimura, K. Machida, M. Enyo, *Electrochim. Acta* **1991**, *36*, 877.

[94] O. Rutten, A. Van Sandwijk, G. Van Weert, *J. Appl. Electrochem.* **1999**, *29*, 87.

[95] S. Wasmus, E. J. Vasini, M. Krausa, H. T. Mishima, W. Vielstich, *Electrochim. Acta* **1994**, *39*, 23.

[96] M. T. Groot, M. T. M. Koper, *J. Electroanal. Chem.* **2004**, *562*, 81.

[97] G. Horanyi, E. M. Rizmayer, *J. Electroanal Chem.* **1982**, *140*, 347.

[98] M. Wasberg, G. Horanyi, *Electrochim. Acta* **1995**, *40*, 615.

[99] D. De, J. D. Englehardt, E. E. Kalu, *J. Electrochem. Soc.* **2000**, *147*, 4224.

[100] D. D. De, J. D. Englehardt, E. E. Kalu, *J. Electrochem. Soc.* **2000**, *147*, 4573.

[101] O. Brylev, M. Sarrazin, D. Belanger, L. Roue, *Appl. Catal. B* **2006**, *64*, 243.

[102] A. C. A. de Vooys, R. A. van Santen, J. A. R. van Veen, *J. Mol. Catal. A* **2000**, *154*, 203.

[103] I. G. Casella, M. Gatta, *J. Electroanal. Chem.* **2004**, *568*, 183.

[104] P. M. Tucker, M. J. Waite, B. E. Hayden, *J. Appl. Electrochem.* **2004**, *34*, 781.

[105] X. K. Xing, D. A. Scherson, C. Mak, *J. Electrochem. Soc.* **1990**, *137*, 2166.

[106] G. E. Dima, G. L. Beltramo, M. T. M. Koper, *Electrochim. Acta* **2005**, *50*, 4318.

[107] B. Simpson, D. Johnson, *Electroanalysis* **2004**, *16*, 7.

[108] K. Tada, K. Shimazu, *J. Electroanal. Chem.* **2005**, *577*, 303.

[109] I. G. Casella, M. Contursi, *J. Electroanal. Chem.* **2006**, *588*, 147.

[110] C. Polatides, G. Kyriacou, *J. Appl. Electrochem.* **2005**, *35*, 421.

[111] K. Bouzek, M. Paidar, A. Sadilkova, H. Bergmann, *J. Appl. Electrochem.* **2001**, *31*, 1185.

[112] C. Levy-Clement, N. A. Ndao, A. Katty, M. Bernard, A. Deneuville, C. Comninellis, A. Fujishima, *Diamond Relat. Mater.* **2003**, *12*, 606.

[113] J. F. E. Gootzen, P. Peeters, J. M. B. Dukers, L. Lefferts, W. Visscher, J. A. R. vanVeen, *J. Electroanal. Chem.* **1997**, *434*, 171.

[114] S. Hwang, J. Lee, J. Kwak, *J. Electroanal. Chem.* **2005**, *579*, 143.

[115] N. Chebotareva, T. Nyokong, *J. Appl. Electrochem.* **1997**, *27*, 975.

[116] R. Prasad, A. Kumar, *J. Electroanal. Chem.* **2005**, *576*, 295.

[117] T. Hiratsu, S. Suzuki, K. Yamaguchi, *Chem. Comm.* **2005**, 4534.

[118] D. Pletcher, Z. Poorabedi, *Electrochim. Acta* **1979**, *24*, 1253.

[119] S. Cattarin, *J. Appl. Electrochem.* **1992**, *22*, 1077.

[120] O. Radovici, G. E. Badea, T. Badea, *Rev. Roum. Chim.* **2003**, *48*, 591.

[121] F. Deganello, L. F. Liotta, A. Macaluso, A. M. Venezia, G. Deganello, *Appl. Catal. B* **2000**, *24*, 265.

[122] Y. Yoshinaga, T. Akita, I. Mikami, T. Okuhara, *J. Catal.* **2002**, *207*, 37.

[123] M. Chollier-Brym, R. Gavagnin, G. Strukul, M. Marella, M. Tomaselli, P. Ruiz, *Catal. Today* **2002**, *75*, 49.

[124] A. Pintar, *Catal. Today* **2003**, *77*, 451.

[125] Y. Wang, J. H. Qu, H. J. Liu, *Chin. Chem. Lett.* **2006**, *17*, 61.

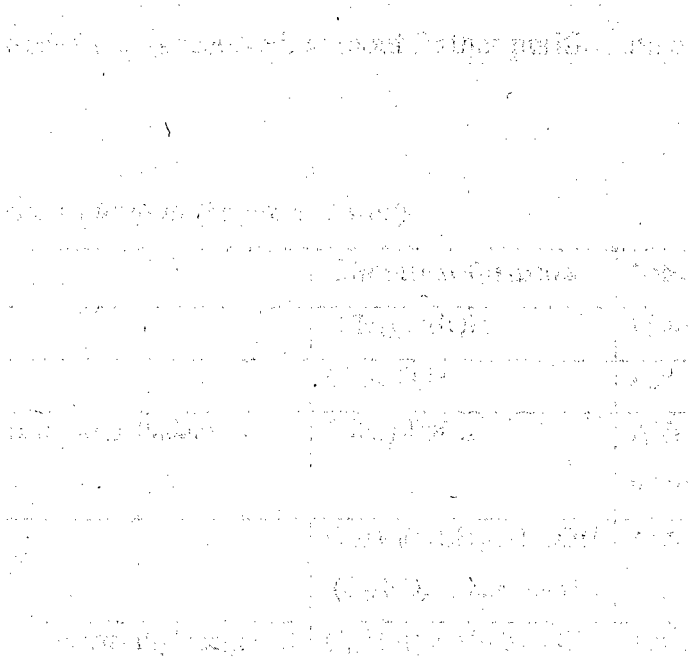

Chapter 2- Experimental

Throughout the course of this research, a range of chemicals, electrode materials and electrical equipment have been used. A summary of these materials and equipment is presented here, followed by the procedures carried out for the preparation and characterisation of Pd, Cu and Cu-Pd films deposited from the hexagonal (H_1) lyotropic liquid crystalline phase of $C_{16}EO_8$ and from non-templating solutions.

2.1- Chemicals and Solutions

All chemicals were used as received, without further purification and are listed in Table 2.1.

Table 2.1 *Chemicals used in the present study.*

Name	Chemical formula	Manufacturer/ grade
2-Propanol	$(CH_3)_2CHOH$	Fisher/ laboratory grade
Acetic acid	CH_3CO_2H	Fisher/ reagent ACS
Ammonium tetrachloropalladate	$(NH_4)_2PdCl_4$	Alfa Aesar/ Premion®, 99.998%
Brij® 56	$C_{16}H_{33}(OCH_2CH_2)_nOH$ ($C_{16}EO_n$, where n~10)	Aldrich
$C_{16}EO_8$ (Octaethyleneglycol monohexadecyl ether)	$C_{16}H_{33}(OCH_2CH_2)_8OH$	Jan Dekker
Copper(II) sulphate pentahydrate	$CuSO_4.5H_2O$	BDH/AnalaR®
Cupric carbonate	$CuCO_3.Cu(OH)_2.H_2O$	BDH/ laboratory reagent
Heptane	$CH_3(CH_2)_5CH_3$	Aldrich/ 99%
Lead(II) carbonate	$PbCO_3$	BDH

Mercury	Hg	Aldrich/ 99.99+ %
Mercury(I) chloride	Hg_2Cl_2	Aldrich/ 99.5+ %
Mercury(I) sulphate	Hg_2SO_4	Aldrich/ 99%
Methanesulfonic acid 70 wt %	CH_3SO_3H	Sigma-Aldrich
Nitric acid 70%	HNO_3	Fisher/ reagent ACS
Palladium(II) acetate	$Pd(CH_3CO_2)_2$	Sigma-Aldrich/ 99.9+ %
Palladium(II) nitrate dihydrate	$Pd(NO_3)_2.2H_2O$	Fluka
Palladium(II) sulphate dihydrate	$PdSO_4.2H_2O$	Alfa Aesar/ 99%
Perchloric acid 60%	$HClO_4$	Fisher/ laboratory grade
Perchloric acid double distilled 70%	$HClO_4$	GFS chemicals
Potassium chloride	KCl	Fisher/ analytical reagent
Potassium sulphate	K_2SO_4	BDH/ AnalaR®
Sodium carbonate	Na_2CO_3	BDH/ AnalaR®
Sodium hydrogen carbonate	$NaHCO_3$	Aldrich/ 99%
Sodium hydroxide	NaOH	Fisher/ laboratory grade
Sodium nitrate	$NaNO_3$	Fisons/ analytical reagent
Sodium nitrite	$NaNO_2$	BDH/ AnalaR®
Sodium sulphide	Na_2S	Aldrich/ 99.99+ %
Sulphuric acid	H_2SO_4	BDH/ ARISTAR®

Aqueous solutions were prepared using deionised water from a Whatman Analyst Water Purifier system. Glassware was soaked in a 5% solution of Decon 90 (Decon Laboratories Limited) and subsequent rinsing with deionised water before use.

2.2- Electrochemical Measurements

2.2.1- Electrode materials

A series of both macroelectrodes and microelectrodes (disc geometry) of different materials were used and a brief description of the different electrodes is made in the following sections.

2.2.1.1- Microelectrodes

Platinum (d = 10 and 25 μm) and gold microdiscs (d = 60 μm) were fabricated by sealing the respective wires in soda glass and were all manufactured at the Glassblowing Workshop, School of Chemistry, University of Southampton.

Palladium microdiscs were made by sealing a short length of the palladium wire (d = 25 μm, Goodfellow, 99.9%) into a soda glass pipette using a butane and propane mix flame. The sealed end of the pipette was then inserted into a heating coil, which caused the glass to melt and to collapse around the microwire, while vacuum was applied at the other end of the pipette. The coil was moved slowly until about 5 mm of the microwire was left exposed inside the pipette. After the vacuum line was opened, the pipette was left to cool for about 5 minutes. The electrical contact between the Pd microwire and a copper wire was made by inserting finely cut indium into the open end of the pipette and heating with a hot air gun until the indium melted. A copper wire was then inserted into the molten indium and pressed to ensure a good contact. The open end of the pipette was finally closed with quick set epoxy resin (RS) to fix the copper wire.

Copper microdiscs were made by sealing the copper wire (d = 50 μm, Goodfellow, 99.9%) into epoxy resin (Struers). Electrical contact was made between the microwire and a copper wire using silver conductive paint (RS).

All microelectrodes were short enough to put inside the SEM and to look at the disc/ film surface before/ after the metal deposition. The diameters of the different microdiscs were confirmed by SEM.

2.2.1.2- Macroelectrodes

Throughout this work, most experiments were carried out with microelectrodes, but copper macroelectrodes were also used for some of the experiments. Copper working electrodes were fabricated by sealing a small rod of copper (d = 3.1 mm, Aldrich, 99.999%,) into epoxy resin (Struers). Electrical contact was made onto the back of the electrode material with a copper wire attached by spot welding.

2.2.1.3- Cleaning of micro and macroelectrodes

All new microelectrodes and macroelectrodes were firstly polished on successively finer grades of abrasive paper (from P600 to P1200, Deer) and after with alumina/ water slurries (alumina: 1.0, 0.3 and 0.05 μm) supported on polishing cloth (all from BUEHLER). Finally, they were washed with water to remove the remaining alumina

powder and dried. Once new electrodes had undergone this initial polishing treatment, polishing with only alumina/ water slurries was sufficient for subsequent experiments.

2.2.1.4- Electrodes for TEM and XRD experiments

For transmission electron microscopy (TEM) and x-ray diffraction (XRD) analysis most part of the films were deposited onto thin film gold electrodes made by evaporation of gold onto chromium-coated glass slides. Some films were also deposited on indium tin oxide (ITO) coated aluminosilicate glass slides (Delta Technologies Ltd, surface resistivity 4-8 Ω). All electrodes were cleaned in an ultrasonic bath of 2-propanol for 30 minutes prior to deposition, then rinsed with deionised water and dried under ambient conditions.

2.2.2- Reference electrodes

2.2.2.1- Saturated mercury/ mercurous sulphate electrode (SMSE)

A Hg/ Hg_2SO_4, K_2SO_4 (saturated) reference electrode was used in some experiments to prevent Cl^- ion contamination into the test solutions. The electrode was a combination of two glass bodies, see Figure 2.1: (a) a glass tube with one closed end through which a

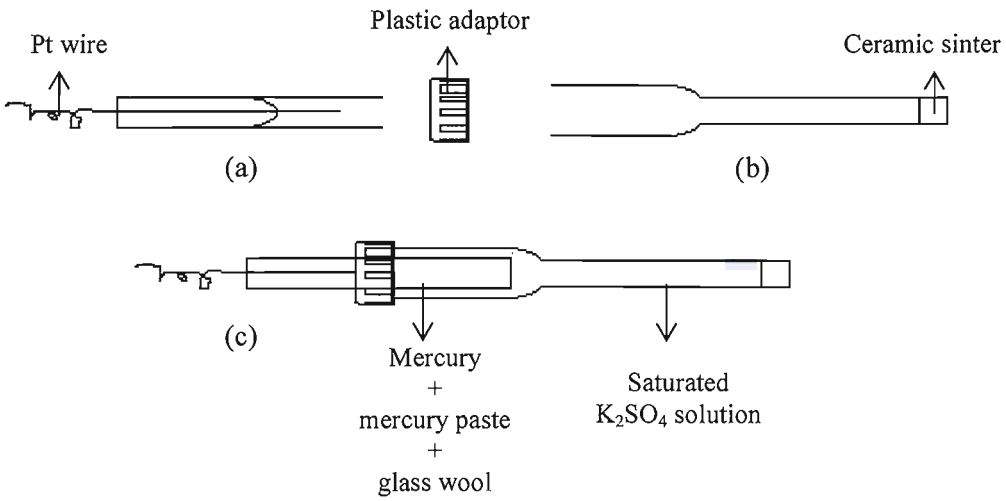

Figure 2.1 *Schematic representation of a reference electrode. (a) Glass tube with sealed Pt wire, (b) glass pipette with sinter and (c) final assembly of the two glass bodies with a plastic connector.*

platinum wire was sealed and (b) a pipette with a sinter at the tip. Drops of mercury were placed into the glass tube until the platinum wire was covered. A paste comprising of K_2SO_4/ Hg_2SO_4 (1/1) mixture and a few drops of saturated K_2SO_4 solution was then placed onto the mercury layer and carefully pressed with a wood stick. Glass wool was inserted into the tube to hold the mercury and the paste in place. The glass tube was then inserted in the glass pipette filled with a saturated K_2SO_4 solution and the two glass bodies were hold together with a plastic adaptor.

The SMSE was stored in saturated K_2SO_4 solution and rinsed with deionised water before use.

2.2.2.2- Saturated calomel electrode (SCE)

A Hg/Hg_2Cl_2, KCl (saturated) electrode was also used as reference electrode in some experiments. The preparation procedure was the same as for the SMSE, except that Hg_2SO_4 was replaced by Hg_2Cl_2 and K_2SO_4 by KCl. The SCE was stored in saturated KCl solution and rinsed with deionised water before use.

2.2.3- Electrochemical cells

Experiments at microelectrodes were undertaken using a two-electrode system, where the reference electrode (either SMSE or SCE) served also as a counter electrode, in a three necked pear-shaped cell. The same type of cell was used for experiments at macroelectrodes but, in this case, with a large surface area Pt mesh working as a counter electrode.

In all experiments carried out with microelectrodes the cell was placed in an aluminium Faraday cage to minimise electrical noise.

The voltammetry was carried out at room temperature, after the solutions had been thoroughly deoxygenated with a stream of oxygen-free nitrogen (BOC GASES). Unless otherwise stated, a stream of nitrogen was always kept above the solution during experiments.

2.2.4- Instrumentation

For most part of the experiments, the potential of the working electrode and the current were recorded using a laboratory built potentiostat (data acquired with NI PCI-6025E card, and the software was developed by D. G. Offin).

The depositions on evaporated gold substrate and on ITO were carried out with a Princeton Applied Research potentiostat/galvanostat (model 263A, equipped with Electrochemistry PowerSuite software for data analysis).

2.3- Electrodeposition of Cu, Pd and Cu-Pd Films from the Hexagonal Mesophase of $C_{16}EO_8$

2.3.1- Preparation of liquid crystalline templating mixtures

2.3.1.1- Palladium templating mixture

The palladium templating mixture followed the composition and procedure described by Bartlett *et al.*[1]. The plating mixture consisted of 12 wt% $(NH_4)_2PdCl_4$, 48 wt% surfactant (Brij® 56 or $C_{16}EO_8$) and 40 wt% deionised water (when indicated in the thesis, the plating mixture also contained 2 wt% heptane). Water and $(NH_4)_2PdCl_4$ were first put in a glass vial and taken to an ultrasonic bath for ~ 10 minutes to ensure completely dissolution of the palladium salt. The surfactant was then added and the mixture was stirred thoroughly for around 5 minutes using a glass rod. To ensure the homogeneity of the viscous mixture, it was heated to 35 °C using a Grant W14 thermostatic water bath and stirred for another 5 minutes until a uniform brown colour was observed. Finally, the plating mixture was allowed to equilibrate at 25 °C for 2 hours before the deposition was carried out.

2.3.1.2- Copper and copper-palladium templating mixtures

Unlike the templating mixture used for the deposition of mesoporous palladium, which is now well established among the Southampton Electrochemistry Group, no successful templating mixture has been reported so far for the electrodeposition of mesoporous copper, or for the deposition of mesoporous copper-palladium films. As a result, a significant amount of work was carried out studying different mixtures and different

compositions to choose the right conditions for the preparation of a suitable plating mixture for each case.

Several copper, palladium and copper-palladium solutions without surfactant were also studied to help to understand the complex electrochemical behaviour observed in some of the templating mixtures.

All the copper templating mixtures prepared are described in detail in Chapter 4 and Chapter 5 reports the studies carried out for the copper-palladium mixtures. In general, the procedure used for their preparation was similar to the one described in the previous section for the palladium templating mixture.

2.3.2- Characterisation of liquid crystalline templating mixtures

For all the templating mixtures the presence of the hexagonal phase was confirmed using a polarizing microscope (Olympus BH2) equipped with a Linkam TMS 90 heating/ cooling stage. Here, thin films of the liquid crystals were prepared by sandwiching the mixture between a glass microscope slide and a cover slip. The hexagonal phase was identified based on its optical texture, which consists of non-uniform light and dark areas and by the presence of air bubbles with an irregular shape due to the viscosity of the mixture. The optical micrographs of the liquid crystalline phases shown in the following chapters were taken with a 10× magnification objective (DPlan Olympus) and the observed features are in the order of micrometers.

The plating mixtures were also studied by low angle X-ray diffraction using a Siemens D5000 diffractometer (CuK_α radiation) with a scan rate of 6° min^{-1}. To record the diffraction pattern, a small amount of the plating mixture was put on a Perspex sample holder and smoothed with a glass microscope slide until a homogeneous film was obtained. To avoid drying of the mixture by the laser beam, the diffraction patterns were acquired only for a short period of time (~10 minutes).

2.3.3- The electrodeposition process

The following sections describe the general procedures for deposition of Pd, Cu and Cu-Pd films from the hexagonal mesophase of $C_{16}EO_8$, but several films were also deposited without the presence of surfactant. The studies carried out with these non-templated films will be mentioned in more detail in the next chapters.

In this thesis, the thickness of the electroplated layers were estimated either from the charge passed using Faraday's law or by observing the edge of the deposit using the SEM. Neither is precise. The Faraday's law calculation assumes that the deposition is 100% efficient. Moreover, in the case of the nanoporous deposits allowance should be made for the volume of the pores. This is, however, dependent on the knowledge of the exact deposit structure. Although the SEM measurement is an accurate measure of the thickness of the deposit at the edge, it is known that the current distribution to a microdisc is non-uniform and the flux to the perimeter is high compared to the centre of the disc. Indeed, the deposit at the edge could sometimes be seen to be thicker.

2.3.3.1- Electrodeposition of Pd films

The mesoporous Pd films used for electrochemical characterisation and for nitrate and nitrite reduction were deposited on Pt microdisc electrodes (d = 10 and 25 μm), at 25 °C, using a two-electrode configuration in a glass vial, with a SCE as reference/ counter electrode.

Before the film deposition, the platinum microdisc electrodes were polished with alumina/ water slurries as described before, rinsed well with water and then potential cycled in 1 M H_2SO_4, at 100 mV s^{-1}, between -0.65 and +0.6 V *vs* SMSE until a stable voltammogram, with the classical features for hydrogen adsorption/desorption and oxide formation/ reduction at polycrystalline Pt[2], was observed, see Figure 2.1.

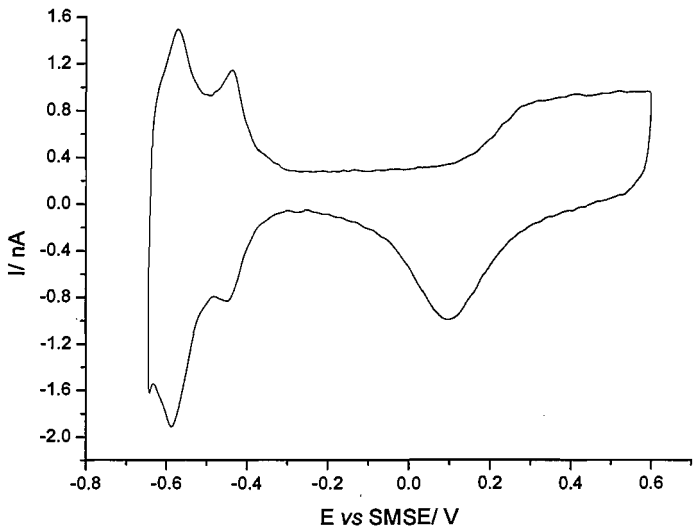

Figure 2.1 *A typical cyclic voltammogram for a Pt microdisc (d = 25 μm) in 1 M* H_2SO_4, $v = 100\ mV\ s^{-1}$.

After cycling in acid, the Pt microdiscs were rinsed with deionised water, dried, and placed in the plating mixture. For the electrodeposition, the potential was stepped from + 0.3 to + 0.1 V *vs* SCE and then kept constant until the desired charge had passed (usually between 0.42 and 3.80 C cm^{-2}) in order to deposit layers with a thickness in the range 0.2 -2 μm.

Films grown for transmission electron microscopy (TEM) and x-ray diffraction (XRD) analysis were deposited onto thin film gold electrodes under the same potentiostatic regime described above. However, in this case, a three-electrode configuration was applied, with the plating mixture sandwiched between the gold electrode, a platinum mesh working as counter electrode and a SCE as reference.

After deposition, the working electrodes were washed thoroughly with water to remove the excess of surfactant and finally soaked in water for at least 3 hours to remove the remaining surfactant from the surface and from within the pores. The films deposited onto thin film gold substrate were usually soaked for a longer period of 24 h.

2.3.3.2- Electrodeposition of Cu films

Copper films from the hexagonal mesophase of $C_{16}EO_8$ were deposited onto Pt (d = 25 μm) and Au (d = 60 μm) microdisc electrodes, using the same set up as described before for mesoporous Pd films.

Before the film deposition, the microdisc electrodes were polished with alumina/ water slurries, rinsed well with water, dried, and placed in the plating mixture.

Initially, to optimize the quality of the Cu films, several depositions were carried out at different potentials (the effect of deposition potential will be discussed later in Chapter 4) and using different charge densities. After these preliminary results, the following depositions were carried out stepping the potential from -0.2 to -0.5 V *vs* SMSE and keeping the potential constant until the desired charge was passed (usually between 0.81 and 4.1 C cm^{-2}) in order to deposit layers with a thickness in the range 0.3 – 1.5 μm.

Copper films for transmission electron microscopy (TEM) and x-ray diffraction (XRD) analysis were deposited onto thin film gold electrodes and onto ITO-coated glass under the same potentiostatic regime described above and using the same set up as for Pd deposition, but with a SMSE as reference electrode. Some depositions were also carried out at constant current.

2.3.3.3- Electrodeposition of Cu-Pd films

Copper-palladium films from the hexagonal mesophase of $C_{16}EO_8$ were deposited on Pt (d = 25 μm) and Au (d = 60 μm) microdisc electrodes, using the same set up as described before for Pd and Cu films.

Before the film deposition, the microdisc electrodes were polished with alumina/ water slurries, rinsed well with water, dried, and placed in the plating mixture.

As with Cu films, some preliminary results were carried out to optimize the deposition conditions and this will be discussed in detail in Chapter 5. The Cu-Pd films were deposited at different potentials in order to obtain deposits with different Cu:Pd ratios. As before, the potential was held constant until the desired charge was passed (usually between 0.81 and 4.1 C cm^{-2}).

Cu-Pd films for transmission electron microscopy (TEM) and x-ray diffraction (XRD) analysis were deposited onto thin film gold electrodes under the same potentiostatic regime described above and using the same set up as for Cu deposition.

2.4- Morphological and Structural Characterisation of Pd, Cu and Cu-Pd Films

SEM images of the different films were obtained in "wet mode" either with a Back Scattered Electron (BSE) or a Gaseous Secondary Electron (GSE) detector, using an environmental scanning electron microscope (XL30 ESEM, Philips). Optimum combination of accelerating voltage, spot size and vapour pressure were selected for each scanning electron micrograph.

Unless otherwise stated, the top view micrographs of the deposits were obtained with the sample at 0° to the beam and the side views with the sample at 65.5°, see Figure 2.2. In this last case, the thickness of the films given by the SEM (t_{SEM}) was corrected to the real value (t_{real}) using Equation 2.1. When appropriate, comparison will be made with the thickness value given by Faraday's Law, which will be mentioned as $t_{Faraday}$.

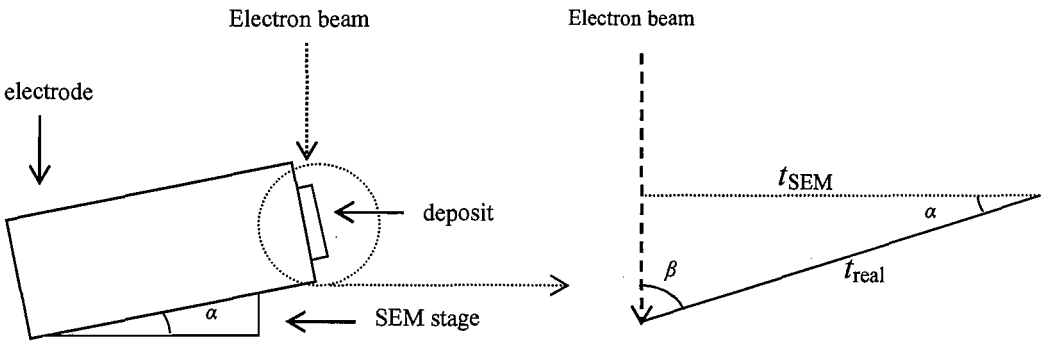

Figure 2.2 *Scheme of the SEM configuration used to obtain side micrographs of the metallic films deposited onto microdiscs.*

$$t_{real} = \frac{t_{SEM}}{\sin 65.5°} \qquad (2.1)$$

The composition of the different films was obtained by EDX (Energy Dispersive X-ray) analysis in different places over the surface. In EDX analysis, the volume of the specimen which is penetrated by electrons (the interaction volume) and the volume of the specimen from which the detected X-rays are generated (the sampling volume) are in the order of few μm^3[3]. The specific volume value depends on (i) the energy of the electron beam, (ii) the energy (wavelength) of the X-ray being studied and (c) the atomic weight of the specimen. No attempt has been made in this work to determine the sampling volume, but the atomic percentages shown in the following chapters are certainly representative of the bulk composition of the analyzed films.

The mesoporous structure of the films was investigated using a JEOL 3010 transmission electron microscope (TEM). Samples were prepared by scraping particles from the films supported on gold substrate into carbon coated Cu or carbon coated Au TEM grids.

Both low angle and wide angle X-ray diffraction spectra were collected using the X-ray diffractometer described in 2.3.2. Unless otherwise stated, the low angle X-ray diffraction was carried out at 6° min^{-1}, for around 1 hour, and the wide angle X-ray spectra were collected for 14 h, at a slower scan rate.

2.5- References

[1] P. N. Bartlett, B. Gollas, S. Guerin, J. Marwan, *Phys. Chem. Chem. Phys.* **2002**, *4*, 3835.

[2] H. Angerstein-Kozlowska, in *Comprehensive Treatise of Electrochemistry, Vol. 9* (Ed.: J. O. M. B. E. Yeager, B.E. Conway, S. Sarangapani), Plenum Press, New York, **1984**, p. 15.

[3] P. Goodhew, J. Humphreys, R. Beanland, *Electron Microscopy and Analysis*, 3rd ed., Taylor & Francis, London, **2001**.

Chapter 3- Mesoporous Palladium Films

3.1- Preparation and Characterisation of the Palladium Templating Mixture

In some preliminary studies, the palladium templating mixture used for the deposition of mesoporous palladium films followed the composition described before by Bartlett *et al.*[1], using the hexagonal (H_1) lyotropic liquid crystalline phase of Brij® 56 or $C_{16}EO_8$ and adding 2 wt% heptane to the mixture. Previous studies carried out with mesoporous platinum showed that the presence of heptane increases the diameter of the pores[2], but in the present work no significant changes were found in the voltammetric response of films obtained from plating mixtures with and without heptane and it was decided not to include the hydrophobic additive in the plating mixture. Hence, all the results shown here are from mixtures composed only by the precursor salt, water and surfactant.

The plating mixtures were prepared as described before in the experimental section and the presence of the hexagonal phase was confirmed by optical microscopy and small angle X-ray diffraction. Figure 3.1 (a) shows a typical example of the texture observed for the palladium plating mixture, at 25 °C. The presence of dark and bright areas resembling a marble texture and the air bubbles with an irregular shape are characteristics of the hexagonal phase. For the composition studied here, the H_1 phase is stable up to 59 °C; above, it gives rise to a micellar solution (L_1). The micellar solution is optically isotropic, so it appears completely black under crossed polarisers and it can also be characterised by its low viscosity, which gives rise to very round air bubbles that move between the glasses when pressed. During slow cooling of the sample to room temperature, the hexagonal phase reappears at 59° C but this time, due to nucleation effects, increase in the size of the domains and formation of monodomain boundaries the H_1 phase shows a fan-like texture, Figure 3.1 (b).

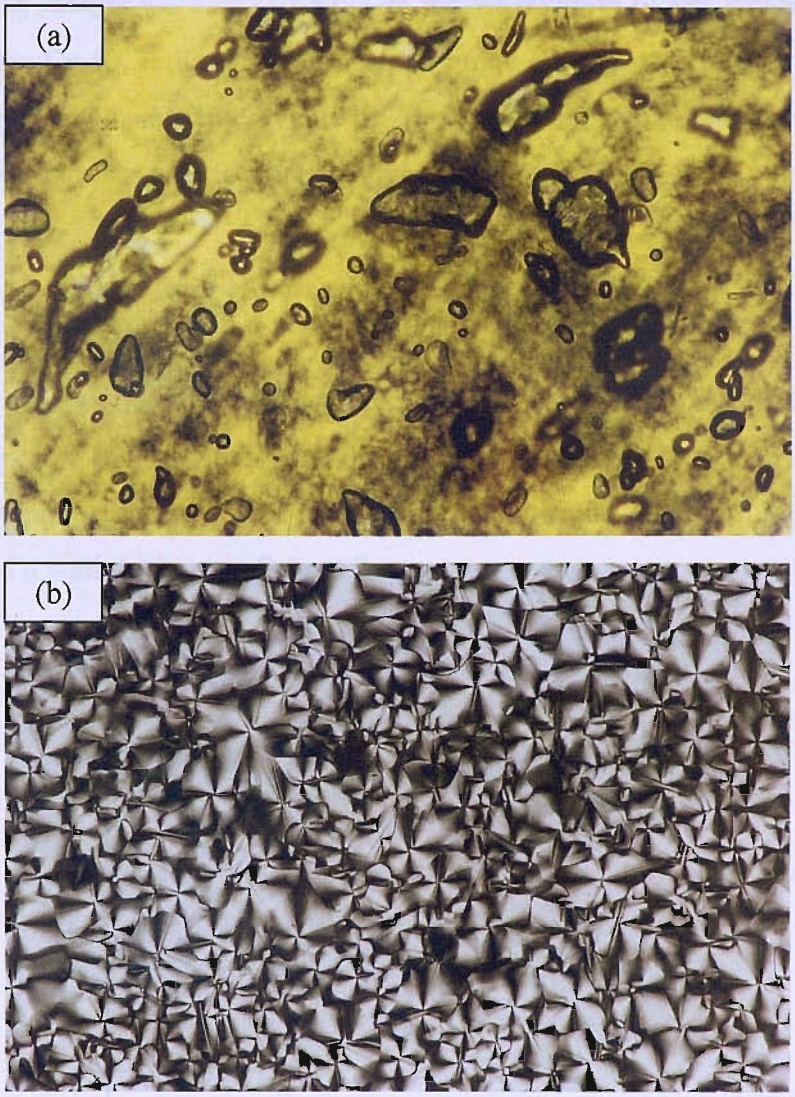

Figure 3.1 *Textures of the hexagonal phase from a plating mixture containing 48 wt% $C_{16}EO_8$, 40 wt% water and 12 wt % $(NH_4)_2PdCl_4$. (a) Picture taken at 25° C, after preparation of plating mixture and (b) picture taken while cooling down sample, at 35.3° C.*

Figure 3.2 shows an example of the small angle X-ray diffraction pattern obtained for the hexagonal phase of the palladium plating mixture after its preparation, i.e., when the texture shown in Figure 3.1 (a) is present. The spectrum shows a diffraction peak corresponding to the (100) diffraction plane of the hexagonal structure and the *d* spacing of the lattice (i.e., the distance between the centres of adjacent rods) for the palladium mixture can be estimated using the Bragg equation

$$n\lambda = 2d\sin\theta \qquad (3.1)$$

where n is an integer (1, 2, 3, ..., n), λ is the wavelength of the incident X-ray beam (1.5406 Å for Cu K_α radiation) and θ is the angle between the incident beam and the diffraction plane. Considering a value of $2\theta = 1.78$, the estimated *d* spacing is 4.96 nm. The pore centre to pore centre distance given by

$$\text{pore centre to pore centre distance} = d/\cos 30° \qquad (3.2)$$

can then be estimated and in this case, a value of 5.7 nm was found, which is similar to the value reported by Bartlett *et al.*[1]. From TEM images obtained from samples of H_1--ePd the authors estimated a pore centre to pore centre distance of 5.8 nm, with a pore diameter and a wall thickness of about 3 nm.

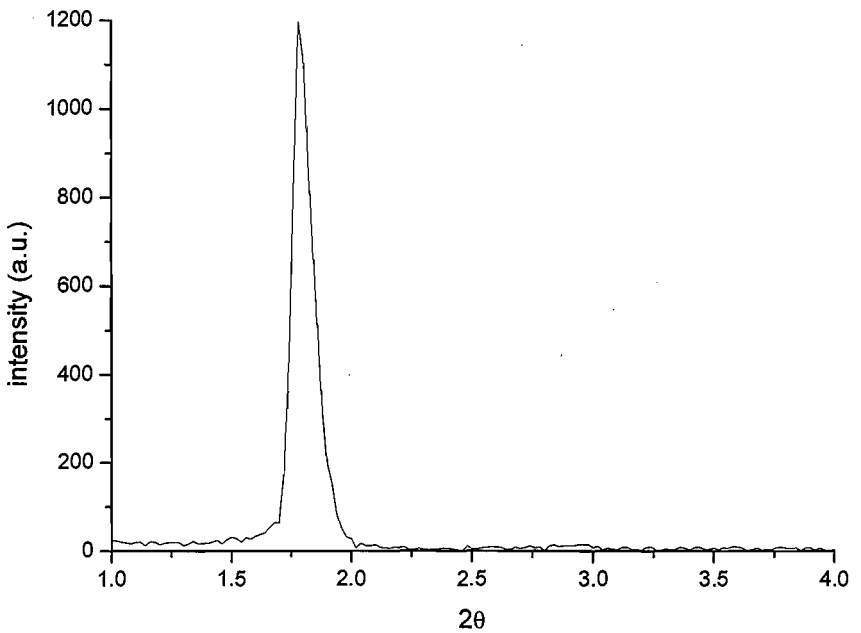

Figure 3.2 *Low angle X-ray diffraction from plating mixture containing 48 wt% $C_{16}EO_8$, 40 wt% water and 12 wt% $(NH_4)_2PdCl_4$.*

3.2- Electrodeposition and Characterisation of Mesoporous Palladium Films

The H_1-ePd films were electroplated onto Pt microdiscs (diameters 10 or 25 μm) from the hexagonal (H_1) lyotropic liquid crystalline phase of Brij® 56 or $C_{16}EO_8$, using a deposition potential of +0.1 V *vs* SCE. At this value, the deposition of palladium occurs under mixed kinetic/diffusion control, as can been observed in Figure 3.3.

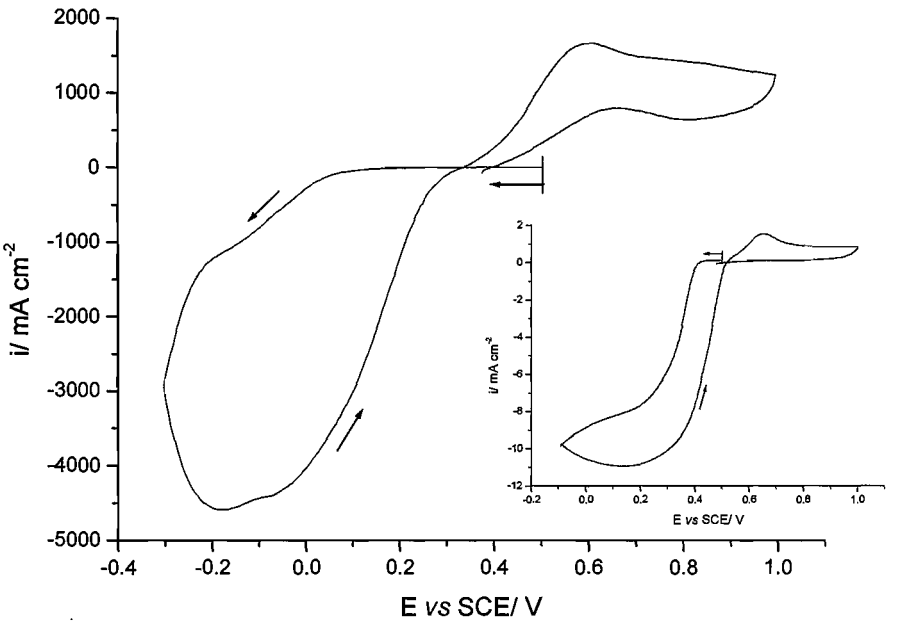

Figure 3.3 *Cyclic voltammogram for a Pt microdisc (d = 10 μm) in a palladium templating mixture containing 48 wt% $C_{16}EO_8$, 40 wt% water and 12 wt % $(NH_4)_2PdCl_4$. Inset shows cyclic voltammogram for a Pt microdisc (d = 25 μm) in 5 mM $(NH_4)_2PdCl_4$ solution. Scan rate = 10 mV s^{-1}.*

The cyclic voltammetry of the plating mixture shows similarities to the voltammetry in aqueous solution, see inset in Figure 3.3. In both voltammograms it is possible to observe a very well defined cathodic wave corresponding to the reduction of Pd(II) ions, and in the reverse scan the presence of a nucleation loop and an oxidation peak. However, the deposition of palladium in the presence of $C_{16}EO_8$ starts at considerably more negative potentials. At the moment it is not possible to give a plausible

explanation for this potential shift, but it is possible that it might be due to some complexation between the Pd species and the surfactant molecules.

The bigger current density observed in the presence of surfactant is a result of the significantly higher concentration of Pd precursor present in the templating mixture (1 M, comparing with 5 mM in the absence of surfactant).

After deposition, all deposits were washed thoroughly with water to remove the excess of surfactant and soaked in water for at least 3 hours before further experiments.

When observed by scanning electron microscopy, the films deposited from Brij® 56 and $C_{16}EO_8$ had a significantly different appearance, see Figure 3.4. The films prepared with the pure surfactant, $C_{16}EO_8$, had a smooth and uniform appearance and the film thicknesses corresponded closely to those estimated from Faraday's law assuming 100% current efficiency for the Pd deposition. In contrast, the films deposited from the

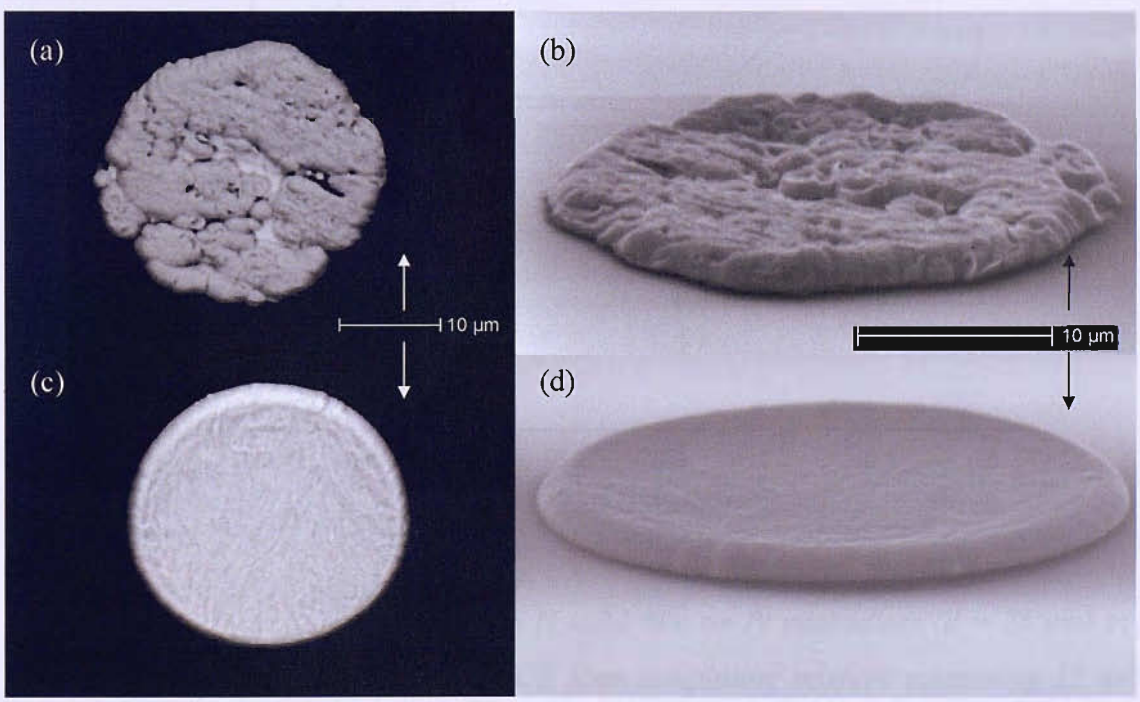

Figure 3.4 *SEM images of H_I-ePd films on Pt microdiscs (d = 25 µm) from templating mixture containing 12 wt% $(NH_4)_2PdCl_4$, 40 wt% water and (a), (b) 48 wt% Brij® 56 or (c), (d) 48 wt% $C_{16}EO_8$. Deposition charge density: 2.0 C cm^{-2}. Deposition potential: +0.1 V vs SCE. (a) and (c) employ BSE detector with sample at 20° to the beam, (b) and (d) employ GSE detector with sample at 73.5° to the beam.*

mixture containing Brij® 56 were not uniform; they showed substantial irregularity with independent areas of deposition and some areas of the microdisc were, at best, thinly covered. Edge effects can be seen from the SEM pictures of the films plated from both liquid crystalline media; a slightly higher rate of deposition to the edge of the microdisc is apparent, reflecting the higher rate of diffusion to the perimeter of the microdiscs. There is also some growth over the glass surround (e.g. after deposition with a charge of 2.0 C cm^{-2}, 25 μm discs were coated with a Pd layer with a diameter ~ 28 μm).

Before any voltammetric studies, all deposits were cycled in 1 M H_2SO_4, at 100 mV s^{-1}, between -0.65 and +0.60 V *vs* SMSE, until a steady state voltammogram with the appearance shown in Figure 3.5 was obtained. During the potential cycling, the peaks

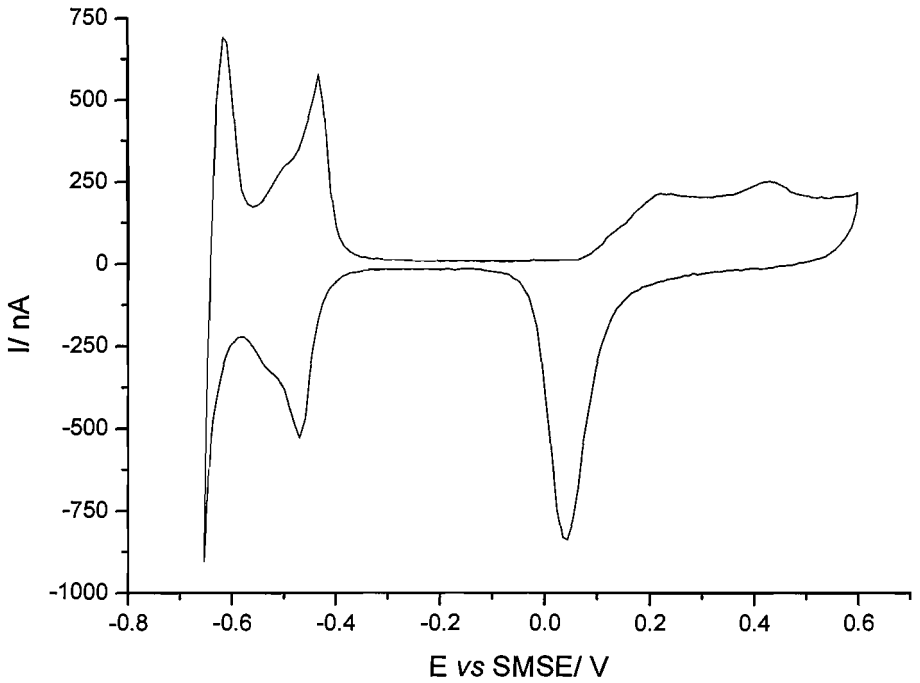

Figure 3.5 *Cyclic voltammogram for a H_1-ePd film on Pt microdiscs (d = 25 μm) in 1 M H_2SO_4. Deposition at + 0.1 V vs SCE from templating mixture containing 12 wt% $(NH_4)_2PdCl_4$, 40 wt% water and 48 wt% $C_{16}EO_8$. Deposition charge density: 2.0 C cm^{-2}. Scan rate = 100 mV s^{-1}.*

for both oxide formation/reduction and hydrogen adsorption/desorption became sharper and the charges associated with the processes increased. A similar behaviour has been observed before for these kind of structures and it has been assigned to the presence of some surfactant inside the pores at the start of the potential cycling and the complete

decontamination by sulphuric acid[1]. Once the response in Figure 3.5 was reached, no further changes were observed. This cleaning procedure is similar to that reported by Solla-Gullón *et al.*[3] for removing Brij® 30 from Pd nanoparticles. In the present study, no decrease in charge associated with oxide reduction was observed during cycling to the positive potential limit of 0.60 V *vs* SMSE; this contrasts with the observations of Gullón *et al.*[3], although they used a more positive potential limit. It should be stressed that the voltammogram of the mesoporous Pd layer in sulphuric acid solution, Figure 3.5, is similar to those reported in the literature[4-6] and shows features consistent with the rapid adsorption and desorption of hydrogen in acidic solution. The sharpness of the peaks and the reproducibility of this voltammogram when repeated during extended series of experiments were taken as an indication that all the surfactant had been removed from the surface. This voltammogram was also used to estimate the electrochemically active surface area of the nanostructured palladium films. The charge associated with the reduction peak of the surface oxide at +0.02 V was determined; it was assumed that a monolayer of oxide had been formed and that this required 424 μC cm^{-2} of active surface area [4].

Surprisingly, in view of the structural differences observed by SEM between the films deposited from Brij® 56 and those from $C_{16}EO_8$, the voltammetry of both types of film was remarkably similar in sulfuric acid. The same oxidation and reduction peaks were observed, at similar potentials, although the absolute current densities were different. The specific surface areas (and hence roughness factors), determined by cyclic voltammetry in 1 M sulfuric acid were consistently higher by a factor of ~ 2 with $C_{16}EO_8$ compared to Brij® 56, see Table 3.1. This may reflect a more ordered nanostructure in the liquid crystal phase with the pure non-ionic surfactant, $C_{16}EO_8$; Brij® 56 has a mixture of chain lengths that inevitably lead to some disorder in the liquid crystal phase. Surfactants are generally used in electroplating and their role in producing smoother deposits is well known [7, 8] so, in this case, the smoother deposit on a micron scale probably results from the different smoothing actions of the two surfactants.

Table 3.1 *Specific surface areas and roughness factors for H_1-ePd films deposited from hexagonal phases prepared with two surfactants. The areas are estimated by cyclic voltammetry from the charge under the palladium oxide reduction peak, in 1 M sulfuric acid, with a positive potential limit of + 0.6 V vs SMSE.*

Surfactant	Diameter Pt disc/ μm	Deposition charge density/ C cm^{-2}	Active surface area/ cm^2	t_{real}/ μm	Specific surface area[(a)]/ m^2 g^{-1}	Roughness factor[(b)]/ cm^2 cm^{-2}
Brij® 56	10	2.2	1.9×10^{-4}	-	20.1	161
	25	2.0	8.8×10^{-4}	-	18.9	160
$C_{16}EO_8$	10	2.2	3.0×10^{-4}	1.4	31.7	275
	10	3.8	5.1×10^{-4}	1.8	30.8	330
	25	0.4	3.5×10^{-4}	0.6	31.3	62
	25	1.6	16×10^{-4}	1.7	29.6	286
	25	2.0	18×10^{-4}	2.1	33.0	283

(a) Specific surface area = active surface area/ mass of palladium given by Faradays' law.

(b) Roughness factor = active surface area/ geometric area of the deposit.

Unless otherwise stated, all cyclic voltammograms reported later in this thesis were obtained with palladium films electroplated from the hexagonal (H_1) liquid crystal phase prepared with $C_{16}EO_8$.

Both the cyclic voltammetry in 1 M H_2SO_4 and the appearance by scanning electron microscopy were employed to 'quality control' the palladium films before and after the different series of experiments.

3.3- The Voltammetry of Mesoporous Palladium Films in 2 M NaOH

Figure 3.6 reports a cyclic voltammogram for a mesoporous palladium film (deposition charge of 1.6 C cm^{-2}) on a 25 μm Pt microdisc, in 2 M NaOH, recorded over a wide potential range and using a potential scan rate of 10 mV s^{-1}. This voltammogram has similarities to examples at other forms of palladium in the literature[9-12] although only two papers at other two high area palladium forms report the processes C_2/A_2 leading to well defined peaks[9, 11]. It should be noted that peak C_2 has the symmetrical shape associated with a surface reaction and it probably arises from the adsorption of hydrogen onto the palladium surface. It is, of course, to be expected that the surface chemistry will be much more prominent at this high area mesoporous Pd than at Pd disc

electrodes or even at smooth Pd films where the peak C_2, in particular, is not observed[10, 12].

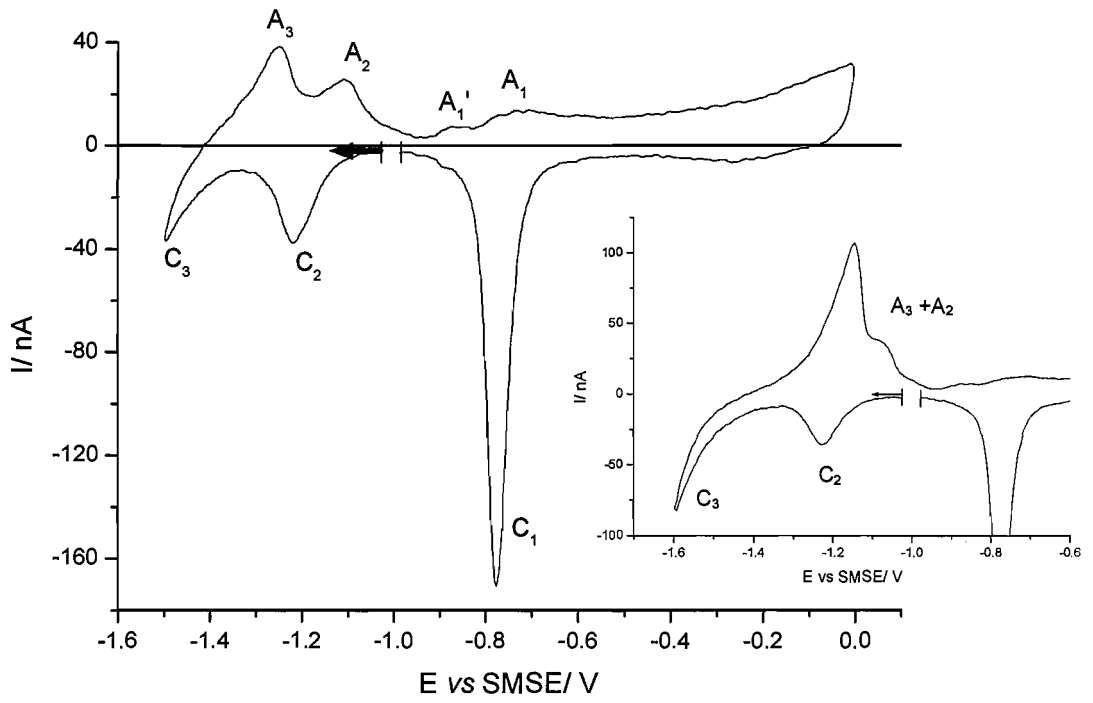

Figure 3.6 *Cyclic voltammogram of a H_I-ePd film on 25 μm diameter Pt microdisc in 2 M NaOH, recorded at 10 mV s^{-1}. Deposition charge density 1.6 C cm^{-2}. Estimated active surface area 1.63×10^{-3} cm^2. Inset shows a cyclic voltammogram recorded using the same conditions, but cycling to -1.6 V.*

There is general agreement that the processes A_1/C_1 are the formation and reduction of a surface palladium oxide, respectively. A_1 has the "wave" shape of an oxide formation process where the oxide continues to thicken as the potential is made more positive, while C_1 has the symmetrical shape expected for the reduction of a surface layer.

With regard to processes C_3/A_3 they are usually assigned to the absorption of hydrogen into the palladium lattice and its reoxidation. In Figure 3.6 the potential scan is reversed while the rate of hydrogen absorption is still relatively low. If the negative potential limit is extended further, a large cathodic current is observed and the anodic peak, A_3, becomes dominant with the increased charge for hydrogen absorption into the palladium lattice. The peak A_3 becomes large and broadens, consequently obliterating the anodic peaks coupled to the cathodic peak C_2, see inset in Figure 3.6. The broadening of the

peak A_3 is well known and arises because this oxidation process requires diffusion of hydrogen through the palladium lattice back to the surface and the timescale of this diffusion process becomes a factor.

In this thesis, special attention will be given to the cathodic peak C_2 and the coupled anodic peaks. Firstly, however, it is essential to define the anodic peaks associated with oxide formation since, under some conditions, the voltammetric peaks for hydrogen desorption overlap those for oxide formation. The overlapping of these two processes does not occur in acidic media, but it has been reported for different types of palladium in basic conditions[12, 13], as a consequence of the rate of diffusion of hydrogen atoms out of the palladium lattice. The voltammogram of Figure 3.6 shows a prepeak, A_1', to the main process associated with the oxidation of the palladium surface. This peak becomes even more evident if the potential is cycled over a shorter range, from -0.95 to -0.60 V *vs* SMSE and increasing the potential scan rate to 300 mV s^{-1}, see Figure 3.7. Under these conditions, it is apparent that there is a corresponding cathodic peak, C_1', on the reverse scan, but this peak is only visible if the charge associated with the peaks A_1/C_1 is kept small. A similar pair of peaks in the initial stage of the palladium oxide film formation has been observed by Bolzán[12] using triangularly modulated

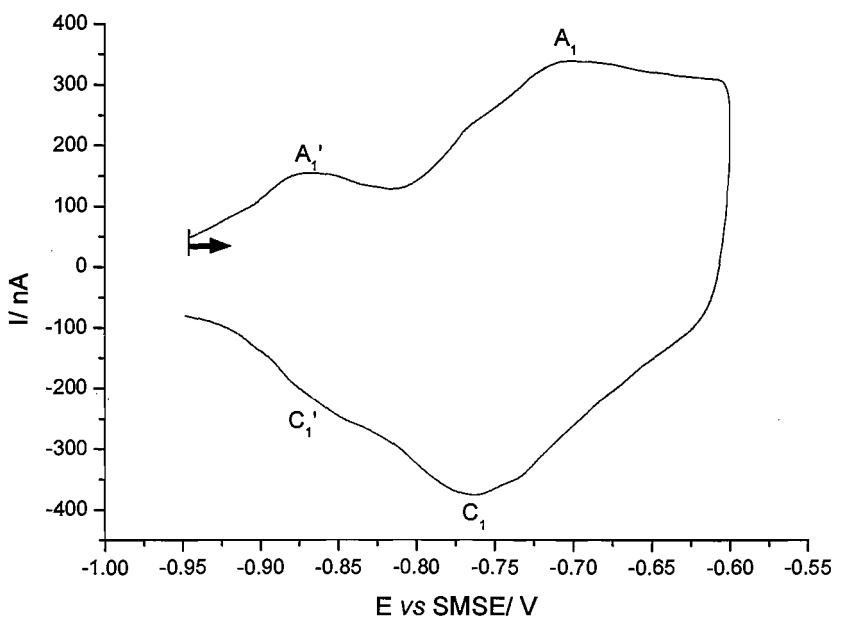

Figure 3.7 *Cyclic voltammogram of a H_1-ePd film on 25 μm diameter Pt microdisc, in 2 M NaOH, at 300 mV s^{-1}. Deposition charge density 1.6 C cm^{-2}. Estimated active surface area 1.63×10^{-3} cm^2.*

voltammetry and it has been assigned to the formation and reduction of Pd(OH) species. The charge associated with the peak A_1' is ~1×10^{-5} C cm^{-2} (considering the active surface area), a value significantly smaller than that required to form a monolayer of oxide over the active palladium surface and which is more likely to correspond to a premonolayer oxidation process. According to Burke and co-workers[10, 14], such a peak can be attributed to the oxidation of surface metal atoms of relatively low bulk lattice coordination number, with the initial product of reaction being an anionic hydrous oxide.

Figure 3.7 seems to show slight shoulders for both peaks A_1 and C_1, indicating that the oxidation of the palladium surface is a complex process; the origin of these shoulders is not known.

To define the origin of the peaks C_2/A_2, a set of voltammograms was recorded at 10 mV s^{-1}, varying the positive potential limit while the negative potential limit was held constant at a value where the peak C_2 is complete and the influence of the processes C_3/A_3 on the voltammogram is minimised, see Figure 3.8. It should be noted that when the initial potential is -1.0 V *vs* SMSE or more positive, the peaks C_2 and A_2 are unchanged. The peak C_2 is symmetrical with the current dropping to close to zero beyond it and the charge under the peak is ~200 μC cm^{-2}. Both features are consistent with the formation of a monolayer of hydrogen atoms over the mesoporous surface. In addition, it should be emphasised that there is no significant steady state current in the potential range -1.00 to -1.40 V *vs* SMSE; when the potential scan is stopped at any potential positive to -1.40 V, the current quickly drops to a very low value.

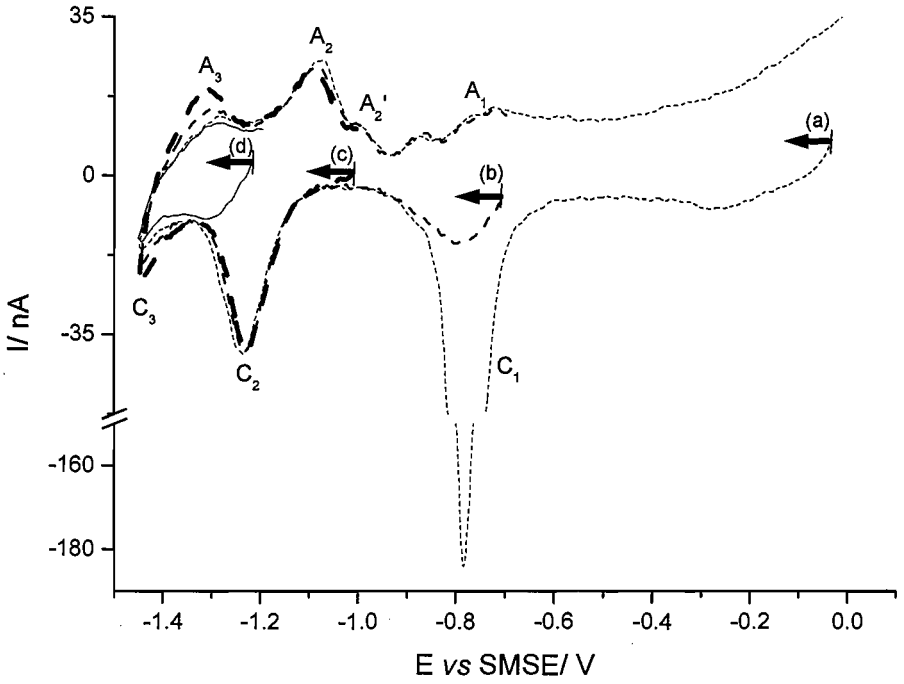

Figure 3.8 *The influence of the positive potential limit on the cyclic voltammograms of a H_I-ePd film on a 25 μm diameter Pt microdisc, in 2 M NaOH, at 10 mV s^{-1}. Positive potential limit (a) 0.0 V, (b) -0.7 V, (c) -1.0 V and (d) -1.2 V vs SMSE. Deposition charge density 2.0 C cm^{-2}. Estimated active surface area 1.39×10^{-3} cm^2.*

On the reverse scan, towards positive potentials, there are two anodic peaks, A_2 and A_2', which seem to be coupled to the cathodic peak C_2. The symmetrical shape of peak A_2 is again an indication of a surface process, but only when the charges associated with both A_2 and A_2' are considered does the charge equate with that for the cathodic peak C_2. When the voltammetry starts at -1.2 V, the charge associated with the peak C_2 is not observed, indicating that the surface is already covered by adsorbed hydrogen and that the processes associated with peaks A_2 and A_2' are essential to return the palladium surface to its original state free of adsorbed hydrogen, i.e., processes A_2 and A_2' are the reverse of C_2 and can be assigned to the desorption of hydrogen atoms. The separation between peaks C_2 and A_2 is, however, of 160 mV, which indicates that the adsorption/ desorption processes are irreversible, i.e., the electron transfer reactions are slow.

The potential scan rate has a large effect on the shape of the cathodic peak, C_2, as can been seen in Figure 3.9. On increasing the potential scan rate from 10 to 300 mV s^{-1}, the peak potential is negatively shifted from -1.25 to -1.37 V *vs* SMSE and the peak clearly

broadens, but the cathodic charge associated with it remains constant (~200 μC cm^{-2}). Both the shift in potential and the broadening of the peak are characteristics consistent with an adsorption process where the electron transfer process is slow. In fact, in order to observe the peak at higher potential scan rates, it is necessary to extend the negative potential limit, which makes it impossible to record the full peak without interference from hydrogen absorption. For this reason, and to ensure that the positive going scans are not complicated by hydrogen leaving the bulk palladium lattice, the responses in Figure 3.9 are obtained with negative potential limits where the current has not dropped to zero beyond the peak. The general behaviour of peak C_2 slightly interferes with the integration of the area under the peak, and the value also depends on the baseline considered, but over the scan rates shown in Figure 3.9 the charge remains in the range 160-200 μC cm^{-2}.

The effect of potential scan rate on the reverse scan is even more dramatic and the response becomes complex. In general, three anodic peaks are seen in the potential range -1.10 to -0.80 V. With increasing potential scan rate, there is a shift in charge from peak A_2 to peak A_2' and both peaks move strongly towards more positive potentials. Indeed, peak A_2' can be seen as a minor process at the slowest scan rate, see Figure 3.9, but it becomes more dominant with increasing potential scan rate. There is, however, always a reasonable charge balance between the processes C_2 and the sum of A_2 and A_2' (e.g. at 50 mV s^{-1}, the charges were 185 μC cm^{-2} and 172 μC cm^{-2}, respectively), showing that both anodic peaks are associated with oxidation of adsorbed hydrogen. The change in the importance of the peaks A_2 and A_2' with scan rate indicates the interconversion of two adsorbed species on the timescale of the voltammetry. It is again clear from the increase in the peak separation with potential scan rate and the breadth of the peaks that the electrochemistry associated with peaks C_2, A_2 and A_2' is highly irreversible. Tateishi *et al.*[9] have reported a similar behaviour for electrodes of ultrafine palladium particles supported on glassy carbon in 1 M NaOH, but it is suggested that the observed features are due to the presence of weakly and strongly adsorbed hydrogen adatoms.

With a positive limit of -0.80 V, the reverse process of peak A_1' (described above during discussion of Figure 3.7) is again seen as a small cathodic peak at -0.87 V, at the commencement of the forward scan. At 300 mV s^{-1}, the irreversibility of the process C_2/ (A_2 + A_2') causes the peaks A_2' and A_1' to overlap.

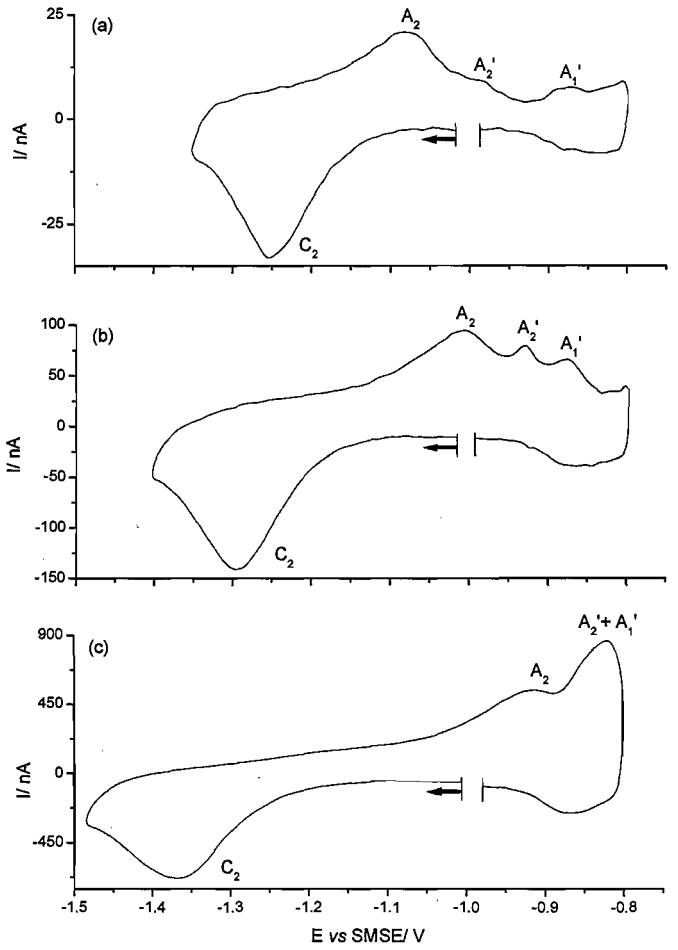

Figure 3.9 *The influence of the potential scan rate on the cyclic voltammograms of a H_I-ePd film on a 25 μm diameter Pt microdisc, in 2 M NaOH. (a) 10 mV s^{-1}, (b) 50 mV s^{-1} and (c) 300 mV s^{-1}. Deposition charge density of 2.0 C cm^{-2}. Estimated active surface area 1.39×10^{-3} cm^2.*

It is clearly oversimplistic to discuss the peaks A_2 and A_2' in terms of oxidation of weakly and strongly adsorbed hydrogen because (a) there is never a cathodic peak at a potential close to the anodic peak A_2' that could be assigned to the formation of strongly adsorbed hydrogen and (b) the peak current ratios indicate interconversion of the adsorbed species on the timescale of the voltammetry; during the positive going scans at slow sweep rates, conversion of the reactants for the peak A_2' into the reactant for A_2 is occurring (if discussed in terms of weakly and strongly adsorbed hydrogen, this would correspond to the conversion of strongly to weakly adsorbed species). Equations 3.3 to

3.6 summarize the proposed mechanism, assuming interconversion between two different species of hydrogen

$$\text{Peak } C_2 \quad H_2O + Pd + e^- \longrightarrow (Pd\text{-}H)_1 + OH^- \qquad (3.3)$$

$$(Pd\text{-}H)_1 \rightleftharpoons (Pd\text{-}H)_2 \qquad (3.4)$$

$$\text{Peak } A_2 \quad (Pd\text{-}H)_1 + OH^- \longrightarrow H_2O + Pd^- + e^- \qquad (3.5)$$

$$\text{Peak } A_2' \quad (Pd\text{-}H)_2 + OH^- \longrightarrow H_2O + Pd^- + e^- \qquad (3.6)$$

where the equilibrium (3.4) lies to the right, but the kinetics of the back reaction are sufficiently fast for the reformation of $(Pd\text{-}H)_1$ to occur on the timescale of the voltammetry, particularly in experiments with a slow scan rate. This way, it is assumed that the direct formation of the species $(Pd\text{-}H)_2$ does not occur. To find the differences between $(Pd\text{-}H)_1$ and $(Pd\text{-}H)_2$ is out of the scope of this thesis and their respective features were not studied in more detail, but they can, for example, correspond to adsorbed hydrogen at different surface sites. In the late seventies, Breiter[15] introduced the idea of a subsurface layer of hydrogen atoms in equilibrium with adsorbed hydrogen atoms on the surface and it is well possible that the species $(Pd\text{-}H)_2$ are associated with that subsurface layer. Such a layer works as the first step of hydrogen incorporation into the palladium lattice. Some surface science studies with a palladium (110) surface [16, 17] have also shown evidence for the formation of this subsurface hydrogen species and indicate that the adsorption of hydrogen on palladium is a complicated process where as many as four different types of surface hydrogen species have been identified by thermal desorption methods.

The voltammetry at this high surface area palladium film (H_1-ePd) certainly leads to better resolved voltammetric peaks (as noted before for another high area form of palladium[9]), which clearly disclose some differences between the surface electrochemistry of palladium and other precious metals in alkaline solutions:

(i) At palladium in alkaline media, the kinetics of the electron transfer reactions involved in hydrogen adsorption/ desorption are very slow, leading to broad peaks and large peak separations of coupled anodic and cathodic processes;

(ii) The voltammetry shows up the oxidation of two types of adsorbed hydrogen that interconvert on the timescale of the voltammetry, but the presence of

only a single reduction peak rules out the formation of strongly and weakly adsorbed hydrogen;

(iii) A sub-monolayer amount of an oxidised palladium surface is formed at potentials negative to the deposition of the 'normal' palladium oxide;

(iv) The potential for the formation of the sub-monolayer palladium oxide and the oxidation of adsorbed hydrogen overlap when increasing the potential scan rate. The response then becomes complex because (a) the current associated with palladium oxidation increases and (b) the charge associated with peak A_2' increases and the peak is shifted positively by the slow electron transfer.

3.4- The Cathodic Reduction of Nitrate and Nitrite at Mesoporous Palladium Films in 2 M NaOH

3.4.1- Nitrate reduction

The reduction of nitrate was carried out at H_1-ePd films in 30 mM $NaNO_3$/ 2 M NaOH. Figure 3.10 illustrates the electrochemical behaviour of this solution at 10 mV s^{-1}. In the presence of nitrate, the voltammogram shows a new symmetric peak at -1.34 V *vs* SMSE, with the current tending to zero after the peak. It is also possible to observe a small decrease in current for the oxide reduction peak, as well as for the hydrogen adsorption peak.

The current density for the nitrate reduction peak (~7.2 mA cm^{-2}) is considerably smaller than the value expected for a diffusion controlled $8e^-$ process (~133 mA cm^{-2} at a 26.6 μm diameter film and assuming D = 6×10^{-6} cm^2 s^{-1}[18]) and considering the symmetry of the peak, it is likely that the reduction of the anion in alkaline media involves surface chemistry.

Figure 3.11 compares the electrochemical behaviour of a non-templated Pd film with the response observed in Figure 3.10 for the mesoporous Pd film in 30 mM $NaNO_3$/ 2 M NaOH. The geometric areas of the two deposits were considered for the calculation of the current density. As it is possible to observe, the non-templated film does not show any response for nitrate and the features related with hydrogen adsorption are also absent.

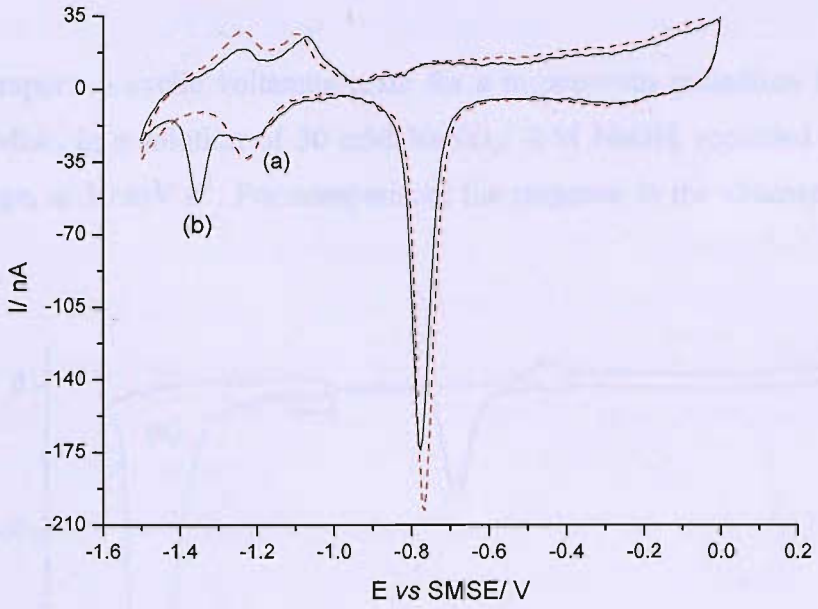

Figure 3.10 *Cyclic voltammogram of a H_1-ePd film on a Pt microdisc (d = 25 μm) in (a) 2 M NaOH and (b) 30 mM $NaNO_3$/ 2 M NaOH, at 10 mV s^{-1}. Deposition charge density = 2.0 C cm^{-2}. Estimated active surface area =1.94×10^{-3} cm^2.*

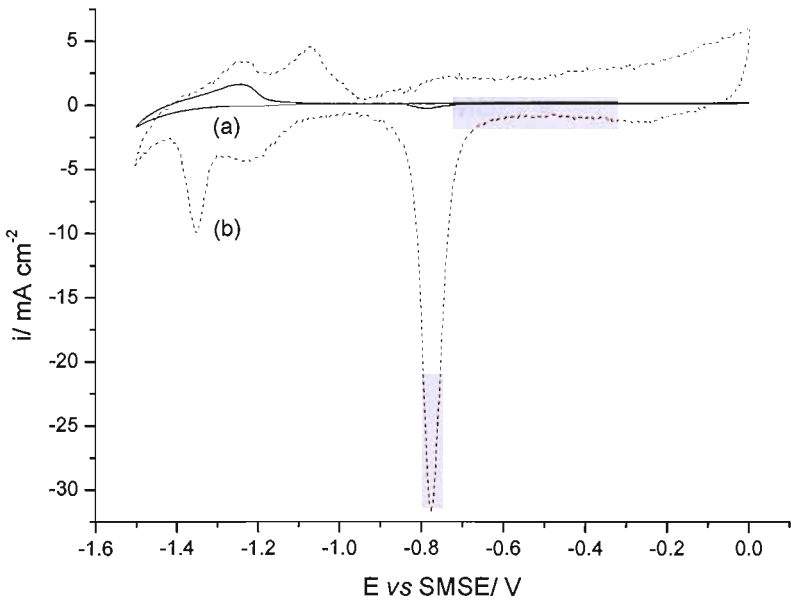

Figure 3.11 *Cyclic voltammogram of (a) a non-templated Pd film and (b) a H_1-ePd film in 30 mM $NaNO_3$/ 2 M NaOH, at 10 mV s^{-1}. Both films deposited on a Pt microdisc (d = 25 μm). Deposition charge density = 2.0 C cm^{-2}.*

3.4.2- Nitrite reduction

Figure 3.12 reports a cyclic voltammogram for a mesoporous palladium film on a 10 μm Pt microdisc, in a solution of 30 mM $NaNO_2$/ 2 M NaOH, recorded over a wide potential range, at 10 mV s^{-1}. For comparison, the response in the absence of nitrite is also shown.

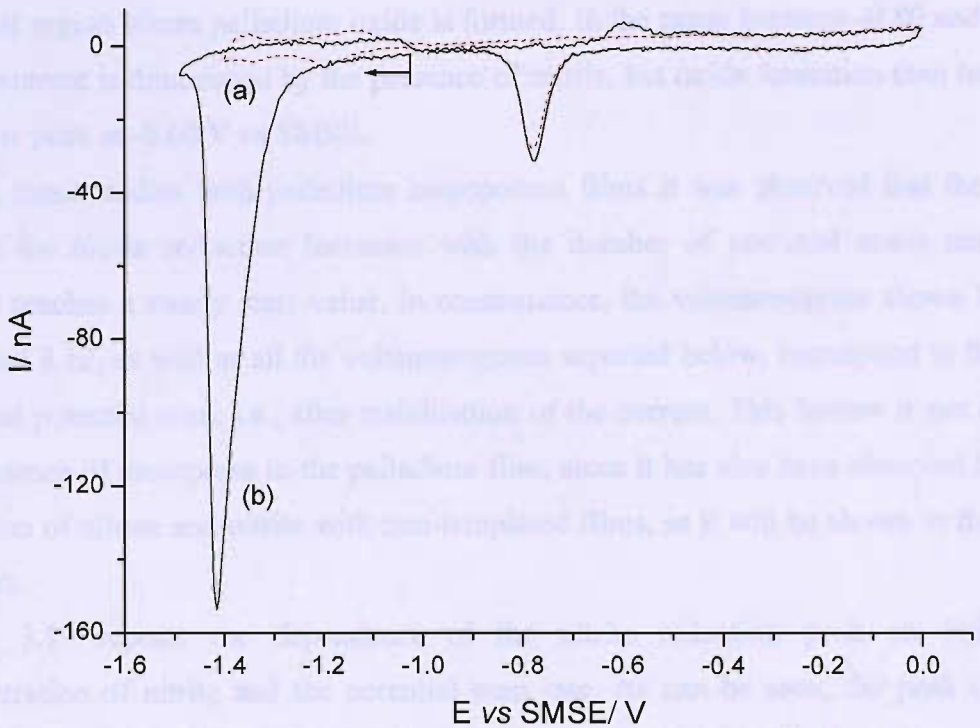

Figure 3.12 *Cyclic voltammogram for a H_I-ePd film on a 10 μm Pt microdisc in (a) 2 M NaOH and (b) 30 mM $NaNO_2$/ 2 M NaOH, at 10 mV s^{-1}. Deposition charge density 2.0 C cm^{-2}. Estimated active surface area 2.56×10^{-4} cm^2.*

The presence of the nitrite ion in the solution gives rise to the large cathodic peak at -1.42 V *vs* SMSE. This peak is present at any potential sweep rate, but the steady state current over its potential range is very low (at the level of the response in the absence of nitrite). The peak assigned to nitrite reduction is again symmetrical in shape, with the current dropping to a low value beyond the peak. Both observations imply an electrode reaction involving surface chemistry. The large charge associated with the peak (~ 4 mC cm^{-2}, based on the active surface area of the mesoporous film) corresponds to the reduction of much more than a monolayer, i.e., the surface involves chemistry where the

reactant at the surface is replenished. It should also be noted that the rise in the cathodic current leading to the peak for nitrite reduction does not commence until potentials negative to the peak for hydrogen adsorption in the absence of nitrite. Similarly, the potential beyond the peak where the current drops down towards zero is more negative in the presence of NO_2^-. On increasing the current sensitivity, the peak for the desorption of a monolayer of hydrogen becomes apparent although it is shifted to a more positive potential. Another observed feature is the change in the response in the potential region where palladium oxide is formed; in the range between -0.80 and -0.65 V, the current is diminished by the presence of nitrite, but oxide formation then leads to a steeper peak at -0.60 V vs SMSE.

During these studies with palladium mesoporous films it was observed that the peak current for nitrite reduction increases with the number of potential scans until the current reaches a steady state value. In consequence, the voltammogram shown before in Figure 3.12, as well as all the voltammograms reported below, correspond to the last recorded potential scan, i.e., after stabilization of the current. This feature is not due to the presence of mesopores in the palladium film, since it has also been observed for the reduction of nitrate and nitrite with non-templated films, as it will be shown in the next chapters.

Figure 3.13 reports the dependence of the nitrite reduction peak on both the concentration of nitrite and the potential scan rate. As can be seen, the peak current increases with both nitrite concentration and potential scan rate, but there is no simple dependence of the peak current on either parameter. Plots of the peak current versus the potential scan rate or the square root of the potential scan rate are non-linear. It is clear that the charge associated with the peak increases markedly with the concentration of nitrite in solution, reaching 12.6 mC cm^{-2} (again, based on the active surface area of the mesoporous film) for 0.1 M nitrite solution. On the other hand, it decreases with increasing potential scan rate, see Figures 3.13 (c) and (d).

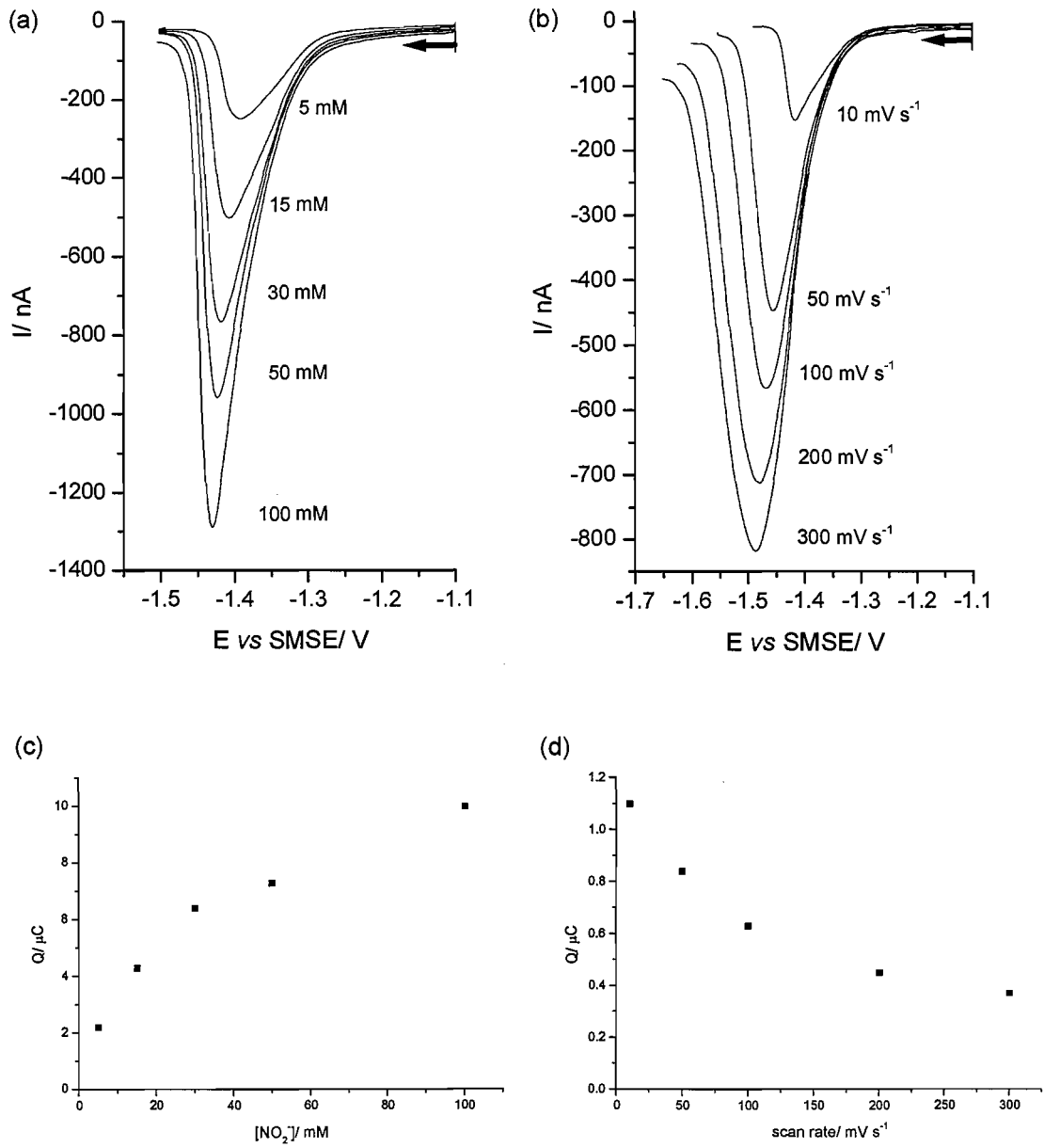

Figure 3.13 *The influence of nitrite concentration and potential scan rate on the reduction of nitrite at H_1-ePd films on Pt microdiscs in 2 M NaOH. (a) Variation of nitrite concentration. Potential scan rate 10 mV s^{-1}; 25 µm Pt microdisc, deposition charge density 2.0 C cm^{-2} and estimated active surface area 8.00×10^{-4} cm^2. (b) Variation of potential scan rate. Nitrite concentration 30 mM; 10 µm Pt microdisc, deposition charge density 2.0 C cm^{-2} and estimated surface area 2.56×10^{-4} cm^2. In both cases, the data are taken from potential scans commenced at 0.0 V. (c) Charges associated with the nitrite reduction peak for the different concentrations and (d) charges associated with the nitrite reduction peak for the different scan rates.*

Two voltammograms recorded at 300 mV s^{-1} for solutions with and without nitrite are compared in Figure 3.14. Focusing on the reverse scan, it can be seen that there are significant differences. Firstly, there appears to be a relatively sharp, single peak for hydrogen desorption in the presence of nitrite and its peak potential would suggest that it corresponds to the peak A_2' for the oxidation of $(Pd\text{-}H)_2$. Secondly, it is very clear that, with nitrite in solution, there is a reduction process occurring in the range between -0.78 and -0.60 V and after that, as reported before at 10 mV s^{-1}, the response for the oxidation of the palladium surface becomes steeper. Indeed, the process A_1 appears to be completely absent.

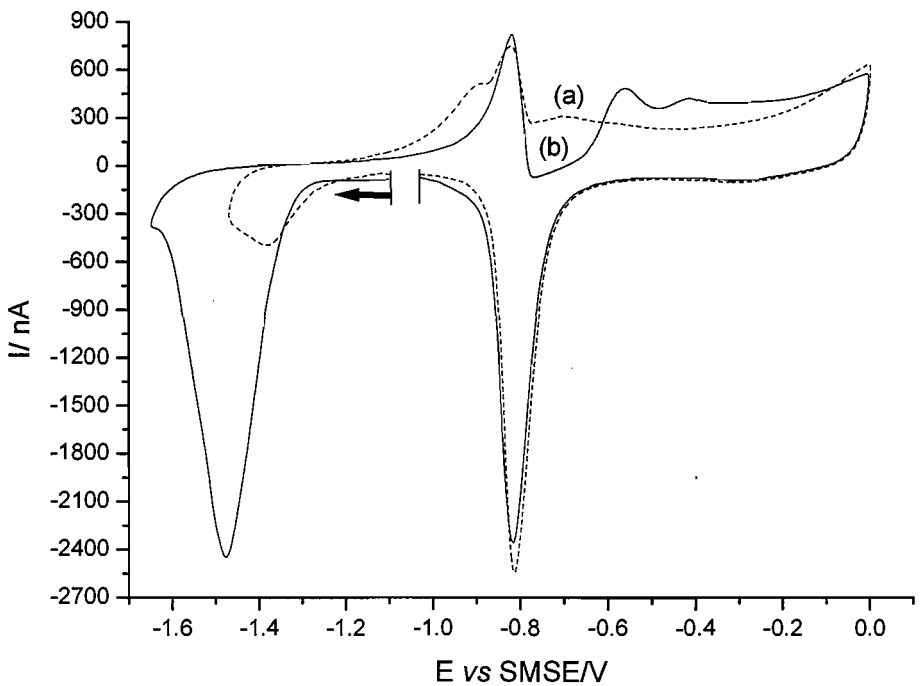

Figure 3.14 *Cyclic voltammogram for a H_1-ePd film on a 25 μm Pt microdisc in (a) 2 M NaOH and (b) 30 mM $NaNO_2$/ 2 M NaOH at 300 mV s^{-1}. Deposition charge density 1.6 C cm^{-2}. Estimated surface area 1.63×10^{-3} cm^2.*

This implies that a key step in the mechanism for nitrite reduction is a chemical reaction between adsorbed hydrogen and adsorbed nitrite,

$$Pd\text{-}H + Pd\text{-}NO_2^- \longrightarrow 2Pd + \text{products} \qquad (3.7)$$

leading to free surface sites where there will be competition between formation of adsorbed hydrogen and re-adsorption of NO_2^-. It must be emphasised that the shape of the nitrite reduction peak indicates conclusively the involvement of surface chemistry and the return of the current to zero beyond the peak (or when holding the potential constant at a value in this potential region) can be associated with the surface becoming fully covered with adsorbed hydrogen. On the other hand, the large charges associated with the peak for nitrite reduction indicate that while the competition between the formation of adsorbed hydrogen and re-adsorption of nitrite at the free sites created is eventually won by the adsorbed hydrogen, the competition is relatively close and re-adsorption of nitrite continues for an extended period. Such strong adsorption of nitrite at these negative potentials is surprising, but further evidence can be found in the voltammetry. Firstly, while the hydrogen adsorption peak in the absence of NO_2^- is seen at -1.21 V, no such peak is seen when the anion is in solution; only the large peak at -1.42 V is obtained (see Figure 3.12). Secondly, the current for the initial oxidation of the palladium surface is shifted positively when nitrite is present (see Figure 3.14). Although adsorption of anions at such negative potentials is surprising, several papers in the literature[19, 20] have discussed the adsorption of both chloride and cyanide ion in this potential region and found that these anions inhibit hydrogen absorption (and, by implication, hydrogen adsorption) and also alter the oxide formation region.

3.5- Conclusion

The application of mesoporous coatings magnifies the response for surface reactions. In consequence, it is possible to see well formed peaks for both the adsorption of hydrogen on palladium and the reduction of nitrate/ nitrite.

The adsorption/ desorption of hydrogen is shown to be a complex process involving both slow electron transfer and equilibrium between adsorbed hydrogen species.

Nitrate and nitrite reduction is shown to involve surface reactions between adsorbed hydrogen species and adsorbed nitrate/ nitrite. It is also a transient process as the Pd surface always becomes fully covered by adsorbed hydrogen. The reaction of nitrite is much faster than nitrate, leading to a much larger cathodic peak.

3.6- References

[1] P. N. Bartlett, B. Gollas, S. Guerin, J. Marwan, *Phys. Chem. Chem. Phys.* **2002**, *4*, 3835.

[2] G. S. Attard, P. N. Bartlett, N. R. B. Coleman, J. M. Elliott, J. R. Owen, J. H. Wang, *Science* **1997**, *278*, 838.

[3] J. Solla-Gullón, V. Montiel, A. Aldaz, J. Clavilier, *J. Electrochem. Soc.* **2003**, *150*, E104.

[4] R. Woods, in *Electroanalytical Chemistry, Vol. 9* (Ed.: A. J. Bard), Marcel Dekker, New York, **1976**, p. 109.

[5] J. P. Chevillot, J. Farcy, C. Hinnen, A. Rousseau, *J. Electroanal. Chem.* **1975**, *64*, 39.

[6] L. H. Dall'Antonia, G. Tremiliosi-Filho, G. Jerkiewicz, *J. Electroanal. Chem.* **2001**, *502*, 72.

[7] R. Vittal, H. Gomathi, K. J. Kim, *Adv. Colloid Interface Sci.* **2006**, *119*, 55.

[8] A. Aragon, M. G. Figueroa, R. E. Gana, J. H. Zagal, *J. Appl. Electrochem.* **1992**, *22*, 558.

[9] N. Tateishi, K. Yahikozawa, K. Nishimura, Y. Takasu, *Electrochim. Acta* **1992**, *37*, 2427.

[10] L. D. Burke, J. K. Casey, *J. Electrochem. Soc.* **1993**, *140*, 1292.

[11] C. C. Hu, T. C. Wen, *J. Electrochem. Soc.* **1994**, *141*, 2996.

[12] A. E. Bolzan, *J. Electroanal. Chem.* **1995**, *380*, 127.

[13] A. Czerwinski, I. Kiersztyn, M. Grden, *J. Electroanal. Chem.* **2000**, *492*, 128.

[14] L. D. Burke, V. J. Cunnane, B. H. Lee, *J. Electrochem. Soc.* **1992**, *139*, 399.

[15] M. W. Breiter, *J. Electroanal. Chem.* **1978**, *90*, 425.

[16] M. G. Cattania, V. Penka, R. J. Behm, K. Christmann, G. Ertl, *Surface Science* **1983**, *126*, 382.

[17] J. W. He, D. A. Harrington, K. Griffiths, P. R. Norton, *Surface Science* **1988**, *198*, 413.

[18] N. G. Carpenter, D. Pletcher, *Anal. Chim. Acta* **1995**, *317*, 287.

[19] J. Horkans, *J. Electroanal. Chem.* **1986**, *209*, 371.

[20] J. McBreen, *J. Electroanal. Chem.* **1990**, *287*, 279.

Chapter 4- Seeking Mesoporous Copper Films

The electrochemical synthesis of mesoporous Cu/CuO_2 films from a plating bath containing low concentration (< 10 wt%) of the anionic surfactant SDS (sodium dodecylsulfonate), water and $CuSO_4.5H_2O$ has been claimed by Zou *et al.*[1].
Characterisation of the films electrodeposited onto conductive glass (type not specified) by small angle XRD revealed four intense diffraction peaks at $2\theta = 2.32°$, 4.52°, 6.70° and 8.92°, indicating highly ordered arrays of uniform mesopores and a pore diameter of 3.40 nm was calculated. According to the authors, the TEM images obtained are further evidence for a highly ordered 2D hexagonal structure with the pore direction parallel to the substrate. The SEM images reported in this work, however, show a film morphology mainly made of cubic crystals of several microns where it is possible to observe many "black holes" about 50 nm in diameter. The authors recognise the inconsistency in the results, but no explanation for the observed morphology or for the presence of the 50 nm "black holes" is given.

The aim of the present study is to investigate the preparation of mesoporous copper films from the hexagonal phase of $C_{16}EO_8$.
The preparation of mesoporous copper using the hexagonal liquid crystalline phase of a non-ionic surfactant has been attempted before by Ghanem[2]. The plating mixture consisted of 45 wt% Brij® 56, 45 wt% water and 10 wt% $CuCl_2$ and the copper deposition was studied at different potentials. SEM images of the copper films showed a very rough surface with a non-uniform growth. The author reported a diffraction pattern for the electrodeposited Cu films with a well defined intensity peak giving a *d* spacing of 5.2 nm, however, TEM showed that the Cu film consisted of a highly random porous structure and that the pores had a non-regular shape. According to the author, the disordered phase might have been the result of the nucleation mechanism and the growth of large grains. The electrochemical characterisation of the resulting copper

structure was done in chloride solution by cyclic voltammetry, but no clear evidence of a high area mesoporous structure was given in this work.

With such a high concentration of Cl^- in the plating mixture studied by Ghanem, the corrosion of the copper film due to the reaction

$$Cu + Cu^{2+} + 4Cl^- \longrightarrow 2CuCl_2^- \qquad (4.1)$$

can be a problem during open circuit, and since no clear evidence for the presence of a mesoporous structure was given, a big part of the work reported in this thesis was focused on the development of a new plating mixture for the electrodeposition of mesoporous copper films from the hexagonal liquid crystalline phase of $C_{16}EO_8$.

Sulfate copper baths are generally used in industry for copper electroplating and for this reason, one of the first approaches for a copper plating mixture consisted of using $CuSO_4.5H_2O$ as a salt precursor.

4.1- Preparation and Characterisation of Copper Films from an Acidic Bath containing $CuSO_4$ and $C_{16}EO_8$

4.1.1- Preparation and characterisation of the copper plating mixture

Several plating mixtures were prepared from $C_{16}EO_8$ and different amounts of $CuSO_4.5H_2O$ to study the effect of copper concentration on the stability of the hexagonal phase and on the quality of the deposits.

The electrodeposition of copper from acid sulphate baths is extensively used for industrial electroplating[3]. Plate characteristics are improved, solution conductivity is increased and anode and cathode polarizations are greatly reduced when sulphuric acid is added to solution. The acid also prevents the precipitation of basic salts like $Cu(OH)_2$.

Before studying the effect of sulphuric acid on the plating mixtures containing copper, some preliminary studies were carried out to study the effect of the acid on $C_{16}EO_8$ only. Two mixtures of similar composition were prepared, one with 50 wt% $C_{16}EO_8$ + 50 wt% water (mixture A), another one with 50 wt% $C_{16}EO_8$ + 50 wt% 0.1 M H_2SO_4 (mixture B). Both mixtures were warmed up to 45 °C for ~3 minutes, mixed with a glass rod until they became homogeneous and then they were allowed to equilibrate for

2 h, at 25 °C. Table 4.1 summarizes the results obtained by polarised optical microscopy and small angle X-ray diffraction for both cases.

Table 4.1 *Characterisation of mixtures of $C_{16}EO_8$ and water and $C_{16}EO_8$ and 0.1 M H_2SO_4 by polarised optical microscopy and small angle X-ray diffraction.*

Mixture	Polarised optical microscopy	Small angle X-ray diffraction
A 50 wt% $C_{16}EO_8$ 50 wt% water	Hexagonal phase stable up to 58 °C	Main diffraction peak at $2\theta = 1.84$ and a smaller one at 2.98
B 50 wt% $C_{16}EO_8$ 50 wt% 0.1 M H_2SO_4	Hexagonal phase stable up to 58 °C	Main diffraction peak at $2\theta = 1.68$ and two smaller ones at 2.76 and 3.12

Apart from the small difference obtained in the position of the main diffraction peak, no significant changes were observed in the presence of 0.1 M H_2SO_4 by polarised optical microscopy. Both mixtures showed a texture typical of the hexagonal phase at room temperature and up to 58 °C, followed by the formation of a micellar phase. Figure 4.1 shows the textures observed for the mixture containing 0.1 M H_2SO_4 at three different stages of the heating/ cooling cycle used in this study.

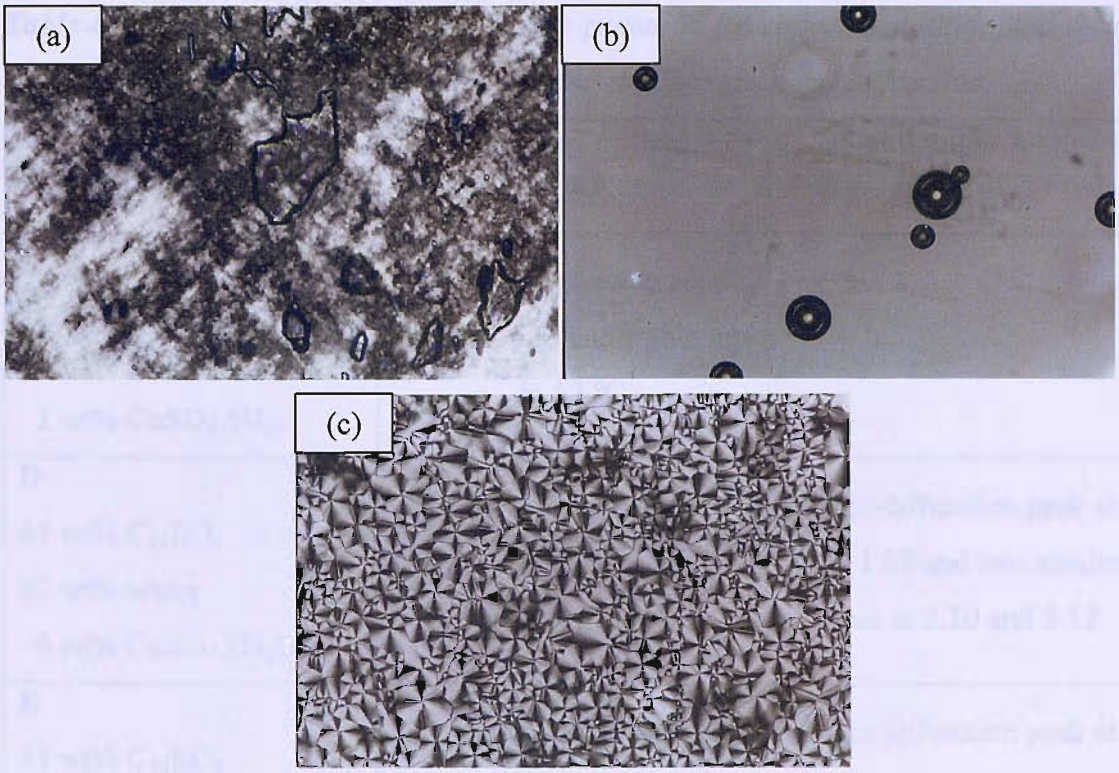

Figure 4.1 *Textures observed by polarised optical microscopy for a mixture containing 50 wt% $C_{16}EO_8$ + 50 wt% 0.1 M H_2SO_4. (a) Hexagonal phase at 25 °C, (b) micellar phase at 63.5 °C and (c) hexagonal phase during cooling of the sample at 56.3 °C.*

To study the effect of copper on the plating mixture, several mixtures with different concentrations of the metal precursor were then prepared. Some of the mixtures were prepared with 0.1 M H_2SO_4 and some other mixtures, of similar composition, with water only. All mixtures were warmed to 45 °C, using a water bath, for ~ 3 minutes, stirred with a glass rod until they became homogeneous and then they were allowed to equilibrate at 25 °C, for 2 hours, before their characterisation with polarised optical microscopy and small angle X-ray diffraction.

Table 4.2 summarises the mixtures prepared for this study, as well as the results from polarised optical microscopy and small angle X-ray diffraction observed for each of them.

Table 4.2 *Summary of the plating mixtures prepared for copper deposition and results obtained by polarised optical microscopy and small angle X-ray diffraction.*

Mixture	Polarised optical microscopy	Small angle X-ray diffraction
C 49 wt% $C_{16}EO_8$ 49 wt% water 2 wt% $CuSO_4.5H_2O$	Hexagonal phase at room temperature and stable up to 53 °C	
D 47 wt% $C_{16}EO_8$ 47 wt% water 6 wt% $CuSO_4.5H_2O$	Hexagonal phase at room temperature and stable up to 43°C	Main diffraction peak at $2\theta = 1.62$ and two smaller ones at 2.10 and 3.12
E 43 wt% $C_{16}EO_8$ 43 wt% water 14 wt% $CuSO_4.5H_2O$	Hexagonal phase at room temperature and stable up to 42 °C	Main diffraction peak at $2\theta = 1.58$ and two smaller ones at 2.06 and 3.06
F 47 wt% $C_{16}EO_8$ 47 wt% 0.1 M H_2SO_4 6 wt% $CuSO_4.5H_2O$	Hexagonal phase at room temperature and stable up to 50 °C	Main diffraction peak at $2\theta = 1.66$ and two smaller ones at 2.18 and 3.18

Comparing the results obtained by polarised optical microscopy for mixtures C, D and E, it is possible to conclude that an increase in $CuSO_4$ concentration decreases the stability of the hexagonal phase. On the other hand, for the same concentration of $CuSO_4$, the presence of 0.1 M H_2SO_4 in the plating mixture seems to stabilise the hexagonal phase up to higher temperatures, compare mixtures D and F.

Figure 4.2 (a) shows a typical example of the texture observed for mixture D, at 25 °C, before the first heating cycle. As for the palladium plating mixture described in Chapter 3 and for the mixture consisting of 50 wt% $C_{16}EO_8$ + 50 wt% 0.1 M H_2SO_4 (mixture B), it is possible to observe the presence of dark and bright areas resembling a marble texture, as well as air bubbles with an irregular shape, due to the viscosity of the mixture. However, while heating up the sample, a different behaviour was observed. For temperatures above 50 °C, some transparent round bubbles start to appear and all

the sample looked like a mixture of oil and water, see Figure 4.2 (b). This phenomenon has been observed for the plating mixture containing $C_{16}EO_8$, $CuSO_4$ and H_2SO_4, but not for $C_{16}EO_8$ in the presence of H_2SO_4 only, or for the copper plating mixtures prepared with water.

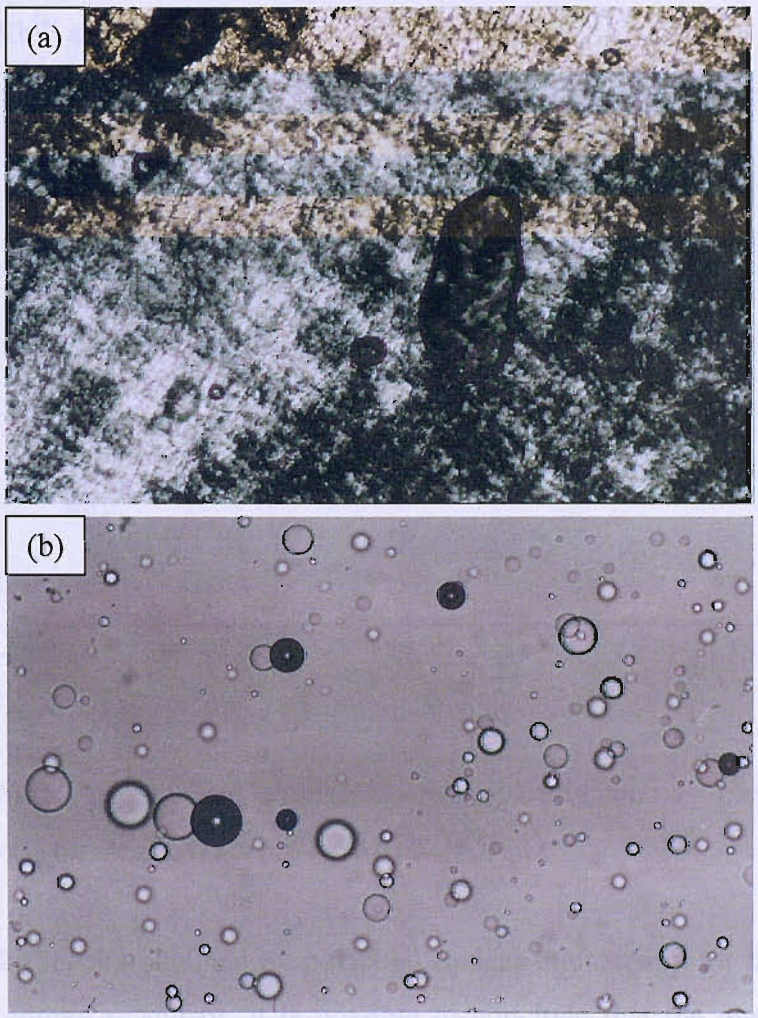

Figure 4.2 *Textures observed by polarised optical microscopy for a mixture containing 47 wt% $C_{16}EO_8$, 47 wt% 0.1 M H_2SO_4 and 6 wt% $CuSO_4.5H_2O$. (a) Hexagonal phase at 25 °C and (b) heterogeneous phase at 50 °C.*

Figure 4.3 shows an example of the small angle X-ray diffraction pattern obtained for mixture F after preparation and equilibration for 2 hours at room temperature, i.e., when the texture shown in Figure 4.2 (a) is present. The spectrum shows a main diffraction peak that corresponds to the (100) diffraction plane of the hexagonal structure and, once again, the *d* space of the lattice for the copper mixtures can be estimated using the Bragg equation (Equation 3.1). Considering the values of 2θ given in Table 4.2, the

estimated *d* spacing is 5.4, 5.6 and 5.3 nm for mixtures D, E and F, respectively. The pore centre to pore centre distance given by *d/cos* 30° was found to be 6.2 (mixture D), 6.5 (mixture E) and 6.1 nm (mixture F). These values are similar to those obtained previously in this study for mesoporous palladium and also to the values reported after deposition from the hexagonal lyotropic liquid crystalline phase formed by $C_{16}EO_8$ for mesoporous Rh[4] and Pt [5].

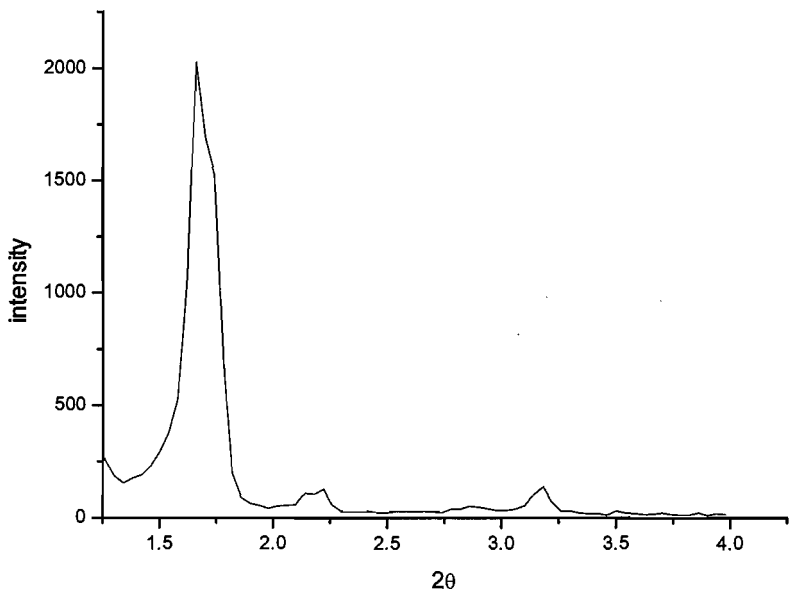

Figure 4.3 *Small angle X-ray diffraction from plating mixture containing 47 wt% $C_{16}EO_8$, 47 wt% 0.1 M H_2SO_4 and 6 wt% $CuSO_4.5H_2O$.*

Comparing the results obtained by polarised optical microscopy for the mixtures with and without copper precursor, it is possible to conclude that the presence of the salt reduces the stability of the hexagonal phase, as the phase is stable only to lower temperatures. From the diffraction pattern, the estimated *d* spacing is 4.8 and 5.2 nm for mixture A and B, respectively. And the pore centre to pore centre was found to be 5.5 (mixture A) and 6.1 (mixture B). These values are close to the ones reported in the presence of copper but, once again, and especially for the mixtures without acid, the presence of the metal seems to affect slightly the structure of the lyotropic liquid crystalline phase.

4.1.2- Electrodeposition and characterisation of copper films

The deposition of Cu films was carried out on Pt (d = 25 μm) and Au microdiscs (d = 60 μm), at 25 °C, stepping the potential from -0.2 to -0.5 V *vs* SMSE and holding the potential at a constant value until the desired charge has passed. At this stage, the

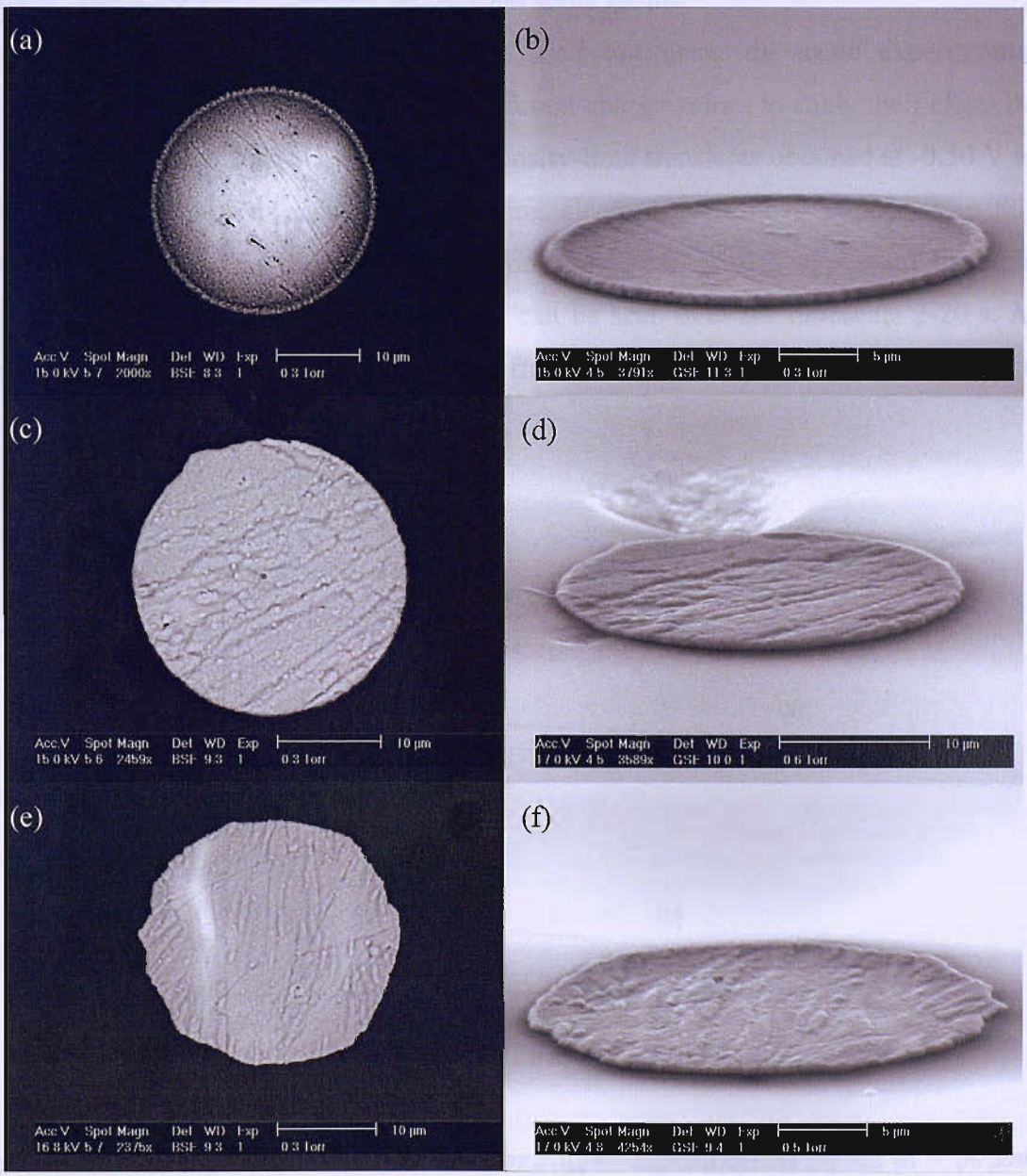

Figure 4.4 *SEM images of copper films on Pt microdiscs (d = 25 μm) obtained from different plating mixtures, stepping the potential from -0.2 to -0.5 V vs SMSE. (a) and (b) mixture C, deposition charge density = 0.73 C cm^{-2}; (c) and (d) mixture D, deposition charge density = 0.81 C cm^{-2}, (e) and (f) mixture E, deposition charge density = 0.81 C cm^{-2}. (a), (c) and (e) employ BSE detector with sample at 0° to the beam. (b), (d) and (f) employ GSE detector with sample at 75° to the beam.*

potential value for the deposition was chosen according to some previous results for copper deposition from 5 mM $CuSO_4.5H_2O$/ 0.1 M H_2SO_4 solution.

Figure 4.4 shows some of the deposits obtained from mixtures C, D and E on Pt. As it is possible to observe from the SEM images, the deposit from mixture C (lower copper concentration) shows an edge effect, but seems a bit smoother than the other two deposits, which are not so uniform and present some grains.

Copper deposition from mixture F was carried out using the same experimental conditions as described above, and trying different charge values to study their effect on the deposits. Figure 4.5 shows two current density-time transients obtained at -0.50 V *vs* SMSE for Pt and Au microelectrodes, during electrodeposition of copper from this plating mixture. At this potential, nucleation and phase growth appear to be rapid processes although some increase in current can be seen over the timescale 2-20 s. At longer times, the deposition appears to be diffusion controlled, since i α 1/r. Figure 4.6 shows the corresponded deposits.

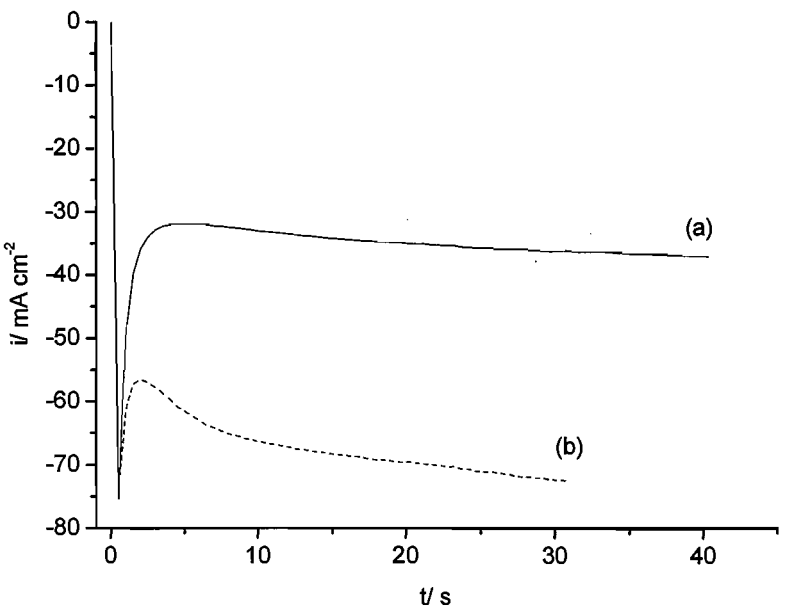

Figure 4.5 *Current density-time transients for copper deposition on (a) Au (d = 60 μm) and (b) Pt microdiscs (d = 25 μm) from plating mixture F. Potential step from -0.2 to -0.50 V vs SMSE, deposition charge density: (a) 1.41 C cm^{-2} and (b) 2.04 C cm^{-2}.*

In the presence of $CuSO_4.5H_2O$, the addition of acid to the plating mixture seems to have a positive effect on the stability of the hexagonal phase (comparing mixtures D and F) and it also seems to affect positively the quality of the deposits. From the top view

images, the film on Pt seems a bit grainier than the one on Au but, from the side pictures, both films look reasonably smooth and well adherent to the substrate.

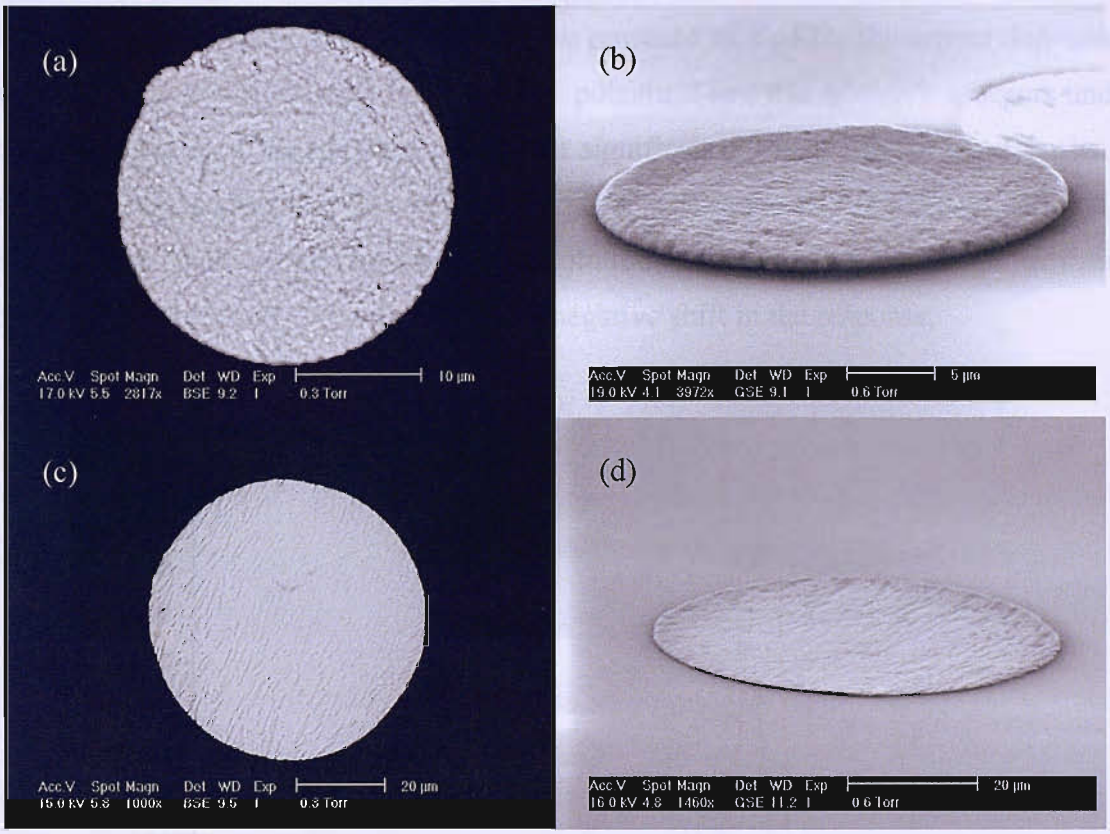

Figure 4.6 *SEM images of copper films deposited from mixture D on different substrates. (a) and (b) Pt (d = 25 µm), (c) and (d) Au microdisc (d = 60 µm). Potential step from -0.2 to -0.5 V vs SMSE. Deposition charge density: (a) and (b) 2.04 C cm^{-2}; (c) and (d) 1.41 C cm^{-2}. Images (a) and (c) employ BSE detector with sample at 0° to the beam. (b) and (d) employ GSE detector with sample at 75° to the beam.*

Considering the stability of the hexagonal phase in the mixture consisting of 47 wt% $C_{16}EO_8$, 47 wt% 0.1M H_2SO_4 and 6 wt% $CuSO_4.5H_2O$ and the quality of the deposits obtained, it was decided to study this plating mixture in more detail and, unless otherwise stated, all the results reported below correspond to this composition.

Figure 4.7 reports the electrochemical behaviour for a Pt microdisc (d = 25 µm) in the copper templating mixture, at 10 mV s^{-1}. As it is possible to observe, the copper deposition starts at -0.38 V and there is a very good charge balance between this process and the copper reoxidation. Indeed, the voltammogram has many of the features outlined for model systems in Section 1.3.3. For comparison, Figure 4.7 also shows the

electrochemical behaviour of the same microdisc in 5 mM $CuSO.5H_2O$/ 0.1 M H_2SO_4. As mentioned before, the potential value that has been used so far for the copper deposition (-0.5 V *vs* SMSE) was chosen based on the electrochemical behaviour of this last solution. However, it is clear that in the presence of $C_{16}EO_8$ the copper deposition starts to occur at significantly more positive potentials and that at -0.5 V it occurs under diffusion control, a situation that can affect significantly the quality of the deposits. It should be emphasised that the concentration of Cu(II) in the simple aqueous solution is much lower than in the liquid crystal solution; this leads to the lower diffusion controlled current and probably also to the negative shift in the response.

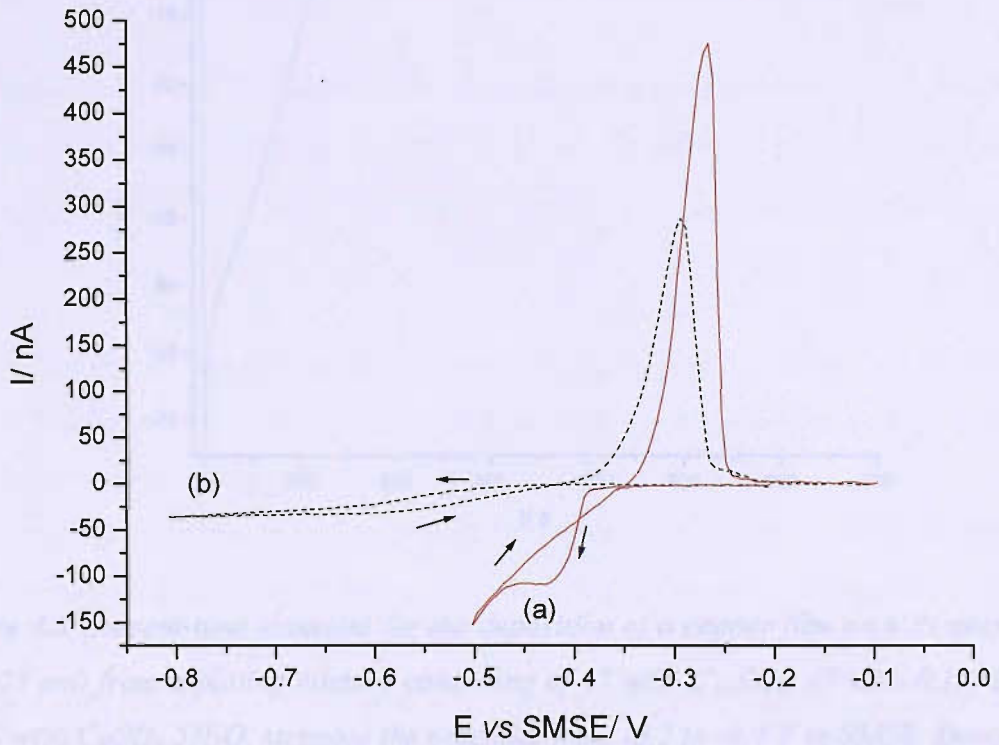

Figure 4.7 *Cyclic voltammogram for a Pt microdisc (d = 25 μm) in (a) a copper templating mixture consisting of 47 wt% $C_{16}EO_8$, 47 wt% 0.1M H_2SO_4 and 6 wt% $CuSO_4.5H_2O$ and (b) 5 mM $CuSO_4.5H_2O$/ 0.1 M H_2SO_4. Scan rate = 10 mV s^{-1}.*

Considering the results observed in Figure 4.7(a), some depositions were then carried out at -0.40 V *vs* SMSE, a potential where copper deposition still occurs under kinetic control. The current-time transients observed at this potential were significantly different from the ones obtained before for copper deposition, see Figure 4.8. Again, nucleation and growth are rapid processes but then a falling transient is observed. The

transient has the shape for the formation of a monolayer before the current drops to a very low value, but the charge passed (~1 C cm^{-2}) is far too large for a monolayer. It appears that deposition is passivated after the deposition of a layer of a certain thickness. Such passivation is consistent with the voltammogram in Figure 4.7, where diffusion controlled deposition is not maintained on the reverse scan. In addition, the quality of the deposits obtained at -0.40 V did not improve. The deposits seemed a bit loose and some areas of the Pt substrate were at best only thinly covered, see Figure 4.9. Considering these results, no further depositions were carried out at this potential.

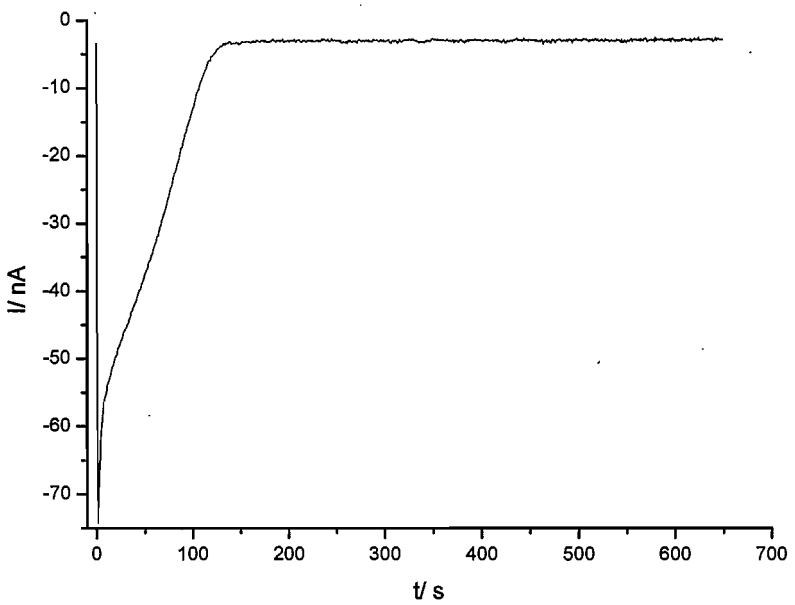

Figure 4.8 *Current-time transient for the deposition of a copper film on a Pt microdisc (d = 25 μm) from a plating mixture consisting of 47 wt% $C_{16}EO_8$, 47 wt% 0.1M H_2SO_4 and 6 wt% $CuSO_4.5H_2O$, stepping the potential from -0.2 to -0.4 V vs SMSE. Deposition charge density = 1.12 C cm^{-2}.*

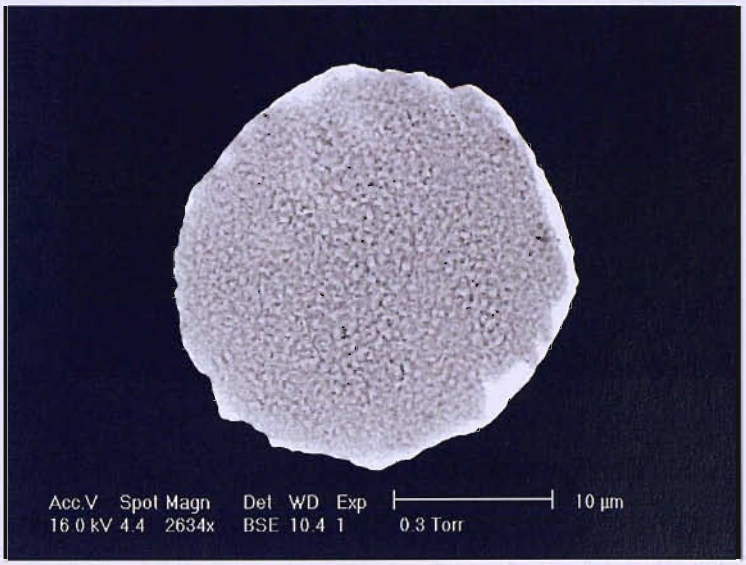

Figure 4.9 *SEM image of a copper film deposited on a Pt microdisc (d = 25 µm) from a plating mixture consisting of 47 wt% $C_{16}EO_8$, 47 wt% 0.1M H_2SO_4 and 6 wt% $CuSO_4.5H_2O$, stepping the potential from -0.2 to -0.4 V vs SMSE. Deposition charge density = 1.12 C cm^{-2}.*

Copper deposition was also carried out on evaporated gold substrate for low angle X-ray and TEM analysis. Figure 4.10 reports a current-time transient for copper deposition onto this substrate, stepping the potential from -0.2 to -0.5 V *vs* SMSE. As with microelectrodes, nucleation and growth of the copper film appear to be rapid processes and a falling transient towards to a steady state value, due to mass transport control is observed. SEM images of the deposit show the presence of a granular film, with small hemispheres deposited along the roughness lines of the gold substrate, see Figure 4.11. Figure 4.12 shows the diffraction pattern obtained for the copper film after cleaning overnight in 2-propanol. The main diffraction peak is now broader comparing with the diffraction peak obtained for the plating mixture, which reflects a more disorganised structure but, the maximum of the peak occurs at similar values. Considering $2\theta = 1.74$ the estimated *d* spacing for the lattice is 5.1 nm and the pore centre to pore centre distance is 5.8 nm. Both values are similar to the ones reported before for the plating mixture.

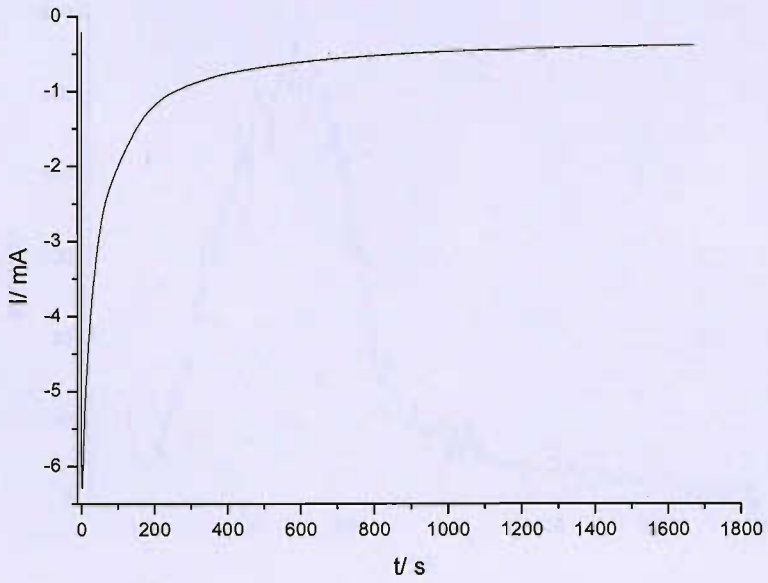

Figure 4.10 *Current-time transient for copper deposition on evaporated gold substrate (area = 0.9 cm^2) from plating mixture consisting of 47 wt% $C_{16}EO_8$, 47 wt% 0.1 M H_2SO_4 and 6 wt% $CuSO_4.5H_2O$. Deposition at -0.5 V vs SMSE. Deposition charge density = 1.4 C cm^{-2}.*

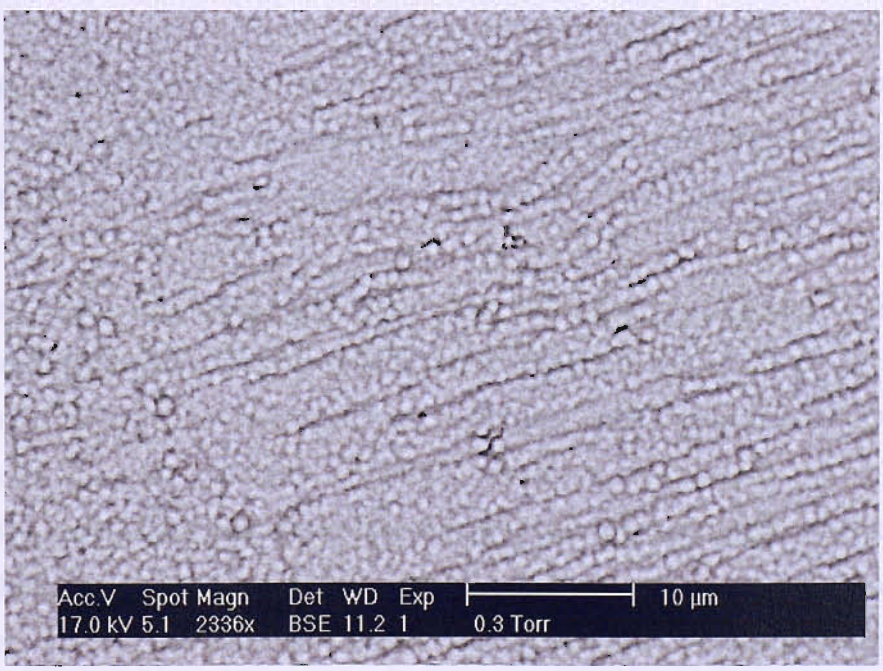

Figure 4.11 *SEM image of a copper film deposited on evaporated gold substrate (area = 0.9 cm^2) from plating mixture consisting of 47 wt% $C_{16}EO_8$, 47 wt% 0.1 M H_2SO_4 and 6 wt% $CuSO_4.5H_2O$. Deposition at -0.5 V vs SMSE. Deposition charge density = 1.4 C cm^{-2}.*

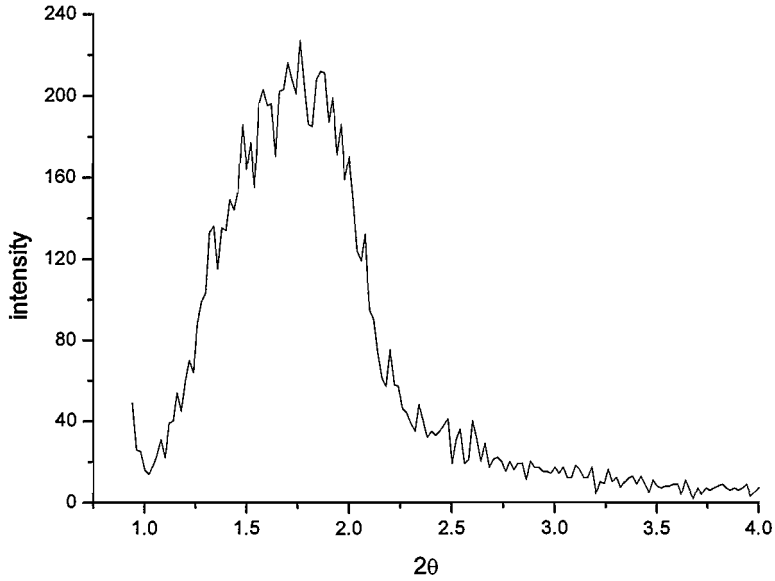

Figure 4.12 *Small angle X-ray diffraction of a copper film deposited on evaporated gold substrate from a plating mixture consisting of 47 wt% $C_{16}EO_8$, 47 wt% 0.1 M H_2SO_4 and 6 wt% $CuSO_4.5H_2O$. Deposition at -0.5 V vs SMSE. Deposition charge density = 1.4 C cm^{-2}.*

Despite the presence of the diffraction peak indicating some hexagonal arrangement in the film, it was not possible to observe a well defined pattern with TEM and the few pores observed in the structure were non-uniform and had a random distribution, see Figure 4.13.

Considering these results, a new templating bath was investigated. This time, a methanesulfonate medium was chosen for further experiments.

Methanesulfonic acid is becoming an emerging electrolyte choice within the electroplating industry because it offers excellent metal salt solubility, high conductivity, ease of effluent treatment, stability and low toxicity[6]. Methanesulfonic acid has already replaced industrial standard electrolytes such as fluoroboric acid for the electroplating of Sn/Pb solder and silver, nickel, zinc and copper electroplating are developing markets[7]. Besides these characteristics, methanesulfonic acid was chosen for further studies during this project since the anion is "more organic" and singly charged.

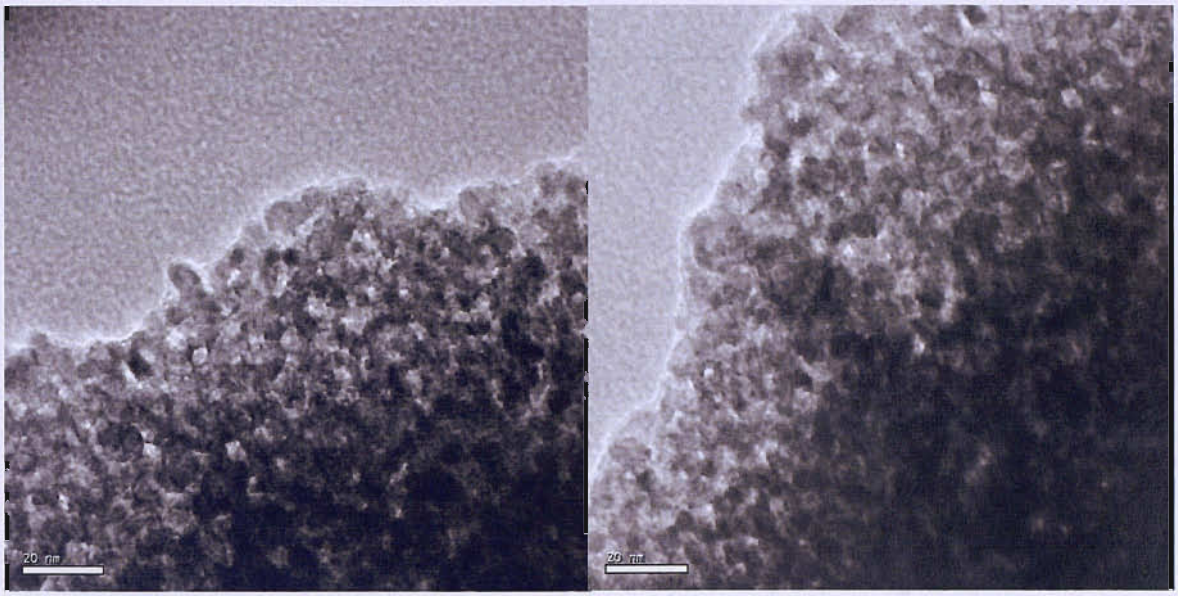

Figure 4.13 *TEM images of a copper film deposited on evaporated gold substrate from a plating mixture consisting of 47 wt% $C_{16}EO_8$, 47 wt% 0.1 M H_2SO_4 and 6 wt% $CuSO_4.5H_2O$. Deposition at -0.5 V vs SMSE. Deposition charge density = 1.4 C cm^{-2}.*

4.2- Preparation and Characterisation of Copper Films from an Acidic Bath containing $Cu(CH_3SO_3)_2$ and $C_{16}EO_8$

4.2.1- Preparation and characterisation of the copper plating mixture

Considering some preliminary results obtained with a mixture of $C_{16}EO_8$ and 0.2 M $Cu(CH_3SO_3)_2$/ 0.1 M CH_3SO_3H solution, it was decided to study the phase diagram for this system in more detail. Several plating mixtures with the compositions indicated in Figure 4.14 were prepared and the different phases were characterised by polarised optical microscopy. Samples from the different plating mixtures were pressed between two glass slides, warmed up at 5 °C min^{-1} to a maximum temperature of 80 °C, and cooled down, at the same rate, to 25 °C. This heating/ cooling cycle was done to confirm the temperature for the different phase transitions. The maximum temperature of 80 °C was chosen to minimize water evaporation from the plating mixtures.

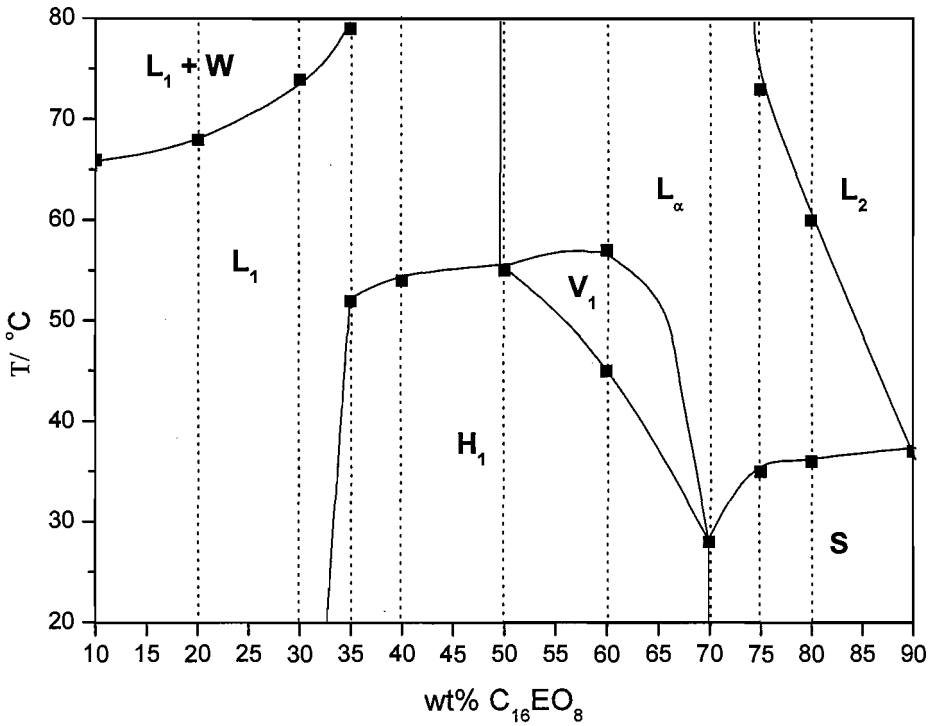

Figure 4.14 *Phase diagram for the system $C_{16}EO_8$ + 0.2 M $Cu(CH_3SO_3)_2$/ 0.1 M CH_3SO_3H. The compositions studied are indicated by a dashed line and the points where a phase transition was observed are indicated by a squared dot (▪). The solid lines are guides to the eye. L_1 = micellar solution, W = water, H_1 = hexagonal phase, V_1 = cubic phase, L_α = lamellar phase, L_2 = surfactant liquid and S = solid.*

For the system studied here, the identification of the phases became more complex with increasing surfactant concentration (especially above 70 wt%), with the heating and cooling cycles giving different temperatures for the phase transitions and also textures that were not always easy to recognize. To help with the identification of the different phases, several mixtures of $C_{16}EO_8$ and water only were prepared, studied by polarised optical microscopy and the results compared with the phase diagram published by Mitchell[8]. In this way, it was possible to recognize more easily the phases for the copper system. Figure 4.14 shows the phase diagram obtained. The hexagonal phase (H_1) is stable from 35 wt% $C_{16}EO_8$ up to compositions with 70 wt% of surfactant, in a temperature range that goes from 20 °C up to 55 °C for some compositions. A typical texture for the hexagonal phase can be seen in Figure 4.15.

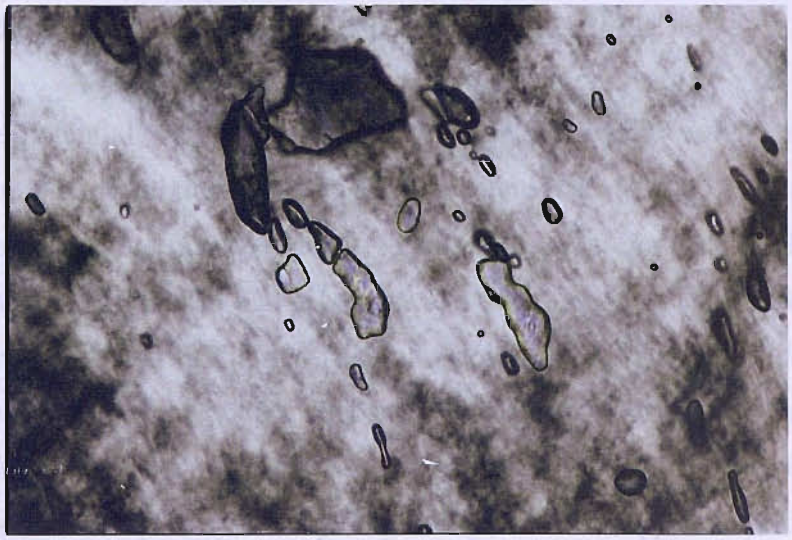

Figure 4.15 *Texture of the hexagonal phase from a plating mixture containing 50 wt% $C_{16}EO_8$ and 50 wt% 0.2 M $Cu(CH_3SO_3)_2$/ 0.1 M CH_3SO_3H. Picture taken at 25 °C.*

The small angle X-ray diffraction pattern for a mixture consisting of 50 wt% $C_{16}EO_8$ and 50 wt% 0.2 M $Cu(CH_3SO_3)_2$/ 0.1 M CH_3SO_3H shows the typical diffraction peak corresponding to the (100) diffraction plane of the hexagonal structure at $2\theta = 1.76$ and two smaller peaks at 2.11 and 3.43, see Figure 4.16.

Unless otherwise stated, all the results shown below were obtained with this composition.

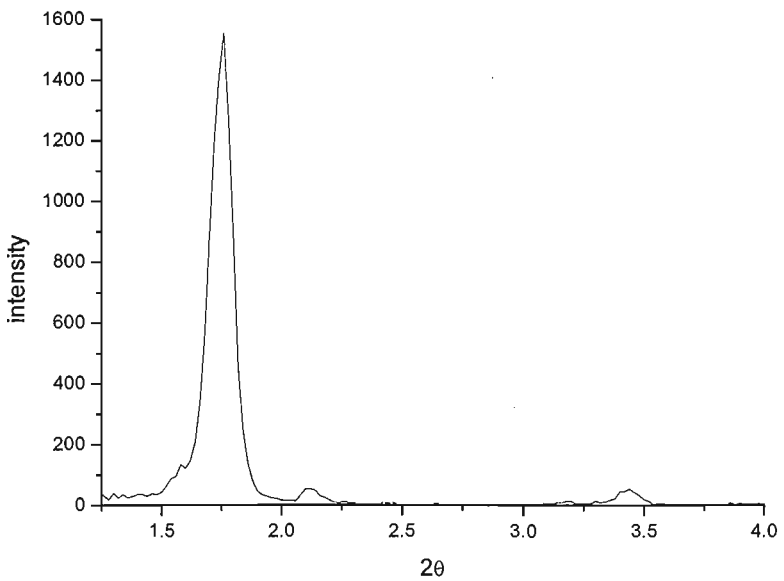

Figure 4.16 *Small angle X-ray diffraction of a plating mixture containing 50 wt% $C_{16}EO_8$ and 50 wt% 0.2 M $Cu(CH_3SO_3)2$/ 0.1 M CH_3SO_3H.*

4.2.2- Electrodeposition and characterisation of copper films

To select the potential for Cu deposition, a series of cyclic voltammograms were obtained in the plating mixture with Pt and Au microdiscs (d = 25 μm) and also with evaporated gold substrate (area ~ 1 cm^2). For Pt and Au microdiscs, the Cu deposition commences at -0.4 V *vs* SMSE and gives rise to a very well defined reduction wave and nucleation loop, as shown in Figure 4.17, for a gold microdisc. A good charge balance can be observed between the copper deposition and stripping peaks, but the latter seems to be a combination of two processes. A closer look at the deposition process reveals a minor feature occurring at the very beginning of the copper deposition in both substrates, see Figure 4.18, but this cannot be related to the presence of the two peaks in the backward scan, since they only appear if the potential is taken more negative than -0.8 V *vs* SMSE. This initial feature is also present in the voltammogram recorded with the evaporated gold substrate, see Figure 4.19, appearing as a shoulder to the main peak, at around -0.45 V. No clear explanation can be given at the moment for its presence, but it is possible that it might be related with some complexation occurring between Cu^{2+} and the surfactant. The presence of some Cl^- impurity in the $C_{16}EO_8$ also cannot be ruled out.

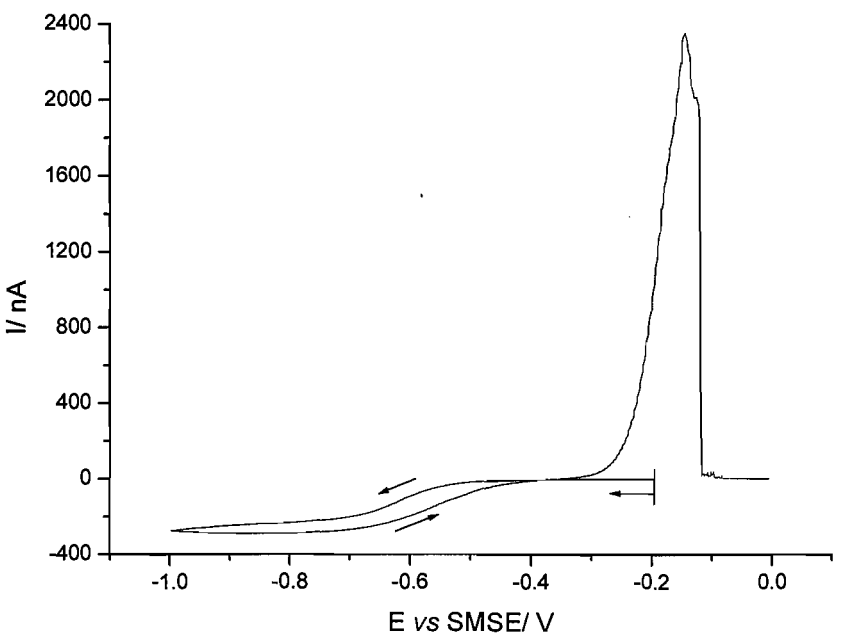

Figure 4.17 *Cyclic voltammetry for a Au microdisc (d = 25 μm) in a plating mixture containing 50 wt% $C_{16}EO_8$ and 50 wt% 0.2 M $Cu(CH_3SO_3)_2$/ 0.1 M CH_3SO_3H. Scan rate 10 mV s^{-1}.*

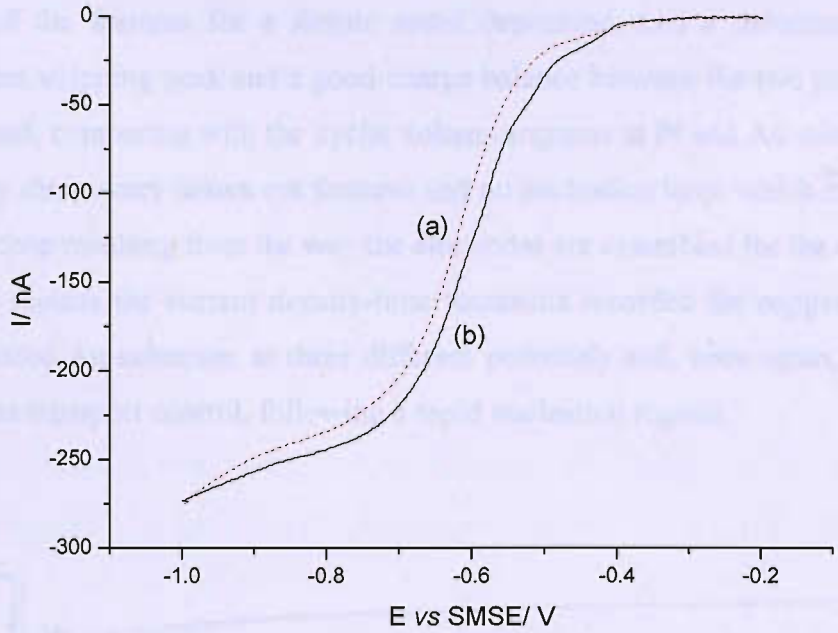

Figure 4.18 *Forward scans for (a) Au and (b) Pt microdiscs (d = 25 μm) in a plating mixture containing 50 wt% $C_{16}EO_8$ and 50 wt% 0.2 M $Cu(CH_3SO_3)_2$/ 0.1 M CH_3SO_3H. Scan rate = 10 mV s^{-1}.*

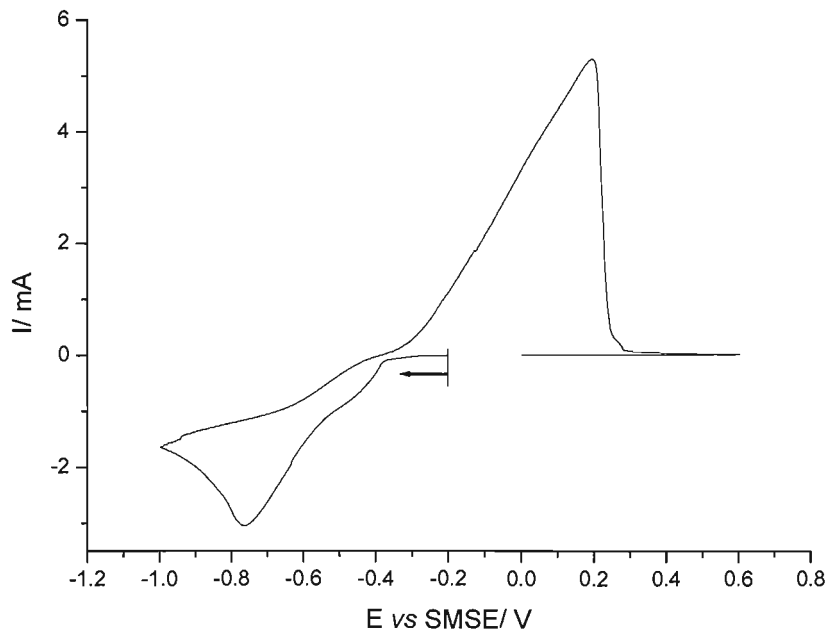

Figure 4.19 *Cyclic voltammetry for evaporated gold substrate (area = 0.52 cm^2) in a plating mixture containing 50 wt% $C_{16}EO_8$ and 50 wt% 0.2 M $Cu(CH_3SO_3)_2$/ 0.1 M CH_3SO_3H. Scan rate = 10 mV s^{-1}.*

Once again, it should be noted that the voltammogram at the larger gold film electrode has many of the features for a simple metal deposition, i.e., a reduction peak, the correspondent stripping peak and a good charge balance between the two processes. On the other hand, comparing with the cyclic voltammograms at Pt and Au microdiscs, the voltammetry shows very drawn out features and no nucleation loop, which might be due to some IR drop resulting from the way the electrodes are assembled for the deposition. Figure 4.20 reports the current density-time transients recorded for copper deposition onto evaporated Au substrate, at three different potentials and, once again, the current tends to mass transport control, following a rapid nucleation regime.

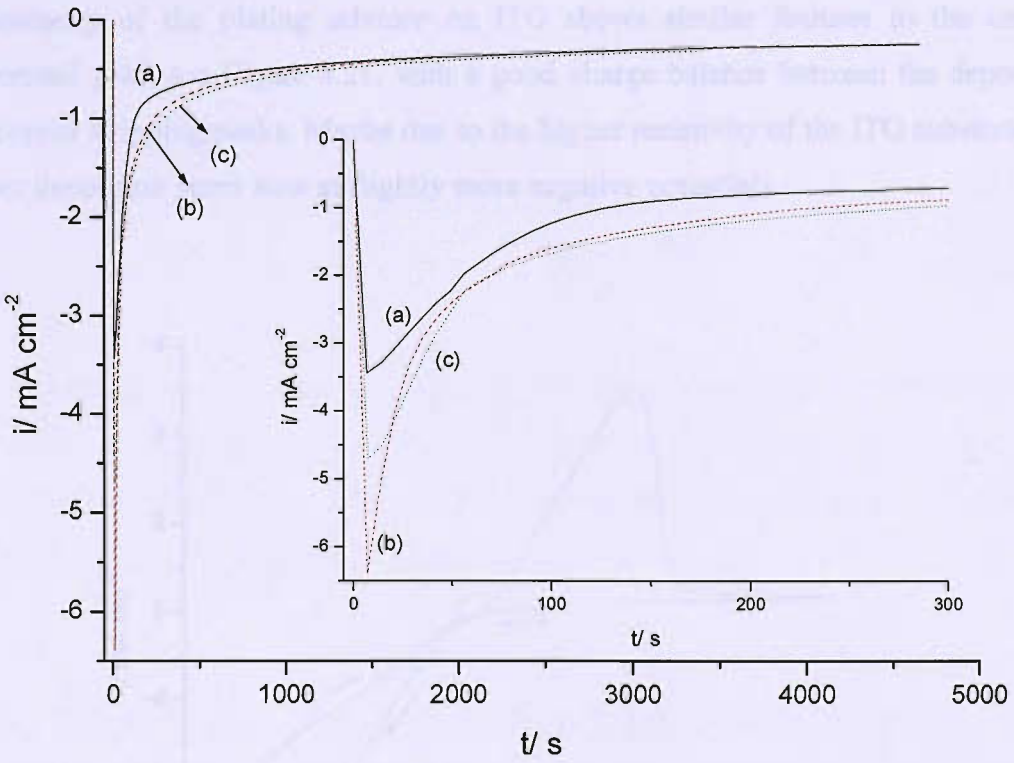

Figure 4.20 *Current density-time transients for copper deposition onto evaporated gold substrates (area ~0.5 cm^2), stepping the potential from -0.20 V to (a) -0.50, (b) -0.60 and (c) -0.65 V vs SMSE. Deposition charge density = 2 C cm^{-2}. Plating mixture containing 50 wt% $C_{16}EO_8$ and 50 wt% 0.2 M $Cu(CH_3SO_3)_2$/ 0.1 M CH_3SO_3H. The inset shows the first 300 s for the three transients.*

After deposition, the copper films were soaked overnight in 2-propanol. This cleaning with 2-propanol took place because previous cleaning with water seemed to trigger a change in colour of the copper deposit and this was taken as an indication that corrosion of the copper was occurring.

By eye, the copper deposits on the evaporated gold substrate looked shiny and well adherent to the substrate, but not covering it completely.

Small angle X-ray diffraction from these deposits did not reveal the presence of any structure and it was possible to observe only a strong background due to the gold substrate for 2θ values ~1.

To avoid the presence of a strong background signal interfering with the pattern from the mesoporous film, some depositions were also carried out on ITO substrate. The voltammetry of the plating mixture on ITO shows similar features to the one on evaporated gold, see Figure 4.21, with a good charge balance between the deposition and copper stripping peaks. Maybe due to the higher resistivity of the ITO substrate, the copper deposition starts now at slightly more negative potentials.

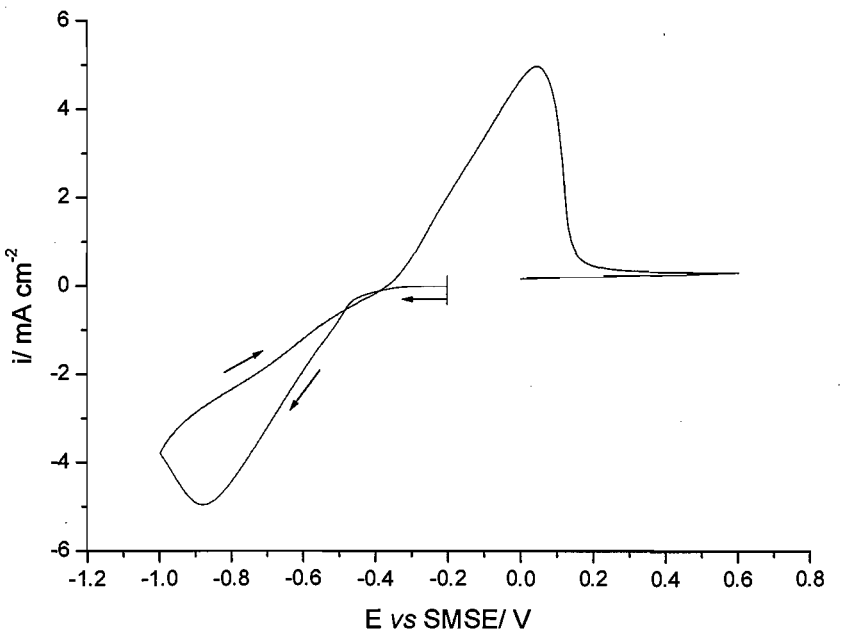

Figure 4.21 *Cyclic voltammetry for ITO substrate (a ~ 0.5 cm^2) in a plating mixture containing 50 wt% $C_{16}EO_8$ and 50 wt% 0.2 M $Cu(CH_3SO_3)_2$/ 0.1 M CH_3SO_3H. Scan rate 10 mV s^{-1}.*

Figure 4.22 shows the current density–time transients for copper deposition on ITO substrate, at two different potentials. Once again, and despite the difference of 100 mV in the deposition potentials, the current tends to the same steady state value in both cases.

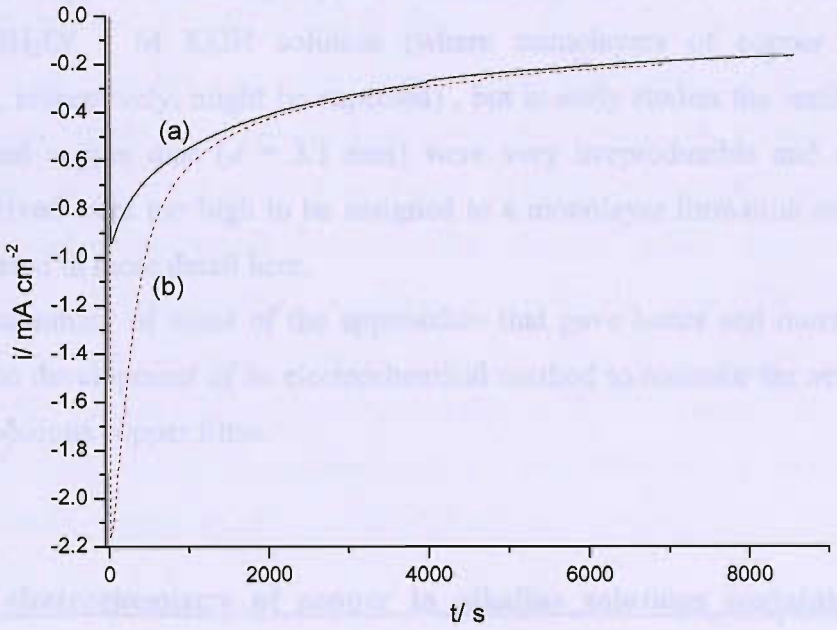

Figure 4.22 *Current density-time transients for copper deposition on ITO substrate (a ~0.5 cm^2), stepping the potential from -0.2 V to (a) -0.5 and (b) -0.6 V vs SMSE. Deposition charge density = 3 C cm^{-2}. Plating mixture containing 50 wt% $C_{16}EO_8$ and 50 wt% 0.2 M $Cu(CH_3SO_3)_2$/ 0.1 M CH_3SO_3H.*

Despite clear evidence for the presence of the hexagonal phase in the plating mixture, small angle X-ray diffraction from the copper films deposited on ITO substrate also did not reveal the presence of the hexagonal arrangement in the final structure.

Since evidence for mesoporous copper structures was elusive, some electrochemical procedures to determine the surface area were investigated.

4.3- Electrochemical Characterisation of High Surface Area Copper Films

Several approaches were carried out to evaluate the electroactive surface area of high surface area copper, including cyclic voltammetry in 1 M KOH and 0.1 M $K_4Fe(CN)_6.3H_2O$/ 1 M KOH solution (where monolayers of copper oxide and $Cu_2Fe(CN)_6$, respectively, might be expected) , but in early studies the results obtained for a polished copper disc (d = 3.1 mm) were very irreproducible and mainly, the charges involved were too high to be assigned to a monolayer formation and they will not be discussed in more detail here.

Below is a summary of some of the approaches that gave better and more promising results for the development of an electrochemical method to measure the active surface area of mesoporous copper films.

4.3.1- The electrochemistry of copper in alkaline solutions containing sodium sulphide

Chialvo *et al.*[9] have studied the electrochemical behaviour of copper in alkaline solutions containing sodium sulphide and a density charge of 130 $\mu C\ cm^{-2}$ was reported for a pair of voltammetric peaks observed between -1.2 and -0.5 V (*vs* NHE). These peaks were assigned to the electroformation and electroreduction of a Cu_2S monolayer, following Reaction 4.2:

$$2Cu + S^{2-} \rightleftharpoons Cu_2S + 2e^- \qquad (4.2)$$

Scharifker *et al.*[10] also investigated the electrodeposition of copper sulphide on copper and a similar pair of peaks was reported for the formation and reduction of a Cu_2S film. The film does not passivate the surface and the fact that the charge ratio for the process was found to be close to 1 and independent of pH (in the range 8-14), of sweep rate and of sulphide concentration, shows that no appreciable dissolution of the electrode or of the film takes place in the potential region studied (-1.2 to -0.5 V *vs* SCE).

To verify if it was possible to observe a pair of peaks that could be assigned to the formation of a monolayer and, consequently, give the active area for high area copper, some experiments were carried out initially at a copper disc (d = 3.1 mm). The voltammetry was first recorded in 0.1 M $NaHCO_3$/ 0.1 M Na_2CO_3 and after in the presence of 1mM Na_2S. In the presence of Na_2S, a new pair of peaks is observed between -1.2 and -0.7 V *vs* SCE, see Figure 4.23. Both peaks increase slightly with number of scans, but become stable after 3 or 4 consecutive cycles. Before each voltammogram, the potential was held at -1.4 V for 10 seconds to ensure complete removal of any film formed on the copper surface. Without this initial delay at a more negative potential, the current for the anodic peak was much smaller and, in some cases, it was not even possible to observe the peak in the first forward scan. The absence of the anodic peak can be due to the spontaneous formation of a copper sulphide layer at open circuit, an effect that has been reported in different studies[9-11]. Holding the potential at -1.4 V for 10 seconds gave reproducible results and the voltammogram of Figure 4.23 is consistent with the formation of a copper sulphide layer as reported by Chialvo *et al.*[9] and Scharifker *et al.*[10]

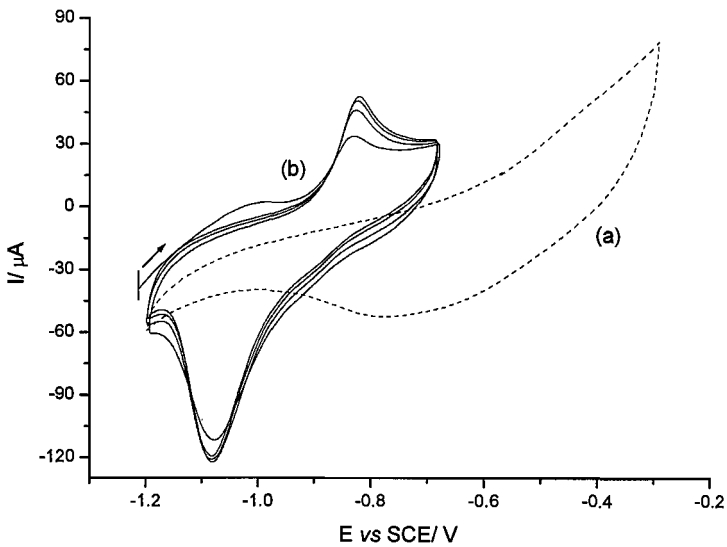

Figure 4.23 *Cyclic voltammograms recorded at a polished Cu disc (d = 3.1 mm) in (a) 0.1 M $NaHCO_3$/ 0.1M Na_2CO_3 and (b) 1mM Na_2S + 0.1 M $NaHCO_3$/ 0.1 M Na_2CO_3 solution, at 200 mV s^{-1}.*

The effect of scan rate was studied and Figure 4.24 shows the first voltammogram recorded at 50, 100 and 200 mV s^{-1}.

The charges associated with both peaks were calculated, considering the first scan recorded for each scan rate and allowing for charging current. The results obtained for the charge densities are bigger than the value of 130 μC cm^{-2} reported by Chialvo[9] however, they are within the values expected for a monolayer formation at an imperfectly flat surface, see Table 4.3. While the peak currents could be proportional to potential scan rate, it is evident that positive to the anodic peak the current does not drop to zero, indicating that the anodic film continues to thicken or further oxidation is occurring.

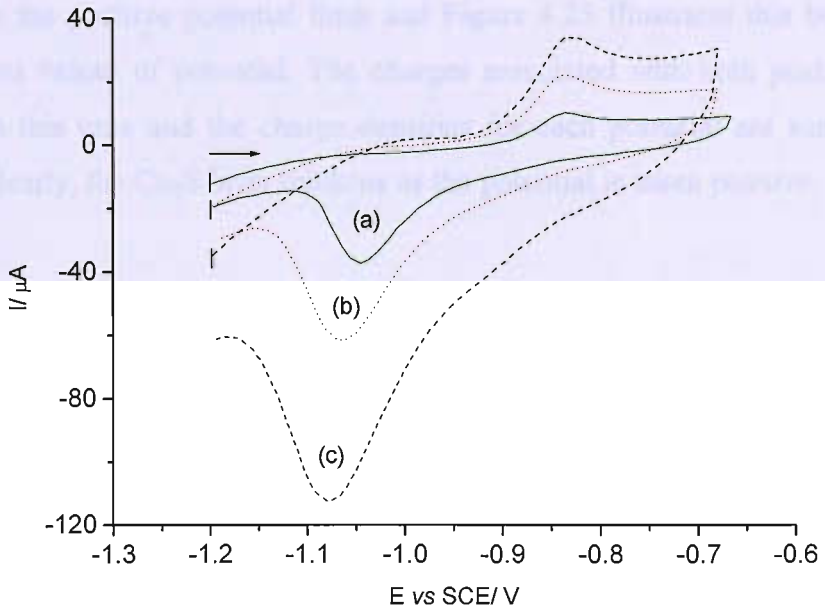

Figure 4.24 *Cyclic voltammograms recorded at a Cu disc (d = 3.1 mm) in 1mM Na_2S + 0.1 M $NaHCO_3$/ 0.1 M Na_2CO_3 solution, at (a) 50, (b) 100 and (c) 200 mV s^{-1}. First recorded cycle is shown.*

Table 4.3 *Charge densities associated with the anodic and cathodic peaks observed at a Cu disc (d = 3.1 mm) in 1 mM Na_2S + 0.1 M $NaHCO_3$/ 0.1 M Na_2CO_3, at different scan rates.*

Scan rate/ mV s^{-1}	Density charge/ μC cm^{-2} (a)		$q_{anodic}/ q_{cathodic}$
	Anodic peak	Cathodic peak	
50	450	442	1.0
100	411	405	1.0
200	358	355	1.0

(a)These values are averages of three different voltammograms obtained for each scan rate.

Moreover, during the experiments with Na_2S it was observed that the cathodic current depended on the positive potential limit and Figure 4.25 illustrates this behaviour for three different values of potential. The charges associated with both peaks were also calculated in this case and the charge densities for each potential are summarized in Table 4.4. Clearly, the Cu_2S layer thickens as the potential is taken positive.

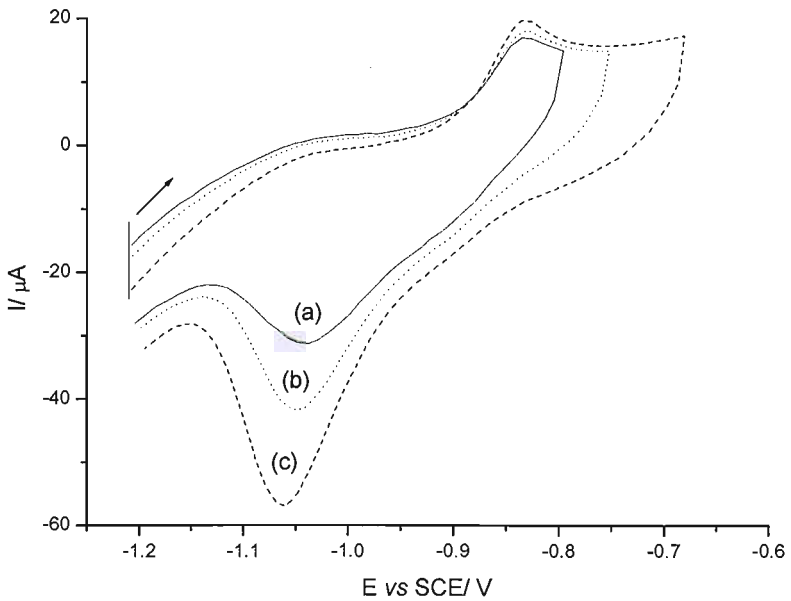

Figure 4.25 *Cyclic voltammograms recorded at a Cu disc (d = 3.1 mm) in 1mM Na_2S + 0.1 M $NaHCO_3$/ 0.1 M Na_2CO_3 solution for different positive potential limits: (a) -0.80, (b) -0.76 and (c) -0.68 V vs SCE. Scan rate = 100 mV s^{-1}. First recorded cycle is shown.*

Table 4.4 *Charge densities associated with the anodic and cathodic peaks observed at a Cu disc (d = 3.1 mm) for 1 mM Na_2S + 0.1 M $NaHCO_3$/ 0.1 M Na_2CO_3, for different positive potential limits. Scan rate = 100 mV s^{-1}.*

Positive potential limit/ V	Density charge/ μC cm^{-2}		$q_{anodic}/ q_{cathodic}$
	Anodic peak	Cathodic peak	
-0.80	151	147	1.0
-0.76	246	225	1.1
-0.68	411	405	1.0

Hence, the estimation of surface area using this solution would require an assumption of the potential where "a monolayer is complete" and the assumption that this potential is independent of surface structure. In addition, measurements at a highly porous surface would necessitate the use of a much more concentrated sulphide solution because of the low pore volume/ pore surface area ratio and the consequent limited availability of sulphide within a pore. On the other hand, a higher sulphide concentration leads to the possibility of multilayer copper sulphide formation. The alternative approach with porous structures is only to carry out long timescale experiments so that diffusion from the bulk solution to the pores does not limit the response.

4.3.2- Underpotential deposition of lead on copper

The underpotential deposition (UPD) of metals, i.e., the formation of metal (sub)monolayers positive to the equilibrium potential, is generally regarded as a reaction very sensitive to the surface structure of the electrode, since it depends on the specific interaction between the surface atoms of the supporting metal and the atoms of the deposited metal[12, 13]. In this way, metal UPD can be used to characterise the surface structure of the electrode and was also studied as a possible method to measure the copper surface area.

4.3.2.1- UPD of lead on copper discs

The underpotential deposition of lead on Cu(100) and Cu(111) single crystal surfaces has been studied by some authors[14-16] and it has been shown that the voltammetric profiles depend on the crystallographic orientation of the surface (different sites have different energies for adsorption) and also on the presence of chloride in the solution, with the peaks becoming sharper and more reversible when the concentration of Cl^- increases. For each copper single crystal surface it is possible to get a very well resolved pair of peaks for the UPD of lead, but no studies have so far been reported on a polycrystalline surface. Hernández[12] has reported the UPD of lead on a polyorientated gold electrode and it is possible to observe in the voltammetry the contribution from three different facets, namely, Au(100), Au(110) and Au(111), so maybe a similar situation can be expected for a polycrystalline copper surface.

The deposition of lead on a copper disc (d = 3.1 mm) was carried out in 6 mM Pb^{2+}/ 0.6 M $HClO_4$ and 60 mM Pb^{2+}/ 0.6 M $HClO_4$ solutions, at different scan rates, and holding the initial potential for 50 s to allow for the initial current to stabilize. The higher Pb^{2+} concentration was selected to increase the availability of this reactant within a porous structure. Figure 4.26 shows the lead bulk deposition starting at –0.48 V and giving rise to a reduction peak with the shape expected for a diffusion controlled reaction. On the

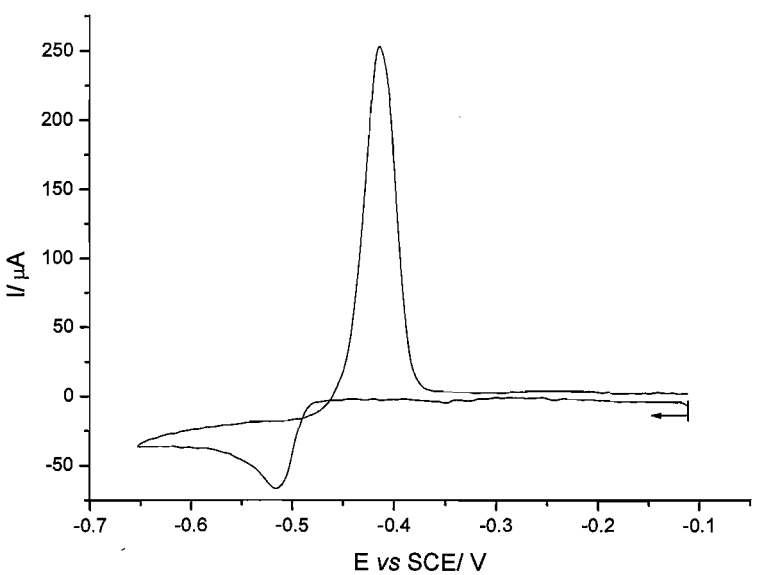

Figure 4.26 *Cyclic voltammetry of a copper disc (d = 3.1 mm) in 6 mM Pb^{2+}/ 0.6 M $HClO_4$. Scan rate = 10 mV s^{-1}.*

reverse scan, a typical nucleation loop is observed, together with a sharp stripping peak at -0.42 V *vs* SCE. A reasonable charge balance between reduction and oxidation processes is obtained.

When the current sensitivity is increased substantially, the UPD of lead can be seen to occur at significantly more positive potentials, with peaks very well resolved from the bulk deposition, see Figure 4.27. In this case, the reduction of lead seems to show two overlapping symmetrical but rather broad peaks, with maxima at -0.30 and -0.33 V, respectively, and a broad oxidation peak at -0.26 V. The two reduction peaks could be assigned to lead UPD at different sites, but the presence of only one stripping peak would be surprising. A significant potential separation between the deposition and stripping peaks for lead UPD has been found even for single copper crystals, which according to Chu[16] is due to slow kinetics of the monolayer deposition process. The difference of ~0.07 V observed in this work could have a similar explanation.

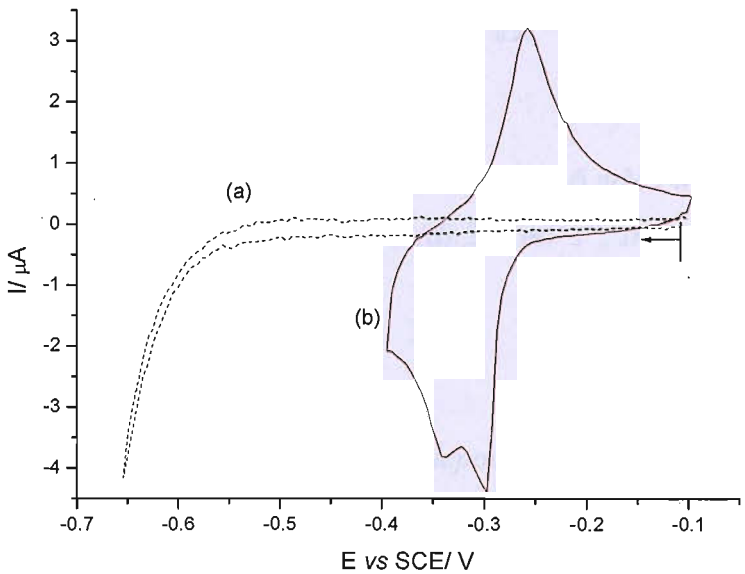

Figure 4.27 *(a) Cyclic voltammetry of a copper disc (d = 3.1 mm) in 0.6 M $HClO_4$ and (b) UPD of lead on the same copper disc in 6 mM Pb^{2+}/ 0.6 M $HClO_4$. Scan rate = 10 mV s^{-1}. Initial potential was held at -0.1 V for 50 s.*

Figure 4.28 shows the cyclic voltammograms recorded for a 6 mM Pb^{2+}/ 0.6 M $HClO_4$ solution at different scan rates and Table 4.5 summarizes the charge density values associated with the deposition (q_c) and stripping (q_a) processes for two different concentrations of lead. As it is possible to observe, there is a good linearity between

current and scan rate and the charges under the UPD peaks are, within experimental error, independent of the scan rate and metal concentration, as expected for the deposition of an underpotential layer.

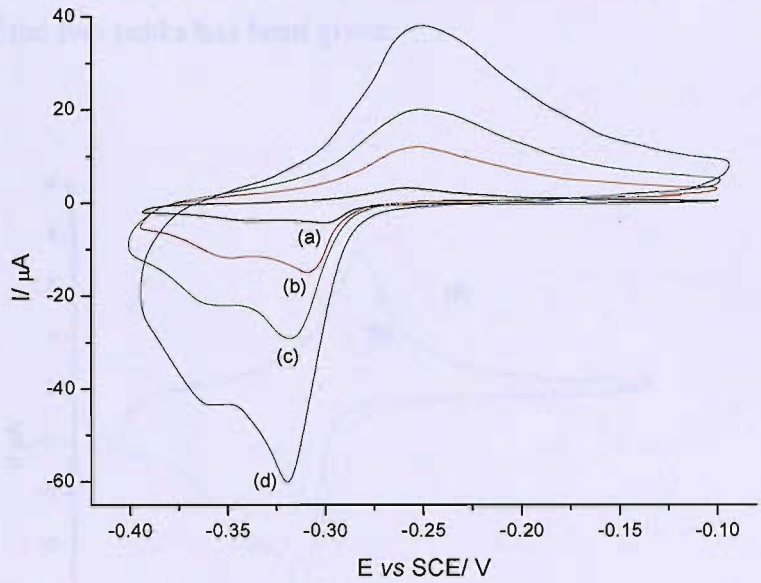

Figure 4.28 *UPD of lead on a copper disc (d = 3.1 mm) in 6 mM Pb^{2+}/ 0.6 M $HClO_4$, at different scan rates: (a) 10, (b) 50, (c) 100 and (d) 200 mV s^{-1}. Initial potential was held at -0.1 V for 50 s.*

Table 4.5 *Charge densities associated with the deposition (q_c) and stripping (q_a) peaks for lead UPD on a copper disc (d = 3.1 mm) in two different concentrations of Pb^{2+}, at different scan rates.*

	10 mV s^{-1}		50 mV s^{-1}		100 mV s^{-1}		200 mV s^{-1}	
Concentration	q_c μC cm^{-2}	q_a μC cm^{-2}	q_c μC cm^{-2}	q_a μC cm^{-2}	q_c μC cm^{-2}	q_a μC cm^{-2}	q_c μC cm^{-2}	q_a μC cm^{-2}
6 mM Pb^{2+}/ 0.6 M $HClO_4$	350	297	287	268	265	270	258	237
60 mM Pb^{2+}/ 0.6 M $HClO_4$	354	288	332	334	297	278	244	221

To verify if the two superimposed peaks in the cathodic region were due to some impurity in the electrolyte, a 60 mM Pb^{2+} solution was prepared with highly pure $HClO_4$ (GFS chemicals) and the voltammetry compared with the one obtained previously,

using reagent grade perchloric acid. As it is possible to observe, see Figure 4.29, there is a small decrease in current when the highly pure $HClO_4$ is used, but the purity of the electrolyte does not seem to affect the shape of the voltammogram, and the overlapping of the two peaks in the deposition process occurs in both cases. A similar behaviour has been reported[14] for Pb UPD on Cu(111) in the absence of Cl^-, but no explanation for the presence of the two peaks has been given.

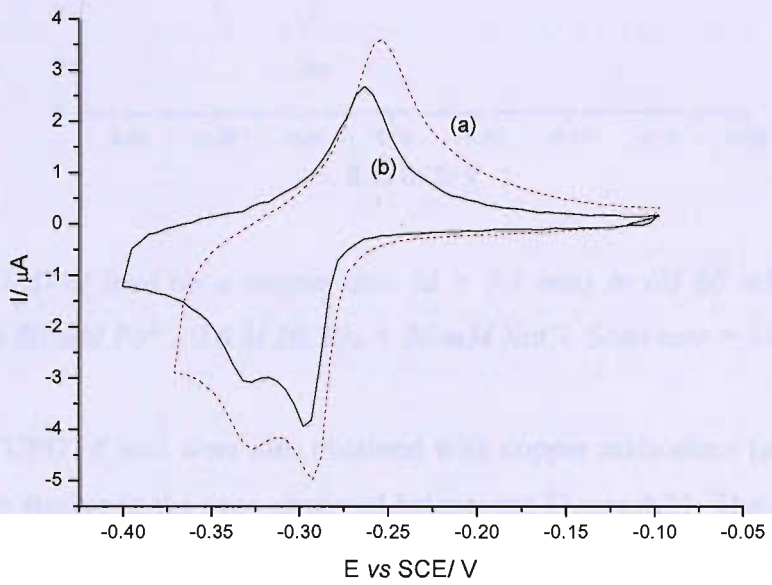

Figure 4.29 *UPD of lead on a copper disc (d = 3.1 mm) in 60 mM Pb^{2+}/ 0.6 M $HClO_4$. (a) Reagent grade and (b) highly pure $HClO_4$. Scan rate = 10 mV s^{-1}. Initial potential was held at -0.1 V for 50 s.*

Brisard[15] and Chu[16] have shown that the presence of chloride can interfere considerably with the voltammetry for lead UPD, with the peaks becoming sharper and the current densities increasing significantly upon addition of chloride. This way, the difference in current observed in Figure 4.29 may be due to the presence of some chloride in the reagent grade $HClO_4$. To study this possibility, some NaCl was added to a solution of lead prepared with highly pure perchloric acid and the results are shown in Figure 4.30. The presence of Cl^- does not seem to affect significantly the sharpness neither the position of the peaks in the present case, but there is in fact a small increase in the current.

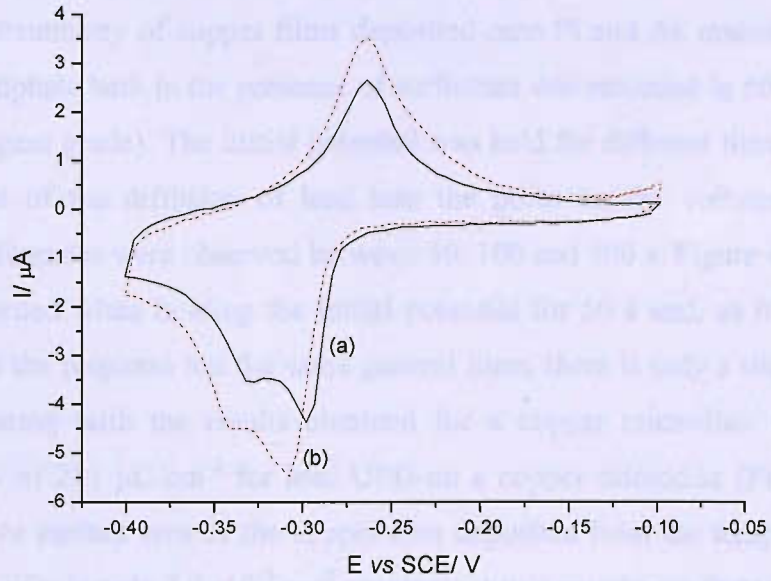

Figure 4.30 *UPD of lead on a copper disc (d = 3.1 mm) in (a) 60 mM Pb^{2+}/ 0.6 M $HClO_4$ and (b) 60 mM Pb^{2+}/ 0.6 M $HClO_4$ + 30 mM NaCl. Scan rate = 10 mV s^{-1}.*

The peaks for UPD of lead were also obtained with copper microdiscs (d = 50 μm) and the features are similar to the ones observed before, see Figure 4.31. The charge balance is not as good as for normal size electrodes (q_c = 281 μC cm^{-2} and q_a = 185 μC cm^{-2}), however, the charge density values are still in good agreement with the formation of a monolayer of lead.

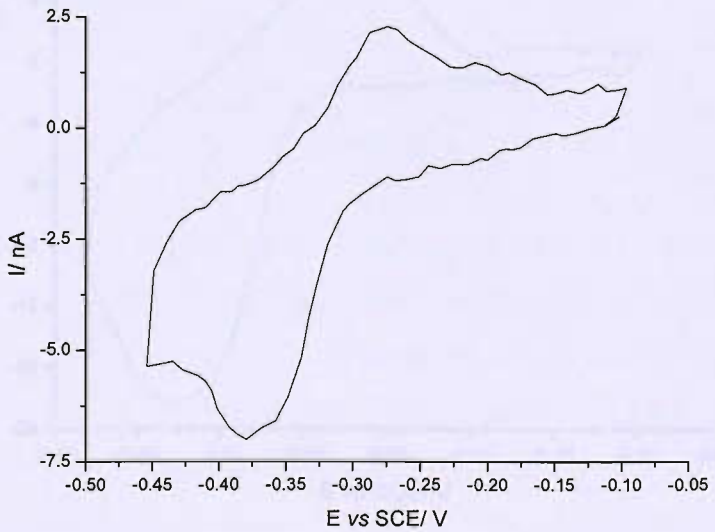

Figure 4.31 *UPD of lead on a copper microdisc (d = 50 μm) in 60 mM Pb^{2+}/ 0.6 M $HClO_4$ (reagent grade). Scan rate = 100 mV s^{-1}.*

4.3.2.2- UPD of lead on electrodeposited copper films

The cyclic voltammetry of copper films deposited onto Pt and Au microdiscs from the copper acid sulphate bath in the presence of surfactant was recorded in 60 mM Pb^{2+}/ 0.6 M $HClO_4$ (reagent grade). The initial potential was held for different times to study any possible effect of the diffusion of lead into the pores on the voltammetry, but no significant differences were observed between 50, 100 and 500 s. Figure 4.32 shows the first scan recorded when holding the initial potential for 50 s and, as it is possible to observe, while the response has the same general form, there is only a slight increase in current comparing with the results obtained for a copper microdisc. Considering a charge density of 281 $\mu C\ cm^{-2}$ for lead UPD on a copper microdisc (Figure 4.31) the estimated active surface area of the copper film deposited from the templating mixture containing $C_{16}EO_8$ is only $5.7\times10^{-5}\ cm^2$ (equivalent to a roughness factor of 2), a value considerably smaller than the values observed before for mesoporous palladium. The concentration of Pb^{2+} was then increased to 600 mM to be sure that there was enough lead to cover all the active surface area without deplection within the pores, but also with this concentration the UPD peaks did not change significantly. Considering these results, there are two possibilities: (i) the UPD of lead is not a suitable method to determine the active surface area of mesoporous copper because, for example, the Pb^{2+} ions cannot enter the pores or (ii) there is no nanostructure present in the Cu film.

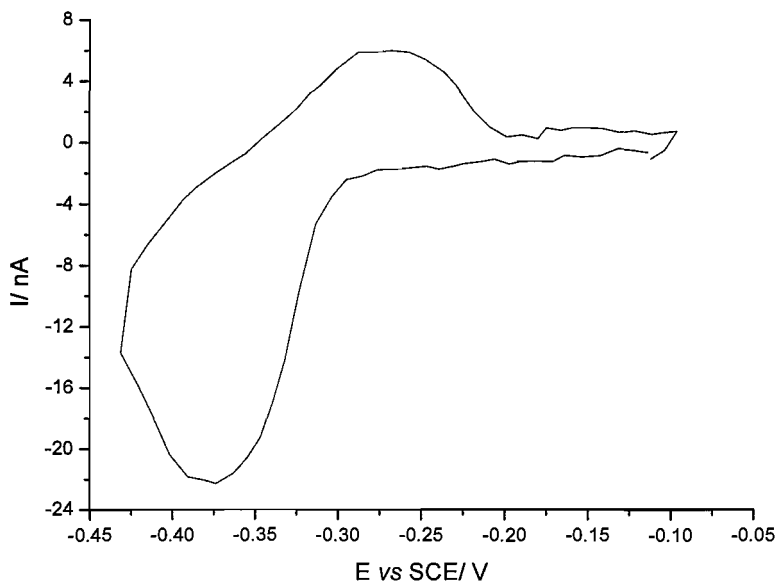

Figure 4.32 *UPD of lead on a copper film deposited on a Au microdisc (d = 60 μm) from a plating mixture containing 47 wt% $C_{16}EO_8$, 47 wt% 0.1 M H_2SO_4 and 6 wt% $CuSO_4.5H_2O$ in 60 mM Pb^{2+}/ 0.6 M $HClO_4$. Scan rate = 100 mV s^{-1}.*

4.4- Nitrate Reduction at Copper Electrodes

4.4.1- Acid medium

In a previous work carried out in acidic media with rotating vitreous carbon disc electrodes[17], a catalytic effect was observed for nitrate reduction in the presence of copper deposited *in situ*, by the electroplating of Cu from $CuSO_4$ in solution. To study the effect of these *in situ* Cu deposits on the reduction of nitrate using microelectrodes a series of experiments was carried out at a Cu microdisc in the presence of a small amount of $CuSO_4.5H_2O$ (4 mM) and the results compared with the response at a Cu film electrodeposited in the presence of $C_{16}EO_8$. Figure 4.33 shows the electrochemical response of a polished copper microdisc, an *in situ* plated copper deposit and a Cu film electrodeposited in the presence of surfactant in 5 mM $NaNO_3$/ 0.1 M H_2SO_4. The effect of $CuSO_4$ in the electrolyte is also shown for comparison.

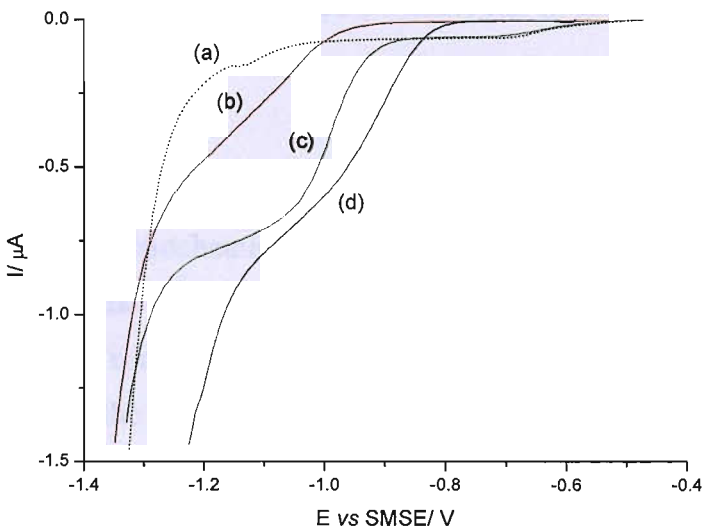

Figure 4.33 *Linear sweep voltammograms recorded at a copper microdisc (d = 50 µm) in (a) 0.1 M H_2SO_4 + 4 mM $CuSO_4$, (b) 5 mM $NaNO_3$/ 0.1 M H_2SO_4 and (c) 5 mM $NaNO_3$/ 0.1 M H_2SO_4 + 4 mM $CuSO_4$. Voltammogram (d) was recorded at a copper film electrodeposited at -0.55 V vs SMSE on a Au microdisc electrode (d = 60 µm) from a plating bath containing 50 wt% $C_{16}EO_8$ and 50 wt% 0.2 M $Cu(CH_3SO_3)_2$/ 0.1 M CH_3SO_3H. Deposition charge density = 1.4 C cm^{-2}. Scan rate = 10 mV s^{-1}.*

For 0.1 M H_2SO_4 in the presence of 4 mM $CuSO_4$, the voltammogram only shows a small cathodic wave at $E_{1/2}$ = -0.6 V, corresponding to the deposition of copper onto the Cu microdisc:

$$Cu^{2+} + 2e^- \longrightarrow Cu \qquad (4.4)$$

In the presence of nitrate, the wave for the *in situ* copper deposition is also evident, but an additional well formed reduction wave at $E_{1/2}$ = -0.98 V is observed, see voltammogram (c). Comparing this last voltammogram with the response at the polished Cu microdisc, voltamogram (b), it is possible to confirm that also with microelectrodes the reduction of nitrate occurs at more positive potentials and the limiting current plateau is better defined at copper films deposited *in situ*. At the copper film deposited in the presence of $C_{16}EO_8$, voltammogram (d), the response for nitrate reduction occurs even at more positive potentials and a positive shift of ~ 200 mV comparing with the response at the polished Cu microdisc is obtained.

4.4.2- Basic medium

Figure 4.34 shows the electrochemical responses of a Cu film deposited from the H_1 mesophase of $C_{16}EO_8$ and of a non-templated Cu film in the presence of 30 mM $NaNO_3$/ 2 M NaOH. For comparison, the response in 2 M NaOH only is also shown for the Cu film deposited in the presence of surfactant and the geometric areas of both films were considered for the calculation of the current densities.

In the presence of nitrate, the non-templated film shows two peaks at -1.65 and -1.92 V *vs* SMSE. Both peaks are definitely associated with the presence of nitrate in solution, since they are not present in the voltammetry of 2 M NaOH only, see voltammogram (c) in Figure 4.34, but they might well be due to the reduction of NO_3^- and some other reaction product. For the templated copper film the first peak at -1.65 V is not so evident but a positive potential shift of ~100 mV can be observed for the second peak. This implies that a high surface area form of copper is present.

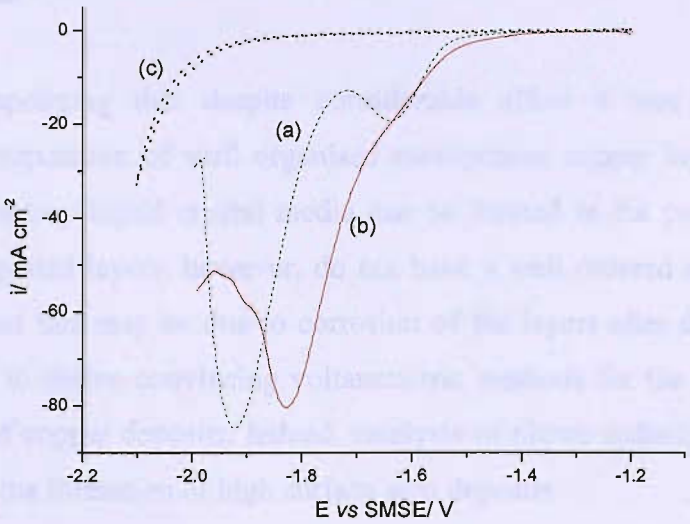

Figure 4.34 *Cyclic voltammograms in 30 mM $NaNO_3$/ 2 M NaOH for (a) a non-templated Cu film deposited from 15 mM $CuSO_4.5H_2O$/ 0.6 M $HClO_4$ solution at -0.55 V vs SMSE and (b) a Cu film deposited from a templating mixture containing 47 wt% $C_{16}EO_8$, 47 wt% 0.1 M H_2SO_4 and 6 wt% $CuSO_4.5H_2O$ at -0.45 V vs SMSE. (c) Cyclic voltammogram for the Cu film of (b) in 2 M NaOH. Both films were deposited on a Pt microdisc (d = 25 μm) using a deposition charge density of 1.4 C Cm^{-2}. Scan rate = 10 mV s^{-1}. (a) and (b) are the forward scans.*

The presence of two cathodic current peaks during NO_3^- reduction at a Cu RDE in weakly alkaline solutions has been reported before by Bouzek *et al.*[18]. According to the authors, the first peak at -1.0 V *vs* SCE corresponds to NO_3^- reduction to NO_2^- and the second peak at -1.3 V *vs* SCE is due to "a series of unspecified reactions" leading from NO_2^- to NH_3.

In 1 M NaOH, Cattarin[19] has also observed a small wave at -1.1 V *vs* SCE and a double peak ~-1.3 V occurring for NO_3^- reduction at a Cu disc electrode. The presence and the shape of the three peaks seems to be dependent on electrode treatment and it is concluded in this study that the peaks at -1.1 V and -1.25 V *vs* SCE are enhanced after reduction of surface oxides produced by mechanical polishing or mild anodization, and decrease after polarization at sufficiently negative potentials. In general terms, Cattarin attributes the changes observed in the voltammetry to surface modifications affecting interfacial properties of relevance to catalytic behaviour.

4.5- Conclusion

It is most disappointing that despite considerable effort it was not possible to demonstrate the deposition of well organised mesoporous copper layers. It has been shown that satisfactory liquid crystal media can be formed in the presence of copper salts. The electroplated layers, however, do not have a well ordered structure; there is some evidence that this may be due to corrosion of the layers after deposition. It was also not possible to define convincing voltammetric methods for the determination of the surface area of copper deposits. Indeed, catalysis of nitrate reduction is perhaps the best evidence for the formation of high surface area deposits

4.6- References

[1] W. Y. Zou, Q. Cai, F. Z. Cui, H. D. Li, *Mater. Lett.* **2003**, *57*, 1934.

[2] M. A. Ghanem, PhD thesis, Southampton **2002**.

[3] W. H. Safranek, in *Modern Electroplating*, third ed. (Ed.: F. A. Lowenheim), John Wiley & Sons, New York, **1974**, p. 183.

[4] P. N. Bartlett, J. Marwan, *Microporous and Mesoporous Materials* **2003**, *62*, 73.

[5] J. M. Elliott, G. S. Attard, P. N. Bartlett, N. R. B. Coleman, D. A. S. Merckel, J. R. Owen, *Chem. Mater.* **1999**, *11*, 3602.

[6] M. D. Gernon, M. Wu, T. Buszta, P. Janney, *Green Chem.* **1999**, *1*, 127.

[7] R. Balaji, M. Pushpavanam, *Trans. Inst. Metal Finish.* **2003**, *81*, 154.

[8] D. J. Mitchell, G. J. T. Tiddy, L. Waring, T. Bostock, M. P. McDonald, *J. Chem. Soc., Faraday Trans. 1* **1983**, *79*, 975.

[9] M. R. G. De Chialvo, A. J. Arvia, *J. Appl. Electrochem.* **1985**, *15*, 685.

[10] B. Scharifker, R. Rugeles, J. Mozota, *Electrochim. Acta* **1984**, *29*, 261.

[11] D. V. Moll, M. R. G. De Chialvo, R. C. Salvarezza, A. J. Arvia, *Electrochim. Acta* **1985**, *30*, 1011.

[12] J. Hernandez, J. Solla-Gullon, E. Herrero, *J. Electroanal. Chem.* **2004**, *574*, 185.

[13] E. Herrero, L. J. Buller, H. D. Abruna, *Chem. Rev.* **2001**, *101*, 1897.

[14] G. M. Brisard, E. Zenati, H. A. Gasteiger, N. M. Markovic, P. N. Ross, *Langmuir* **1995**, *11*, 2221.

[15] G. M. Brisard, E. Zenati, H. A. Gasteiger, N. M. Markovic, P. N. Ross, *Langmuir* **1997**, *13*, 2390.

[16] Y. S. Chu, I. K. Robinson, A. A. Gewirth, *Phys. Rev. B* **1997**, *55*, 7945.

[17] N. G. Carpenter, D. Pletcher, *Anal. Chim. Acta* **1995**, *317*, 287.

[18] K. Bouzek, M. Paidar, A. Sadilkova, H. Bergmann, *J. Appl. Electrochem.* **2001**, *31*, 1185.

[19] S. Cattarin, *J. Appl. Electrochem.* **1992**, *22*, 1077.

Chapter 5- Cu-Pd Films Electrodeposited from Templating Baths Containing $C_{16}EO_8$

The catalysts typically used in liquid phase nitrate hydrogenation consist of a combination of a noble and a non-noble metal[1]. It is generally accepted that these bimetallic combinations have a substantial higher activity for nitrate reduction when compared with the activity of each metal alone. Usually, in these systems, the noble metal component is highly active for the reduction of nitrite (considered as an intermediate in the reaction) to nitrogen and the second metal plays a special role in the activation of nitrate for reduction. Considering the catalytic activities for these reactions of Pd and Cu, respectively, several studies have been focused on the supported Cu-Pd bimetallic system for the liquid phase hydrogenation of NO_3^- and NO_2^-[1-4]. In terms of the electrochemical reduction of these two anions, however, only few studies have been dedicated to the electrochemical behaviour of Cu-Pd[5-7].

In this chapter, special attention will be given to the preparation and characterisation of Cu-Pd films deposited from templating mixtures containing $C_{16}EO_8$, in order to study their activity for the electrochemical reduction of nitrate and nitrite. To better understand the electrochemistry of the different templating mixtures, it was first necessary to study a bit more in detail the voltammetry of the two metal precursor salts in solution and a significant number of the experiments reported here is related to the voltammetry of Cu(II), Pd(II) and Cu(II)-Pd(II) solutions.
Several Cu-Pd films were also electrodeposited from aqueous solution and their response for nitrate reduction was compared with the response at Cu films obtained from the hexagonal phase of $C_{16}EO_8$.

5.1- Electrochemical Characterisation of Cu, Pd and Cu-Pd Solutions in the Presence of H_2SO_4

Ammonium tetrachloropalladate was the salt precursor used before for the deposition of mesoporous palladium films. The salt dissolves very well in aqueous media and, as mentioned in Chapter 3, produces a stable hexagonal phase in the presence of $C_{16}EO_8$, allowing the deposition of a mesoporous structure. However, when depositing Cu-Pd films, the presence of chloride in the medium can induce the corrosion of copper and it is necessary to find a suitable palladium salt without chloride to prepare the plating mixture for this bimetallic system. Palladium(II) sulphate, palladium(II) nitrate and palladium(II) acetate are all chloride free, but significantly more difficult to dissolve than ammonium tetrachloropalladate. The solubility of these salts was studied in several media such as sulphuric acid, nitric acid and acetic acid, but even at low concentrations (~5 mM) none of the salts dissolves completely, leaving a small amount of a brown residue. Despite the presence of this residue, some solutions were studied by cyclic voltammetry.

Figure 5.1 shows the cyclic voltammograms obtained for a Pt microdisc in 5 mM $PdSO_4.2H_2O$/ 0.1 M H_2SO_4, 5 mM $CuSO_4.5H_2O$/ 0.1 M H_2SO_4 and 5 mM $CuSO_4.5H_2O$ + 5 mM $PdSO_4.2H_2O$ / 0.1 M H_2SO_4.

For a 5 mM $PdSO_4.2H_2O$/ 0.1 M H_2SO_4 solution it is possible to observe the deposition of palladium starting at ~-0.2 V *vs* SMSE and giving rise to a very well defined wave in the forward scan, with the current reaching the value expected for a diffusion controlled process (~ 30 nA for a $2e^-$ process and considering D = 6×10^{-6} cm^2 s^{-1}), see voltammogram (a). The presence of a nucleation loop shows that the deposition of palladium continues in the reverse scan and it is thermodynamically favourable up to ~0.0 V, however, no stripping peak was observed in this medium.

The reduction of copper in 5 mM $CuSO_4.5H_2O$/ 0.1 M H_2SO_4 starts at more negative potentials and, once again, the limiting current is in accordance with the value expected for a diffusion controlled process, see voltammogram (b). The voltammogram shows in this case a sharp stripping peak at -0.30 V *vs* SMSE and there is a good charge balance between the copper deposition and stripping processes.

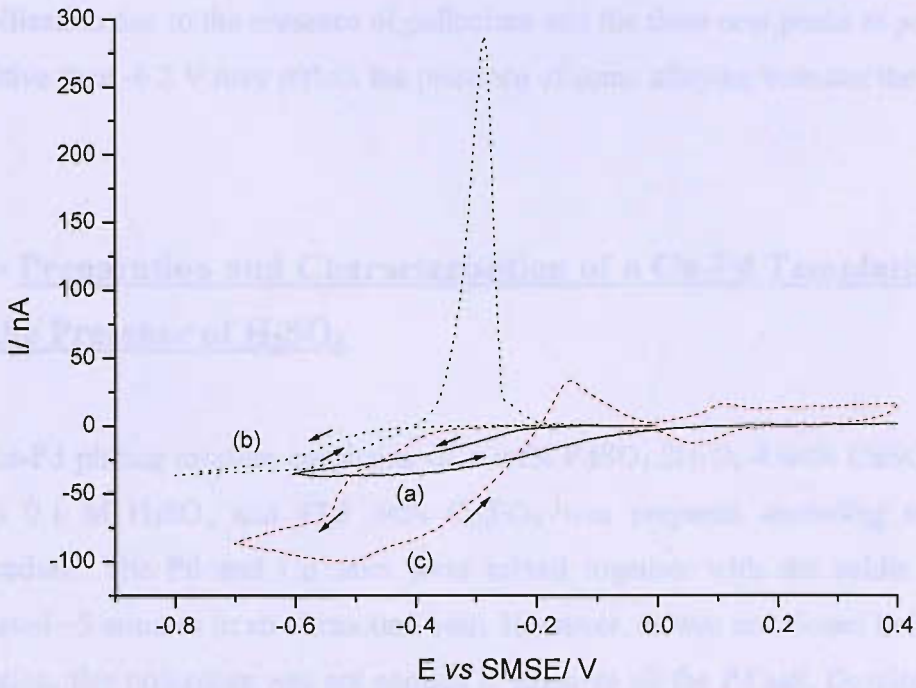

Figure 5.1 *Cyclic voltammograms for a Pt microdisc (d = 25 μm) in (a) 5 mM $PdSO_4.2H_2O$/ 0.1 M H_2SO_4, (b) 5 mM $CuSO_4.5H_2O$/ 0.1 M H_2SO_4 and (c) 5 mM $CuSO_4.5H_2O$ + 5 mM $PdSO_4.2H_2O$ / 0.1 M H_2SO_4. Scan rate =10 mV s^{-1}.*

When the two metals are present in the same solution, however, the voltammetry is quite different from the sum of the two individual metal ions responses, clearly showing the formation of new species. For 5 mM $CuSO_4.5H_2O$ + 5 mM $PdSO_4.2H_2O$ / 0.1 M H_2SO_4 it is possible to observe two distinct processes occurring between -0.40 and -0.55 V in the forward scan and in the reverse scan deposition continues to -0.2 V and there are two new small peaks at -0.15 and 0.1 V *vs* SMSE. The copper dissolution peak is absent and there is no charge balance between deposition and dissolution. If the scan is reversed at 0.4 V, another peak appears at ~ 0.05 V. Comparing with the voltammetry of each metal ion alone, the voltammetry for the Cu-Pd solution seems to show the deposition of Pd occurring at more negative potentials and, on the other hand, a catalytic effect for the reduction of copper(II). The large cathodic current in the reverse scan between -0.5 and -0.2 V is certainly well above that possible for palladium deposition alone and clearly shows that in the Cu-Pd solution the deposition of copper occurs at considerably more positive potentials than in 5 mM $CuSO_4$/ 0.1 M H_2SO_4. The

absence of the sharp copper stripping peak can also be an indication of some copper stabilisation due to the presence of palladium and the three new peaks at potentials more positive than -0.2 V may reflect the presence of some alloying between the two metals.

5.2- Preparation and Characterisation of a Cu-Pd Templating Mixture in the Presence of H_2SO_4

A Cu-Pd plating mixture consisting of 1 wt% $PdSO_4.2H_2O$, 4 wt% $CuSO_4.5H_2O$, 47.5 wt% 0.1 M H_2SO_4 and 47.5 wt% $C_{16}EO_8$ was prepared according to the normal procedure. The Pd and Cu salts were mixed together with the acidic solution and agitated ~5 minutes in an ultrasound bath. However, as was mentioned before for the Pd solution, this procedure was not enough to dissolve all the Pd salt. Despite the presence of some brown residue, the surfactant was added and the mixture was warmed up to 45 °C for ~3 minutes and mixed with a glass rod to ensure its homogeneity. The plating mixture was then allowed to equilibrate at 25 °C for 2 hours. During this last step, the colour of the plating mixture changed from green olive to brown, which can be due to some palladium ion reduction by the surfactant (the OH groups present in the surfactant chains can be potential sites for oxidation).

The analysis of the plating mixture by optical microscopy, at room temperature, shows the irregular air bubbles and bright and dark areas that usually characterise the hexagonal phase, but the presence of the brown residue is also evident, with very tiny particles giving a "smoky" aspect to the texture, see Figure 5.2(a). In these conditions, the hexagonal phase is stable only up to 45 °C. At ~ 60 °C a larger number of particles can be observed, moving around the typical round air bubbles of the micellar phase, see Figure 5.2(b), and with a further increase in temperature the solid becomes more and more evident. Cooling down the plating mixture to room temperature does not give back the texture of the hexagonal phase, because the increase in temperature clearly facilitates the surfactant oxidation and at the end there is a big interference of the palladium residue in all sample, as it is possible to observe in Figure 5.2(c). However, since the deposition of Cu-Pd films could be carried out without any annealing of the plating mixture and since the presence of the brown residue seems to have a minimum effect at 25 °C, some further studies were carried out with this plating mixture.

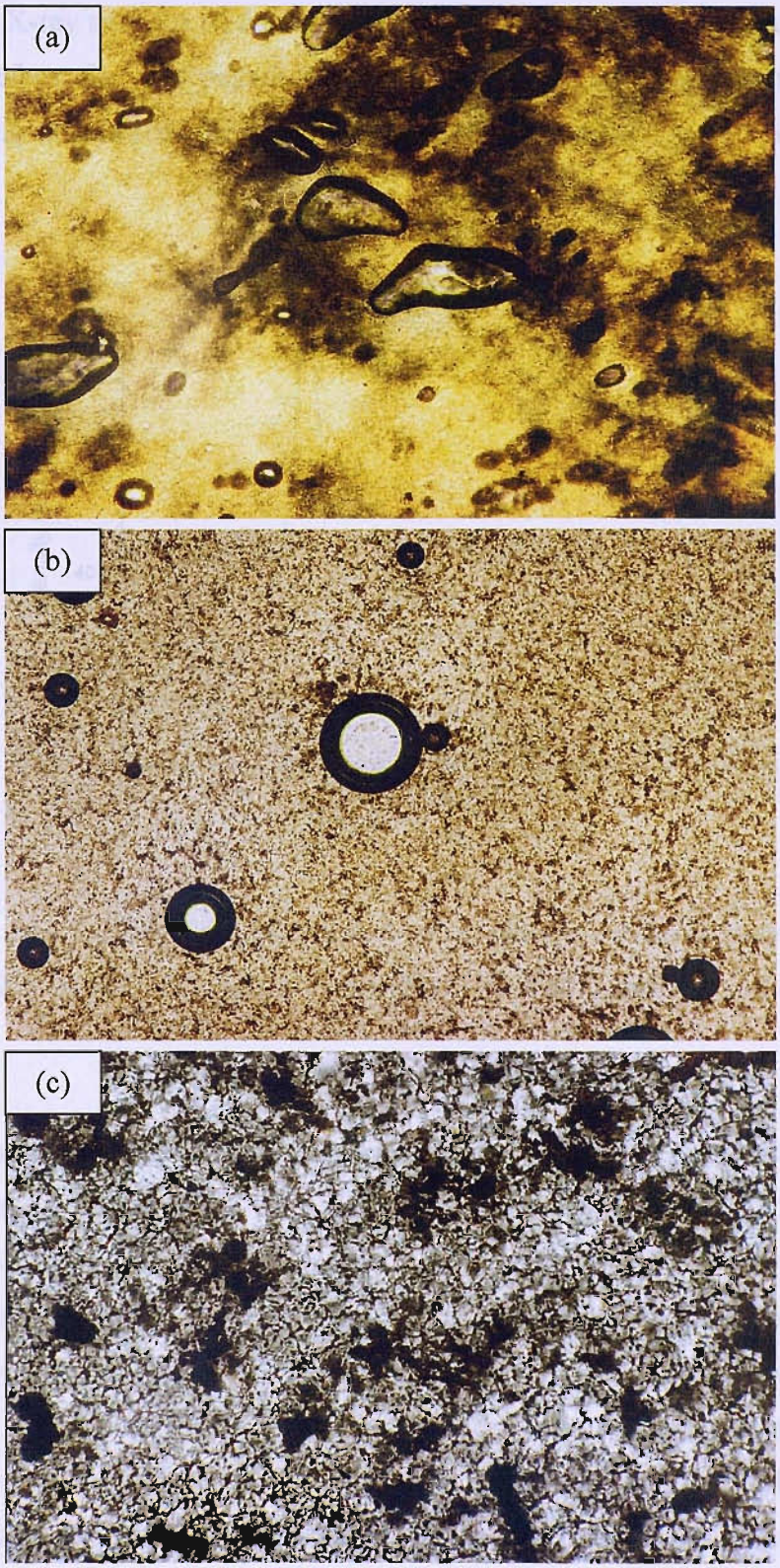

Figure 5.2 *Textures of a plating mixture containing 1 wt% $PdSO_4.2H_2O$, 4 wt% $CuSO_4.5H_2O$, 47.5 wt% 0.1 M H_2SO_4 and 47.5 wt% $C_{16}EO_8$ at (a) 19.5 °C, after preparation of plating mixture, (b) 61.2 °C, while heating up sample and (c) 20 °C, cooling down sample, after heating up to 83 °C.*

Small angle X-ray analysis of the mixture gives a diffraction pattern similar to the ones observed before for the palladium and copper plating mixtures, with the peak corresponding to the (100) diffraction plane of the hexagonal structure at 2θ ~1.86, see Figure 5.3.

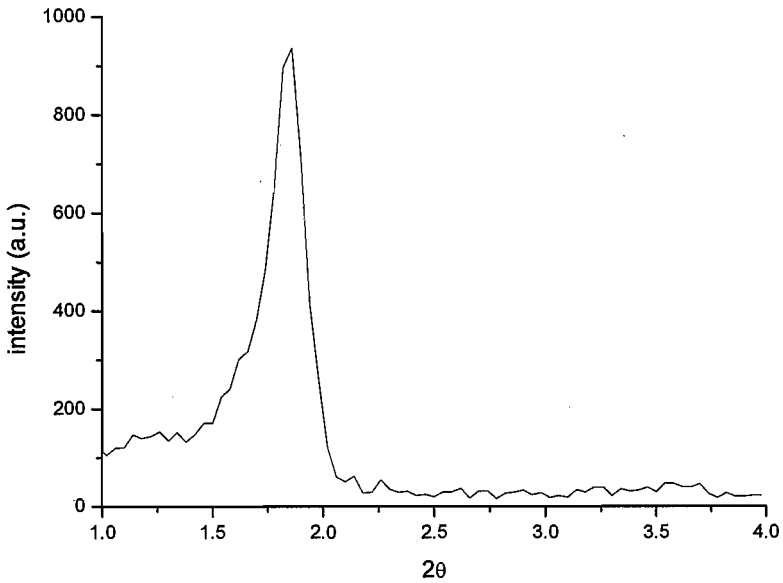

Figure 5.3 *Low angle X-ray diffraction of a plating mixture containing 1 wt % $PdSO_4.2H_2O$, 4 wt % $CuSO_4.5H_2O$, 47.5 wt% 0.1 M H_2SO_4 and 47.5 wt% $C_{16}EO_8$.*

The voltammetry for the Cu-Pd plating mixture, see Figure 5.4, shows two well formed reduction waves, which might be assigned to the deposition of Pd and Cu on the Pt microdisc, occurring only at slightly more positive potentials than in aqueous solution, compare with Figure 5.1, voltammogram (c). A significant difference between the voltammetry of the Cu(II)-Pd(II) solution shown in Figure 5.1 and the voltammetry of the plating mixture can be observed, however, in the reverse scan, where two superimposed peaks appear now between -0.3 and 0.0 V *vs* SMSE. The charge associated with these anodic peaks (11 μC) is smaller than the value for the reduction processes occurring in the forward scan (16 μC), but there is no doubt that these features are correlated and the fact that the peaks in the reverse scan are significantly different from those observed in Pd(II) and Cu(II) solutions, see Figure 5.1, clearly indicates the formation of an alloy. It is obvious that the voltammetry of a Cu-Pd solution is not a simple addition of the features observed for the two metals alone and the presence of the surfactant introduces even more changes in the voltammogram. Either in solution or in

the plating mixture, the formation of some Cu-Pd alloys and/or Cu-Pd mixtures can not be ruled out, which makes difficult the correct assignment of all the features.

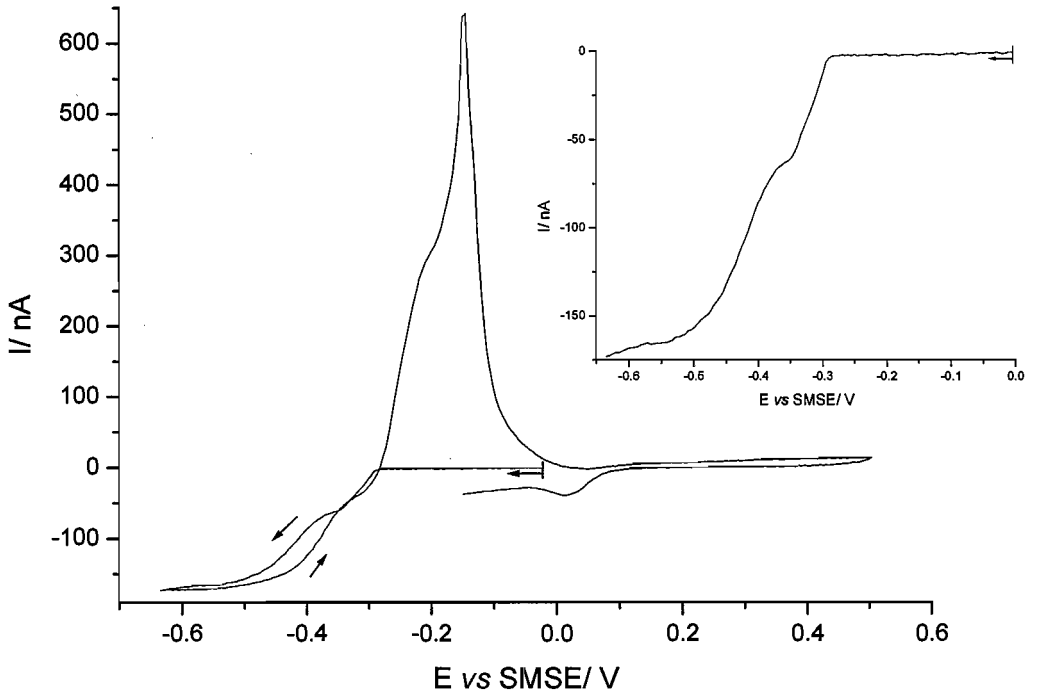

Figure 5.4 *Cyclic voltammogram for a Pt microdisc (d = 25 μm) in a Cu-Pd plating mixture consisting of 1 wt % $PdSO_4.2H_2O$, 4 wt % $CuSO_4.5H_2O$, 47.5 wt% 0.1 M H_2SO_4 and 47.5 wt% $C_{16}EO_8$. Scan rate = 5 mV s^{-1}. The inset shows the forward scan.*

The different Cu/Pd ratios present in the Cu(II)-Pd(II) solution reported in Figure 5.1 and in the Cu-Pd templating mixture also contribute to the differences observed in the reverse scans, but this effect will be discussed in more detail in Section 5.5.

5.3- Electrodeposition and Characterisation of Cu-Pd Films from a Templating Mixture in the Presence of H_2SO_4

The deposition of Pd-Cu films was carried out as before for Pd and Cu only, on Pt and Au microdiscs. The potential was stepped from -0.10 V to different potential values and it was kept constant until the desired charge was passed. Figure 5.5 shows two examples of the current-time transients obtained with Pt microdiscs for depositions at -0.31 V and -0.40 V *vs* SMSE and Figure 5.6 the correspondent deposits.

As expected, the deposition at more negative potentials reaches higher current values and is faster. In both cases the initial current indicates the rapid formation of a phase. While transient (a) soon reaches a steady state current that can correspond to the thickening of the initial layers, transient (b) shows a further rise in current over the timescale 30-100 s. This could be due to the growth of a different phase or the growth of the deposit over the glass surrounding the microdisc substrate (although the latter was not apparent in the SEM). There is no doubt that the current-time transients show significantly different features and that is clearly reflected on the deposits.

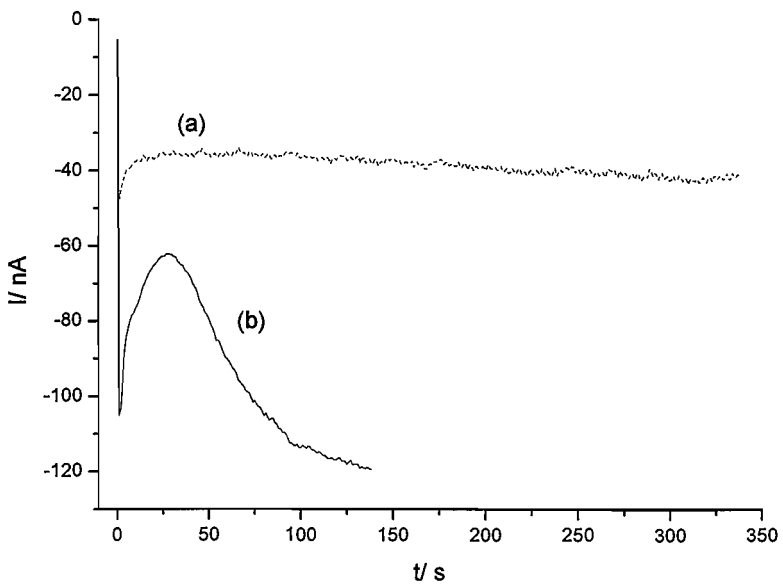

Figure 5.5 *Current-time transients recorded during the deposition of Cu-Pd films on Pt microdiscs (d = 25 μm) at (a) -0.31 and (b) -0.40 V vs SMSE. Plating mixture containing 1 wt % $PdSO_4.2H_2O$, 4 wt % $CuSO_4.5H_2O$, 47.5 wt% 0.1 M H_2SO_4 and 47.5 wt% $C_{16}EO_8$. Deposition charge density = 2.6 C cm^{-2}.*

Both deposits are adherent to the substrate, but not so smooth and uniform as observed before for Pd and Cu alone, and it is clear that the deposition potential plays a major role in the appearance of the films, as well as in their composition. EDX analysis shows that the deposit obtained at more negative potential (-0.40 V *vs* SMSE) is richer in Cu (ratio Cu/ Pd = 4.6, considering the atomic percentage given by EDX) and stepping the potential to -0.31 V gave rise to deposits richer in Pd (ratio Cu/ Pd = 0.5).

A similar trend was observed for the deposits obtained on Au microdiscs, with the copper percentage increasing for more negative potentials. Figure 5.7 shows a Cu-Pd deposit obtained at -0.31 V *vs* SMSE, where EDX analysis gave a Cu/ Pd ratio of 0.37.

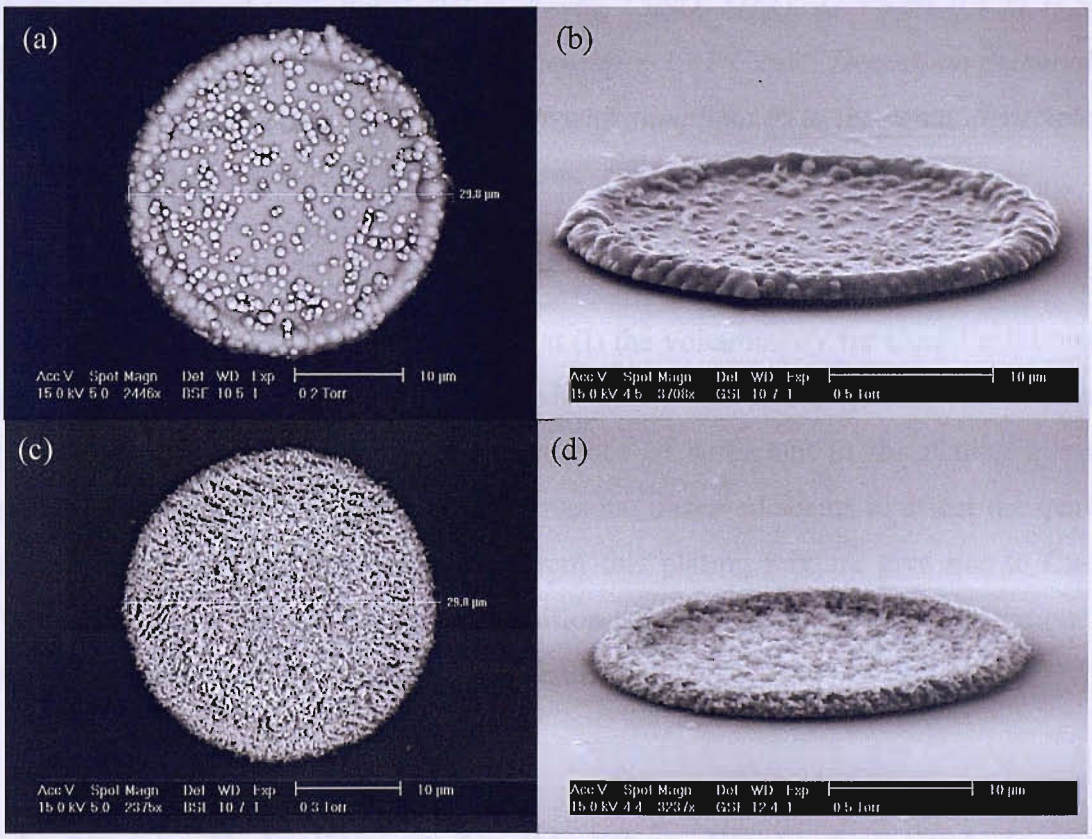

Figure 5.6 *SEM images of Cu-Pd films on Pt microdiscs (d = 25 μm) from a plating mixture containing 1 wt% $PdSO_4.2H_2O$, 4 wt% $CuSO_4.5H_2O$, 47.5 wt% 0.1 M H_2SO_4 and 47.5 wt% $C_{16}EO_8$. Deposition charge density = 2.6 C cm^{-2}. (a) and (b) film deposited at -0.31 V and (c) and (d) film deposited at -0.40 V vs SMSE. (a) and (c) employ BSE detector with sample at 0° to the beam, (b) and (d) employ GSE detector with sample at 75° to the beam.*

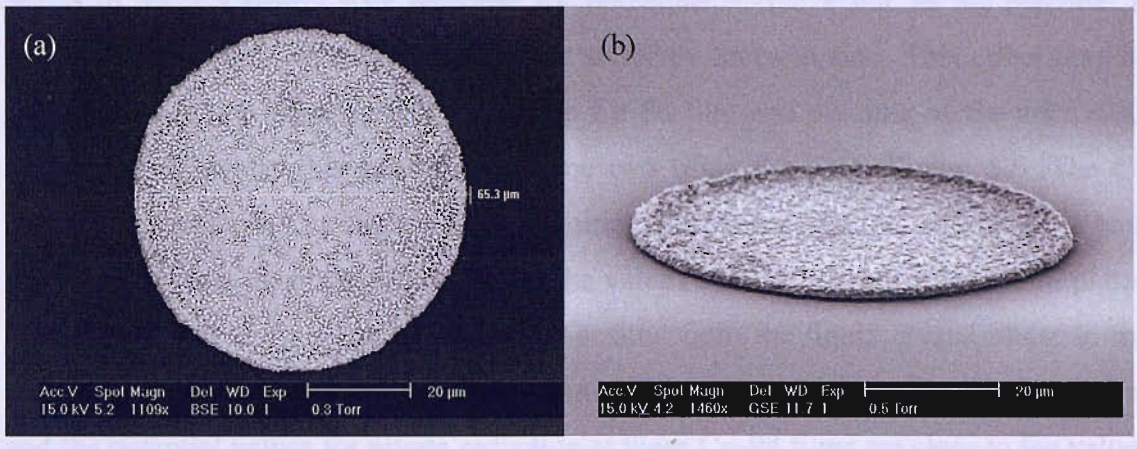

Figure 5.7 *SEM images of a Cu-Pd film on Au microdisc (d = 60 µm) from a plating mixture containing 1 wt% $PdSO_4.2H_2O$, 4 wt% $CuSO_4.5H_2O$, 47.5 wt% 0.1 M H_2SO_4 and 47.5 wt% $C_{16}EO_8$. Deposition charge density = 1.41 C cm^{-2}. Deposition potential = -0.31 V vs SMSE. (a) employs BSE detector with sample at 0° to the beam, (b) employs GSE detector with sample at 75 ° to the beam.*

So far in this section, it has been shown that (i) the voltammetry for Cu-Pd solutions is quite different from the sum of the two individual metal ions responses and it clearly shows the formation of alloys; (ii) the presence of surfactant in the plating mixture reduces the palladium ions and the brown residue observed seems to affect the quality of the deposits and (iii) the depositions from this plating mixture give rise to Cu-Pd films which composition depends on deposition potential, with higher concentrations of copper being obtained at more negative potential values.

5.4- Nitrate Reduction at Cu-Pd Films Electrodeposited from a Templating Mixture in the Presence of H_2SO_4

5.4.1- Acid medium

The reduction of nitrate at Cu-Pd films was carried out in 15 mM $NaNO_3$/ 0.1 M H_2SO_4, however, the electrochemical response of the films in this solution was not very stable. At the beginning of the voltammetry, the current starts to increase and it almost

seems to reach a steady state response for potentials ~ -1.2 V but, as the potential is driven to more negative values, the current suddenly drops to zero. This effect may be due to some gas evolution occurring at the Cu-Pd film and blinding of the microdisc. Figure 5.8 illustrates this behaviour for the two films shown in Figure 5.6. The Cu richer film gives rise to a slightly higher limiting current for NO_3^- reduction, but in both cases the currents observed are similar to the values obtained before at an *in situ* plated copper film and at a copper film electrodeposited from the liquid crystal phase in the presence of CH_3SO_3H. However, no positive shift in potential can be observed this time and the potential values for nitrate reduction at these Cu-Pd films are close to the values obtained before at *in situ* plated copper.

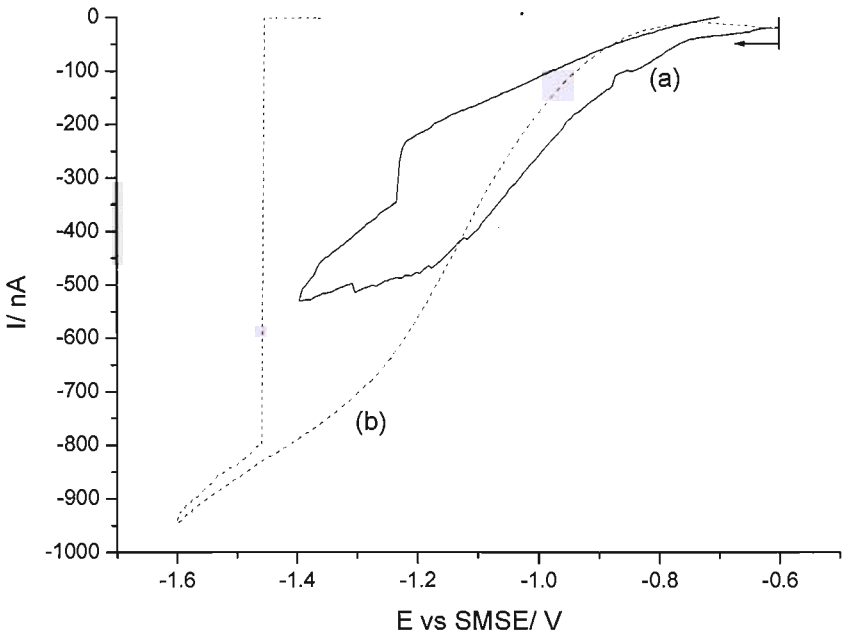

Figure 5.8 *Cyclic voltammograms for two Cu-Pd films deposited on Pt microdiscs (d = 25 μm) in 15 mM $NaNO_3$/ 0.1 M H_2SO_4. (a) Cu:Pd = 35:65 and (b) Cu:Pd = 82:18 . Scan rate = 10 mV s^{-1}.*

5.4.2- Basic medium

For 15 mM $NaNO_3$ in 2 M NaOH, the response is, in some way, close to the results obtained before with Pd for nitrite reduction, with NO_3^- also giving rise to a peak at around -1.4 V *vs* SMSE. Figure 5.9 illustrates the response obtained for two Cu-Pd films with different compositions. As in acid medium, the film richer in Cu gives a

bigger cathodic current for nitrate reduction, but the value is still lower than the current value expected for a diffusion controlled $8e^-$ process (414 nA at a 29.8 μm diameter film and assuming $D = 6\times10^{-6}$ cm^2 s^{-1}[8]).

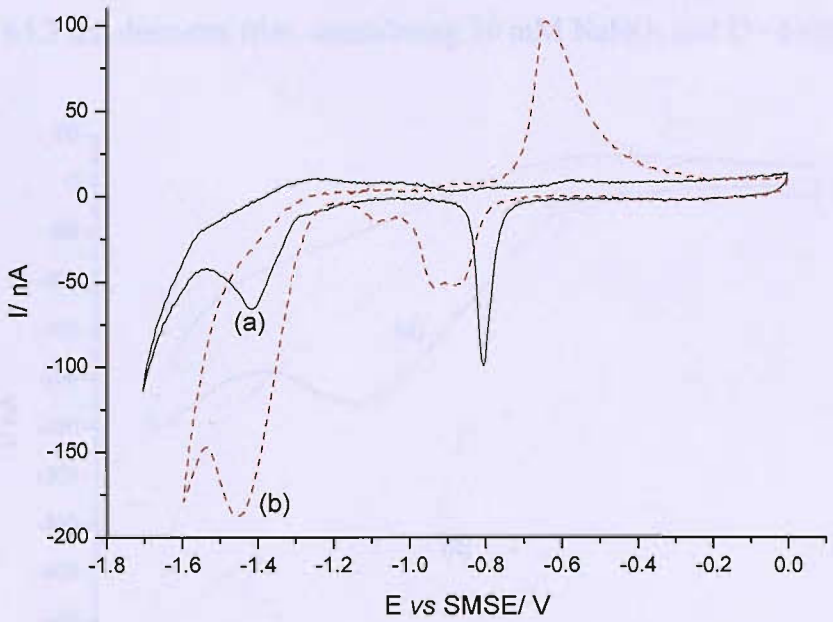

Figure 5.9 *Cyclic voltammograms for two Cu-Pd films deposited on Pt microdiscs (d = 25 μm) in 15 mM $NaNO_3$/ 2 M NaOH. (a) Cu:Pd = 35:65 and (b) Cu:Pd = 82:18 . Scan rate = 10 mV s^{-1}.*

The features observed positive to -0.9 V in Figure 5.9 for the deposit richer in Pd resemble those observed for Pd only, with the oxide formation region between -0.7 and 0.0 V and the correspondent oxide stripping peak appearing at -0.8 V *vs* SMSE.

For the deposit with higher concentration of copper, the anodic peak at -0.65 V can be assigned to the formation of Cu(II) species, either as $Cu(OH)_2$, CuO, $HCuO_2^-$ or CuO_2^{2-} [9, 10]. The cathodic peaks between -0.8 and -1.2 V are likely to be related with the reduction of these species, but they appear at significantly more positive potentials than the ones reported by Medina *et al.*[10] for the electrochemical behaviour of copper only in NaOH solutions. The presence of palladium certainly plays a role here and, once again, the voltammetry shows that the electrochemistry of these Cu-Pd films is not a simple addition of what has been reported so far for Pd and Cu alone. It is also worth pointing out that in Figure 5.9 the film richer in palladium does not show any feature that can be related with copper, despite the presence of 35 at% of this metal.

Figure 5.10 reports the electrochemical behaviour of a Cu-Pd film deposited on a Au microdisc (film shown before in Figure 5.7) for two different concentrations of nitrate. The peak current changes proportionally to the concentration but, once again, the values obtained are lower than the ones expected for a mass transport controlled $8e^-$ process (1.8 μA at a 65.3 μm diameter film, considering 30 mM $NaNO_3$ and $D= 6\times10^{-6}$ cm^2 s^{-1}).

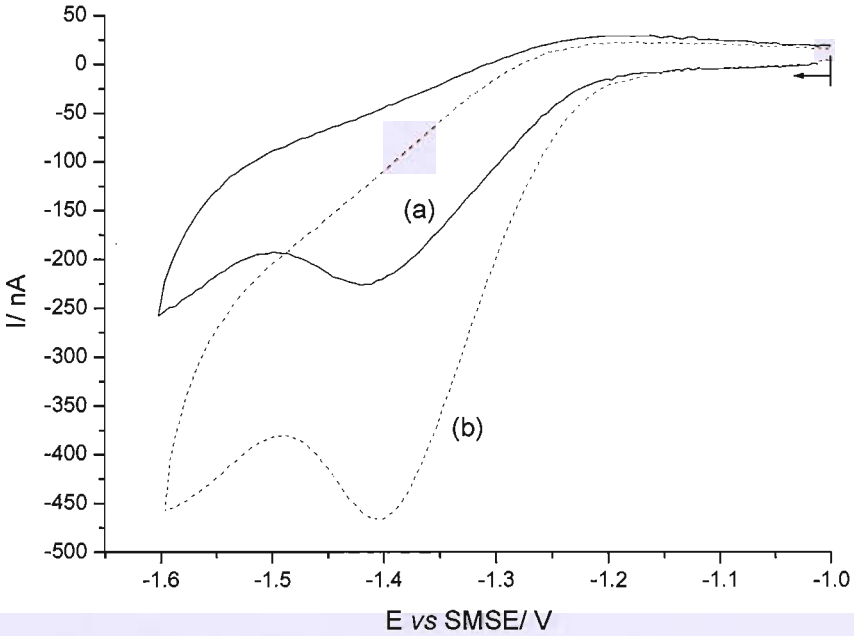

Figure 5.10 *Cyclic voltammograms for a Cu-Pd film deposited on a Au microdisc (d = 60 μm) in (a) 15 mM $NaNO_3$/ 2 M NaOH and (b) 30 mM $NaNO_3$/ 2 M NaOH. Cu:Pd = 27:73. Scan rate = 10 mV s^{-1}.*

As reported before for nitrite reduction with mesoporous palladium, see Chapter 3, the current for nitrate reduction with Cu-Pd films also depends on the positive potential limit and increases with the number of cycles. As it is possible to observe in Figure 5.11, cycling to 0.0 V *vs* SMSE increases the nitrate reduction current to more than the double of the value that is obtained when cycling only up to -1.0 V. To avoid the dissolution of copper in the medium, the potential scan should not go more positive than -1.0 V *vs* SMSE, but this clearly compromises the results for nitrate reduction.

SEM images of the Cu-Pd deposit obtained after contact with the nitrate solution and a series of consecutive scans up to 0.0 V *vs* SMSE showed that the deposit was still in very good condition and did not suffer major changes, see Figure 5.12. However, EDX analysis revealed a change in the Cu/ Pd ratio from 0.37 to 0.89 due to loss of some Pd.

Once again, and despite the initial presence of 27 at% Cu, the voltammogram reported in Figure 5.11 for the Cu-Pd film does not show any feature that can be assigned to the surface electrochemistry of this metal in a medium with 2 M NaOH. In particular, the absence of any feature related with copper corrosion, strongly suggests the stabilization of the metal by the presence of palladium.

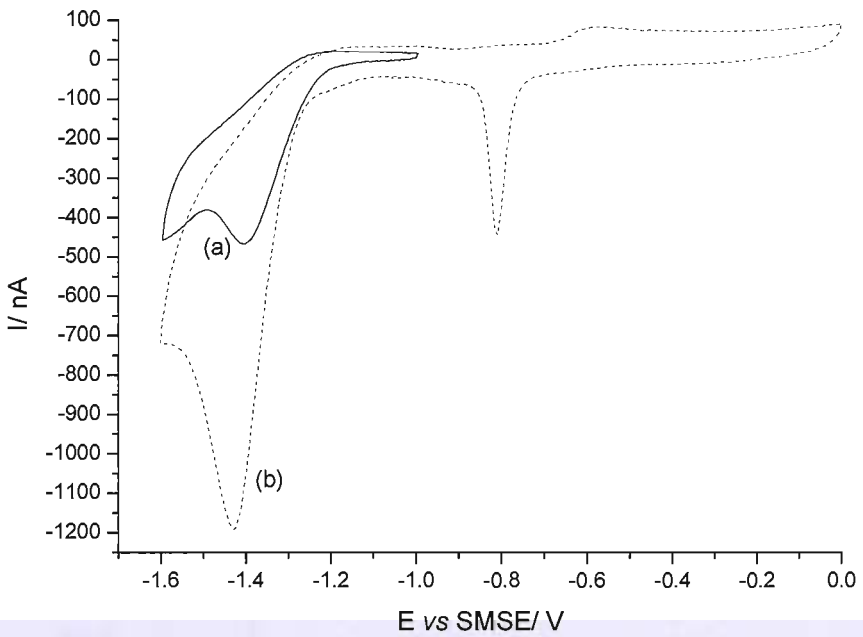

Figure 5.11 *Cyclic voltammograms of a Cu-Pd film deposited on a Au microdisc (d = 60 μm) in 30 mM $NaNO_3$/ 2 M NaOH. Cu:Pd = 27:73. Cycling between (a) -1.0 and -1.6 V and (b) 0.0 and -1.6 V. Scan rate = 10 mV s^{-1}.*

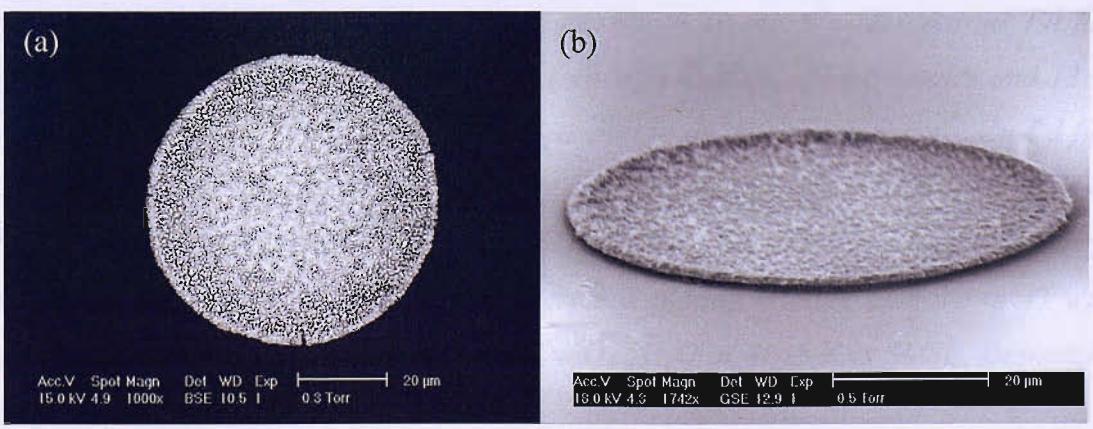

Figure 5.12 *SEM images of a Cu-Pd film deposited on a Au microdisc (d = 60 μm) after contact with nitrate solution and a series of potential scans up to 0.0 V vs SMSE.*

Comparing the results obtained for nitrate reduction at mesoporous Pd, Cu films deposited from the liquid crystal media and now at these Cu-Pd films, it is possible to conclude that in 2 M NaOH (i) nitrate reduction at mesoporous Pd and Cu-Pd films occurs at ~-1.4 V *vs* SMSE in both cases, but considerably higher currents are observed for the Cu-Pd films and (ii) nitrate reduction at mesoporous Pd and Cu-Pd films occurs at significantly more positive potentials than at the Cu films from the liquid crystal media, however, considerably higher currents are obtained in last case, see Figure 5.13. The geometric areas of the deposits were considered for the calculation of the current density.

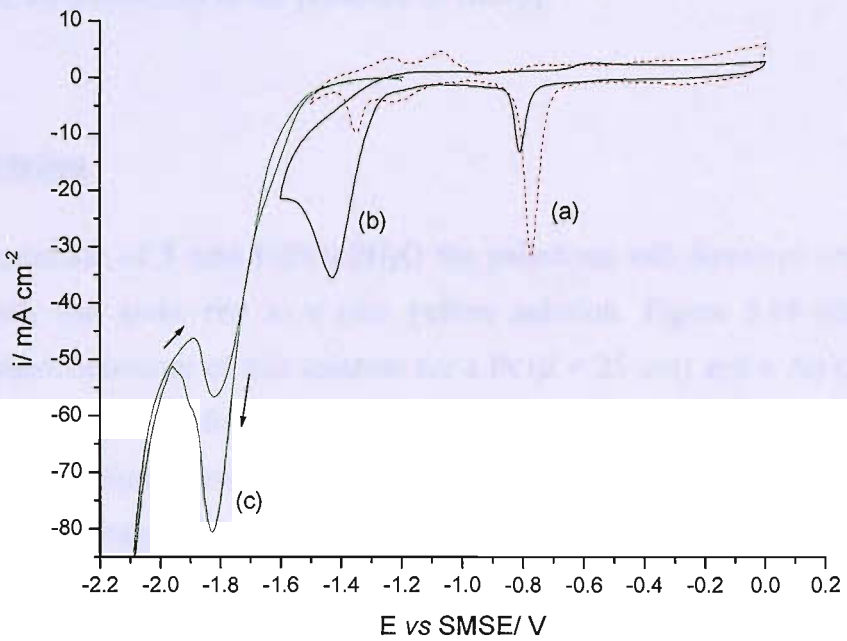

Figure 5.13 *Cyclic voltammograms for (a) mesoporous Pd film (b) Cu-Pd film and (c) Cu film in 30 mM $NaNO_3$/ 2 M NaOH. Scan rate = 10 mV s^{-1}. Mesoporous Pd film deposited from a plating mixture containing 48 wt% $C_{16}EO_8$, 40 wt% water and 12 wt % $(NH_4)_2PdCl_4$ at -0.3 V vs SCE. Deposition charge density = 2.0 C cm^{-2}. Cu-Pd film deposited from a plating mixture containing 1 wt% $PdSO_4.2H_2O$, 4 wt% $CuSO_4.5H_2O$, 47.5 wt% 0.1 M H_2SO_4 and 47.5 wt% $C_{16}EO_8$ at -0.31 V vs SMSE. Deposition charge density = 1.41 C cm^{-2}. Cu film deposited from a plating mixture containing 47 wt% $C_{16}EO_8$, 47 wt% 0.1 M H_2SO_4 and 6 wt% $CuSO_4.5H_2O$ at -0.45 V vs SMSE. Deposition charge density = 1.41 C cm^{-2}.*

5.5- Electrochemical Characterisation of Pd, Cu and Cu-Pd Solutions in the Presence of $HClO_4$

Another Cu-Pd templating mixture studied throughout this work consisted of 25 wt% 0.1 M $CuSO_4.5H_2O$/ 0.6 M $HClO_4$, 25 wt% 0.03 M $PdSO_4.2H_2O$/ 0.6 M $HClO_4$ and 50 wt% $C_{16}EO_8$. This time, the palladium salt dissolved better in the initial solution and it did not give rise to the formation of the brown precipitate observed before. The preparation and characterisation of this plating mixture will be discussed in detail in Section 5.7, but first, special attention will be given to the electrochemical behaviour of Pd, Cu and Cu-Pd solutions in the presence of $HClO_4$.

5.5.1- Pd solution

For a concentration of 5 mM $PdSO_4.2H_2O$ the palladium salt dissolves completely in 0.6 M $HClO_4$ and gives rise to a nice yellow solution. Figure 5.14 illustrates the electrochemical behaviour of this solution for a Pt (d = 25 μm) and a Au (d = 60 μm) microdisc after degassing for ~10 minutes with a N_2 stream. For both substrates, the deposition of palladium starts at -0.42 V *vs* SMSE and gives rise to a very well defined wave, with a limiting current value proportional to the disc radius and therefore corresponding to a diffusion controlled process. The nucleation loop is also clearly evident, with deposition continuing to ~0.0 V on the reverse scan. As in the presence of H_2SO_4, no anodic dissolution occurs in the perchloric acid solution. If the potential is taken even slightly more negative than -0.6 V *vs* SMSE, hydrogen starts to interfere with the voltammetry and it is possible to observe some new peaks that might well be related with Pd/ H oxidation, see Figure 5.15.

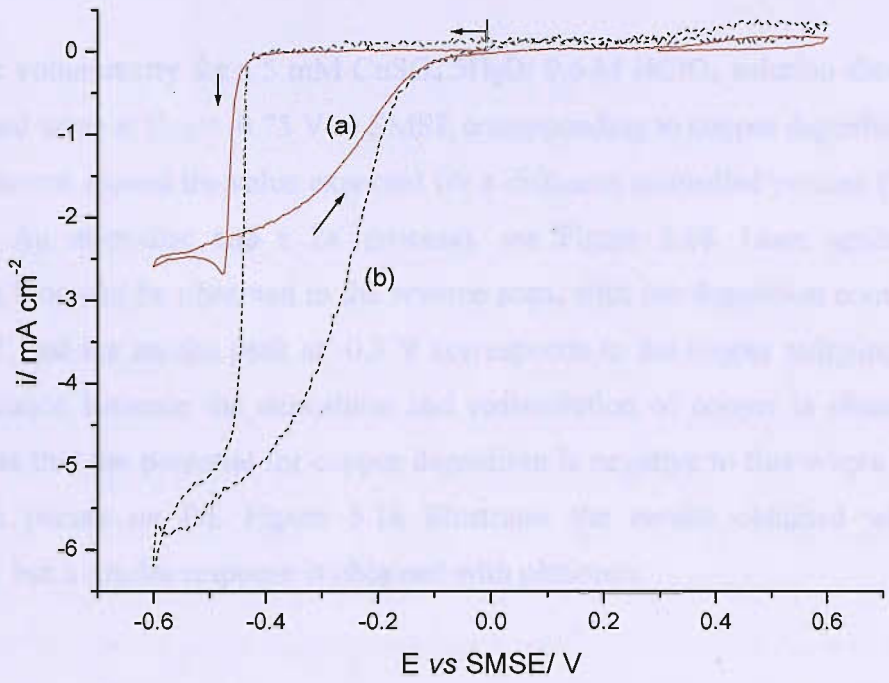

Figure 5.14 *Cyclic voltammograms for (a) Au microdisc (d = 60 μm) and (b) Pt microdisc (d = 25 μm) in 5 mM $PdSO_4.2H_2O$/ 0.6 M $HClO_4$. Scan rate = 10 mV s^{-1}.*

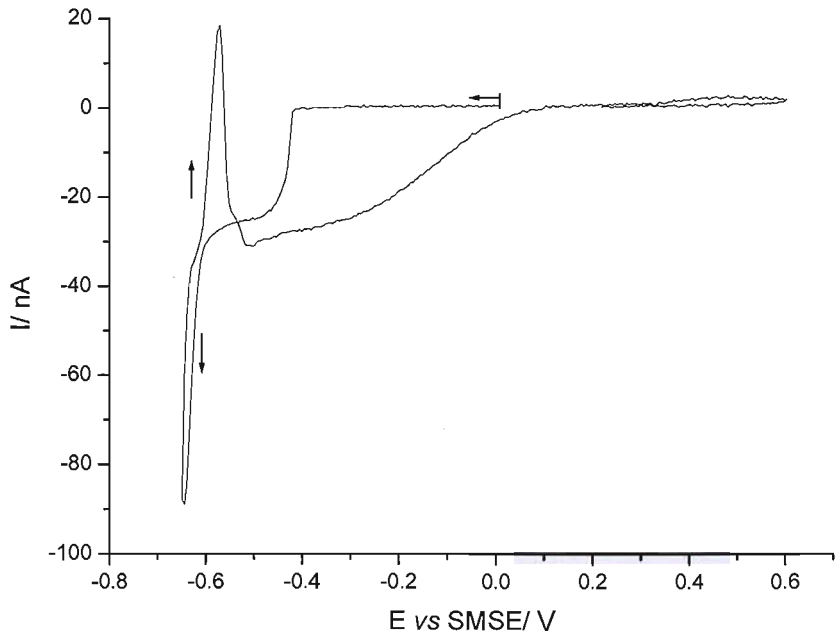

Figure 5.15 *Cyclic voltammogram for a Pt microdisc (d = 25 μm) in 5 mM $PdSO_4.2H_2O$/ 0.6 M $HClO_4$. Scan rate = 10 mV s^{-1}.*

5.5.2- Cu solution

The cyclic voltammetry for a 5 mM $CuSO_4.5H_2O$/ 0.6 M $HClO_4$ solution shows a very well defined wave at $E_{1/2}$ = -0.75 V *vs* SMSE corresponding to copper deposition, with a limiting current around the value expected for a diffusion controlled process (70 nA for a 60 μm Au microdisc and a $2e^-$ process), see Figure 5.16. Once again, a clear nucleation loop can be observed in the reverse scan, with the deposition continuing up to -0.45 V, and the anodic peak at -0.3 V corresponds to the copper stripping. A good charge balance between the deposition and redissolution of copper is obtained. One should note that the potential for copper deposition is negative to that where hydrogen absorption occurs on Pd. Figure 5.16 illustrates the results obtained with a Au microdisc, but a similar response is obtained with platinum.

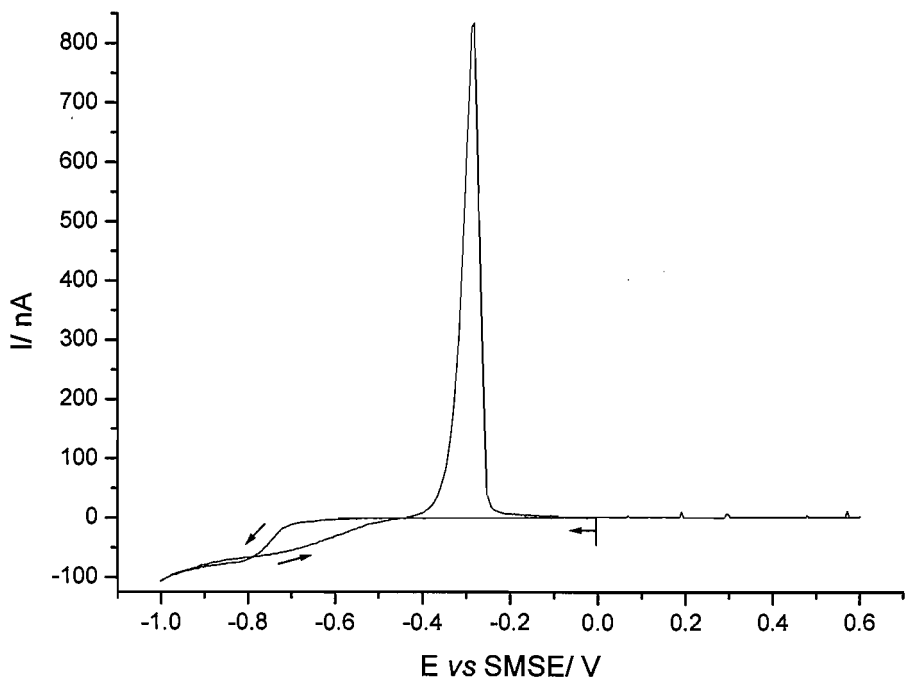

Figure 5.16 *Cyclic voltammogram for a Au microdisc (d = 60 μm) in 5 mM $CuSO_4.5H_2O$/ 0.6 M $HClO_4$. Scan rate = 10 mV s^{-1}.*

5.5.3- Cu-Pd solutions

5 mM $CuSO_4.5H_2O$ + 5 mM $PdSO_4.2H_2O$ in 0.6 M $HClO_4$

Figure 5.17 shows a cyclic voltammogram for a Pt microdisc (d = 25 μm) in a solution containing 5 mM $CuSO_4.5H_2O$ + 5 mM $PdSO_4.2H_2O$ in 0.6 M $HClO_4$. An initial wave with a limiting current around 20 nA appears at -0.45 V, in the potential range where one can expect the palladium deposition to occur, according to the results shown before in Figure 5.14. However, if the forward scan is reversed at -0.55 V, just in the plateau of the first wave, the voltammetry reveals some new anodic peaks between -0.4 and -0.1 V *vs* SMSE, see inset in Figure 5.17. These peaks are not present in the voltammetry of Pd(II) alone, which means that the initial wave does not correspond only to the deposition of palladium, and these anodic peaks are also very broad compared to copper dissolution. In addition, the limiting current at -0.7 V seems to correspond to the reduction of both Cu(II) and Pd(II) although in the Cu(II) only solution the Cu(II) is not reduced at this potential. The presence of Pd(II) is certainly aiding Cu(II) reduction and alloys are being formed.

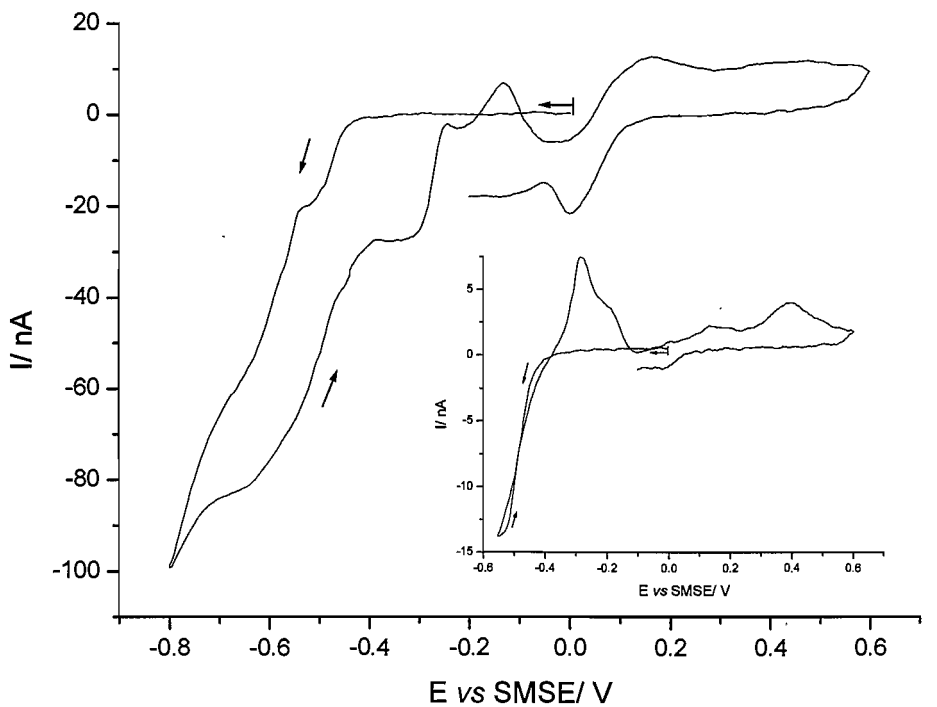

Figure 5.17 *Cyclic voltammograms for a Pt microdisc (d = 25 μm) in 5 mM $CuSO_4.5H_2O$ + 5 mM $PdSO_4.2H_2O$/ 0.6 M $HClO_4$. Inset shows voltammogram when the forward scan is reversed at -0.55 V vs SMSE. Scan rate = 10 mV s^{-1}.*

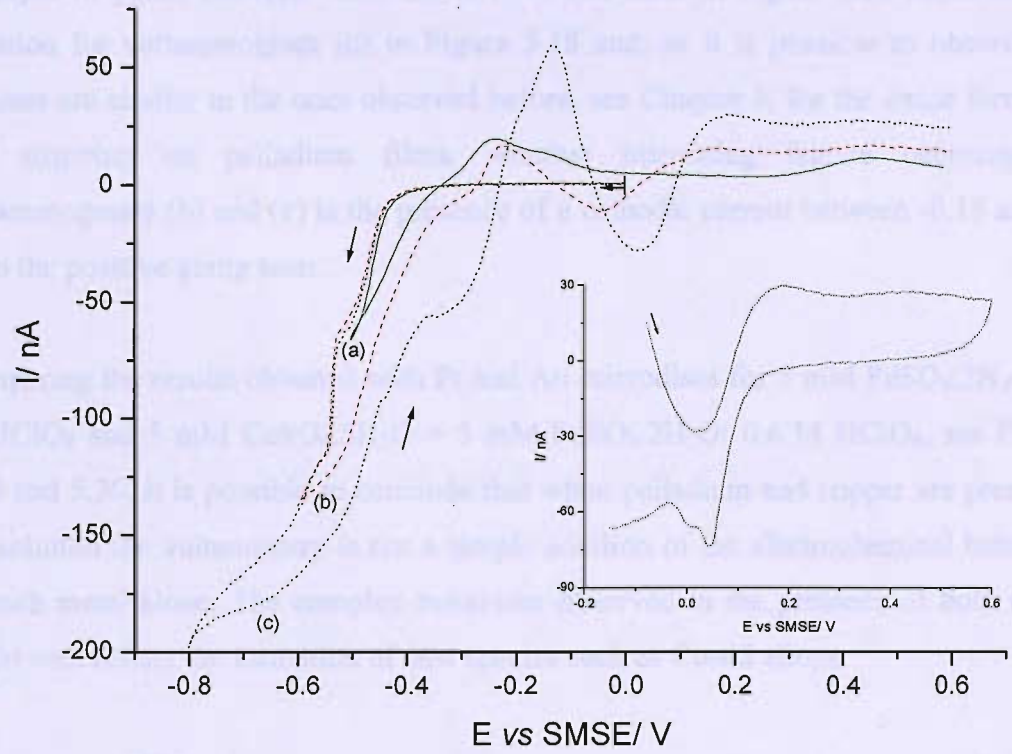

Figure 5.18 *Cyclic voltammograms for a Au microdisc (d = 60 μm) in 5 mM $CuSO_4.5H_2O$ + 5 mM $PdSO_4.2H_2O$/ 0.6 M $HClO_4$ with different negative potential limits: (a) -0.5, (b) -0.6 V and (c) -0.8 V vs SMSE. Inset shows in more detail voltammogram (c) when the scan is reversed at 0.6 V in the negative direction. Scan rate = 10 mV s^{-1}.*

With a Au microdisc the voltammetry is similar, but the features in the forward scan are better defined and at least three different processes seem to occur between -0.4 and -0.8 V *vs* SMSE, see Figure 5.18. The three waves could be assigned with palladium deposition, copper deposition and finally hydrogen absorption, but again, the correct assignment of all the features is difficult and it is well possible that some of them correspond to the deposition of alloys or Cu-Pd mixtures. Figure 5.18 clearly shows that the voltammetry is dependent on the negative potential limit and that the charge balance between reduction and oxidation processes becomes worse when cycling to more negative values, despite the deposition of more metal. For a question of simplification, the reverse scans in Figure 5.18 are shown only until 0.6 V *vs* SMSE, but if the scan is reversed at this potential in the negative direction again, the three voltammograms show

a couple of peaks between -0.05 and 0.1 V. The inset in Figure 5.18 illustrates this situation for voltammogram (c) in Figure 5.18 and, as it is possible to observe, the features are similar to the ones observed before, see Chapter 3, for the oxide formation and stripping on palladium films. Another interesting feature occurring for voltammograms (b) and (c) is the presence of a cathodic current between -0.15 and 0.1 V on the positive going scan.

Comparing the results obtained with Pt and Au microdiscs for 5 mM $PdSO_4.2H_2O$/ 0.6 M $HClO_4$ and 5 mM $CuSO_4.5H_2O$ + 5 mM $PdSO_4.2H_2O$/ 0.6 M $HClO_4$, see Figures 5.19 and 5.20, it is possible to conclude that when palladium and copper are present in the solution the voltammetry is not a simple addition of the electrochemical behaviour of each metal alone. The complex behaviour observed in the presence of both metals might well reflect the formation of new species such as Cu-Pd alloys.

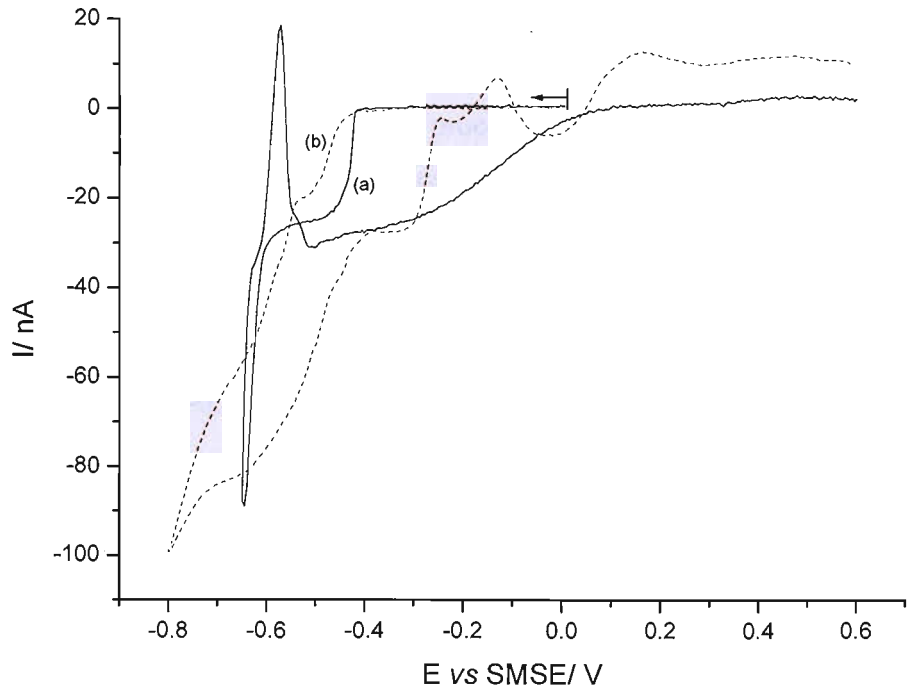

Figure 5.19 *Cyclic voltammograms for a Pt microdisc (d = 25 μm) in (a) 5 mM $PdSO_4.2H_2O$/ 0.6 M $HClO_4$ and (b) 5 mM $CuSO_4.5H_2O$ + 5 mM $PdSO_4.2H_2O$/ 0.6 M $HClO_4$. Scan rate = 10 mV s^{-1}.*

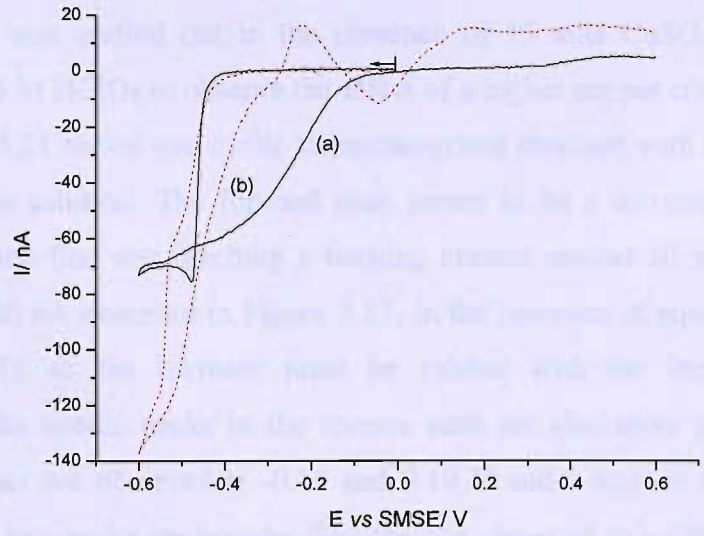

Figure 5.20 *Cyclic voltammograms for a Au microdisc (d = 60 μm) in (a) 5 mM $PdSO_4.2H_2O$/ 0.6 M $HClO_4$ and (b) 5 mM $CuSO_4.5H_2O$ + 5 mM $PdSO_4.2H_2O$/ 0.6 M $HClO_4$. Scan rate = 10 mV s^{-1}.*

Despite the fact that the initial reduction process in the Cu(II)-Pd(II) solution starts at potentials where only Pd deposition could be expected, EDX analysis of a film deposited at -0.48 V *vs* SMSE onto platinum confirms a higher concentration of copper (Cu/Pd ratio = 6.9). This might seem like a contradiction at the beginning, but one should be reminded that in the voltammetry shown in the inset of Figure 5.17, when the potential is reversed at -0.55 V, it is possible to observe in the reverse scan a stripping peak at ~-0.3 V that can be assigned to the presence of copper. According to these results, the presence of palladium seems to catalyze the deposition of copper; from the reverse scan of the solution containing only Cu(II), the metal deposition is thermodynamically possible up to -0.45 V, i.e., in the potential region where the first wave for the Cu(II)-Pd(II) solution is observed.

Electroless copper deposition is a technique widely applied to the printed circuit board manufacturing, where it is necessary to activate the surface of the specimen before copper deposition. This step in the metallization process is normally accomplished by Pd-seeding techniques and it is well known that palladium catalyses the electroless deposition of copper[11-14]. Therefore, it is possible that the palladium has a similar catalytic effect for the deposition of copper in the Cu(II)-Pd(II) solutions studied in this work.

15 mM $CuSO_4.5H_2O$ + 5 mM $PdSO_4.2H_2O$ in 0.6 M $HClO_4$

A similar study was carried out in the presence of 15 mM $CuSO_4.5H_2O$ + 5 mM $PdSO_4.2H_2O$/ 0.6 M $HClO_4$ to observe the effect of a higher copper concentration in the solution. Figure 5.21 shows two cyclic voltammograms obtained with a Pt microdisc (*d* = 25 μm) in this solution. The forward scan seems to be a mixture of at least two processes, with the first one reaching a limiting current around 50 nA. This value is bigger than the 20 nA observed in Figure 5.17, in the presence of equal amounts of Pd and Cu (5 mM), so the increase must be related with the increase in copper concentration. The anodic peaks in the reverse scan are also more pronounced. Two large anodic peaks are observed at -0.16 and 0.10 V and a smaller one at 0.23 V *vs* SMSE. The first two peaks are broader than the one observed in a Cu(II) only solution and occur at more positive potentials. It is likely that these peaks correspond to the dissolution of alloy phases. The charge balance is, however, only ~75% indicating that some metal is not reoxidised. The peak above 0.2 V can, once again, be assigned to the formation of the palladium oxide, with the correspondent oxide stripping peak occurring at ~ 0.0 V if the scan is allowed to continue to negative enough potentials.

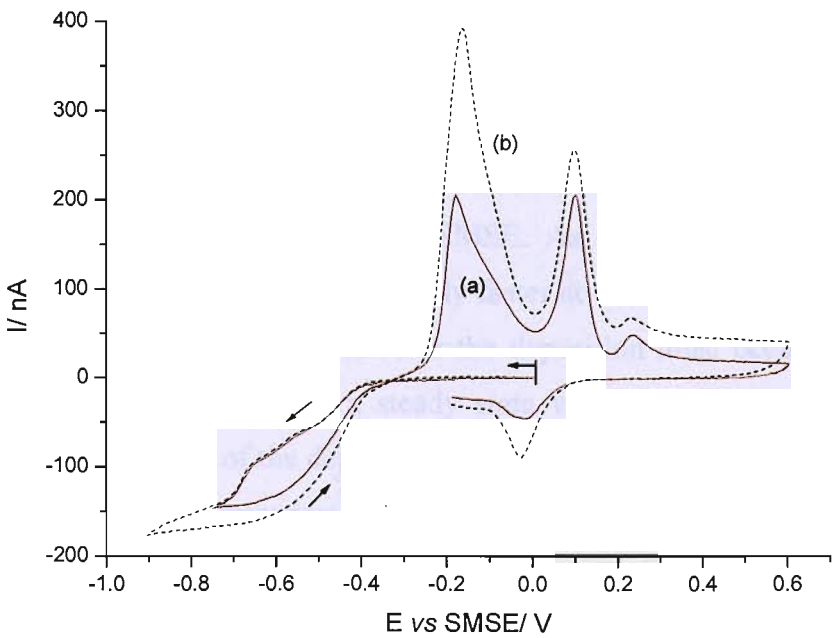

Figure 5.21 *Cyclic voltammograms for a Pt microdisc (d = 25 μm) in 15 mM $CuSO_4.5H_2O$ + 5 mM $PdSO_4.2H_2O$/ 0.6 M $HClO_4$ when reversing the negative potential at (a) -0.75 and (b) -0.90 V vs SMSE. Scan rate = 10 mV s^{-1}.*

Similar features can be observed with gold. Figure 5.22 shows the effect of the negative potential limit on the voltammetry.

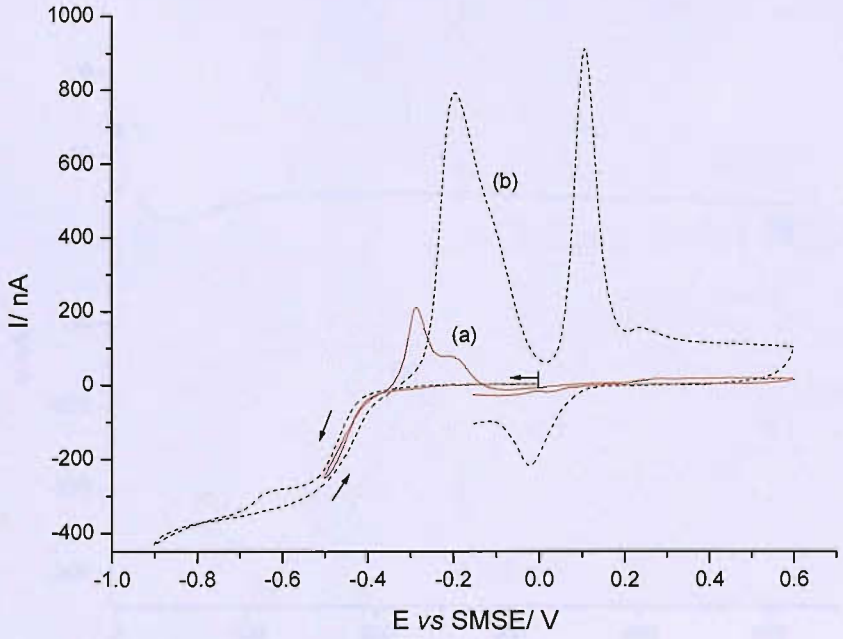

Figure 5.22 *Cyclic voltammograms for a Au microdisc (d = 60 μm) in 15 mM $CuSO_4.5H_2O$ + 5 mM $PdSO_4.2H_2O$/ 0.6 M $HClO_4$ when reversing the negative potential limit at (a) -0.50 and (b) -0.90 V vs SMSE. Scan rate = 10 mV s^{-1}.*

Figure 5.23 reports the current-time transients for the deposition of Cu-Pd films on gold microdiscs at -0.50, -0.55 and -0.60 V *vs* SMSE. As expected, the current reaches higher values and the deposition is significantly faster at -0.60 V. Transients (a) and (b) show a similar behaviour and for both cases the deposition must occur under kinetic control. The current reaches almost a steady state value for t > 50 s, which must correspond to the thickening of the deposit. On the other hand, the deposition at -0.60 V seems to occur under mass transport control and, as can be seen in Figure 5.24, this affects considerably the quality of the deposit. The deposits corresponding to transients (a) and (b) are smooth, uniform and well adherent to the substrate, while the deposition at -0.60 V gives rise to the formation of some dendrites, specially around the edge of the deposit.

EDX analysis from different areas of each film show a uniform distribution of Pd and Cu in the deposits, with the concentration of Pd increasing for the depositions at more negative potentials. Table 5.1 summarizes the data obtained by EDX.

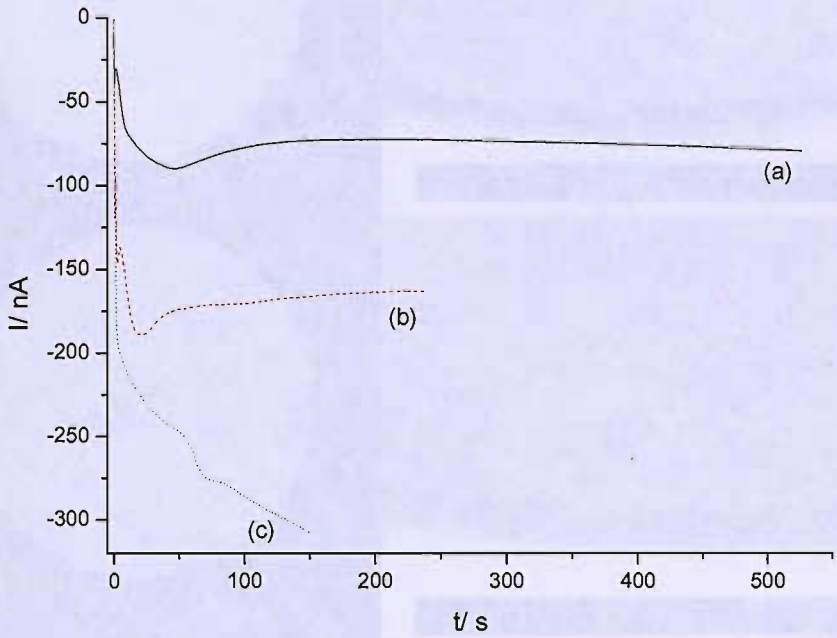

Figure 5.23 *Current-time transients for the deposition of Cu-Pd films from 15 mM $CuSO_4.5H_2O$ + 5 mM $PdSO_4.2H_2O$ / 0.6 M $HClO_4$ on Au microdiscs (d = 60 μm) at: (a) -0.50, (b) -0.55 and (c) -0.60 V vs SMSE. Deposition charge density = 1.4 C cm^{-2}.*

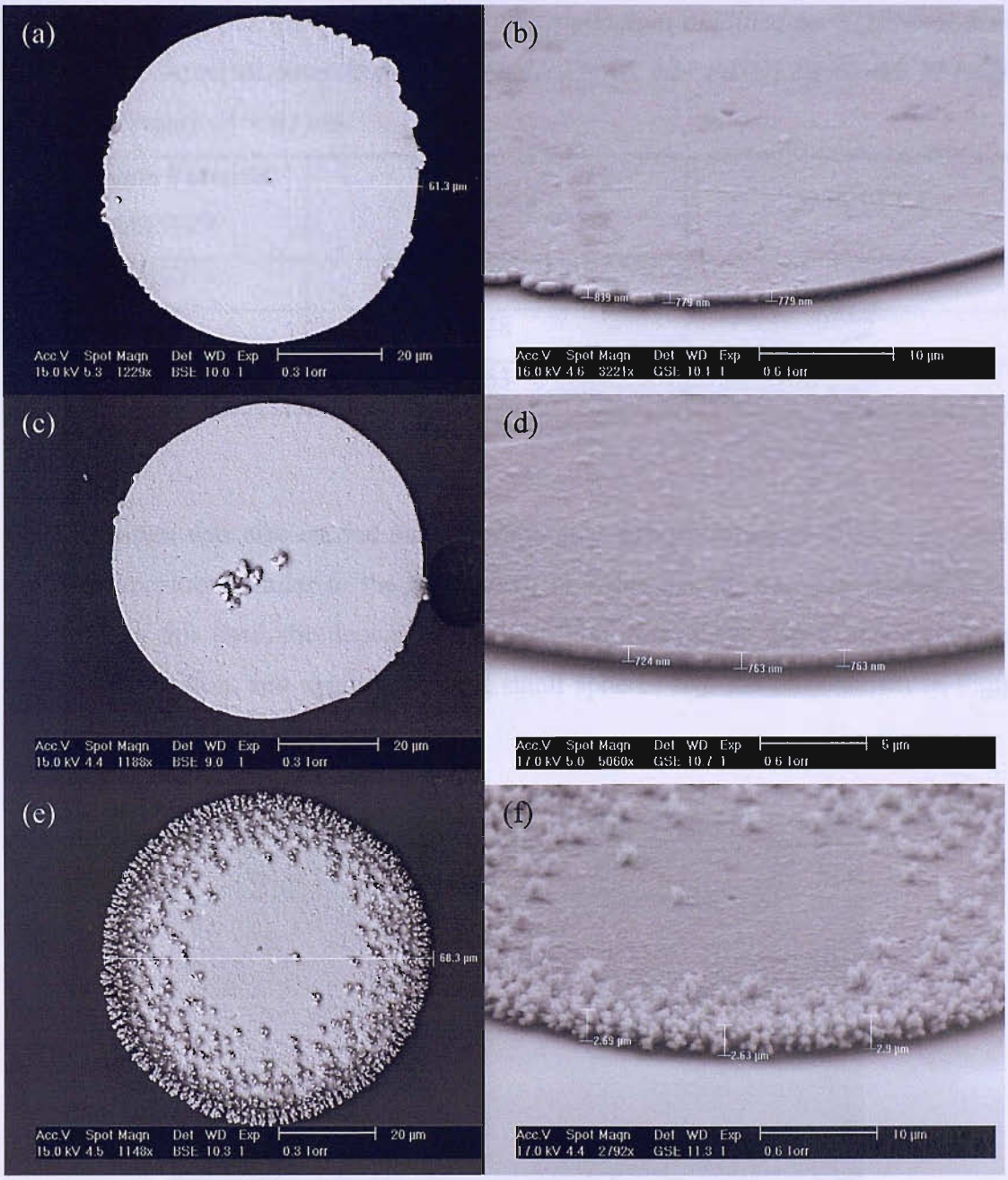

Figure 5.24 *SEM images of Cu-Pd films deposited from 15 mM $CuSO_4.5H_2O$ + 5 mM $PdSO_4.2H_2O$/ 0.6 M $HClO_4$ on Au microdiscs (d = 60 µm) at: (a) -0.50, (b) -0.55 and (c) -0.60 V vs SMSE. Deposition charge density = 1.4 C cm^{-2}.*

Table 5.1 *Atomic percentages of copper and palladium obtained by EDX analysis of Cu-Pd films deposited from 15 mM $CuSO_4.5H_2O$ + 5 mM $PdSO_4.2H_2O$/ 0.6 M $HClO_4$ on Au microdiscs (d = 60 μm).*

Deposition Potential *vs* SMSE/ V	**at % of Cu**	**at % of Pd**
-0.50	90	10
-0.55	78	22
-0.60	63	37

The deposition was also carried out on evaporated gold substrate at -0.50 V *vs* SMSE and a composition similar to the one shown in Table 5.1 for the same potential was observed. In this case, the deposit was not so uniform, maybe due to the bigger area used for deposition, and agglomerates of small spheres like the ones shown in Figure 5.25 were present all over the film.

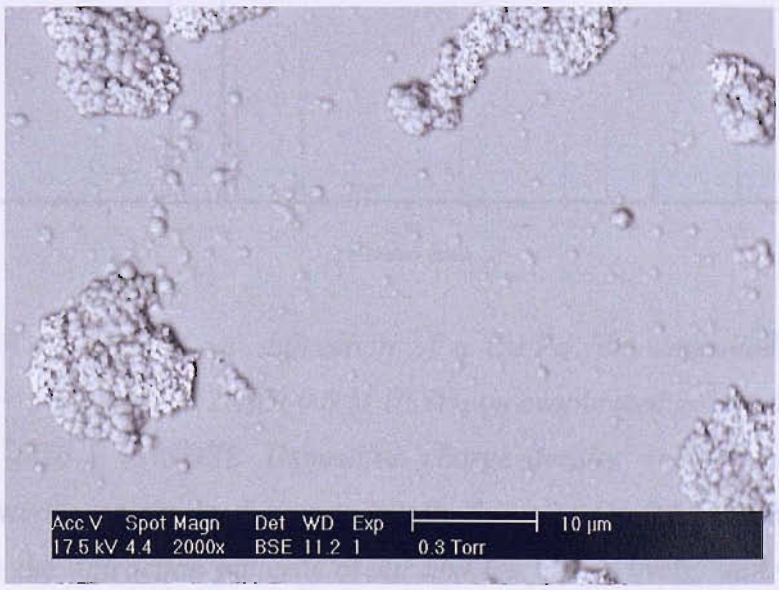

Figure 5.25 *SEM image of a Cu-Pd film deposited from 15 mM $CuSO_4.5H_2O$ + 5 mM $PdSO_4.2H_2O$/ 0.6 M $HClO_4$ on evaporated gold substrate (area = 0.35 cm^2) at -0.50 V vs SMSE. Deposition charge density = 2.0 C cm^2.*

Although there is clear evidence for the formation of alloys shown by cyclic voltammetry, it was not possible to confirm their presence by wide angle X-ray diffraction. For the film shown in Figure 5.25, for example, the diffraction pattern revealed only the presence of Au (from the substrate) and Cu and no peaks could be assigned with Pd, despite the 10 % atomic concentration of this metal given by EDX analysis, see Figure 5.26.

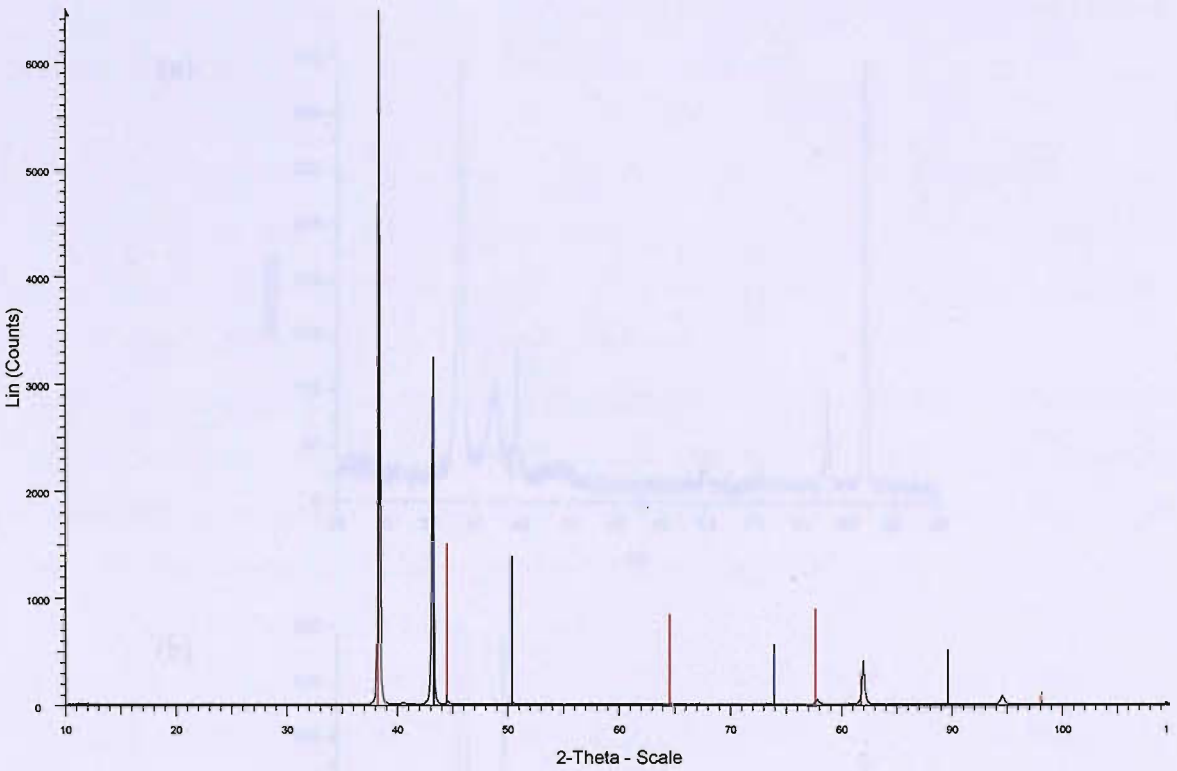

Figure 5.26 *Wide angle X-ray diffraction of a Cu-Pd film deposited from 15 mM $CuSO_4.5H_2O$ + 5 mM $PdSO_4.2H_2O$/ 0.6 M $HClO_4$ on evaporated gold substrate (area = 0.35 cm^2) at -0.50 V vs SMSE. Deposition charge density = 2.0 C cm^2. The black diffraction pattern was obtained experimentally from the Cu-Pd film, the red and the blue lines are the diffraction patterns of Au and Cu, respectively, and were obtained from the Joint Committee on Powder Diffraction Standards (JCPDS) database.*

A possible explanation for the absence of Pd in the diffraction pattern is that the metal is not crystalline, but it exists in an amorphous state. This way, the presence of some Cu-Pd alloys cannot be ruled out and it is well possible that they are also present in an amorphous phase.

In some studies, the identification of crystalline phases of Cu-Pd alloys by X-ray diffraction has been achieved only after thermal treatment of the samples[15]. Considering this approach, some of the Cu-Pd films prepared in this study were heated for 3 hours, in air, at 300 °C before X-ray analysis and the results compared with the ones obtained before treatment. Figure 5.27 shows an example of the diffraction patterns obtained for a Cu-Pd film before and after thermal treatment. As it is possible

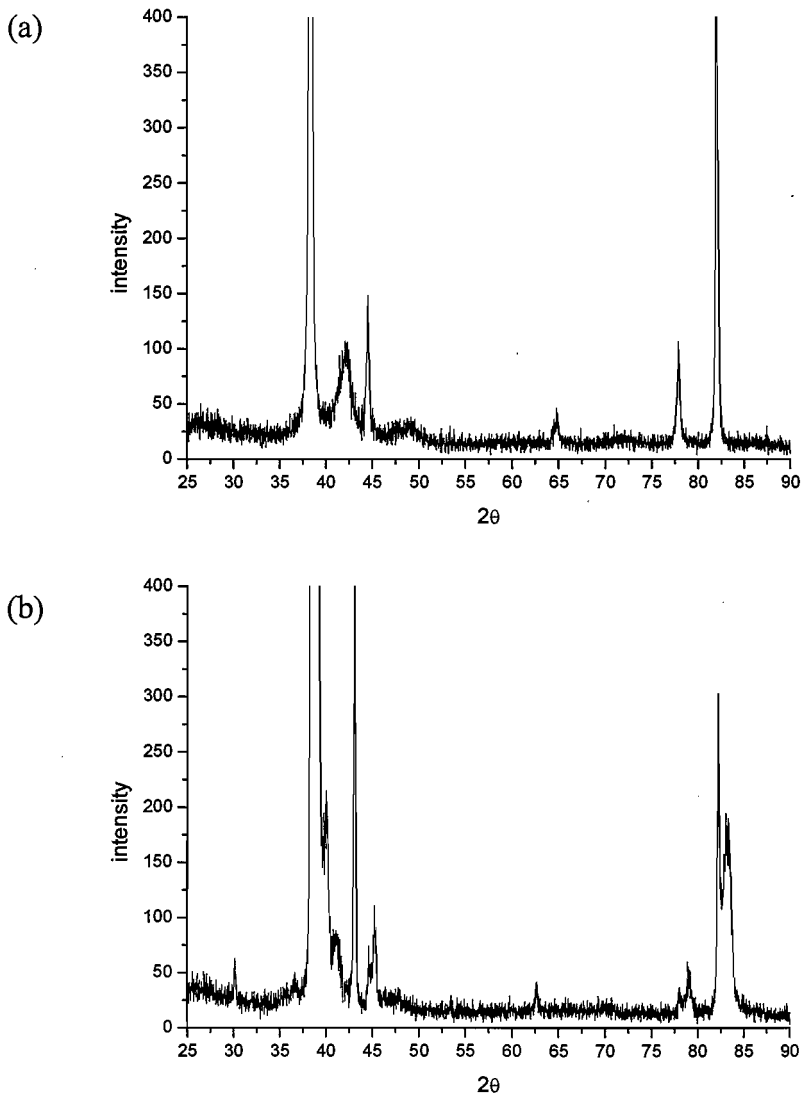

Figure 5.27 *Wide angle X-ray diffraction of a Cu-Pd film deposited from 15 mM $CuSO_4.5H_2O$ + 5 mM $PdSO_4.2H_2O$/ 0.6 M $HClO_4$ on evaporated gold substrate (a ~ 0.5 cm^2) at 0.62 mA cm^{-2}. (a) Before thermal treatment and (b) after 3 h at 300 °C.*

to observe, the diffraction pattern changed significantly after the thermal treatment, but the correct assignment of all the peaks was difficult. Some of the peaks suggest the formation of palladium silicon (Pd_4Si), copper silicon (Cu_4Si) and Cu-Au alloys. The presence of silica is certainly due to the glass slide where the evaporated gold is deposited and it seems that, even at temperatures well below the melting point of the glass, it can interfere significantly with the Cu-Pd film composition if the thermal treatment is carried out. In a similar way, the presence of Cu-Au alloys must be due to some interaction between the evaporated gold substrate and the electrodeposited copper. No indication for the formation of Cu-Pd alloys was found

Some Cu-Pd films were deposited on evaporated gold substrate at constant current, instead of the potentiostatic regime described so far. Figure 5.28 shows SEM images of two deposits obtained from a solution containing 15 mM $CuSO_4.5H_2O$ + 5 mM $PdSO_4.2H_2O$ / 0.6 M $HClO_4$ at 1.2 and 4.4 mA cm^{-2}.

As it is possible to observe, the film deposited at higher current density is considerably rougher and it seems to show a dendritic morphology like the one observed before for Cu-Pd films deposited on microdiscs at -0.60 V *vs* SMSE, compare with Figure 5.24(e). Also by eye, this rougher film showed a black colour, while the film deposited at 1.2 mA cm^{-2} had a nice metallic grey.

Table 5.2 shows the atomic percentages of Pd and Cu given by EDX analysis of different areas of the two deposits and a similar trend to the one obtained before with depositions at constant potential is obtained now, with the Pd concentration increasing with the deposition current density.

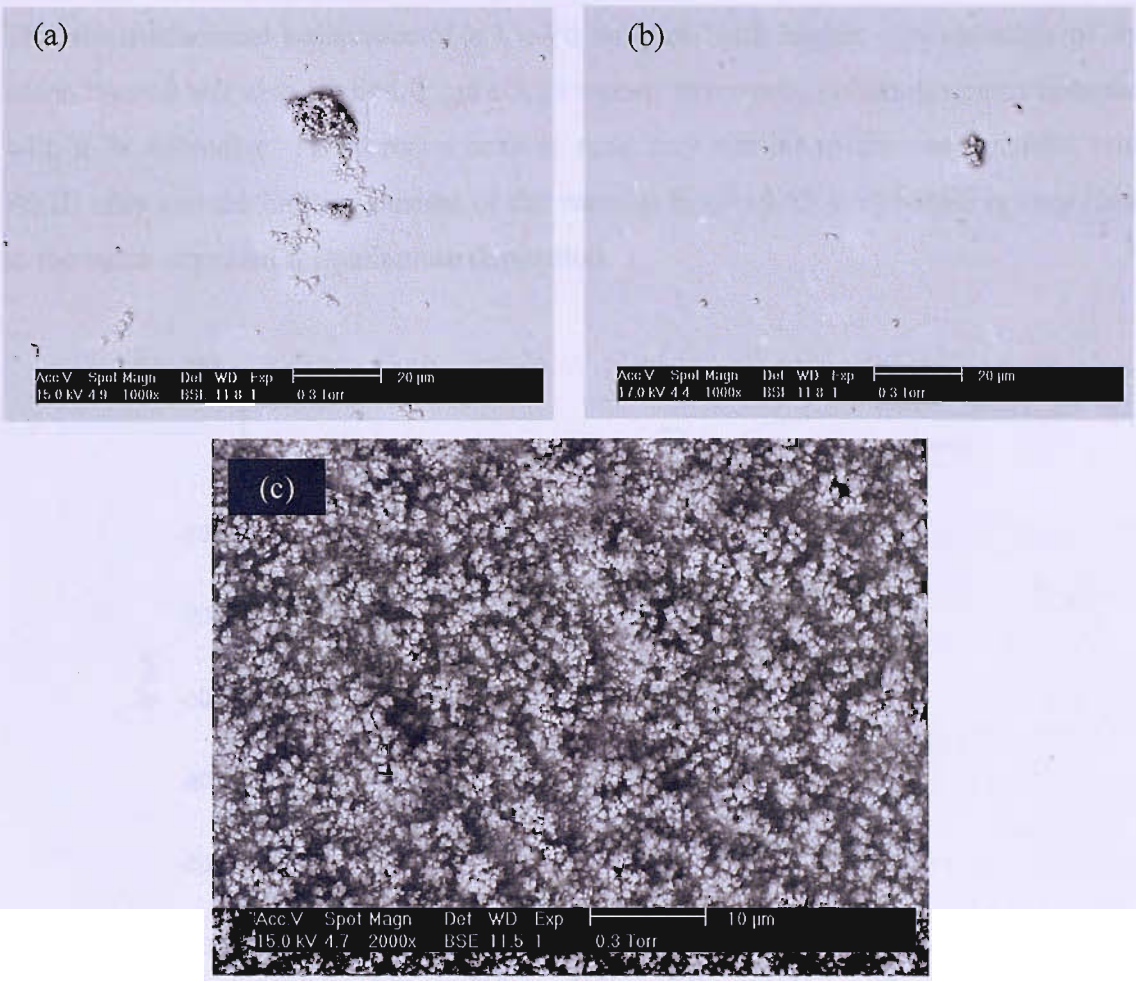

Figure 5.28 *SEM image of Cu-Pd films deposited on evaporated gold substrate (area~ 0.5 cm^2) at (a) and (b) 1.2 and (c) 4.4 mA cm^{-2} from a solution containing 15 mM $CuSO_4.5H_2O$ + 5 mM $PdSO_4.2H_2O$ / 0.6 M $HClO_4$.*

Table 5.2 *Atomic percentages of copper and palladium obtained by EDX analysis of Cu-Pd films deposited from 15 mM $CuSO_4.5H_2O$ + 5 mM $PdSO_4.2H_2O$/ 0.6 M $HClO_4$ on evaporated gold substrate at constant current.*

Deposition current density (mA cm^{-2})	**at % of Cu**	**at % of Pd**
1.2	87	13
4.4	74	26

5 mM $CuSO_4.5H_2O$ + 15 mM $PdSO_4.2H_2O$ in 0.6 M $HClO_4$

The electrochemical behaviour of a Cu-Pd solution with higher concentration of the second metal was also studied. Figure 5.29 reports two cyclic voltammograms obtained with a Pt microdisc. The forward scan is now very similar to the one obtained with Pd(II) only and the limiting current of the wave at $E_{1/2}$ = -0.53 V *vs* SMSE is very close to the value expected for palladium deposition.

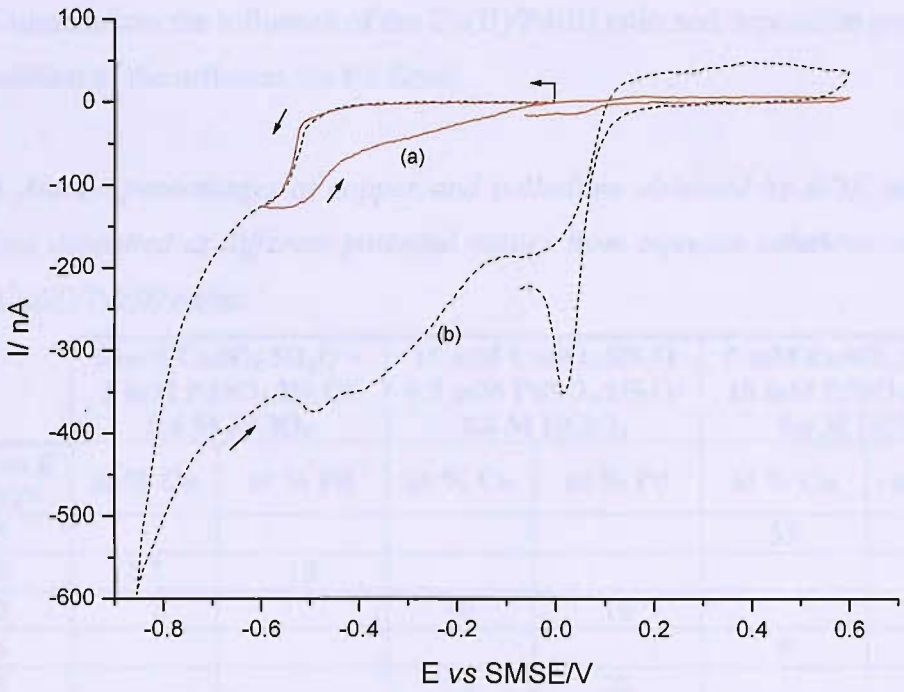

Figure 5.29 *Cyclic voltammograms for a Pt microdisc (d = 25 μm) in 5 mM $CuSO_4.5H_2O$ + 15 mM $PdSO_4.2H_2O$/ 0.6 M $HClO_4$ when reversing the negative potential limit at (a) -0.60 and (b) -0.85 V vs SMSE. Scan rate = 10 mV s^{-1}.*

As before, the negative potential limit has a strong influence in the reverse scan and cycling to more negative potentials introduces new features. The current values in the reverse scan are clearly above the ones expected for the deposition of palladium and copper, compare with Figure 5.15 and 5.16, but, surprisingly, there is no signal of an anodic stripping peak.

Although the initial response in the forward scan resembles the deposition of Pd(II) only, cycling to more negative potentials seems to lead to further deposition of this metal, since a bigger response is obtained in the area corresponding to the palladium oxide formation and reduction. This observation, together with the big currents obtained

in the reverse scan, seem to indicate that the film is actually spreading over the glass. Similar results were obtained with Au microdiscs.

EDX analysis of Cu-Pd films deposited from this solution at -0.45 and -0.54 V *vs* SMSE revealed only a slightly higher copper concentration in the first case, with a Cu/ Pd ratio of 1.1. The concentration of palladium increased dramatically for the deposition at -0.54 were a Cu/ Pd ratio of 0.06 was obtained.

Table 5.3 summarizes the influence of the Cu(II)/Pd(II) ratio and deposition potential on the composition of the different Cu-Pd films.

Table 5.3 *Atomic percentages of copper and palladium obtained by EDX analysis of Cu-Pd films deposited at different potential values from aqueous solutions containing different Cu(II)/Pd(II) ratios.*

	5 mM $CuSO_4.5H_2O$ + 5 mM $PdSO_4.2H_2O$/ 0.6 M $HClO_4$		**15 mM $CuSO_4.5H_2O$ + 5 mM $PdSO_4.2H_2O$/ 0.6 M $HClO_4$**		**5 mM $CuSO_4.5H_2O$ + 15 mM $PdSO_4.2H_2O$/ 0.6 M $HClO_4$**	
Deposition E *vs* SMSE/V	**at % Cu**	**at % Pd**	**at % Cu**	**at % Pd**	**at % Cu**	**at % Pd**
-0.45					53	47
-0.48	87	13				
-0.50			90	10		
-0.54					6	94
-0.55			78	22		
-0.60			63	37		

Petró *et al.*[15, 16] have reported an electrochemical polarization study for a series of Cu-Pd alloy powders of different composition (0 to 80 at% Cu), where they have assigned different features to the presence of unalloyed Pd, Cu_3Pd phases (ordered and disordered) and unalloyed Cu. Some of these features, and specially the peaks assigned with the presence of alloy phases, are remarkably similar to the voltammetry shown here for the different Cu(II)-Pd(II) solutions, which reinforces the idea that Cu-Pd alloys are being formed. The fact they could not be identified by X-ray diffraction might be due to their presence in an amorphous phase.

Mallát and Petró[16] also concluded that the overall Cu content must be kept low (below about 40 at%) to obtain a catalyst surface containing only alloy phases. At higher Cu

content (close to the theoretical composition of Cu_3Pd), the main constituent will be unalloyed Cu.

Lu and co-workers[17] have reported the preparation of Cu-Pd alloy particles from 1 M $HClO_4$ + 1 mM $PdSO_4$ solution containing Cu(II) ion at different deposition potentials in the UPD region of Cu(II). According to the authors, in this potential region, the fraction of Pd in the alloy particles is not dependent on the concentration of Cu(II) in solution and decreases as the deposition potential is made more negative.

From the results shown here for the Pd(II), Cu(II) and Cu(II)-Pd(II) solutions in the presence of $HClO_4$ it is possible to conclude that: (i) the electrochemical behaviour of Cu(II)-Pd(II) solutions is significantly different from the addition of the responses obtained for each metal ion alone and it depends on the relative concentration of the two metals; (ii) the presence of Pd(II) seems to catalyse the copper deposition; (iii) in a Cu(II)-Pd(II) solution new species are formed and the observed features strongly suggest the formation of Cu-Pd alloys and (iv) the composition of the Cu-Pd films depends on deposition potential and relative concentration of both metal ions in solution.

5.6- Nitrate Reduction at Non-Templated Cu-Pd Films Deposited in the Presence of $HClO_4$

Figures 5.30 and 5.31 illustrate the electrochemical behaviour of two non-templated Cu-Pd films for two different nitrate concentrations in 2 M NaOH, at 10 mV s^{-1}. The geometric area of the films was considered for the calculation of the current density.

The features observed positive to -1.2 V *vs* SMSE can be assigned to the formation and reduction of copper and palladium oxides, since they are present in the voltammetry for 2 M NaOH only. In the presence of nitrate, both films show two new waves/peaks at -1.45 and -1.65 V *vs* SMSE and the film with higher copper content seems to give slightly higher current densities. The presence of these waves/peaks is definitely related with NO_3^- reduction and maybe with the reduction of a reaction product resulting from this first step. Moreover, the current limit for the first reduction step is a significant fraction of the current expected for a $8e^-$ process under mass transport control (44% in the case shown in Figure 5.30).

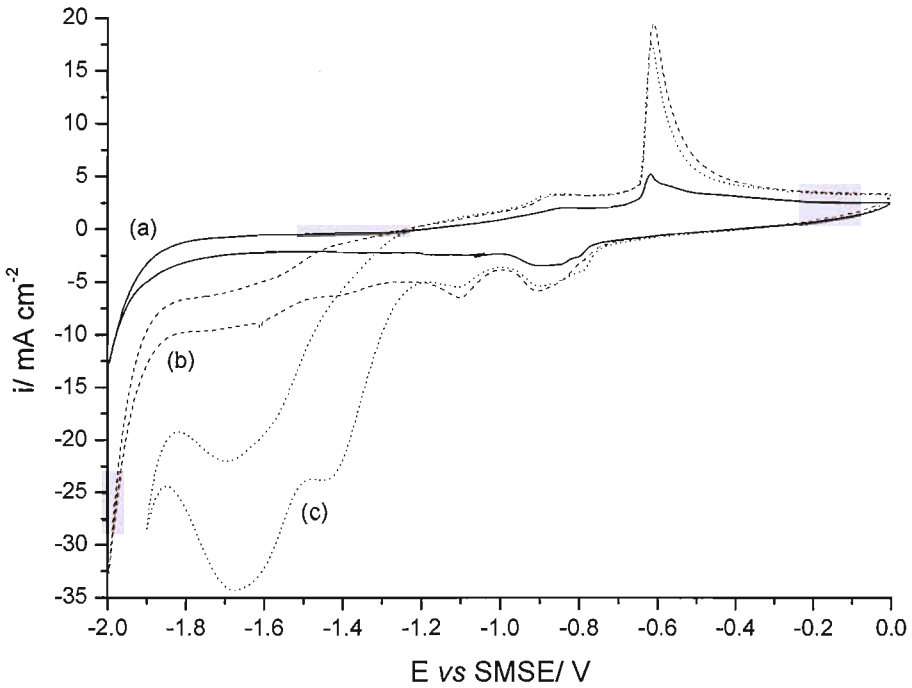

Figure 5.30 *Cyclic voltammograms for a Cu-Pd film deposited from 15 mM $CuSO_4.5H_2O$ + 5 mM $PdSO_4.2H_2O$/ 0.6 M $HClO_4$ on Au microdiscs (d = 60 μm) at -0.55 V vs SMSE in (a) 2 M NaOH, (b) 15 mM $NaNO_3$/ 2 M NaOH and (c) 30 mM $NaNO_3$/ 2 M NaOH. Deposition charge density = 1.4 C cm^{-2}. Film composition = 78 at% Cu + 22 at% Pd. Scan rate = 10 mV s^{-1}.*

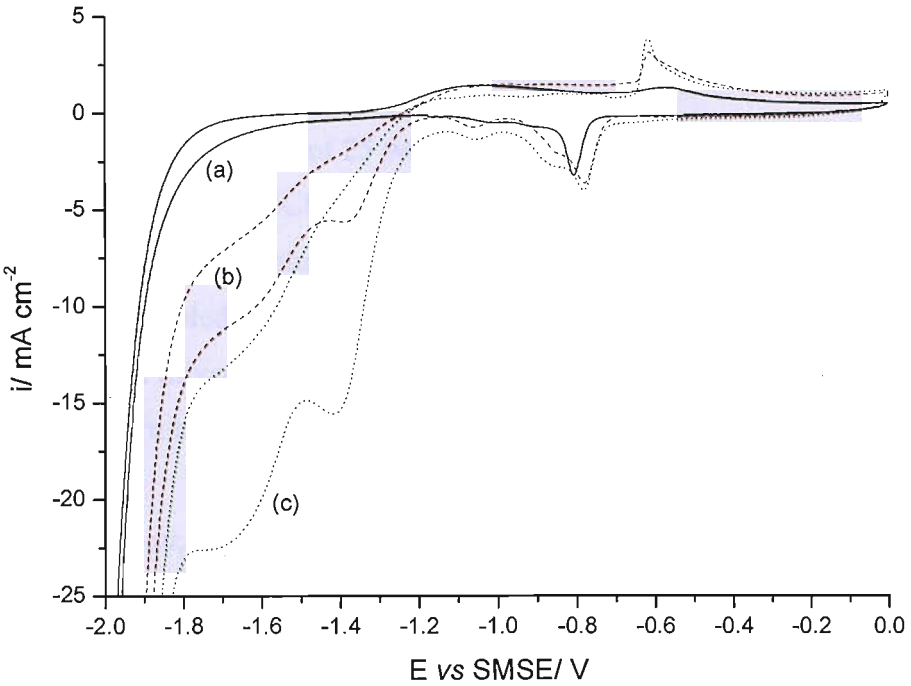

Figure 5.31 *Cyclic voltammograms for a Cu-Pd film deposited from 15 mM $CuSO_4.5H_2O$ + 5 mM $PdSO_4.2H_2O$/ 0.6 M $HClO_4$ on Au microdiscs (d = 60 μm) at -0.60 V vs SMSE in (a) 2 M NaOH, (b) 15 mM $NaNO_3$/ 2 M NaOH and (c) 30 mM $NaNO_3$/ 2 M NaOH. Deposition charge density = 1.4 C cm^{-2}. Film composition = 63 at% Cu and 37 at% Pd. Scan rate = 10 mV s^{-1}.*

It has been shown before in this study that the current for nitrate and nitrite reduction is dependent on the positive potential limit used in the voltammetry, with higher currents being observed when the voltammogram extends to 0.0 V *vs* SMSE. In the case of Pd-Cu films, however, this potential limit clearly implies the dissolution of copper during cycling and significant changes occur in the voltammetry positive to -1.2 V, as can be seen in Figures 5.30 and 5.31. To increase the durability of these deposits, one might then need to compromise the amount of signal obtained for nitrate reduction and carry out the voltammetry in a narrower range of potential.

5.7- Preparation and Characterisation of Cu-Pd Templating Mixtures in the Presence of $HClO_4$

A templating mixture consisting of 25 wt% 20 mM $PdSO_4.2H_2O$/ 0.6 M $HClO_4$, 25 wt% 50 mM $CuSO_4.5H_2O$/ 0.6 M $HClO_4$ and 50 wt% $C_{16}EO_8$ was prepared in the usual way. A proper amount of the two solutions was first mixed in a small glass container and the surfactant was then added. In this case, the plating mixture was warmed up to 72 °C with a hot plate and mixed with a glass rod until it became homogeneous. It was then allowed to cool down to 25 °C using a water bath and it was kept at this temperature for 2 hours.

By optical microscopy, the mixture shows the typical texture of the hexagonal phase up to 73 °C. This temperature is considerably higher than what has been observed before, during the preparation of mesoporous Pd and Cu films, and may be due to the presence of $HClO_4$.

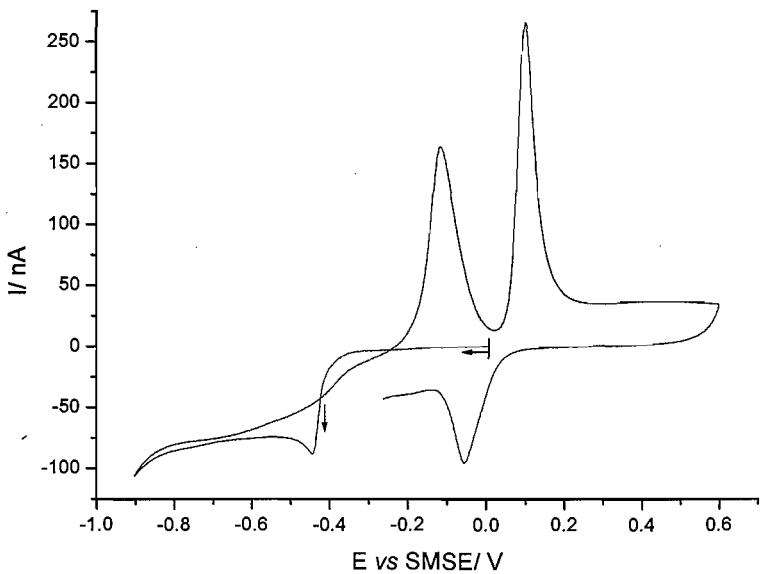

Figure 5.32 *Cyclic voltammogram for a Au microdisc (d = 60 μm) in a plating mixture containing 25 wt% 20 mM $PdSO_4.2H_2O$/ 0.6 M $HClO_4$, 25 wt% 50 mM $CuSO_4.5H_2O$/ 0.6 M $HClO_4$ and 50 wt% $C_{16}EO_8$. Scan rate = 10 mV s^{-1}.*

The electrochemical behaviour of this plating mixture, see Figure 5.32, shows some similarities to the voltammetry shown before for the solution containing 15 mM $CuSO_4.5H_2O$ + 5 mM $PdSO_4.2H_2O$ in 0.6 M $HClO_4$ however, two main differences can

be found in the presence of $C_{16}EO_8$: (i) the forward scan shows only one reduction wave and (ii) the absence of the small peak at ~0.25 V *vs* SMSE.

5.8- Electrodeposition and Characterisation of Cu-Pd Films from a Templating Mixtures in the Presence of $HClO_4$

Several depositions were carried out at different potential values to study the effect of the deposition potential on the composition of the films. Figure 5.33 shows some examples of the current-time transients obtained and, as it is possible to observe, despite the small difference in deposition potential, the current tends to a steady state value and the deposition seems to occur under mass transport control.

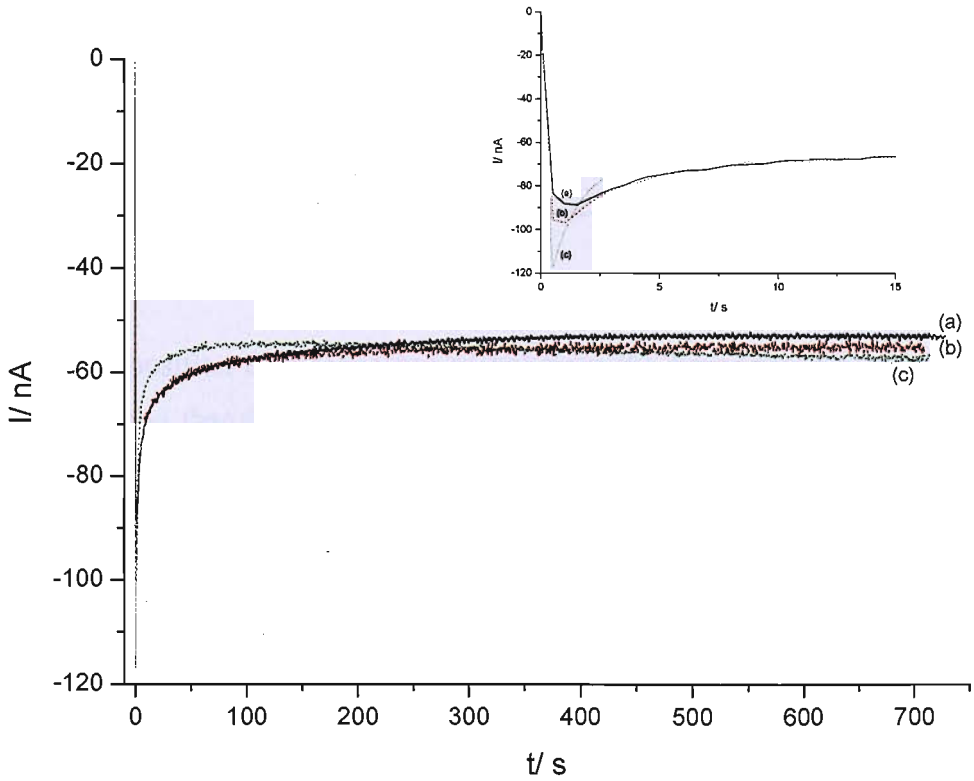

Figure 5.33 *Current-time transients for the deposition of Cu-Pd films on Au microdiscs (d = 60 μm) from a plating mixture containing 25 wt% 20 mM $PdSO_4.2H_2O$/ 0.6 M $HClO_4$, 25 wt% 50 mM $CuSO_4.5H_2O$/ 0.6 M $HClO_4$ and 50 wt% $C_{16}EO_8$. Deposition potential: (a) -0.40 V, (b) -0.42 V and (c) -0.44 V vs SMSE. Deposition current density = 1.41 C cm^{-2}. The inset shows in more detail the first 15 s of the three transients.*

Table 5.3 summarizes the results obtained by EDX analysis of Cu-Pd films deposited at four different potentials. Surprisingly, the trend observed now in the presence of surfactant, with the atomic percentage of palladium decreasing for depositions at more negative potentials, is the opposite to the one obtained for 15 mM $CuSO_4.5H_2O$ + 5 mM $PdSO_4.2H_2O$ in 0.6 M $HClO_4$, compare Tables 5.1 and 5.3. No explanation can be given at the moment but, once again, the surfactant seems to play an important role in determining the behaviour of the solutions.

Table 5.3 *Atomic percentages of copper and palladium obtained by EDX analysis of Cu-Pd films deposited at four different potentials from a templating mixture containing 25 wt% 20 mM $PdSO_4.2H_2O$/ 0.6 M $HClO_4$, 25 wt% 50 mM $CuSO_4.5H_2O$/ 0.6 M $HClO_4$ and 50 wt% $C_{16}EO_8$.*

Deposition Potential *vs* SMSE/ V	**at % of Cu**	**at % of Pd**
-0.40	51	49
-0.41	61	39
-0.42	64	36
-0.44	67	33

For the deposition of mesoporous nickel from the hexagonal phase of Brij® 56 it has been reported that the annealing of the plating mixture just before deposition helps to improve the quality of the deposits in terms of structure and increases the active surface area of the nanostructure[18]. Considering this, some depositions were carried out at different potentials and, for the first time in this study, the plating mixture was annealed before some of the depositions to verify the influence of this procedure on the quality of the Cu-Pd films. Some microdiscs were placed in the plating mixture and the mixture was then warmed up to 60 °C with a water bath, and allowed to cool down again to 25 °C. After the annealing, the deposition was carried out at 25 °C, according to the normal procedure. Figures 5.34 shows some SEM images of the deposits obtained.

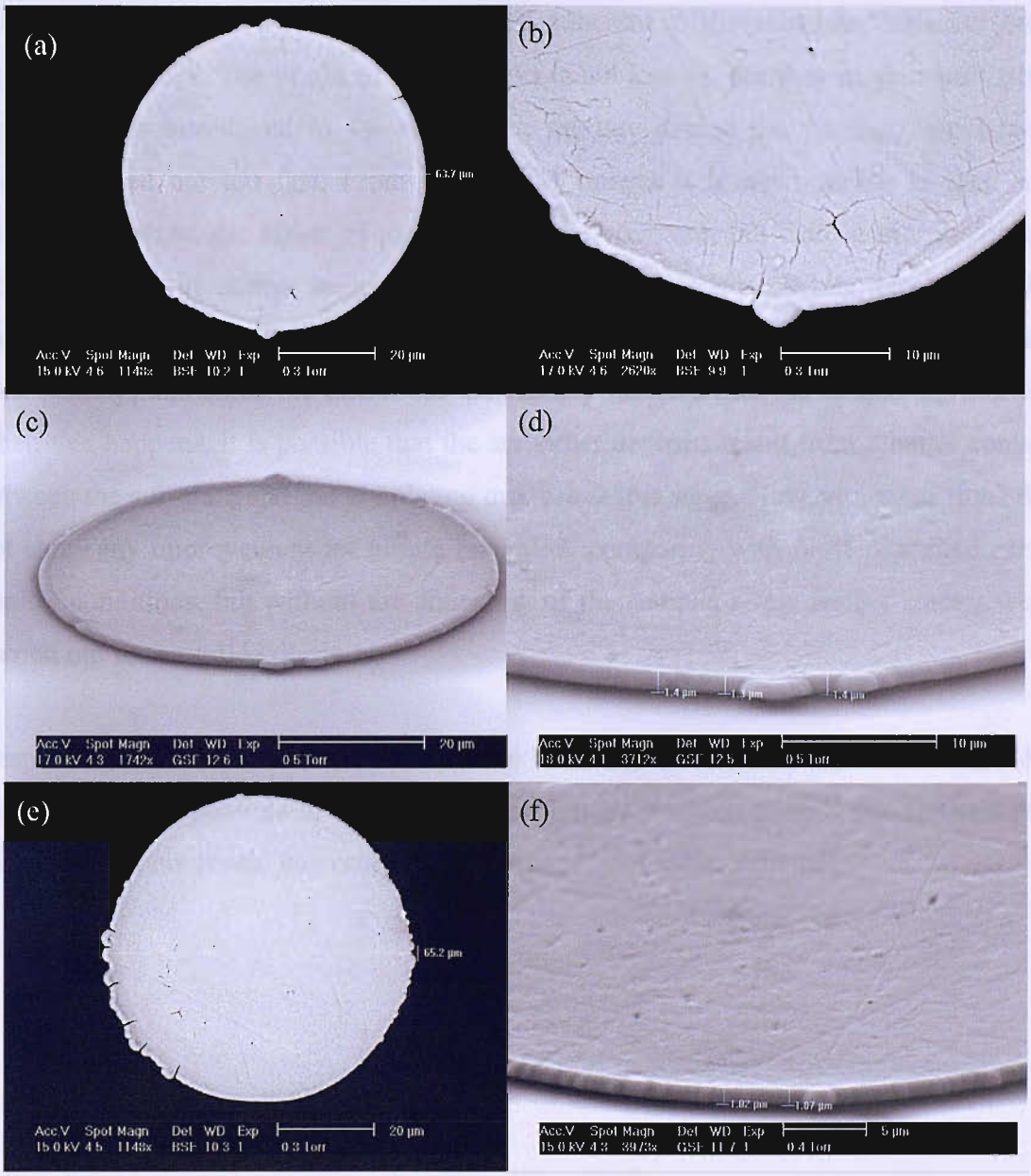

Figure 5.34 *SEM images of Cu-Pd films deposited on Au microdiscs (d = 60 µm) from a plating mixture containing 25 wt% 20 mM $PdSO_4.2H_2O$/ 0.6 M $HClO_4$, 25 wt% 50 mM $CuSO_4.5H_2O$/ 0.6 M $HClO_4$ and 50 wt% $C_{16}EO_8$, after annealing of the plating mixture. Deposition potential: (a)-(d) -0.40 V and (e), (f) -0.42 V vs SMSE. Deposition current density = 1.41 C cm^{-2}. Figures (a) to (d) correspond to the same film.*

As it is possible to observe, the two films deposited after the annealing of the plating mixture are very uniform, smooth and well adherent to the substrate, however both show some cracks. The origin of these cracks is not known, but they might result from some stresses introduced in the templating mixture during the cooling, which was maybe carried out too fast. From these SEM images it is not possible to take any conclusions about the effect of annealing on the structure, but from a morphological point of view, it seems to give rise to smoother deposits. While increasing the temperature during annealing, the viscosity of the templating mixture decreases considerably, and since the electrodes are already inserted into the templating mixture when this happens, it is possible that the smoother deposits result from a better contact between the substrate and the templating mixture at this stage. However, these films did not show any improvement for nitrate reduction, comparing with films deposited using similar conditions, but without the annealing of the sample, so no further studies were carried out for annealed deposits.

Despite all the efforts carried out to obtain well organized and nanostructured Cu-Pd films, it was not possible to obtain any structural information from X-ray analysis and TEM also did not reveal any ordered pore arrangement in the structure.

5.9- Nitrate Reduction at Cu-Pd Films Electrodeposited in the Presence of $C_{16}EO_8$ and $HClO_4$

Figure 5.35 reports the electrochemical behaviour of a Cu-Pd film in 2 M NaOH and in the presence of 30 mM $NaNO_3$.

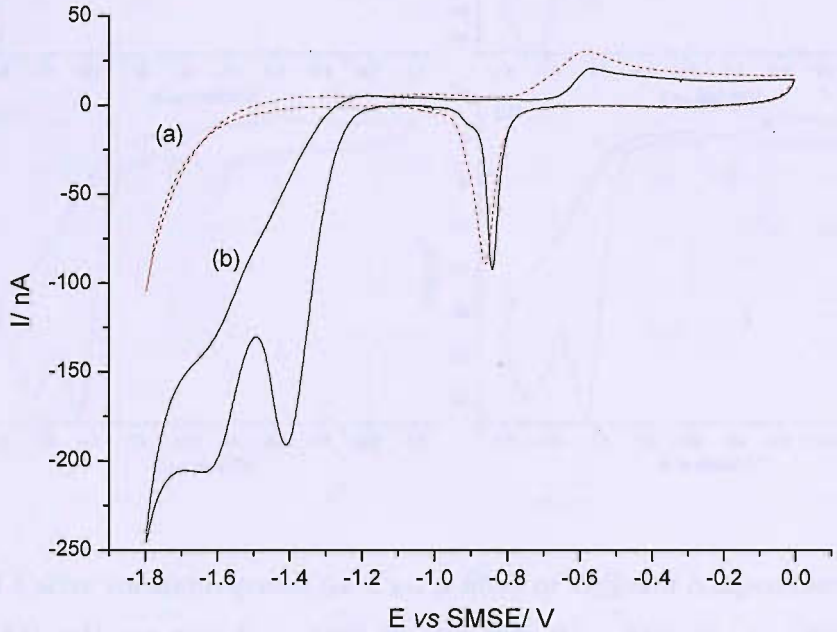

Figure 5.35 *Cyclic voltammograms for a Cu-Pd film deposited on a Pt microdisc (d = 25 μm) from a plating mixture containing 25 wt% 20 mM $PdSO_4.2H_2O$/ 0.6 M $HClO_4$, 25 wt% 50 mM $CuSO_4.5H_2O$/ 0.6 M $HClO_4$ and 50 wt% $C_{16}EO_8$ in (a) 2 M NaOH and (b) 30 mM $NaNO_3$/ 2 M NaOH. Film composition: 49 at% Pd + 51 at% Cu. Scan rate =10 mV s^{-1}.*

Despite the presence of similar concentrations of both metals in the deposit (49 at% Pd and 51 at% Cu), the features positive to -1.2 V are similar to the behaviour of palladium only in 2 M NaOH. As with the non-templated Cu-Pd films, in the presence of 30 mM $NaNO_3$ one reduction peak appears at -1.4 and a wave at -1.6 V *vs* SMSE, but again the current value corresponding to the first process is below the value expected for a 8e- diffusion controlled process. In Figure 5.36 the electrochemical response of four Cu-Pd films, with different compositions, in the presence of 30 mM $NaNO_3$ is compared. The geometric areas of the deposits were considered for the calculation of the current density values.

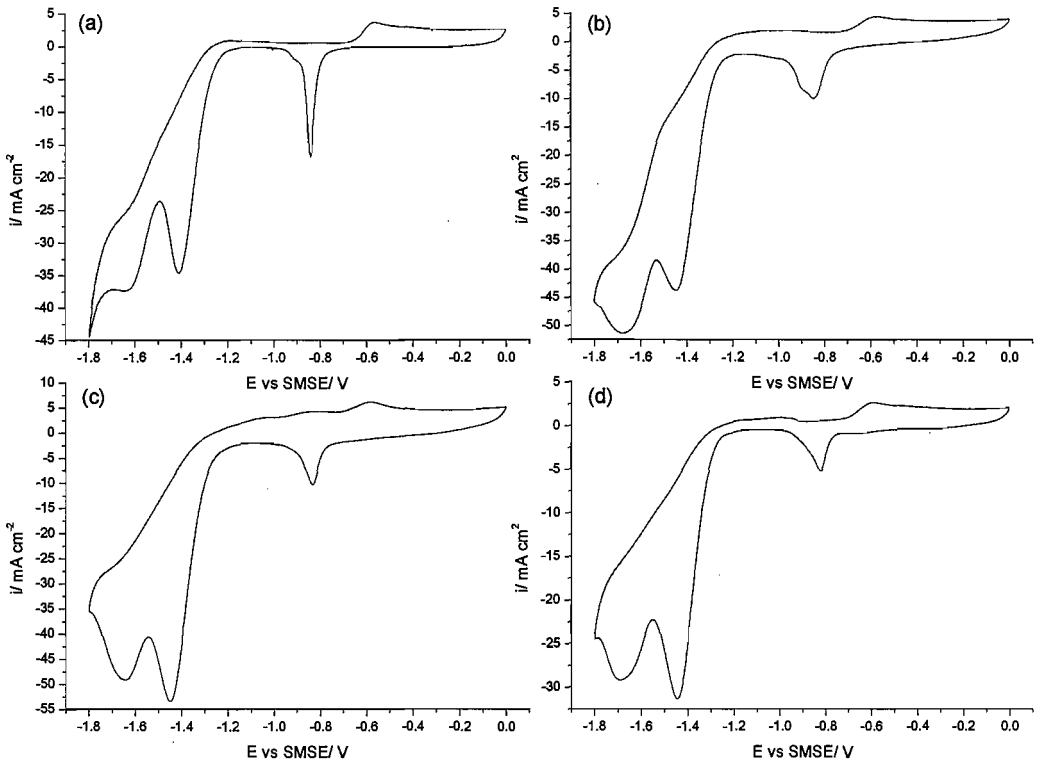

Figure 5.36 *Cyclic voltammograms for Cu-Pd films of different compositions in 30 mM $NaNO_3$/ 2 M NaOH. (a) 49% Pd + 51% Cu, (b) 39% Pd + 61% Cu, (c) 36% Pd + 64% Cu and (d) 33% Pd + 67% Cu. Scan rate = 10 mV s^{-1}.*

All deposits show two peaks associated with nitrate reduction. The first peak ~-1.4 V and the second one at ~-1.6 V. The current densities are slightly higher for compositions (b) and (c), i.e., 39% Pd + 61% Cu and 36% Pd + 64% Cu, but since the composition range studied here is very narrow, it is not possible to conclude if this effect is due to the Cu-Pd ratio only, or if there are some other factors affecting the response of the deposits.

The peak at -0.6 V is present in the four deposits and, once again, can be assigned to the formation of Pd oxide, with the correspondent reduction peak appearing at ~-0.85 V. The broadening of this peak in the last three voltammograms, together with a slight increase in anodic current between -1.2 and -0.7 V might be related with the presence of copper, but it is remarkable how even in the presence of 67 at% Cu the voltammetry positive to -1.2 V looks so similar to the one obtained for Pd only in the same medium.

Nishimura *et al.*[19] have studied the electrochemical response of Cu-Pd and Au-Pd alloys of different compositions in 1 M NaOH and similar effects to the ones observed in Figure 5.36 have been reported. In their work, the Cu-Pd alloys have been studied in a shorter range of potential to avoid Cu oxidation, but it is possible to observe how even small contents of Cu affect significantly the response in the Pd-H oxidation region, with the peak for hydrogen desorption disappearing completely in the presence of only 28.5 at% of Cu in the alloy.

The Au-Pd alloys have been studied in a potential range similar to the one used in the present work and, in this case, the following features have been observed: (i) the current for the Pd-H desorption peak decreases with the increase in Au content; (ii) the alloys give a single oxide reduction peak over a wide range of compositions, except for Au rich alloys such as $Au_{80}Pd_{20}$, at which two peaks are seen and (iii) only for this composition, or higher content of Au, one starts to observe a peak due to gold oxidation.

Comparing the responses obtained for the Cu-Pd films deposited from the templating mixture with the responses shown before for the non-templating films, compare Figures 5.30, 5.31 and 5.36, it is possible to conclude that they are similar. It is possible that the small differences obtained in the current are due to the different composition of the films, but no significant improvement for nitrate reduction has been observed in the presence of the templating films.

5.10- Conclusion

It has been shown that the electrochemical response of Cu(II)-Pd(II) solutions in H_2SO_4 and $HClO_4$ is significantly different from the addition of the voltammetric responses obtained for each metal ion alone. Despite the fact that it was not possible to obtain any diffraction pattern proving the presence of Cu-Pd alloys in the electrodeposited film, the electrochemical results clearly show the formation of alloys.

The composition of the plating bath and the deposition potential strongly influence the Cu:Pd ratio present in the electrodeposited films and different trends were found in the presence and absence of surfactant.

The higher solubility of $PdSO_4.2H_2O$ in $HClO_4$, comparing with H_2SO_4, clearly improves the quality of the deposits obtained in the presence of $C_{16}EO_8$.

As with Cu films, the Cu-Pd films give a sigmoidal shape for the reduction of nitrate in acid media with a limiting current reaching the value expected for a diffusion controlled process. The response in 2 M NaOH shows the formation of two peaks/ waves due to the presence of NO_3^-, but the correct assignment of both features cannot be done.

5.11- References

[1] A. Pintar, *Catal. Today* **2003**, *77*, 451.

[2] F. Deganello, L. F. Liotta, A. Macaluso, A. M. Venezia, G. Deganello, *Appl. Catal. B* **2000**, *24*, 265.

[3] Y. Yoshinaga, T. Akita, I. Mikami, T. Okuhara, *J. Catal.* **2002**, *207*, 37.

[4] M. Chollier-Brym, R. Gavagnin, G. Strukul, M. Marella, M. Tomaselli, P. Ruiz, *Catal. Today* **2002**, *75*, 49.

[5] A. C. A. de Vooys, R. A. van Santen, J. A. R. van Veen, *J. Mol. Catal. A* **2000**, *154*, 203.

[6] Y. Wang, J. H. Qu, H. J. Liu, *Chin. Chem. Lett.* **2006**, *17*, 61.

[7] M. Ilieva, V. Tsakova, W. Erfurth, *Electrochim. Acta* **2006**, *52*, 816.

[8] N. G. Carpenter, D. Pletcher, *Anal. Chim. Acta* **1995**, *317*, 287.

[9] U. Bertocci, D. R. Turner, in *Encyclopedia of Electrochemistry of the Elements, Vol. II* (Ed.: A. J. Bard), Marcel Dekker, New York, **1974**, pp. 383.

[10] A. M. C. L. d. Medina, S. L. Marchiano, A. J. Arvia, *J. Appl. Electrochem.* **1978**, *8*, 121.

[11] K. Kondo, F. Ishikawa, N. Ishida, M. Irie, *Chem. Lett.* **1992**, 999.

[12] J. H. Lin, Y. Y. Tsai, S. Y. Chiu, T. L. Lee, C. M. Tsai, P. H. Chen, C. C. Lin, M. S. Feng, C. S. Kou, H. C. Shih, *Thin Solid Films* **2000**, *377*, 592.

[13] S. Y. Chang, C. W. Lin, H. H. Hsu, J. H. Fang, S. J. Lin, *J. Electrochem. Soc* **2004**, *151*, C81.

[14] C. A. Deckert, *Plat. Surf. Fin.* **1995**, *82*, 58.

[15] J. Petro, T. Mallat, S. Szabo, F. Hange, *J. Electroanal. Chem.* **1984**, *160*, 289.

[16] T. Mallat, J. Petro, *J. Electroanal. Chem.* **1988**, *239*, 409.

[17] D. L. Lu, M. Ichihara, K. Tanaka, *Electrochim. Acta* **1998**, *43*, 2325.

[18] P. A. Nelson, PhD thesis, University of Southampton **2003**.

[19] K. Nishimura, K. I. Machida, M. Enyo, *J. Electroanal. Chem.* **1988**, *251*, 103.

Chapter 6- Conclusions

It was been confirmed that it is possible to electrodeposit mesoporous Pd films (H_1-ePd) from the hexagonal lyotropic liquid crystalline phase of Brij® 56 and $C_{16}EO_8$ onto Pt microdisc electrodes. The films electrodeposited from $C_{16}EO_8$ are well adherent to the substrate, considerably smoother than the films from Brij® 56 and with specific surface areas consistently higher by a factor of ~2. These mesoporous Pd films allow the study of additional surface processes and show a higher response for nitrate and nitrite electroreduction when compared with bulk Pd and smooth Pd films.

The cathodic reduction of nitrate at H_1-ePd films in 2 M NaOH shows a small symmetric peak at -1.34 V *vs* SMSE and its characteristics clearly indicate that the reduction of the anion in alkaline media involves surface chemistry. A similar situation is observed in the presence of nitrite, however, the response of the mesoporous Pd films is substantially higher in this case. The presence NO_2^- in 2 M NaOH also introduces significant changes in the anodic part of the voltammogram, comparing with the response obtained in the presence of NO_3^- and 2 M NaOH only. The observed features suggest a chemical reaction between adsorbed hydrogen and adsorbed nitrite as a key step in the mechanism for nitrite reduction.

The electrodeposition of mesoporous Cu films proved to be a difficult task, but certainly the results reported in this thesis can help further studies. It has been shown that it is possible to obtain a stable hexagonal phase in the presence of $CuSO_4.5H_2O$, H_2SO_4 and $C_{16}EO_8$ up to ~50 °C, but the increase in temperature gives rise to a heterogeneous phase. TEM analysis of copper films electrodeposited from this templating mixture revealed the presence of a non-uniform porous structure, with the pores having a random distribution. Templating mixtures containing $C_{16}EO_8$ and methanesulfonic acid also allow the formation of a hexagonal phase and clearly overcome some of the problems found in the presence of H_2SO_4. The phase diagram for the system $C_{16}EO_8$ + 0.2 M $Cu(CH_3SO_3)_2$/ 0.1 M CH_3SO_3H was studied in detail and a stable hexagonal

phase can be observed for compositions between 35 and 70 wt% surfactant and temperatures between 20 and 55 °C. Based on the phase diagram, a templating mixture consisting of 50 wt% $C_{16}EO_8$ and 50 wt% 0.2 M $Cu(CH_3SO_3)_2$/ 0.1 M CH_3SO_3H was investigated. This plating mixture allowed the deposition of smooth and adherent Cu films, but it was not possible to confirm the presence of a porous structure during the timescale of this project.

In terms of electrochemical characterisation, the voltammetry of copper in alkaline solutions containing sodium sulphide revealed a pair of peaks between -1.2 and -0.7 V *vs* SCE. The charges under these peaks could be associated with the formation and reduction of a monolayer, but it was evident from their shape and their peak current dependence on the positive potential limit that a more complex process was occurring and that this method would not be appropriate for the correct estimation of the copper surface area. The underpotential deposition of lead on copper seems to be a more promising approach, however, it was not possible to confirm the presence of a high area copper surface with this method either.

Despite all the difficulties faced while trying to find a suitable method for the electrochemical characterisation of a high surface area copper film and the fact that TEM analysis shows only the presence of some irregular pores, the copper films electrodeposited in the presence of $C_{16}EO_8$ show a considerable positive shift for the nitrate reduction potential in acidic medium when compared with the response at a polished Cu disc or even with the response at a Cu film deposited *in situ*. In basic media, a positive potential shift of ~100 mV is also observed at Cu films deposited in the presence of surfactant, when compared with the response at a non-templated Cu film.

The results reported in the last chapter of this thesis are, to the best of our knowledge some of the few results published so far in terms of Cu(II)-Pd(II) electrochemistry. The complex response in the presence of the two metal ions strongly suggests the formation of Cu-Pd alloys, as well as a catalytic effect on the electrodeposition of copper due to the presence of Pd(II).

The low solubility of $PdSO_4.2H_2O$ in 0.1 M H_2SO_4 interferes with the preparation of a templating mixture containing $C_{16}EO_8$ and it is evident that in this medium an increase in temperature clearly favours the palladium ion reduction by the surfactant. In the

presence of $HClO_4$ the complete dissolution of the palladium salt precursor is achieved and smooth and well adherent Cu-Pd films can be obtained.

The response for nitrate electroreduction at Cu-Pd films in acidic media is close to the one obtained at *in situ* plated Cu films. In basic media, the peak current for nitrate reduction is smaller than at Cu films electrodeposited from the liquid crystalline phase, but it occurs at more positive potentials. Comparing with the results observed at mesoporous Pd, it has been shown that a small amount of Cu (~ 25 wt%) clearly improves the response for nitrate. However, no significant differences were observed between the responses obtained at smooth Cu-Pd films and at Cu-Pd films electrodeposited in the presence of surfactant. It is clear from the voltammetry that the nitrate response depends on the Cu:Pd ratio present on the deposit and this factor must be taken into account when comparing the results obtained at different Cu-Pd films. It has been shown that the ratio of the two metals depends on the deposition potential and composition of solution/ plating mixture, but different trends have been observed in the presence and absence of surfactant.

The electrochemistry of the Cu-Pd films in 2 M NaOH shows only minor features that can be related with the surface electrochemistry of copper in this medium, which strongly suggests some kind of stabilization due to the presence of palladium.

Some fundamental questions have also been raised throughout this project and even if a clear explanation cannot be given for some of them, at least they are not ignored. How does the presence of surfactant, in this case $C_{16}EO_8$, affect the metal electrodeposition in this templating method? It is clear from the results shown for Pd, for example, that the surfactant is not only a "simple spectator", providing the template for the metal deposition. The voltammetry strongly suggests some complexation between $C_{16}EO_8$ and Pd(II). How does the metal electrodepositon around the surfactant rods occur? Does it obey the basic fundaments of deposition and growth observed at a macrodisc, for example? Some of the current-time transients obtained seem to reveal a more complex process. The cleaning of the Cu films electrodeposited in the presence of surfactant and all the protective procedures between the time of their preparation and analysis are some other issues. It was observed that the cleaning with water triggers the oxidation of the films. The cleaning in 2-propanol seems to delay the process while the deposits are in solution, but oxidation occurs as soon as they are exposed to air. The possibility that highly ordered mesoporous Cu structures have been formed during this project and that

they have been destroyed by corrosion cannot be ruled out. It is interesting to notice, for example, that the most successful mesoporous metallic structures electrodeposited so far from the hexagonal liquid crystal template of non-ionic surfactants are Pt, Pd and Ni, which are metals that do not corrode reversibly.

As mentioned in the introduction of this thesis, the electrodeposition of different metals from the hexagonal lyotropic liquid crystalline phase of non-ionic surfactants has been achieved by different authors and some remarkable results have been reported. During the timescale of this project it was not possible to demonstrate the presence of a well organised porous structure in the Cu and Cu-Pd films studied here, but I am convinced that the results shown are a step further for the fabrication of mesoporous Cu and Cu-Pd films.